NMR Spectroscopic Investigations on Aminocatalysis: Catalysts and Intermediates, Conformations and Mechanisms

Dissertation

zur Erlangung des Doktorgrades
der Naturwissenschaften (Dr. rer. nat.)
der Fakultät für Chemie und Pharmazie
der Universität Regensburg

vorgelegt von

Markus Schmid
aus Regensburg

2011

Die vorliegende Dissertation beruht auf Arbeiten, die zwischen Oktober 2007 und Januar 2011 im Arbeitskreis von Professor Dr. Ruth M. Gschwind am Institut für organische Chemie der Universität Regensburg durchgeführt wurden.

Promotionsgesuch eingereicht am: 21.01.2011

Die Arbeit wurde angeleitet von: Prof. Dr. Ruth M. Gschwind

Prüfungsausschuss:

Vorsitzender:	Prof. Dr. Dominik Horinek
1. Gutachter:	Prof. Dr. Ruth M. Gschwind
2. Gutachter:	Dr. Kirsten Zeitler
3. Prüfer:	Prof. Dr. Bernhard Dick

An dieser Stelle sei allen gedankt, die zum Gelingen dieser Arbeit beigetragen haben. Meiner Doktormutter Professor Dr. Ruth M. Gschwind bin ich in erster Linie zu Dank verpflichtet für den großen Freiraum bei der Entwicklung des Forschungsvorhabens, für ihr Vertrauen, für die intensiven Diskussionen und die fruchtbare Begleitung des Fortschreitens meiner Arbeit. Herzlich möchte ich Dr. Kirsten Zeitler danken für viele wertvolle Hinweise und Anregungen, für das Teilen ihres Wissens, für ihren unermüdlichen Fleiß und für ihr großes Interesse an meinen Forschungsergebnissen. Professor Dr. Dominik Horinek und Professor Dr. Bernhard Dick danke ich für ihre Bereitschaft, als Vorsitzender bzw. Prüfer im Prüfungsausschuss mitzuwirken. Ich bedanke mich bei Professor Dr. Burkhard König für viele hilfreiche Anmerkungen im Seminar und Professor Dr. Armin Buschauer als Sprecher des Graduiertenkollegs „Medizinische Chemie“ für die Möglichkeit, im Rahmen des GRK 760 zu lernen und zu forschen.
Ferner möchte ich allen Kooperationspartnern danken, deren Rat und Tat das Gelingen verschiedener Forschungsprojekte ermöglichten: Dr. Kirsten Zeitler und Johannes Franz (Institut für organische Chemie) für die synthetische Unterstützung der Organokatalyseprojekte; PD Dr. Wolfram Gronwald (Institut für funktionelle Genomik), Professor Dr. Oliver Reiser und Dr. Valerio D´Elia (Institut für organische Chemie) sowie Professor Dr. Burkhard Luy (Karlsruher Institut für Technologie) für ihre Beiträge zu den Foldamerstudien; Professor Dr. Armin Buschauer, Professor Dr. Günther Bernhardt und Christian Textor (Institut für Pharmazie) für die Zusammenarbeit an medizinisch-chemischen Forschungsprojekten; Dr. Evgeny Katayev (Institut für organische Chemie) sowie Professor Dr. Reinhard Sterner, Dr. Alexander Ehrmann, Harald Guldan und Florian Busch (Institut für Biophysik und physikalische Biochemie) für die Einblicke in die supramolekulare Chemie und die biochemische Forschung. Den Forschungspraktikantinnen Doris Heiß, Ancilla Neu, Carolin Holzhauser, Veronika Kropf und Carina Koch danke ich für ihre Mitarbeit und ihr Engagement.

Besonders herzlich möchte ich allen meinen Kollegen danken, die dafür sorgten, dass die Stimmung im Labor, im Sozialraum, im Salon, am Spektrometer, im „Doku-Zentrum“, im Computerraum, in der Mensa und in den Kaffee-, Kuchen-, Mittags-, Weißwurst- und Eispausen oft erfreulicher war als die Umstände. Vielen Dank Euch allen! Dr. Guido Federwisch, Dr. Tobias Gärtner und Dr. Roland Kleinmaier, Katrin Schober, Evelyn Hartmann und Christian Feldmeier, Diana Drettwan, Maria Neumeier und Nils Sorgenfrei. Matthias Fleischmann und Felicitas von Rekowski danke ich zudem für die Zusammenarbeit an einzelnen Teilprojekten dieser Arbeit. Dem Nachwuchs, Carina Koch, Michael Haindl und Michael Hammer, viel Erfolg und Durchhaltevermögen.
Ich danke Nikola Kastner-Pustet und Ulrike Weck für die Hilfsbereitschaft in allen technischen und bürokratischen Fragen, den Mitarbeitern der NMR-Abteilung, Dr. Thomas Burgemeister, Fritz Kastner, Annette Schramm und Georgine Stühler, für die Unterstützung am Spektrometer, Dr. Manfred Zabel, Sabine Stempfhuber und Dr. Stefanie Gärtner für die Kristallstrukturanalysen und die Hilfe im Umgang damit.

Schließlich habe ich dem Cusanuswerk und der Studienstiftung des deutschen Volkes zu danken für die finanzielle und ideelle Förderung während meiner Promotion sowie der Deutschen Forschungsgemeinschaft (GRK 760 und SPP 1179) für die finanzielle Unterstützung meiner Forschungsprojekte.

Vor allem aber gilt mein Dank meinen Eltern, Geschwistern und Freunden für Rückhalt und Unterstützung. Herzlichen Dank.

„Und?
Gefällt es Ihnen?“

—

„Ich habe es gesehen.
Es ist sehr schwer.“

NMR Spectroscopic Investigations on Aminocatalysis: Catalysts and Intermediates, Conformations and Mechanisms

Contents

1 Introduction and Outline

During the past decade, organocatalysis, *i.e.* the catalysis of chemical reactions with the help of small organic molecules, has experienced a tremendous increase in research activities and the scientific progress in the field has reached a breathtaking pace. Various general catalytic concepts, such as non-covalent catalysis through hydrogen bonding or phase transfer and covalent catalysis through Brønsted acids or Lewis bases, have been identified, developed to competitive chemical tools, and very successfully applied to an enormous number of chemical transformations. In particular organocatalysis by secondary amines, offering enamine, iminium, or SOMO activation modes, has proven to be one of the most widely applicable principles. By typically employing amine catalysts originating from the chiral pool, chemical reactions can be catalyzed in an asymmetric fashion with ease, which has contributed substantially to the interest in and to the popularity of modern amine organocatalysis. Accordingly, besides biocatalysis and metal catalysis, organocatalysis can nowadays be termed the third pillar of asymmetric catalysis and often even outperforms its two predecessors in the field of stereoselective catalysis in terms of experimental convenience, versatility, low cost, non-toxicity and sustainability.

Yet, with respect to the huge number of synthetic applications of asymmetric organocatalysis, studies aiming at a more detailed understanding of the underlying principles, mechanisms, and modes of stereoselection are rather sparse. Therefore, Seebach´s statement from 2008 that "the field is in its exploratory discovery phase before it can become contemplating" (*Helv. Chim. Acta* **2008**, *91*, 2002.) basically still holds true today. On the other hand, this lack of knowledge on the stabilities of catalysts and intermediates as well as on their conformations and reaction pathways may turn out to be an obstacle for the future development and further improvement of asymmetric organocatalysis, since a better mechanistic understanding is essential for the design and optimization of tailored catalytic systems and reaction conditions.

The goal of this thesis was therefore to shed more light on conformational and mechanistic issues of amine catalysis. A variety of modern NMR spectroscopic techniques was developed and applied to study catalyst properties, to monitor reaction profiles, to detect and characterize intermediate species, to investigate interconversion pathways, to elucidate conformational aspects, and to explore novel chemical transformations in order to generally advance the understanding of organocatalyzed reactions.

In chapter 2, organocatalytically active peptidic foldamers are analyzed conformationally in solution by a combined NMR/MD approach. Residual dipolar couplings are thereby established as novel NMR structural parameters for short linear peptides. RDCs are applied to validate structure coordinates for molecular dynamics simulations and to gather information on the peptide backbone and side-chain conformations.

Chapter 3 describes the first *in situ* detection and NMR characterization of proline enamine key intermediates in aldehyde self-aldolizations. Trends towards the enamine stabilization by appropriate solvents and substitution patterns are disclosed and the direct enamine formation from the isomeric oxazolidinones is revealed by EXSY analyses. In addition, the proline enamine stabilization by deuteration or deprotonation of the carboxylic group is elucidated and the detections of an α-oxy-aldehyde-derived proline enamine and of a tripeptide enamine are presented.

The mechanism of the direct enamine formation from the oxazolidinones in dipolar aprotic solvents is addressed in chapter 4 by means of selective 1D EXSY methods. Experimental evidence is provided that H-bonding interactions with urea derivatives accelerate the oxazolidinone-oxazolidinone interconversion. In contrast, the oxazolidinone-enamine exchange is enhanced by nucleophilic rather than by basic additives. Altogether, an S_N2-assisted proton relay mechanism is suggested for the oxazolidinone-enamine interconversion.

In chapter 5, the proline-catalyzed aldol addition and condensation of aldehydes are evidenced to be competing rather than consecutive reaction pathways. The condensation reaction is shown to most probably proceed via a Mannich-type mechanism with dual enamine/iminium activation of the substrate. Moreover, its detrimental impact on the stereoselectivity of the aldol addition is demonstrated. Further, the first proline dienamine intermediate is detected *in situ* and the parasitic character of proline intermediate formation with aromatic aldol acceptors is examined.

Detailed investigations on the formation and the stability of both prolinol and prolinol ether enamine intermediates in solution are presented in chapter 6. Thereby, the first *in situ* detection of a prolinol enamine in solution and the observation of a prolinol-derived carbinolamine are reported. The dependence of the delicate interplay between selectivity and reactivity on the catalyst structure as well as parasitic equilibria are elucidated and utilized to rationalize the different performances of prolinol(ether)s as organocatalysts.

Chapter 7 deals with the conformations of prolinol (ether) enamines in solution. Distinct conformational preferences of prolinol or prolinol ether enamines, respectively, are described and accounted for by H-bonding and CH/π interactions. Thus, long-standing discussions on conformational issues of such intermediates are solved so that the presented findings substantially help to explain the stereoinduction of prolinol (ether) organocatalysts. In addition, the aggregation behaviour of amine catalysts is studied and the silyl ether cleavage in solution is investigated.

In chapter 8, the origin of decreasing activities of polymer-supported prolinol ether catalysts after recycling is addressed. With the help of NMR signal suppression strategies, the presence of a residual non-hydrolyzed product iminium species could be evidenced. Based on the proposal of product inhibition, a straightforward approach to the restorage of the catalytic activity could be developed.

Chapter 9 details two unprecedented reaction pathways of nitroalkenes in the presence of amine catalysts. The organocatalytic homo- and heterodimerization of nitroalkenes and the subsequent fragmentation to enynes is discovered and a potential mechanism for this transformation is proposed. Furthermore, an intramolecular γ-cyclopropanation of an ϵ-iodo-substituted nitroalkene is observed.

The preliminary results of a study on the organocatalytic Michael addition of aldehydes to nitroalkenes are summarized in chapter 10. Substantial amounts of kinetically rather stable α-branched product enamines, derived from proline and prolinol, are observed. Investigations on a reaction cascade consisting of a Michael addition and an intramolecular alkylation furthermore evidence an eventual deactivation mechanism of amine organocatalysts, triggered by the release of HI in the course of the reaction.

2 RDCs in Short Peptidic Foldamers

Communication

"Residual Dipolar Couplings in Short Peptidic Foldamers: Combined Analyses of Backbone and Side-Chain Conformations and Evaluation of Structure Coordinates of Rigid Unnatural Amino Acids"

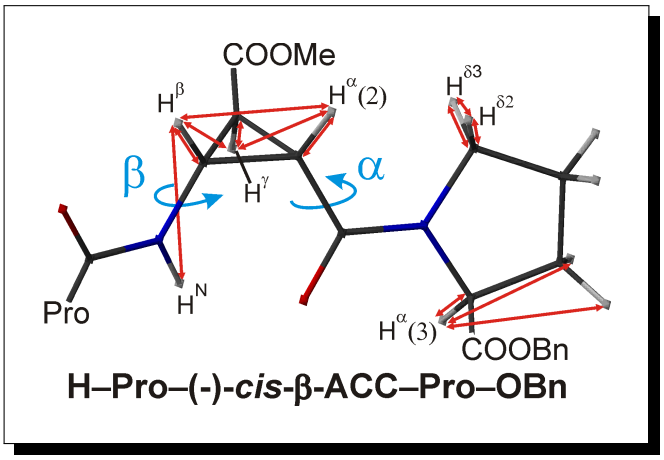

The syntheses of all peptides studied were performed by Valerio D´Elia. The NMR spectra of **1** and **6** and the PRODRG based β-ACC parameterization were accomplished in close collaboration with Matthias Fleischmann. M. F. also conducted the conformational investigations on **2**.

Markus B. Schmid, Matthias Fleischmann, Valerio D'Elia,
Oliver Reiser, Wolfram Gronwald, and Ruth M. Gschwind

ChemBioChem **2009**, *10*, 440–444.

http://dx.doi.org/10.1002/cbic.200800736

2.1 Abstract

Residual dipolar couplings (RDCs) have been shown to be highly potent structural parameters to determine the configuration of small molecules by NMR, but RDC-supported detailed conformational studies of short open-chain structures have not been reported so far. This study demonstrates that RDCs at natural abundance can provide essential structural information even in the case of short linear peptides with unnatural amino acids. Tripeptidic foldamers, composed of proline and *cis*-β-aminocyclopropanecarboxylic acid (*cis*-β-ACC), which has been successfully incorporated into NPY analogs, integrin ligands, and organocatalysts, are investigated as exemplary systems. An RDC-based approach to select appropriate structures for the force field parameterization of rigid non-standard amino acids is presented. Its relevance is demonstrated by conformational analyses of H-(L)-Pro-(L)-Pro-(-)-*cis*-β-ACC-OBn, for which slight alterations in the proton positions of unnatural amino acids lead to significant deviations in backbone and side-chain conformations. In addition, RDCs in combination with *cis*-β-ACC as a probe for molecular alignment allow to obtain conformational information on the backbone of H-(L)-Pro-(-)-*cis*-β-ACC-(L)-Pro-OBn. In this peptide, RDCs support also the elucidation of preferences of proline side-chain conformations.

2.3 Supporting Information

Experimental Section

Compounds **1** and **2** were synthesized following the published protocol.[17]

NMR spectra were recorded on a Bruker Avance DRX 600 spectrometer (600.13 MHz) (temperature was controlled by a BVT 3000 unit) and on a Bruker Avance III 600 (600.25 MHz) equipped with a TCI cryoprobe with z-gradient.

Sample concentrations of 40 mM to 140 mM were applied for NMR measurements of **1** at 240 K and 300 K depending on sensitivity requirements of the different spectra, while aggregation in this concentration and temperature range could be excluded by comparison of chemical shifts and by diffusion measurements with convection artefact suppression.[29] Due to the relatively small size of the investigated molecules and therefore slow NOE buildup a mixing time of 350 ms had to be used in the 2D ^{1}H,^{1}H-NOESY spectra. ^{1}H,^{13}C-P.E.HSQC[22] spectra for the determination of RDCs were measured in $CDCl_3$ and in a strained $CDCl_3$/PDMS gel[23] which provided a $CDCl_3$ line splitting of 20.5 Hz.

^{1}H,^{1}H-NOESY and ^{1}H,^{13}C-HSQC-NOESY spectra (due to severe signal overlap) of a 270 mM sample of **2** were recorded in $CDCl_3$ at 273 K.

NMR data were processed and evaluated with Bruker´s TOPSPIN 2.1 and the included DAISY program was used for spectra simulation whenever necessary. NOESY spectra were integrated and evaluated with AUREMOL;[30] its REFINE module was used for full relaxation matrix calculations.

Assignments of proton and carbon resonances of the conformations with Xxx-Pro *trans*-peptide bonds of **1** and **2** were obtained by the use of one- and two-dimensional NMR spectra. ^{1}H-spectra and ^{13}C-spectra (gated decoupled, power-gated, DEPT-135) in combination with ^{1}H,^{1}H-COSY, ^{1}H,^{1}H-NOESY, ^{1}H,^{13}C-HSQC and ^{1}H,^{13}C-HMBC allowed for the almost complete assignment of all resonances of **1** and **2** (Table 2.1).

MD simulations were performed with CNS 1.1 (Crystallography & NMR System).[25] The simulated annealing protocol included a high temperature stage (2,000 steps at 50,000 K of 7.5 fs each) in torsion angle space, an annealing stage to 0 K (2,000 250 K-steps of 7.5 fs each) and a final energy minimization following the conjugate gradient method in ten cycles of 200 steps each.

The unnatural amino acid *cis*-β-ACC was implemented into CNS on the basis of the DFT minimized structures, as discussed below, and force field parameters were created by the Dundee PRODRG2 Server[19] and XPLO2D.[31] The benzyl protecting group was parameterized on the basis of the available data for the natural amino acid phenylalanine.

The solvent for structure refinement was simulated by a cubic box of 50 Å length filled with 1,000 molecules of chloroform (obtained from VEGA ZZ 2.0.8[32]), for which periodic boundary conditions were assumed. The $CHCl_3$ geometry as well as atomic charges were taken from literature data[33] and force field parameters were generated by XPLO2D.

Calculated structures were visualized and evaluated with MOLMOL 2K.2.[34]

Additional Information

Nomenclature of 1

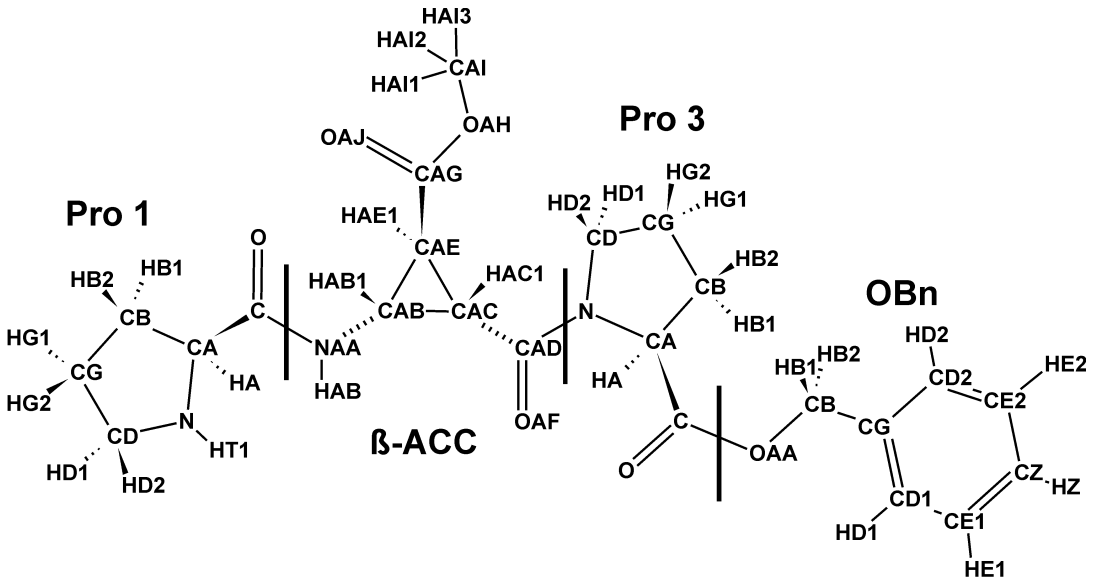

Figure 2.7: Nomenclature of **1** as used for CNS and within this Supporting Information. The same atom names were used for **2**. Only the primarily populated conformation of **1** (with a *trans* Xxx-Pro peptide bond) is depicted as only this one was investigated in detail.

Quality check of different *cis*-β-ACC coordinates with RDC data

In order to generate an appropriate β-ACC parameterization for MD simulations, various *cis*-β-ACC coordinate files were generated with the help of the Spartan 06 program package[35] (Table 2.2). Three different starting structures were used for that purpose: one structure that was directly built within Spartan, a second structure which was generated by the Dundee PRODRG2 Server, and a third one by inverting the stereocenters of a crystal structure of the enantiomer of **3**[18] followed by addition of hydrogen atoms with Spartan. Different equilibrium geometry calculation algorithms were applied to these structures: a molecular mechanics approach (MMFF force field), a semi-empirical calculation (RM1 method) and an ab initio calculation (Hartree-Fock with 6-31G* basis set). In addition, density functional theory calculations (B3LYP, 6-31G* basis set) on the crystal structure and its MM minimized offspring were performed. All these structures were fitted to 6 RDCs within the rigid β-ACC moiety with the help of the PALES[20,21] bestFit module (using singular-value decomposition). The results in terms of alignment tensors and bond and angle parameters as well as quality factors Q are summarized in Figure 2.8 and Table 2.2 (see footnote of Table 2.2 for structure code).

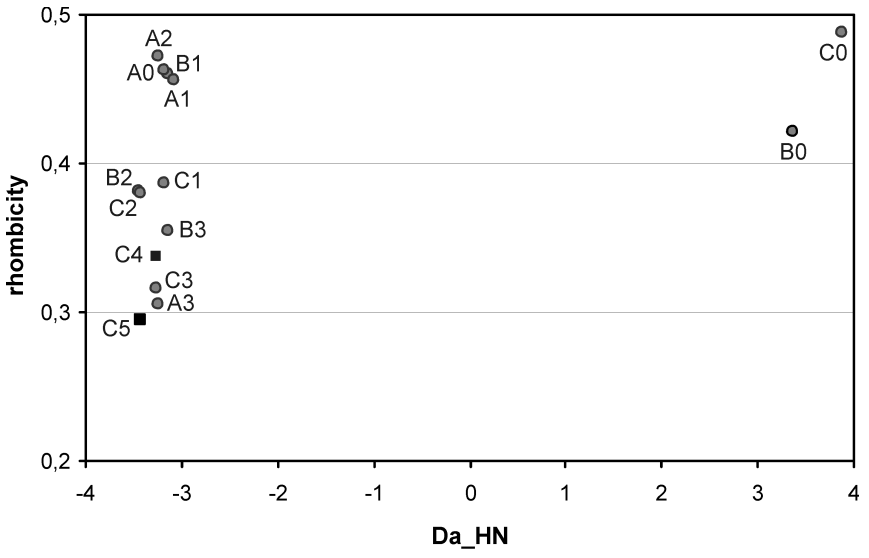

Figure 2.8: Alignment tensors (represented by their normalized axial components and their rhombicities) based on experimental β-ACC RDCs and the 14 different coordinate sets of **3** (see Table 2.2).

It can be concluded that B0 and C0 (the PRODRG structure and the crystal structure to which hydrogen atoms had been added simply by Spartan) yielded insufficient Q factors and erroneous alignment tensors due to the wrong hydrogen positions (decisive parameters are highlighted in Table 2.2). All the other equilibrium geometry calculation methods, however, resulted in acceptable Q factors and both similar parameters and alignment tensors within the range of experimental errors. The two geometries obtained by the DFT calculations were used as the basis for the applied CNS parametrization of *cis*-β-ACC.

Resonance Assignment of 1 and 2

resonance assignment of **1** ($CDCl_3$, 298 K/300 K)				
amino acid	proton	$\delta(^1H)$/ppm	carbon	$\delta(^{13}C)$/ppm
Pro1	HT1	2.08	C	176.4
	HA	3.70	CA	60.8
	HB1	2.07	CB	30.8
	HB2	1.91		
	HG1	1.59	CG	26.2
	HG2	1.69		
	HD1	2.87	CD	47.2
	HD2	2.81		
β-ACC	HAB	8.58	CAD	167.1
	HAB1	4.12	CAB	36.6
	HAC1	2.58	CAC	26.1
	HAE1	2.44	CAE	28.0
			CAG	171.2
	HAI*	3.69	CAI	52.4
Pro3			C	171.6
	HA	4.55	CA	59.1
	HB1	2.17	CB	29.3
	HB2	2.00		
	HG1	2.01, 2.06	CG	24.7
	HG2			
	HD1	3.65	CD	47.5
	HD2	3.87		
OBn	HB1	5.09, 5.12	CB	66.7
	HB2			
			CG	135.7
	HD*	7.32	CD*	128.1
	HE*	7.34	CE*	128.7
	HZ	7.31	CZ	128.4

resonance assignment of **1** ($CDCl_3$, 240 K)				
amino acid	proton	$\delta(^1H)$/ppm	carbon	$\delta(^{13}C)$/ppm
Pro1	HT1	—	C	176.2
	HA	3.75	CA	59.9
	HB1	2.09	CB	30.4
	HB2	1.90		
	HG1	1.59	CG	26.0
	HG2	1.68		
	HD1	2.87	CD	46.8
	HD2	2.74		
β-ACC	HAB	8.97	CAD	166.8
	HAB1	4.18	CAB	36.2
	HAC1	2.61	CAC	25.4
	HAE1	2.46	CAE	27.8
			CAG	171.0
	HAI*	3.67	CAI	52.4
Pro3			C	171.2
	HA	4.53	CA	58.5
	HB1	2.17	CB	28.8
	HB2	2.00		
	HG1	2.02 - 2.05	CG	24.3
	HG2			
	HD1	3.65	CD	47.2
	HD2	3.91		
OBn	HB1	5.04, 5.09	CB	66.5
	HB2			
			CG	134.8
	HD*	7.34	CD*	127.9
	HE*	7.36	CE*	128.4
	HZ	7.33	CZ	128.2

resonance assignment of **2** ($CDCl_3$, 273 K)				
amino acid	proton	$\delta(^1H)$/ppm	carbon	$\delta(^{13}C)$/ppm
Pro1	HT1	—	C	—
	HA	3.89	CA	58.8
	HB1	2.15	CB	30.1
	HB2	1.80		
	HG1	1.81	CG	26.0
	HG2	1.73		
	HD1	2.92	CD	47.3
	HD2	3.13		
Pro2			C	—
	HA	4.53	CA	59.9
	HB1	1.90	CB	27.5
	HB2	2.19		
	HG1	1.88-1.92	CG	24.7
	HG2			
	HD1	3.47	CD	46.5
	HD2	3.40		
β-ACC	HAB	7.65	CAD	—
	HAB1	3.91	CAB	35.8
	HAC1	2.52	CAC	26.5
	HAE1	2.31	CAE	28.2
			CAG	—
	HAI*	3.65	CAI	52.2
OBn	HB1	5.06, 5.08	CB	66.9
	HB2			
			CG	134.8
	HD*	7.31	CD*	127.9
	HE*	7.33	CE*	128.4
	HZ	7.32	CZ	128.3

Table 2.1: Assignment of proton and carbon resonances of **1** and **2** (major conformation with *trans* peptide bonds only, see Figure 2.7 for atom nomenclature). Chemical shifts were referenced to solvent signals ($\delta(^1H)_{CHCl3} = 7.26$ ppm, $\delta(^{13}C)_{CDCl3} = 77.16$ ppm).

bond lengths / Å																	
			A0	A1	A2	A3	B0	B1	B2	B3	C0	C1	C2	C3	C4	C5
	CAB	CAC	1.56	1.51	1.53	1.50	1.56	1.51	1.53	1.50	1.47	1.51	1.53	1.50	1.52	1.52
	CAB	CAE	1.56	1.52	1.52	1.51	1.57	1.52	1.53	1.52	1.54	1.52	1.53	1.51	1.52	1.52
	CAC	CAE	1.56	1.51	1.53	1.50	1.56	1.51	1.53	1.50	1.51	1.51	1.53	1.49	1.54	1.50
	CAB	NAA	1.47	1.44	1.44	1.42	1.51	1.43	1.43	1.42	1.44	1.44	1.43	1.42	1.42	1.43
	CAC	CAD	1.53	1.48	1.50	1.50	1.58	1.49	1.49	1.50	1.48	1.49	1.50	1.50	1.50	1.51
	CAE	CAG	1.53	1.49	1.49	1.50	1.56	1.48	1.48	1.49	1.50	1.48	1.48	1.49	1.49	1.49
	CAB	HAB1	1.10	1.09	1.11	1.07	1.00	1.09	1.11	1.07	1.10	1.09	1.11	1.07	1.08	1.08
	CAC	HAC1	1.10	1.09	1.11	1.07	1.00	1.09	1.11	1.07	1.10	1.09	1.10	1.07	1.08	1.08
	CAE	HAE1	1.10	1.09	1.11	1.07	1.00	1.09	1.11	1.07	1.10	1.09	1.11	1.07	1.09	1.09
	NAA	HAB	1.01	1.01	1.01	1.00	1.00	1.02	1.02	1.00	1.01	1.02	1.02	1.00	1.02	1.01

bond angles / °																
			A0	A1	A2	A3	B0	B1	B2	B3	C0	C1	C2	C3	C4	C5
CAB	CAC	CAE	60.0	59.8	60.1	60.0	59.8	59.5	60.0	59.7	60.3	59.7	60.0	59.3	59.5	59.2
CAC	CAE	CAB	60.0	59.8	60.2	59.5	60.0	60.1	60.2	59.3	57.5	60.0	60.2	60.1	59.5	60.2
CAE	CAB	CAC	60.0	60.4	59.7	60.6	60.2	60.4	59.8	61.0	62.2	60.3	59.9	60.6	61.0	60.6
NAA	CAB	CAC	117.3	121.7	118.1	121.9	121.2	121.0	119.8	112.1	118.8	121.5	118.8	121.5	121.3	120.8
NAA	CAC	CAE	117.3	121.1	118.2	121.0	121.3	121.5	117.7	121.2	116.3	121.0	117.2	118.7	120.5	119.2
CAD	CAC	CAB	117.3	121.9	119.2	121.0	122.7	122.0	118.4	120.6	118.2	120.2	117.4	118.0	118.5	117.1
CAD	CAC	CAE	117.3	118.6	117.1	117.3	121.7	118.4	117.1	116.9	119.1	119.5	117.0	116.4	115.8	115.8
CAG	CAE	CAB	117.3	120.9	116.9	118.5	122.3	119.7	116.1	118.1	123.3	119.4	118.9	120.5	120.6	120.7
CAG	CAE	CAC	117.3	117.5	116.0	117.2	121.4	119.6	116.1	117.2	119.9	120.5	119.3	120.6	120.9	121.0
HAB1	CAB	CAC	117.3	116.6	118.9	114.8	135.0	116.1	116.9	115.0	135.1	116.2	117.7	115.2	116.6	115.5
HAB1	CAB	CAE	117.3	116.7	119.1	115.7	134.9	117.0	118.5	115.6	133.1	116.7	119.1	117.4	117.0	117.5
HAC1	CAC	CAB	117.3	116.8	118.8	113.8	134.6	114.0	117.6	113.6	135.3	116.9	119.1	115.5	115.1	115.6
HAC1	CAC	CAE	117.3	115.4	118.5	113.6	135.6	118.5	117.6	114.5	134.5	115.8	117.5	116.4	114.7	116.6
HAE1	CAE	CAB	117.3	113.9	118.2	114.9	134.6	115.9	119.2	116.6	134.6	117.0	120.4	117.6	116.2	117.4
HAE1	CAE	CAC	117.3	118.6	119.6	115.7	135.4	117.1	120.4	116.7	137.6	117.6	119.0	115.4	115.3	114.2
HAB1	CAB	NAA	116.0	111.7	113.1	113.3	88.4	112.0	113.9	112.7	93.0	112.1	113.9	113.6	111.9	113.5
HAC1	CAC	CAD	116.0	113.8	113.3	118.0	87.3	114.0	115.2	118.4	91.7	114.2	114.9	118.1	119.2	118.8
HAE1	CAE	CAG	116.0	115.2	115.1	118.0	87.7	114.1	114.5	116.7	88.1	112.8	110.9	112.9	113.9	113.4

PALES-output																
		A0	A1	A2	A3	B0	B1	B2	B3	C0	C1	C2	C3	C4	C5
	Q RDC_RMS	0.054	0.098	0.081	0.036	0.357	0.039	0.066	0.058	0.310	0.062	0.057	0.007	0.021	0.036
	Da_HN	-3.18	-3.07	-3.25	-3.23	3.37	-3.13	-3.44	-3.14	3.87	-3.19	-3.42	-3.27	-3.27	-3.43
	rhombicity	0.46	0.46	0.47	0.30	0.42	0.46	0.38	0.35	0.49	0.39	0.38	0.32	0.34	0.29

structure code:

A	structure built within spartan	0	starting structure
B	PRODRG structure	1	molecular mechanics: MMFF
C	crystal structure	2	semi-empirical: RM1
C4	DFT: B3LYP, 6-31G*, starting from C0	3	Hartree-Fock: 6-31G*
C5	DFT: B3LYP, 6-31G*, starting from C1		

Table 2.2: Comparison of geometric parameters of the generated β-ACC coordinates of **1** and their RDC evaluation with PALES.

Structure investigation of 1

Structure investigation of 1 at 240 K. 28 negative NOE contacts (spin diffusion limit), detected in 2D ^{1}H,^{1}H-NOESY (350 ms mixing time) spectra at 240 K, were used as restraints in MD simulations. At first, relatively loose distance restraints were used to restrict the available conformational space, employing uniform upper and lower bounds of 0.500 nm and 0.175 nm, respectively. Using the standard simulated annealing protocol, described in chapter 2.3, 100 structures were calculated. Of these, 5 structures with low total and NOE energies were selected as a representative set for further analysis. Each member of this ensemble together with the NOESY crosspeak volumes (determined with AUREMOL) was used as input for the full relaxation matrix calculation (with the REFINE module (to be published) included in AUREMOL) in order to take spin diffusion effects into account. The refined sets of distance restraints were then applied for the next round of structure calculations. In total 5 rounds of structure calculations were performed until convergence of both distance restraints and calculated structures was reached. Solvent refined structures were obtained by subsequent refinement employing a chloroform box with periodic boundary conditions. Figure 2.9 shows the obtained structure ensemble.

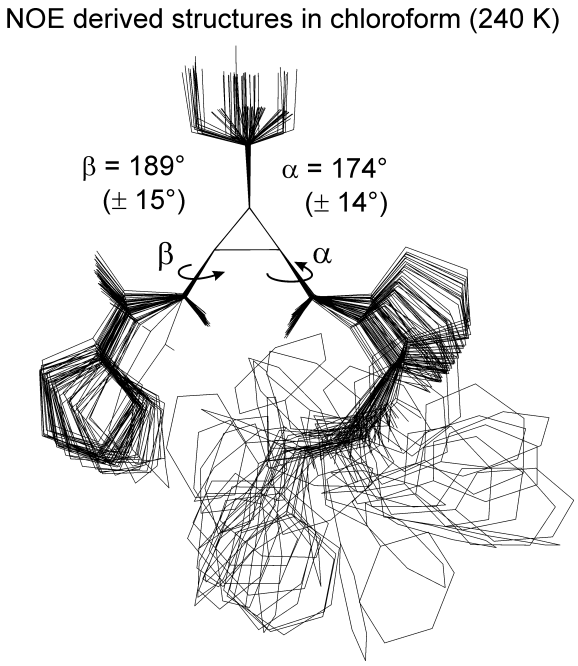

Figure 2.9: Ensemble of 50 structures refined in a chloroform box with 28 NOE distance restraints at 240 K derived from full relaxation matrix calculations.

The range of the β angle populated by the structure ensemble is in agreement with the large J coupling between the amide proton and the β-proton of *cis*-β-ACC (9.69 Hz at 240 K). As no Karplus curve has become available for *cis*-β-ACC so far, the quantum-mechanically calculated Karplus curve for **4**[36] was compared to the one calculated for **5** by an empirically generalized Karplus equation.[37]

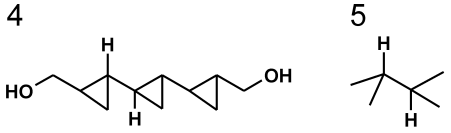

Thus, it was concluded that the cyclopropane ring scales down the scalar coupling constant in comparison to aliphatic chains as substituents. This was transferred onto the well-known Karplus curve for $^3J_{HN,H\alpha}$ of natural α-amino acids.[38] Hence, the observed J coupling of 9.69 Hz was interpreted in terms of a population of β values of 180° ± 30° (Figure 2.4C).

Structure investigation of 1 at 300 K based on NOEs. At 300 K, only four NOEs carrying quantifiable α- and β-relevant structural information could be identified (HAC1 - HD*(Pro3) for α and HAB - HAC1 as well as HAB - HAE1 for β). The quantification of this NOE information was additionally hampered by chemical exchange processes involving the amide proton. Therefore, no global calibration of NOE intensities was possible at 300 K and the REFINE module of AUREMOL could not be applied for spin diffusion corrections either.

When trying to translate relative NOE intensities relevant for α directly into angular information as shown in Figure 2.4B (right), proline side-chain conformations become important as they influence interatomar distances, too. In order to take this into account, a two-state approximation was made for Pro3 (the two conformations of low energy are usually referred to as "*up*" and "*down*")[39] and the population of these two conformations was estimated to be approximately 30 %:70 % *up*:*down* with the help of J couplings.[28] This ratio was used for the theoretical calculation of NOE intensities (Figure 2.4B, it was also used for Figure 2.4D) which includes the assumption that the populations of α and proline side-chain conformations are independent.

In order to additionally obtain upper limit distance restraints for MD simulations, the structurally relevant four NOEs that carry conformational information about the angles α and β were quantified according to equation 2.1: Two β-relevant contacts involving the amide proton were calibrated to the NOE HAB-HAB1 (r_{ref} = 3.0 Å) whose distance cannot exceed 3 Å so that the applied restraints represent upper limits on any account. Two further restraints, meaningful for α, were calibrated to the geminal peak of the δ-protons of Pro3. The upper limit of all these restraints was extended to 1.07*r_{ref} ($\approx$ 1.5*NOE_{ref}/NOE_{XY}) in order to concede spin diffusion influences and shortcomings in NOE integration. The generated structure ensemble is displayed in Figure 2.5A in the communication (chapter 2.2).

$$r_{XY} = r_{ref} \cdot \left(\frac{NOE_{ref}}{NOE_{XY}}\right)^{1/6} \tag{2.1}$$

Structure investigation of 1 at 298 K based on RDCs. A second set of structures was calculated employing residual dipolar couplings (RDCs) as conformational restraints. 23 RDCs could be determined experimentally from well-resolved 1D proton spectra and P.E.HSQC spectra at 298 K. They are summarized together with their estimated errors in Table 2.3. However, only 8 of them (highlighted in Table 2.3) were suited for interpretation as all the others were heavily influenced by internal dynamics.

Experimental errors of 0.2 Hz were assumed for $^3D_{H,H}$ determined from multiplet analysis of 1D proton spectra. For $^1D_{C,H}$ from P.E.HSQC spectra, the error was estimated to be 1 Hz in case the RDC could be extracted directly from peak splitting in ω2 and 2 Hz in case the multiplets in ω2 had to be simulated with DAISY due to higher order influences. Errors in $^2D_{H,H}$ from the peak tilt in P.E.HSQC spectra were estimated dependent on the peak quality as 0.4 Hz or 0.7 Hz. These errors were also used for the alignment tensor determination and Q calculation with PALES.

Concerning the angle α, the RDCs $^2D_{H\delta2,H\delta3}$, $^1D_{C\delta,H\delta2}$, $^1D_{C\delta,H\delta3}$ and $^1D_{C\alpha,H\alpha}$ bear conformational information, but in principle they all depend on the proline side-chain conformation which impedes their straightforward interpretation. However, $^1D_{C\alpha,H\alpha}$ shows almost no dependence on the proline side-chain conformation (Figure 2.10) and is therefore suited to extract information on α.

				D / Hz	ΔD / Hz	source
Pro1	$^1D_{C,H}$	CA	HA	0.1	1.0	P.E.HSQC
		CB	HB1	0.5	1.0	P.E.HSQC
			HB2	2.7	1.0	P.E.HSQC
		CG	HG1	2.6	1.0	P.E.HSQC
			HG2	3.7	1.0	P.E.HSQC
		CD	HD1	-0.8	1.0	P.E.HSQC
			HD2	-1.1	1.0	P.E.HSQC
	$^2D_{H,H}$	HB1	HB2	2.9	0.4	P.E.HSQC
		HG1	HG2	3.8	0.4	P.E.HSQC
		HD1	HD2	2.0	0.4	P.E.HSQC
β-ACC	$^1D_{C,H}$	CAB	HAB1	-7.4	1.0	P.E.HSQC
		CAC	HAC1	5.2	2.0	P.E.HSQC
		CAE	HAE1	2.9	2.0	P.E.HSQC
	$^3D_{H,H}$	HAB	HAB1	-0.9	0.2	1D ^{1}H
		HAB1	HAC1	-0.3	0.2	1D ^{1}H
		HAB1	HAE1	0.5	0.2	1D ^{1}H
		HAC1	HAE1	1.8	0.2	1D ^{1}H
Pro3	$^1D_{C,H}$	CA	HA	5.0	1.0	P.E.HSQC
		CD	HD1	-1.9	1.0	P.E.HSQC
			HD2	-0.3	1.0	P.E.HSQC
	$^2D_{H,H}$	HD1	HD2	3.7	0.7	P.E.HSQC
	$^3D_{H,H}$	HA	HB1	3.0	0.2	1D ^{1}H
			HB2	1.3	0.2	1D ^{1}H

Table 2.3: Experimentally determined residual dipolar couplings.

For the use of RDCs as CNS restraints, the alignment tensor defined for the *cis*-β-ACC residue was applied. As the "axial" input in CNS is dependent on D_{max}, i.e. on the internuclear distance, three different scaling factors for the "axial" value of $^3D_{HN,H\beta}$ (the only applied RDC for which the distance cannot be assumed to be fixed) were used which were supposed to cover the available distance range. However, the structures of low energy generated with these three different scaling factors were identical, resulting in the 40 structures (out of 300) that are displayed in the communication.

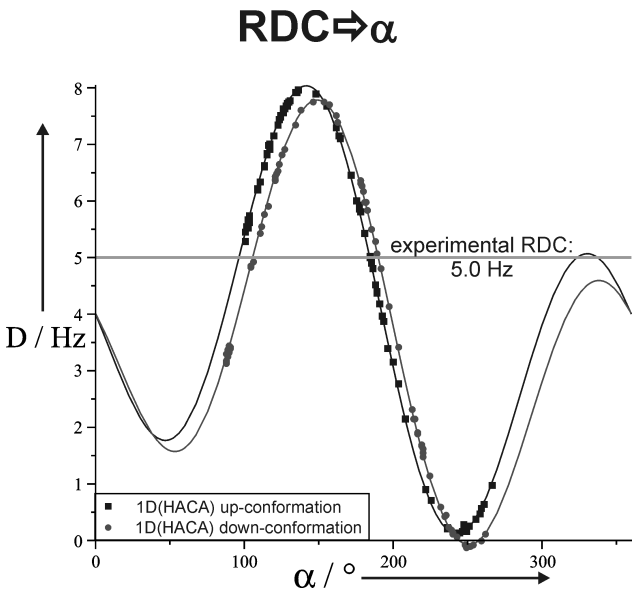

Figure 2.10: $^1D_{C\alpha,H\alpha}$ shows almost no dependence on the side-chain conformation of Pro3. (A ratio of 30:70 *up*:*down* was used for Figure 2.4D.)

Statistical information on the calculated structures of 1 and 2

	Figure 2.3B	Figure 2.9	Figure 2.5A	Figure 2.5B
number of selected structures	50	50	40	40
number of restraints (NOE/RDC, respectively)	54	28	4	11
rmsd (heavy atoms without BZA residue) / Å	0.39 ± 0.27	0.61 ± 0.24	0.52 ± 0.20 *	0.31 ± 0.14 *
E (NOE/RDC) / kJ/mol	2.0 ± 0.1	1.4 ± 1.8	< 1	< 1
E (total) / kJ/mol	39.2 ± 0.1	-153.0 ± 11.3	12.0 ± 0.2	19.7 ± 2.6

* Only those heavy atoms being directly affected by the applied restraints were concerned for rmsd calculation.

Table 2.4: Statistical information on the calculated structure ensembles displayed in the communication (chapter 2.2) and the Supporting Information.

2.4 Additional Experimental Findings

2.4.1 NMR Evidence for an Intraresidual H-Bond within β-ACC

A surprisingly stable conformation of **1** around the backbone angles α and β is observed by NMR spectroscopy on the basis of chemical shifts, scalar couplings, NOE and RDC data.[40] As the main source of this conformational stability, an intraresidual hydrogen bond within β-ACC is suggested by room temperature IR spectroscopy of **1** in chloroform.[18,41] Still, as an additional experimental proof, direct NMR evidence for this H-bonding interaction would be highly appreciated. The typically employed NMR indicator for intramolecular H-bonds in proteins, however, a small temperature coefficient of the amide proton chemical shift, has to be handled with care in the case of short, partially folded peptides because of the interfering influences of potential conformational changes.[42] The temperature-dependence of the amide proton resonance of **1** can hence not provide unambiguous insights into the H-bonding pattern of **1**.[28] Therefore, H-D exchange and DMSO titration experiments were performed as further NMR approaches that can prove the existence of intramolecular H-bonds.

Well-established for a long time in the field of protein structure investigations,[43] hydrogen-deuterium exchange studies had not found widespread applications to the study of intramolecular hydrogen bonds in small molecules.[44] Only recently could the scope of H-D exchange experiments be extended to small peptides in organic solvents by the addition of deuterated methanol.[45] In this approach, the reduced rate of deuterium exchange can be used as an indicator of H-bond donors and acceptors. In analogy to this study, **1** was dissolved in a mixture of 10 vol% MeOH-d_4 in $CDCl_3$ and the progress of the amide deuteration should be monitored by one-dimensional proton spectra at 300 K. But unfortunately, the amide ^{1}H resonance had already disappeared completely until the first measurement after 45 seconds. This finding is in agreement with the short half-life of the amide proton in chloroform (containing traces of water) that was estimated from EXSY analyses to be on the order of 1-2 seconds at 300 K. This unexpected result can be explained by the close proximity of the β-ACC amide proton and *N*-terminus of **1** (see Figures 2.5 and 2.9). Since the *N*-terminus is readily deuterated, it might act as a deuterium rod and thereby facilitate the amide deuteration. Thus, just like the amide proton temperature coefficient, the hydrogen-deuterium exchange rate is not suited to elucidate the intramolecular H-bond in our experimental system.

A further NMR-based method to identify intramolecular H-bonds in small molecules is the NMR-monitored stepwise addition of competing H-bond acceptors to the solute under investigation. This is due to the fact that the resonances of those analyte protons involved in intramolecular H-bonds should experience a much lower downfield shift than the resonances of solvent-exposed H-bond donors. Indeed, DMSO titration to analyte solutions in chloroform has been successfully applied to systems from medicinal chemistry[46] as well as from foldamer research.[47,48] Therefore, DMSO-d_6 was added stepwise to a 40 mM solution

of **1** in $CDCl_3$ and 1D ^1H NMR spectra were recorded for each DMSO-d_6/$CDCl_3$ ratio at 300 K so that the amide proton chemical shifts could be determined straightforwardly from these spectra. The result of this DMSO titration is displayed in Figure 2.11.

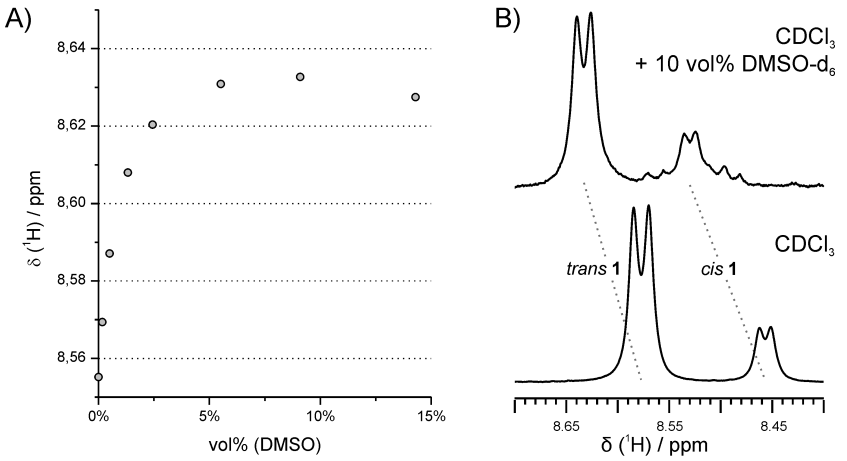

Figure 2.11: A) Development of the chemical shift of the amide proton of the major *trans* conformation of **1** upon addition of DMSO-d_6 at 300 K. B) Amide proton region of the ^1H spectra of **1** in $CDCl_3$ (bottom) and $CDCl_3$/10 vol% DMSO-d_6 (top).

The most striking observation is the low overall downfield shift of the amide proton resonance (below 0.08 ppm) upon the addition of DMSO (Figure 2.11A). This contrasts sharply with the downfield shift of about 0.9 ppm that is experienced by the *N*-terminal proton (data not shown). From this discrepancy and in comparison with literature data,[a] it becomes obvious that the amide proton is indeed involved in an intramolecular H-bond; in contrast, the *N*-terminal amine must be readily accessible for hydrogen-bond acceptor solvent molecules (*i.e.* DMSO). In addition to the chemical shift of the amide proton, the scalar coupling constant $^3J_{HN,H\beta}$ within β-ACC remains unchanged during the DMSO titration (Figure 2.11B). This reveals that the β-ACC backbone conformation is not detectably influenced by competing H-bond acceptors. The correlated stabilities of $\delta(H^N)$ and $^3J_{HN,H\beta}$ can hence be taken as a further support for the hypothesis that an intraresidual H-bond within β-ACC is mainly responsible for the conformational backbone stabilization of **1**.

Altogether, in our experimental system, the DMSO titration experiment reveals the stability of the amide proton chemical shift and of the backbone scalar coupling against addition of competing H-bond acceptors. This provides direct NMR evidence for an intraresidual hydrogen-bond within β-ACC in **1** that could not be obtained by analysis of chemical shift temperature coefficients or hydrogen-deuterium exchange experiments. This finding is also in excellent agreement with the results from both IR spectroscopy and the above-mentioned NMR structural parameters in combination with MD simulations. It hence supports the accuracy of the conformational investigations on the tripeptide **1**.

[a] Downfield shifts of 0.13 ppm,[46] about 0.3 ppm,[47] and up to 0.69 ppm[48] in $CDCl_3$/DMSO titration studies were reported for intramolecularly hydrogen-bonded NH protons.

2.4.2 Investigations on Further β-ACC-Containing Peptides

The methodology established on the example of **1** was also meant to be used for related peptidic foldamers with a closer link to the applications of β-ACC-containing peptides in medicinal chemistry and organocatalysis. Therefore, **6** (Figure 2.12A) was chosen as an extended peptide sequence with regard to medicinal chemistry and **7** (Figure 2.12B) as a *C*-terminally deprotected analog that had been successfully applied in asymmetric organocatalysis. Both compounds were subject to a preliminary screening process to identify promising experimental systems for more detailed studies.

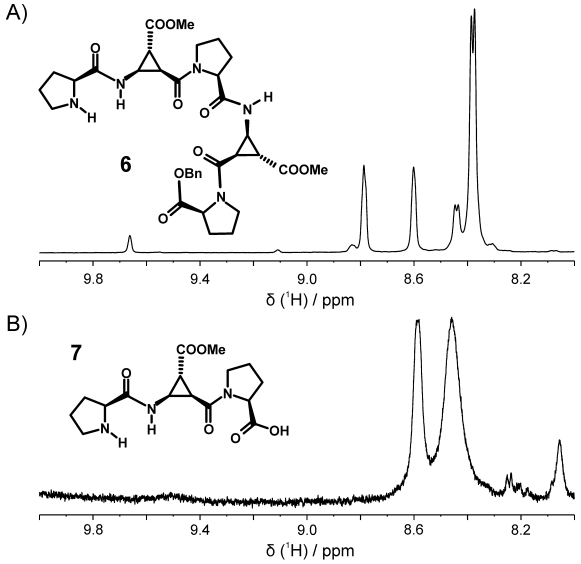

Figure 2.12: Preliminarily investigated β-ACC-containing peptides and amide sections of their ^{1}H spectra: A) H-(L)-Pro-▲-(L)-Pro-▲-(L)-Pro-OBn **6** and B) H-(L)-Pro-▲-(L)-Pro-OH **7**.

However, the proton spectrum of **6** in $CDCl_3$ revealed various sets of signals (Figure 2.12A). This indicates a mixture of manifold stable, most probably interconverting conformers in solution. This experimental system was therefore considered to be too complex for detailed and meaningful conformational investigations. Thus, so far no further efforts have been made towards detailed conformational analyses of **6**.

For **7**, just like for **1** and in contrast to **6**, only two strongly preferred conformations were observed in the proton spectrum (Figure 2.12B). Nevertheless, in this case, the structure analysis was hampered by the severe aggregation of **7** in chloroform, as evidenced by DOSY and additionally indicated by broad proton resonances and by negative NOEs (slow tumbling limit). Attempts to alleviate the problem of aggregation by reduced analyte concentrations or by addition of up to 10 vol% of MeCN-d_3 failed, too. Hence, no conformational investigations were conducted on the organocatalyst **7** itself in chloroform. Instead, the stabilization of reaction intermediates of **7** (most probably coming along with deaggregation, see chapter 3.4) is envisaged as the method of choice for gathering conformational information on **7** as well as on the stereoinduction effectuated by **7** in asymmetric aldol reactions.

2.5 References

[1] J. H. Prestegard, C. M. Bougault, A. I. Kishore, *Chem. Rev.* **2004**, *104*, 3519–3540.

[2] B. Simon, M. Sattler, *Angew. Chem. Int. Ed.* **2002**, *41*, 437–440.

[3] C. Farès, J. Hassfeld, D. Menche, T. Carlomagno, *Angew. Chem. Int. Ed.* **2008**, *47*, 3722–3726.

[4] C. M. Thiele, *Conc. Magn. Reson.* **2007**, *30A*, 65–80.

[5] C. M. Thiele, S. Berger, *Org. Lett.* **2003**, *5*, 705–708.

[6] C. M. Thiele, A. Marx, R. Berger, M. Biel, A. Giannis, *Angew. Chem. Int. Ed.* **2006**, *45*, 4455–4460.

[7] J. Klages, C. Neubauer, M. Coles, H. Kessler, B. Luy, *ChemBioChem* **2005**, *6*, 1672–1678.

[8] U. M. Reinscheid, J. Farjon, M. Radzom, P. Haberz, A. Zeeck, M. Blackledge, C. Griesinger, *ChemBioChem* **2006**, *7*, 287–296.

[9] A. Schuetz, J. Junker, A. Leonov, O. F. Lange, T. F. Molinski, C. Griesinger, *J. Am. Chem. Soc.* **2007**, *129*, 15114–15115.

[10] A. Schuetz, T. Murakami, N. Takada, J. Junker, M. Hashimoto, C. Griesinger, *Angew. Chem. Int. Ed.* **2008**, *47*, 2032–2034.

[11] S. A. Dames, R. Aregger, N. Vajpai, P. Bernado, M. Blackledge, S. Grzesiek, *J. Am. Chem. Soc.* **2006**, *128*, 13508–13514.

[12] S. Ohnishi, D. Shortle, *Proteins Struct. Funct. Genet.* **2003**, *50*, 546–551.

[13] R. Beumer, C. Bubert, C. Cabrele, O. Vielhauer, M. Pietzsch, O. Reiser, *J. Org. Chem.* **2000**, *65*, 8960–8969.

[14] S. De Pol, C. Zorn, C. D. Klein, O. Zerbe, O. Reiser, *Angew. Chem. Int. Ed.* **2004**, *43*, 511–514.

[15] N. Koglin, C. Zorn, R. Beumer, C. Cabrele, C. Bubert, N. Sewald, O. Reiser, A. G. Beck-Sickinger, *Angew. Chem. Int. Ed.* **2003**, *42*, 202–205.

[16] S. Urman, K. Gaus, Y. Yang, U. Strijowski, N. Sewald, S. De Pol, O. Reiser, *Angew. Chem. Int. Ed.* **2007**, *46*, 3976–3978.

[17] V. D´Elia, H. Zwicknagl, O. Reiser, *J. Org. Chem.* **2008**, *73*, 3262–3265.

[18] C. Zorn, Ph.D. Thesis, Universität Regensburg (Germany), **2001**.

[19] A. W. Schüttelkopf, D. M. F. van Aalten, *Acta Cryst.* **2004**, *D60*, 1355–1363.

[20] M. Zweckstetter, A. Bax, *J. Am. Chem. Soc.* **2000**, *122*, 3791–3792.

[21] M. Zweckstetter, *Nat. Protoc.* **2008**, *3*, 679–690.

[22] P. Tzvetkova, S. Simova, B. Luy, *J. Magn. Reson.* **2007**, *186*, 193–200.

[23] J. C. Freudenberger, P. Spiteller, R. Bauer, H. Kessler, B. Luy, *J. Am. Chem. Soc.* **2004**, *126*, 14690–14691.

[24] H. J. Dyson, P. E. Wright, *Ann. Rev. Biophys. Biophys. Chem.* **1991**, *20*, 519–538.

[25] A. T. Brünger, P. D. Adams, G. M. Clore, W. L. DeLano, P. Gros, R. W. Grosse-Kunstleve, J.-S. Jiang, J. Kuszewski, M. Nilges, N. S. Pannu, R. J. Read, L. M. Rice, T. Simonson, G. L. Warren, *Acta Cryst.* **1998**, *D54*, 905–921.

[26] M. Cai, Y. Huang, J. Liu, R. Krishnamoorthi, *J. Biomol. NMR* **1995**, *6*, 123–128.

[27] Z. L. Mádi, C. Griesinger, R. R. Ernst, *J. Am. Chem. Soc.* **1990**, *112*, 2908–2914.

[28] M. Schmid, Diploma Thesis, Universität Regensburg (Germany), **2007**.

[29] A. Jerschow, N. Müller, *J. Magn. Reson.* **1997**, *125*, 372–375.

[30] W. Gronwald, H. R. Kalbitzer, *Prog. Nucl. Magn. Reson. Spectrosc.* **2004**, *44*, 33–96.

[31] G. J. Kleywegt, K. Henrick, E. J. Dodson, D. M. F. van Aalten, *Structure* **2003**, *11*, 1051–1059.

[32] A. Pedretti, L. Villa, G. Vistoli, *J. Comput.-Aided Mol. Des.* **2004**, *18*, 167–173.

[33] M. E. Martín, A. Muñoz Losa, I. F. Galván, M. A. Aguilar, *J. Mol. Struct. (THEOCHEM)* **2006**, *775*, 81–86.

[34] R. Koradi, M. Billeter, K. Wüthrich, *J. Mol. Graphics* **1996**, *14*, 51–55.

[35] `http://www.wavefun.com`.

[36] A. G. M. Barrett, R. A. James, G. E. Morton, P. A. Procopiou, C. Boehme, A. deMeijere, C. Griesinger, U. M. Reinscheid, *J. Org. Chem.* **2006**, *71*, 2756–2759.

[37] C. A. G. Haasnoot, F. A. A. M. de Leeuw, C. Altona, *Tetrahedron* **1980**, *36*, 2783–2792.

[38] V. F. Bystrov, *Prog. Nucl. Magn. Reson. Spectrosc.* **1976**, *10*, 41–82.

[39] G. N. Ramachandran, A. V. Lakshminarayanan, R. Balasubramanian, G. Tegoni, *Biochim. Biophys. Acta Prot. Struct.* **1970**, *221*, 165–181.

[40] M. B. Schmid, M. Fleischmann, V. D'Elia, O. Reiser, W. Gronwald, R. M. Gschwind, *ChemBioChem* **2009**, *10*, 440–444.

[41] V. D´Elia, Ph.D. Thesis, Universität Regensburg (Germany), **2009**.

[42] N. H. Andersen, J. W. Neidigh, S. M. Harris, G. M. Lee, Z. Liu, H. Tong, *J. Am. Chem. Soc.* **1997**, *119*, 8547–8561.

[43] B. M. P. Huyghues-Despointes, J. M. Scholtz, C. N. Pace, *Nat. Struct. Biol.* **1999**, *6*, 910–912.

[44] C. L. Perrin, T. J. Dwyer, J. Rebek, R. J. Duff, *J. Am. Chem. Soc.* **1990**, *112*, 3122–3125.

[45] L. R. Steffel, T. J. Cashman, M. H. Reutershan, B. R. Linton, *J. Am. Chem. Soc.* **2007**, *129*, 12956–12957.

[46] A. Jansma, Q. Zhang, B. Li, Q. Ding, T. Uno, B. Bursulaya, Y. Liu, P. Furet, N. S. Gray, B. H. Geierstanger, *J. Med. Chem.* **2007**, *50*, 5875–5877.

[47] D. Yang, J. Qu, B. Li, F.-F. Ng, X.-C. Wang, K.-K. Cheung, D.-P. Wang, Y.-D. Wu, *J. Am. Chem. Soc.* **1999**, *121*, 589–590.

[48] G. V. M. Sharma, P. Nagendar, P. Jayaprakash, P. Radha Krishna, K. V. S. Ramakrishna, A. C. Kunwar, *Angew. Chem. Int. Ed.* **2005**, *44*, 5878–5882.

3 The Elusive Proline Enamine Intermediate

Communication

"The Elusive Enamine Intermediate in Proline-Catalyzed Aldol Reactions: NMR Detection, Formation Pathway, and Stabilization Trends"

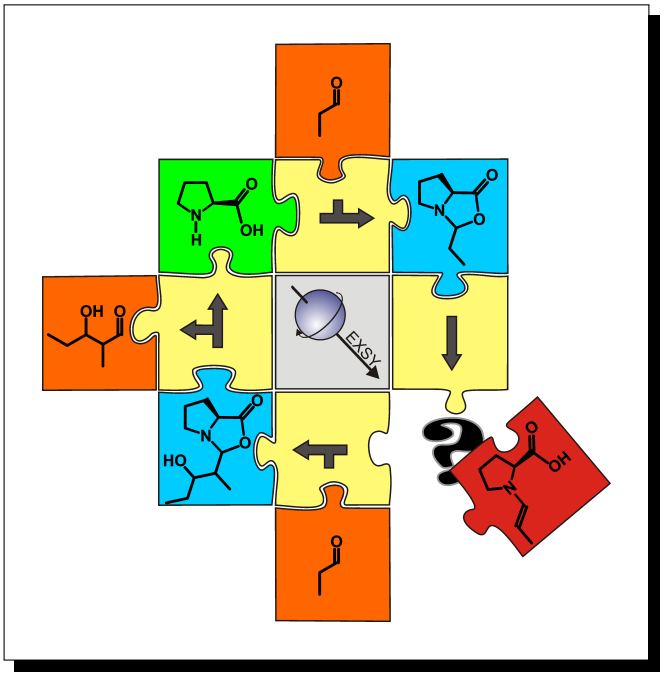

Markus B. Schmid, Kirsten Zeitler, and Ruth M. Gschwind

Angew. Chem. Int. Ed. **2010**, *49*, 4997–5003.

http://dx.doi.org/10.1002/anie.200906629

3.1 Abstract

The elusive experimental detection of enamine intermediates in proline-catalyzed aldol reactions has been the central matter of dispute for the otherwise commonly accepted mechanism of enamine catalysis. Here, the first *in situ* detection of enamine intermediates in proline-catalyzed aldol reactions by real-time NMR is reported and new insights into their stabilization and their formation pathway in dipolar aprotic solvents are presented. Exclusively, *E*-configured s-*trans*-enamines are detected; in DMSO, these enamines are formed directly from oxazolidinones and not via central iminium or iminium-like intermediates as evidenced by EXSY analyses. The position of these oxazolidinone-enamine equilibria is not affected by additional water or the amount of catalyst. But strong hydrogen-bond acceptor and missing hydrogen-bond donor properties of the solvent increase the amount of enamines. Ketones and α-branched aldehydes show no or very low enamine concentrations, while β-alkyl substituents of propionaldehydes cause enamine stabilization. Our results corroborate not only the central role of enamines in proline-catalyzed aldol reactions, but also elucidate a new role of the oxazolidinones as a hinge between aldehydes and enamines in dipolar aprotic solvents. In conclusion, the presented first detailed insights into the oxazolidinone-enamine exchange processes should allow for rational and directed optimizations of proline-catalyzed reactions.

3.3 Supporting Information

Experimental Details

Organocatalytic reactions were conducted inside a standard 5 mm NMR tube by adding 30 μmol freshly distilled aldehyde to a suspension of 30 μmol (100 mol%) or 6 μmol (20 mol%) L-proline, respectively, in 0.6 mL deuterated solvent. The NMR tube was transferred to the spectrometer immediately after starting the reaction.

NMR spectra were recorded at 300 K on a Bruker Avance DRX 600 (600.13 MHz) and on a Bruker Avance III 600 (600.25 MHz) spectrometer, the latter equipped with a TCI cryoprobe with z-gradient. 1D ^{1}H NMR experiments were performed in order to monitor the reaction and to identify appropriate time slots for further intermediate studies. For the characterization of the intermediates, ^{1}H,^{1}H-COSY, ^{1}H,^{1}H-NOESY/EXSY, ^{1}H,^{13}C-HSQC, ^{1}H,^{13}C-HMBC, and ^{1}H-DOSY spectra were recorded. For the NOESY/EXSY spectrum a mixing time of 700 ms was used, the DOSY experiment was performed with a diffusion delay of 50 ms. NMR data were processed and evaluated with Bruker´s TOPSPIN 2.1 and the included DAISY program was used for the simulation of 1D ^{1}H spectra.

Additional Information

Reaction profile of the self-aldolization of 1 under L-Pro-catalysis (100 mol%) and detection of product intermediates

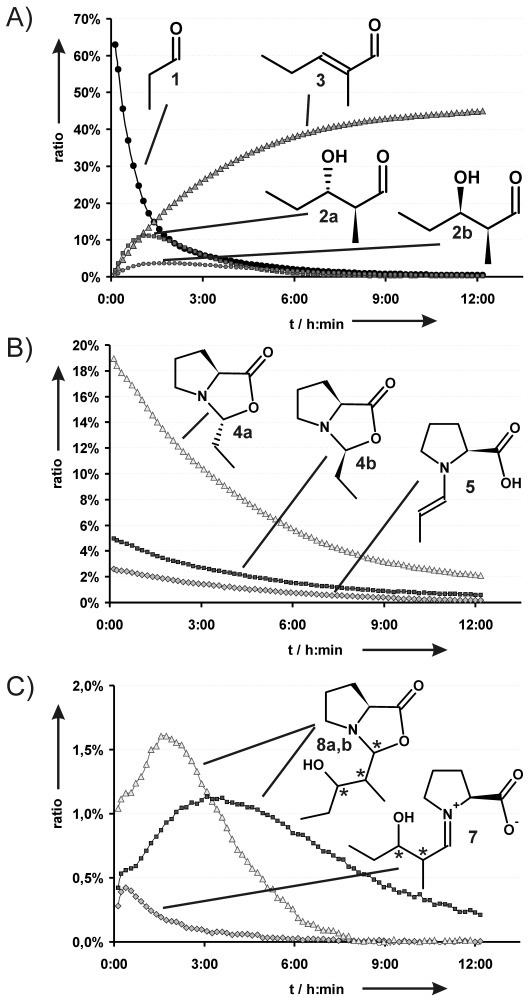

Figure 3.8: Reaction profile of the proline-catalyzed aldol reaction of **1** with 100 mol% of catalyst: A) substrate **1** and aldol products **2a**,**b** and **3**; B) substrate intermediates **4a**,**b** and **5**; C) product intermediates **7** and **8a**,**b**.

NMR assignment of 5

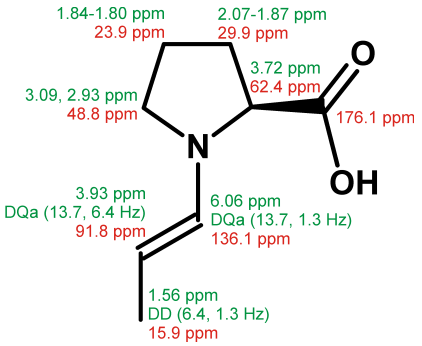

Figure 3.9: Complete ^{1}H and ^{13}C assignment of enamine intermediate **5** and multiplet pattern for the ene-unit. Proton information is given in green, carbon information in red.

Influence of the amount of catalyst on the equilibrium of 4a,b and 5

When increasing the catalyst amount offered from 20 mol% to 100 mol%, no significant change in the position of the oxazolidinone-enamine equilibrium was observed, but only a general increase of the intermediate concentrations.

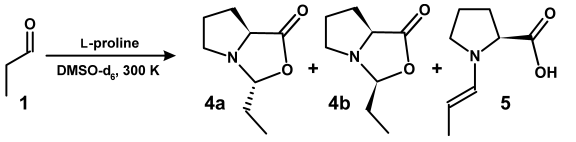

amount of catalyst[a]	4a	4b	5	4a+4b+5 / C_3-moieties[b]
20 mol%	72 %	18 %	10 %	8 %
100 mol%	71 %	19 %	10 %	32 %

a) related to 100 mol% **1**,
b) The total amount of all C_3-moieties stemming from **1**, detected in the first spectrum, was set to 100%; both values were determined at about 10 minutes after the reaction had been started; the water contents of the samples were 1.2 and 1.3 equivalents, respectively.

Figure 3.10: There is no influence of the catalyst amount on the equilibrium ratios of **4a**,**b** and **5**.

Influence of the amount of water on the equilibrium of 4a,b and 5

Addition of increasing amounts of water to the reaction mixtures of propionaldehyde/L-Pro or 3-methyl-butyraldehyde/L-Pro in DMSO leads to an overall decrease of the intermediate concentrations, as expected for reversible reactions releasing water according to Le Chatelier´s principle. (The moderate quality of the data is attributed to a number of potential error sources such as the complex reaction mixture, the lack of control on reproducible sample mixing within the NMR spectrometer, the time dependence of the intermediate concentrations as well as the integration of the broad and overlapping water resonance.)

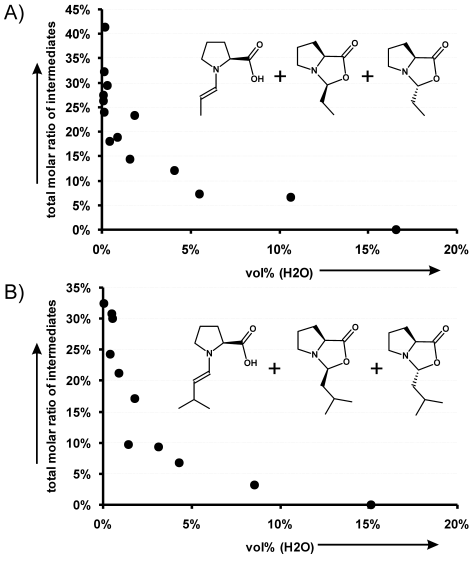

Figure 3.11: The total intermediate concentrations decrease with increasing amounts of water present in the reaction mixtures of A) propionaldehyde/L-Pro and B) 3-methyl-butyraldehyde/L-Pro in DMSO-d_6.

However, as long as relative intermediate ratios can be determined by NMR resonance integration (above about 2 vol% of water, oxazolidinone resonances are broadened and hence integration is not reliable any longer), these ratios remain unaffected for both reaction mixtures. (Note: The stability of this ratio was also assumed for the calculation of the total intermediate amounts of Figure 3.11 when integration of the oxazolidinones was not possible any more.)

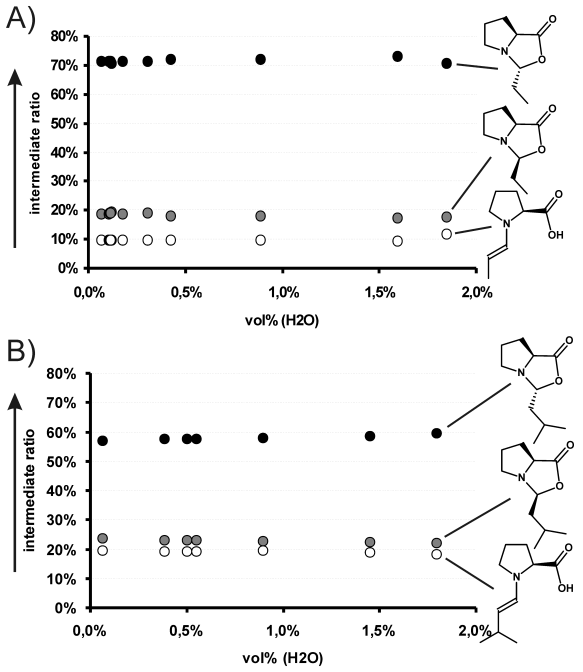

Figure 3.12: The relative ratios of the intermediates are independent of the amount of water present in the reaction mixtures of A) propionaldehyde/L-Pro and B) 3-methylbutyraldehyde/L-Pro in DMSO-d_6.

The addition of water also influences the appearance of the NMR resonances of the intermediate species: The oxazolidinone resonances are broadened and experience a significant downfield shift whereas there is virtually no effect of water on the enamine intermediate resonance. This is in line with our findings that there are different equilibration processes for the exchanges aldehyde-oxazolidinone and oxazolidinone-enamine operative.

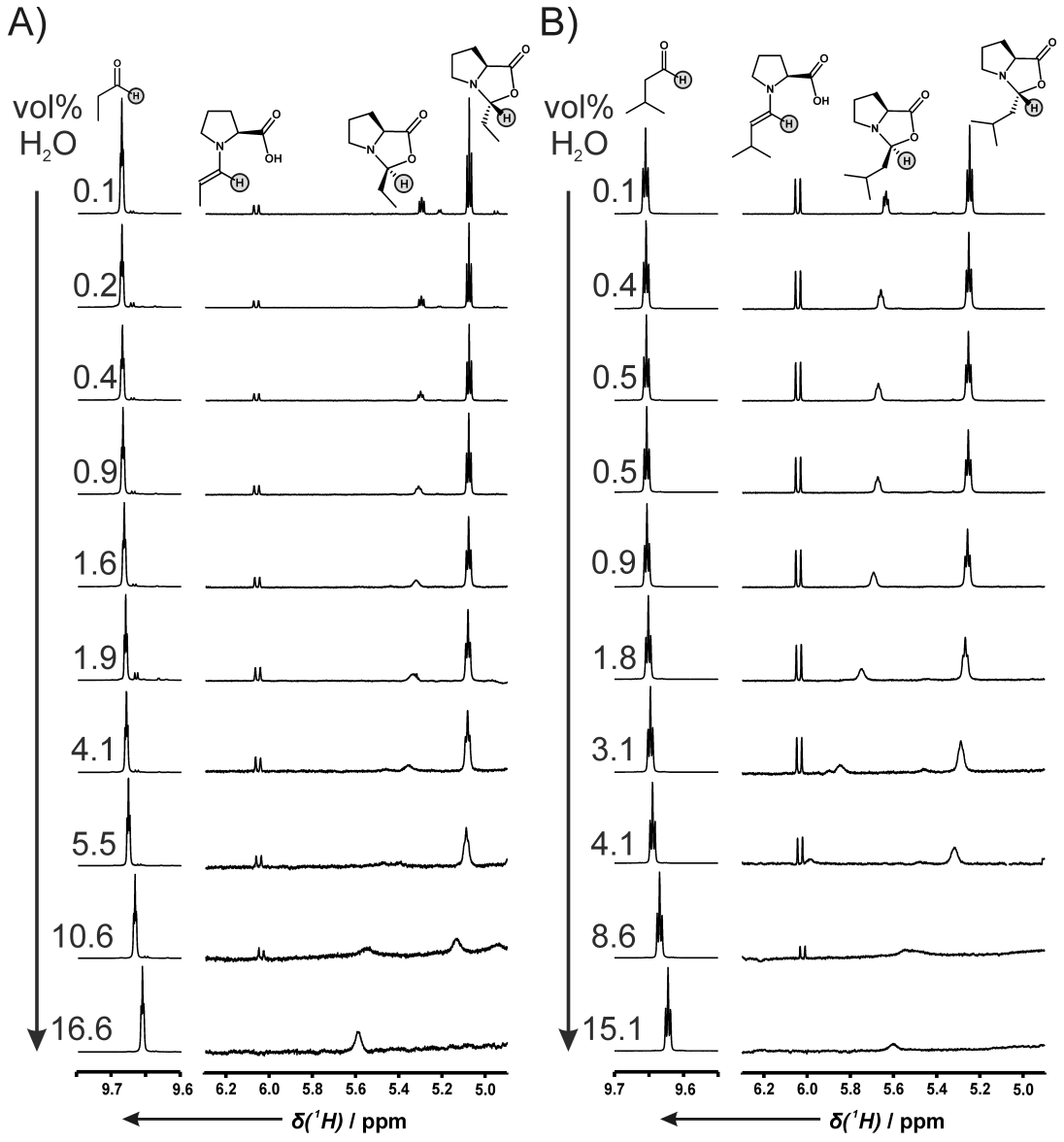

Figure 3.13: Influence of water addition (from top to down) on the intermediates in the reaction mixtures of A) propionaldehyde/L-Pro and B) 3-methyl-butyraldehyde/L-Pro in DMSO-d_6. (All spectral sections were scaled individually in order to reach optimal clarity.)

DOSY findings concerning 5-solvent-aggregates

The evaluation of DOSY experiments that are performed during the course of a reaction is hampered because not only diffusion, but also the progress of the reaction changes the signal intensities. Nevertheless, as we had shown that there is an equilibrium between **4a**,**b** and **5**, the resonances of **4a**,**b** and **5** are identically affected by the reaction so that their observed diffusion properties can be compared with each other. Figure 3.14 shows signal attenuations of the DOSY experiment (slower signal attenuation corresponds to slower molecular diffusion). The significantly slower diffusion of **5** compared to **4a** and **4b** cannot simply be explained by the different shapes of the molecules, instead we believe this to be due to the strong interaction of the carboxylic group of **5** with solvent molecules, which in effect increases molecular size and hence decelerates the diffusion of **5**.

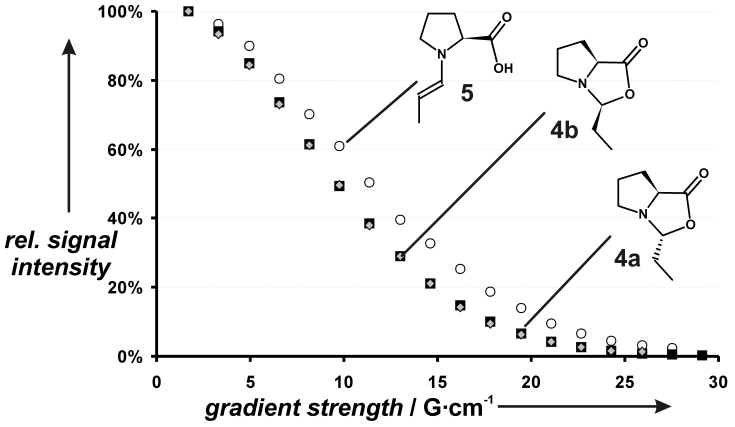

Figure 3.14: Signal attenuation of **4a**,**b** and **5** during a DOSY experiment with variation of the gradient strength from 5 % to 95 % of the maximum. (Signal intensities at the lowest gradient strength were set to 100 % for each compound separately.)

NMR spectra of enamine/oxazolidinone mixtures

See following pages.

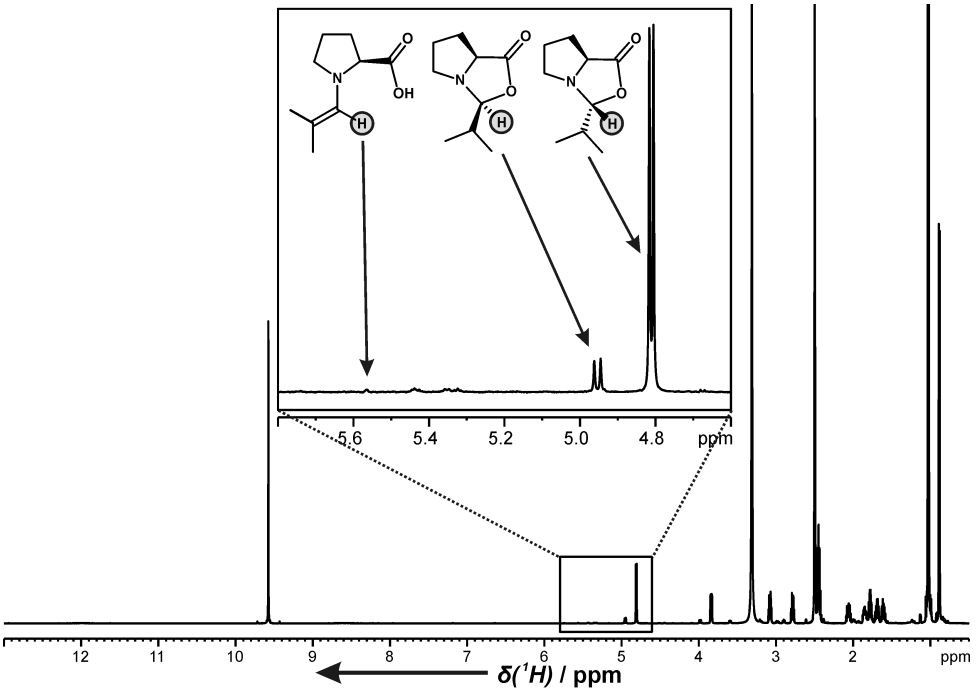

Figure 3.15: 1D ^{1}H spectrum of the reaction mixture of isobutyraldehyde/100 mol% L-Pro after 11 minutes. The characteristic resonances of oxazolidinone and enamine intermediates are shown in the expansion.

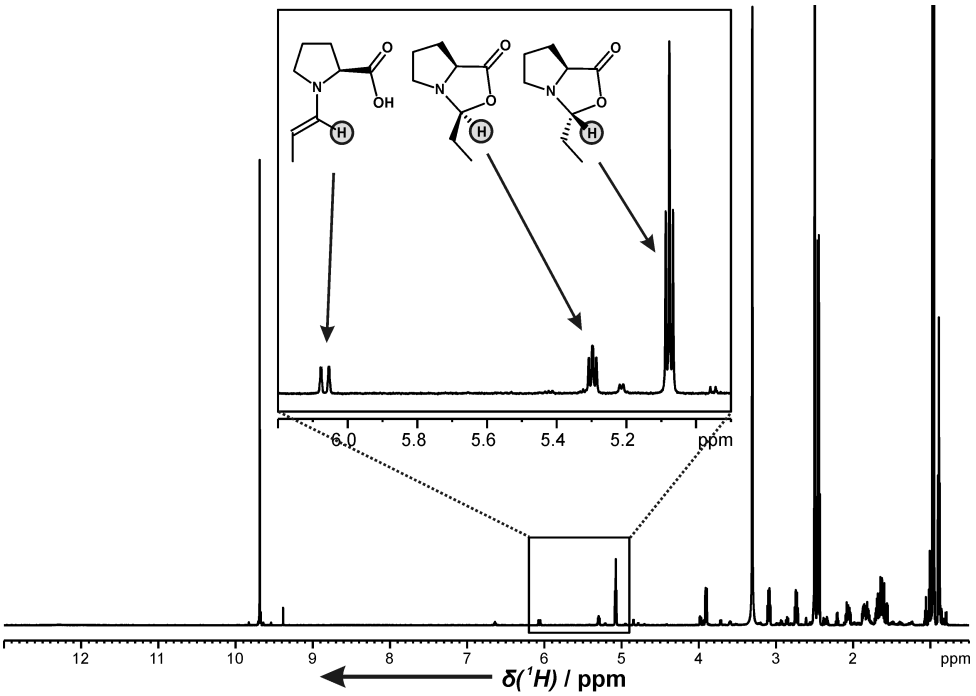

Figure 3.16: 1D ^{1}H spectrum of the reaction mixture of propionaldehyde/100 mol% L-Pro after 8 minutes. The characteristic resonances of oxazolidinone and enamine intermediates are shown in the expansions.

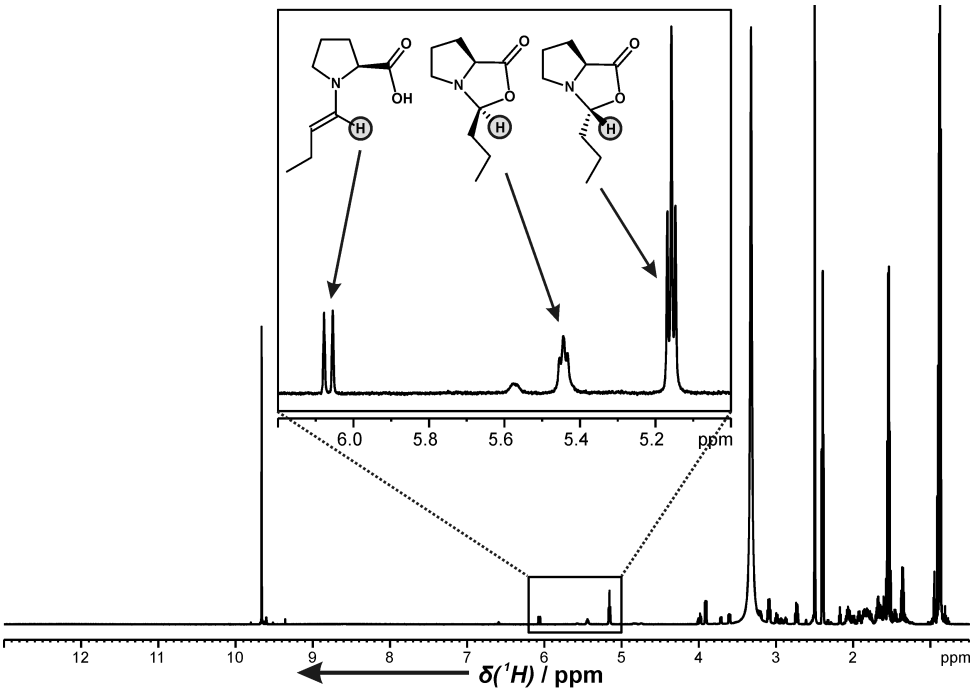

Figure 3.17: 1D ^{1}H spectrum of the reaction mixture of butyraldehyde/100 mol% L-Pro after 7 minutes. The characteristic resonances of oxazolidinone and enamine intermediates are shown in the expansion.

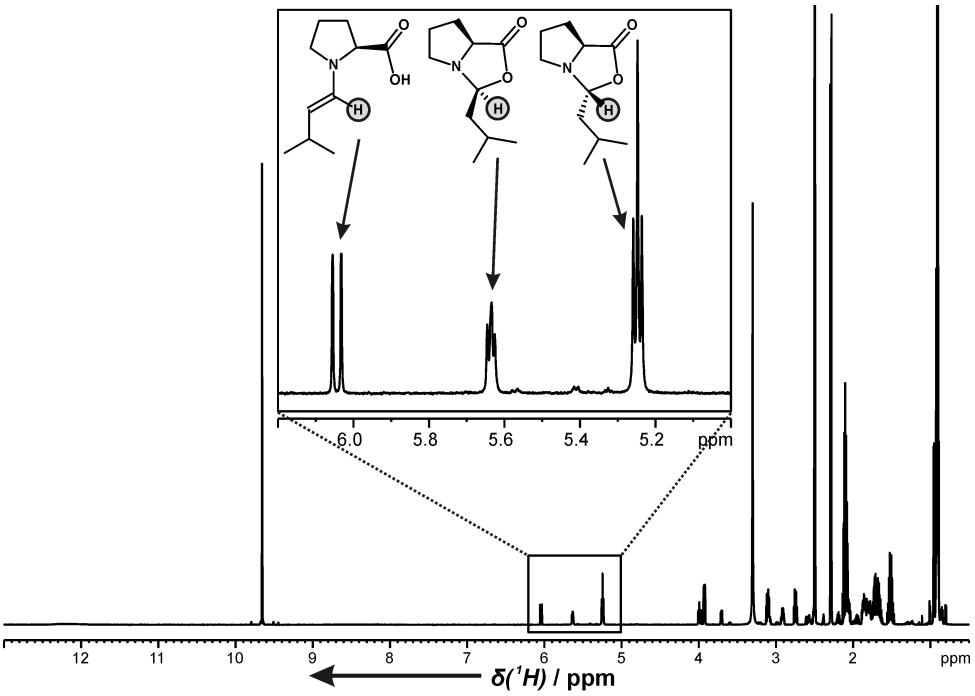

Figure 3.18: 1D ^{1}H spectrum of the reaction mixture of 3-methyl-butyraldehyde/100 mol% L-Pro after 10 minutes. The characteristic resonances of oxazolidinone and enamine intermediates are shown in the expansion.

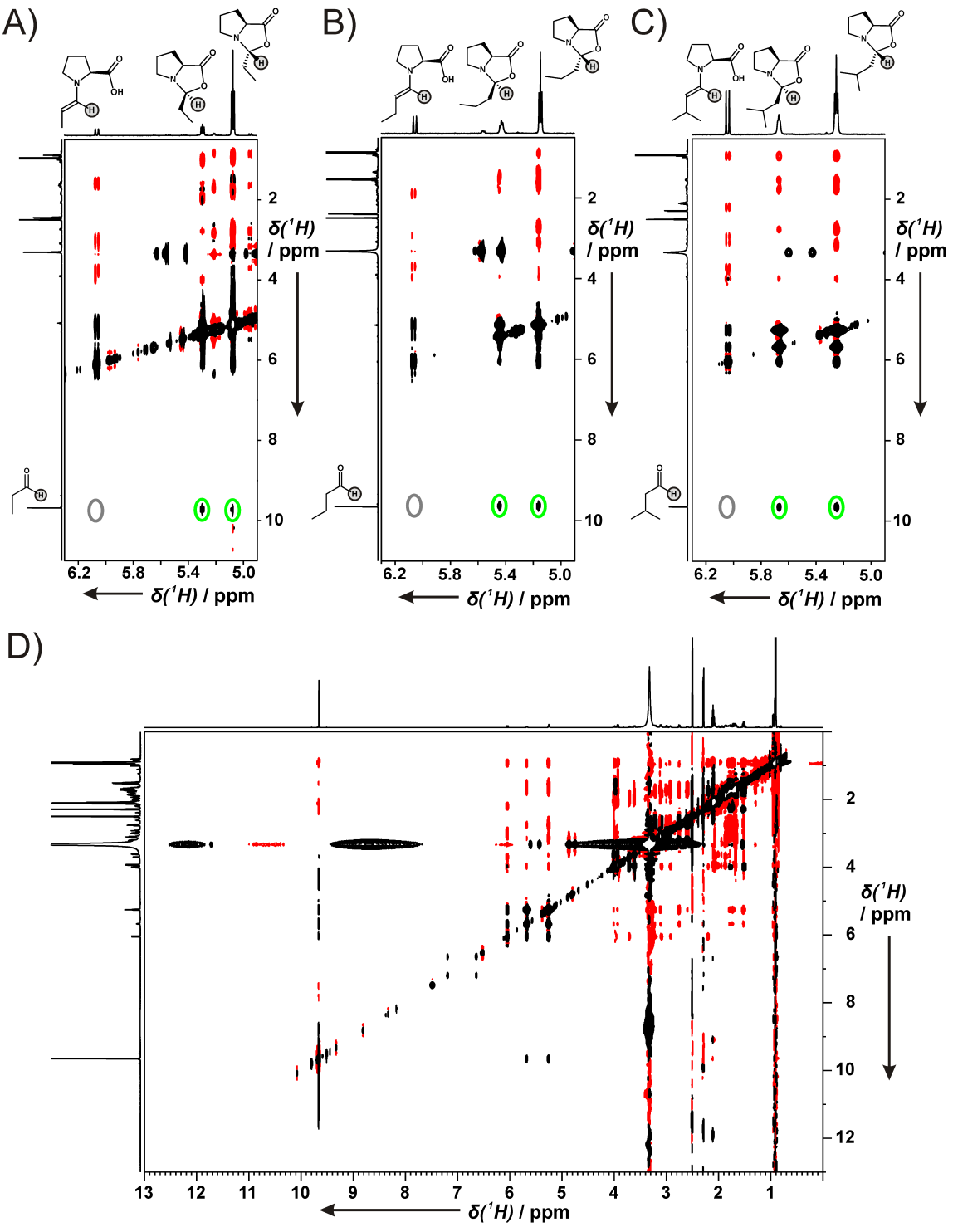

Figure 3.19: Relevant sections of ^{1}H,^{1}H-NOESY/EXSY spectra of the reaction mixtures of A) propionaldehyde/L-Pro, B) butyraldehyde/L-Pro and C) 3-methyl-butyraldehyde/L-Pro in DMSO as well as exemplarily the full spectrum of C). Positive (exchange) peaks are shown in black, negative NOEs are shown in red. In A), B), and C), relevant exchange peaks between aldehydes and oxazolidinones are highlighted by green circles, missing exchange between enamines and aldehydes is marked with grey circles.

3.4 Additional Experimental Findings

3.4.1 Transient Proline Enamine Stabilization by Deuteration

Introduction

For the rationalization of the solvent dependence of the amounts of proline enamine, we proposed H-bonding interactions between the carboxylic proton of the enamine and DMSO/DMF molecules as strong hydrogen-bond acceptors and we could support this suggestion experimentally with the help of DOSY data (chapter 3.2). If the stabilization of proline enamines is in fact related to favorable interactions of the carboxylic protons, one may expect that measures to stabilize the carboxylic proton should also increase the amount of proline enamines in their equilibria with the oxazolidinones. In principle, the exchange of hydrogen by deuterium is a suitable means to overall stabilize carboxylic groups: Though H-bonds will be weaker to deuterium than to hydrogen (Ubbelohde effect),[54] this effect is only small[55,56] and should therefore be overcompensated by the lower zero-point vibrational energy of the O-D bond compared to the O-H bond. In addition, deuteration of the enamine carboxylic group may stabilize the enamine kinetically if the rate determining step of the ring closure to the oxazolidinones is associated with O-D bond cleavages either of COO-D or DO-D (primary isotope effect). One can thus expect a significant impact of the deuteration of the carboxylic acid group on the enamine amount in its equilibrium with the oxazolidinones. If this H/D isotope effect is of thermodynamic nature, it does not only prove the protonation of the detected proline enamine (which is important against the background of the recent work of the Mayr group),[57] but also highlight the importance of the carboxylic group for the stabilization of proline enamines. If it is of kinetic nature, it evidences that O-D bond cleavages are involved in the rate limiting step of the enamine-oxazolidinone interconversion and hence allows for mechanistic conclusions.

Results and Discussion

To check these hypotheses, 3-methyl-butyraldehyde **I-^{i}Pr** was mixed with 100 mol% of L-proline in DMSO-d_6 containing different amounts of D_2O (up to 2 vol%, which was found to be the limit of reliable oxazolidinone integration, chapter 3.3). This aldehyde/catalyst/solvent combination had provided not only the highest enamine ratio (chapter 3.2),[58] but also a constant enamine concentration over one day. The solvent additive D_2O virtually immediately exchanges all the NH and COOH protons against deuterium while, in contrast, the deuteration of the α-position of all **I-^{i}Pr**-derived species proceeds substantially more slowly (see also chapter 5.2). Hence, shortly after preparing the reaction mixture, the species distribution in solution should be dominated by α-protonated, but carboxylically deuterated compounds, in particular the enamine h-**V-^{i}Pr**, bearing a COOD-group, and the isomeric oxazolidinones h,h-**IV-^{i}Pr** (left side of Figure 3.20). From these early stages of the reaction, the approximate equilibrium ratio of the COOD-enamine can be extracted and can be compared to the previously reported ratio of the

COOH-enamine (chapter 3.2) in order to explore potential isotope effects. Since the latter had been shown to be independent of the amount of added H_2O, changes in the enamine ratio upon addition of D_2O to DMSO cannot be explained by general changes in the solvent properties or microsolvation, but must be really ascribed to explicit isotope effects.

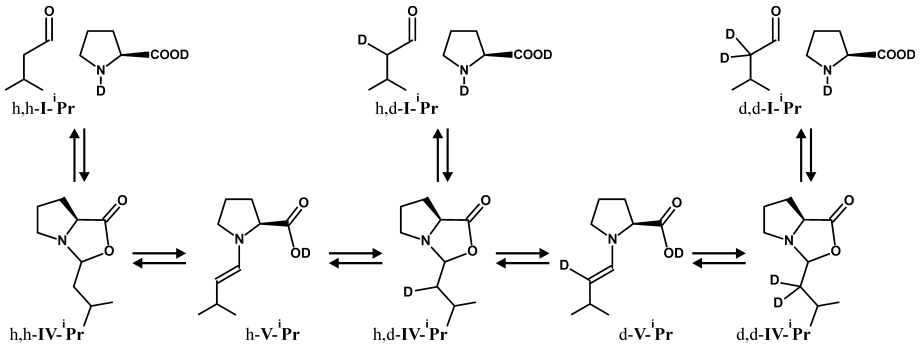

Figure 3.20: Aldehyde-oxazolidinone-enamine equilibria leading to the eventual α-deuteration.

For the reaction mixtures in DMSO with increasing amounts of D_2O, two significant trends are observed. First, the overall concentration of the intermediates **IV-^{i}Pr** and **V-^{i}Pr**, derived from proline and 3-methyl-butyraldehyde **I-^{i}Pr**, decreases with increasing amounts of D_2O present (Figure 3.21A). This finding parallels the effect of the addition of H_2O to the solvent (chapter 3.3)[58] and is rationalized by the shift of the equilibrium position from the intermediates and water towards the starting material according to Le Chatelier´s principle. Second and more interestingly, an isotope effect on the enamine concentration is observed experimentally: With increasing amounts of added D_2O (up to 2 vol%), the initially observed enamine ratio in the equilibrium with the oxazolidinones (after about 9 minutes, each) rises from 19 % without D_2O to almost 50 % in the presence of 2 vol% D_2O (Figure 3.21B). As outlined above, we can take the increased enamine ratio as an indication of the relative stabilization of the enamine h-**V-^{i}Pr** with respect to the oxazolidinones h,h-**IV-^{i}Pr** by the replacement of the carboxylic proton by a deuteron in the beginning of the reaction. This may be either due to a thermodynamic or a kinetic isotope effect. On this basis, the increase of the enamine ratio with higher amounts of D_2O may be explained by a gradual shift of the balance between COOH and COOD and between H_2O, HDO, and D_2O in favor of the deuterated species.

However, the stabilization of the enamine is not permanent, but only a temporary effect (Figure 3.22A). In the case of 1 vol% of D_2O, the initial excess of the enamine ratio vanishes within about 1.5 hours and a constant equilibrium value of about 18 % is reached which is, within the experimental error, identical to the value for the D_2O-free case (19 %, chapter 3.2).[58] As can be deduced from the isotope-induced chemical shift changes (Figure 3.22B, *cf.* chapter 5), the unusually high initial enamine concentration is mainly due to the presence of h-**V-^{i}Pr** in the early stages of the reaction (Figure 3.22). However, with increasing reaction times, the α-deuteration of the enamine **V-^{i}Pr**, of the oxazolidinones **IV-^{i}Pr** and also of 3-methyl-butyraldehyde **I-^{i}Pr** takes place and accordingly, the equilib-

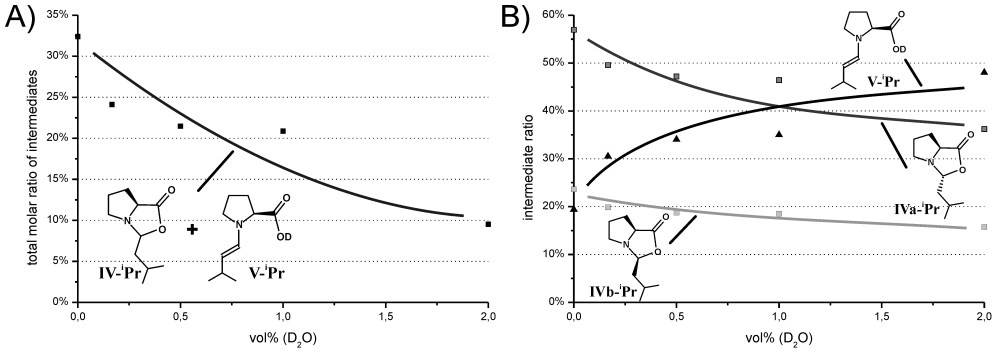

Figure 3.21: Impact of the addition of D_2O to the reaction mixture of **I-^{i}Pr** and 100 mol% L-proline in DMSO-d_6: A) decrease of the overall intermediate concentration and B) increase of the initial enamine ratio in the equilibrium with the oxazolidinones, measured after about 9 minutes (Lines are just meant as a guide to the eye.).

ria displayed in Figure 3.20 are eventually shifted to the right side. After about 1.5 hours, the α-deuteration process has reached its equilibrium state, as is evidenced by the evaluation of the isotopologue amounts of **I-^{i}Pr** (data not shown). The time-correspondence of the reduction of the enamine excess with the progress of the α-deuteration also suggests two rationalizations for the decay of the enamine concentration to a constant value: From the thermodynamic point of view, in the early reaction mixture, the virtually immediate deuteration of the enamine carboxylic group is the main source of isotopic stabilization and hence shifts the equilibrium between the enamine **V-^{i}Pr** and the oxazolidinones **IV-^{i}Pr** towards the enamine. In contrast, when the significantly slower α-deuteration process is finished after 1.5 hours, the isotopic stabilization of the enamine d-**V-^{i}Pr** by one C-D bond and one O-D bond may be balanced by the isotopic stabilization in the oxazolidinones d,d-**IV-^{i}Pr** by two C-D bonds. Thus, the equilibrium position between d-**V-^{i}Pr** and d,d-**IV-^{i}Pr** can be expected to be close to the one observed for the deuterium-free case. From the kinetic point of view, one may argue that the enamine h-**V-^{i}Pr**, once formed from h,h-**IV-^{i}Pr**, is trapped kinetically:[b] While in its formation, only one DO-D bond must be broken for the deuteration of the carboxylic group, one DO-D bond and one COO-D bond must be cleaved for the formation of h,d-**IV-^{i}Pr**, which reduces the rate of the oxazolidinone formation (primary kinetic isotope effect). On the other hand, the back-reaction to h,h-**IV-^{i}Pr**, including only one COO-D bond dissociation, is disfavored statistically owing to the overabundance of D_2O against H_2O. The lack of readily viable cyclization pathways may hence explain the temporary excess of the enamine until the establishment of the thermodynamic equilibrium of all interconverting species.

These interpretations are backed by the investigation of a reaction mixture of isobutyraldehyde (c = 50 mM) and 100 mol% L-proline in DMSO-d_6 with 0.5 vol% of D_2O (data not shown). In the case of isobutyraldehyde, the exchange between the enamine and the oxazolidinone is drastically decelerated (see chapter 4.1). This results in a delayed buildup of the enamine concentration on the one hand (maximum enamine equilibrium

[b] The involvement of one water molecule in the oxazolidinone-enamine exchange is assumed here (see chapter 4).

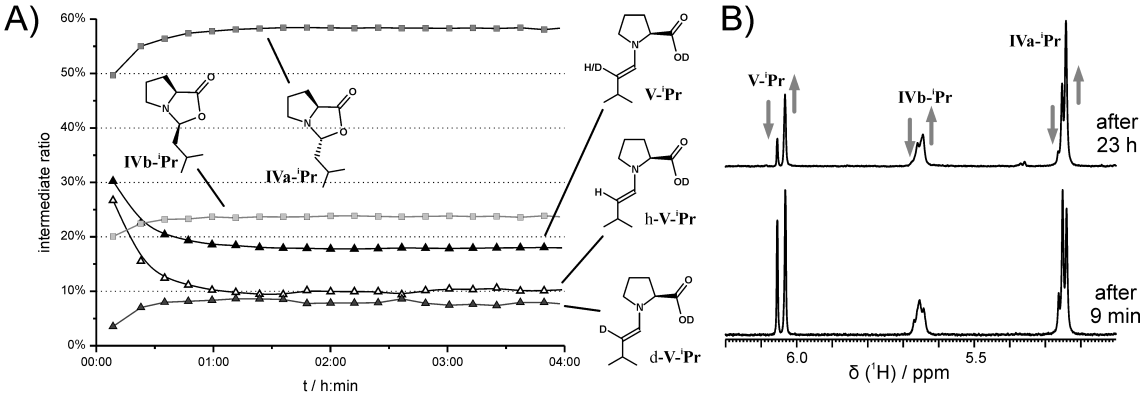

Figure 3.22: A) Time-dependence of the equilibrium ratios of enamines and oxazolidinones in the presence of 1 vol% of D_2O in DMSO-d_6; B) sections of exemplary 1D ^1H spectra of **IVa-^{i}Pr**, **IVb-^{i}Pr**, and **V-^{i}Pr**, revealing isotope-induced shifts of the relative amounts and of the signal shapes (gray arrows) of the intermediates. (Isotopologue distributions have not been determined for the oxazolidinones.).

ratio after 2.5 hours) and in a slow deuteration of the oxazolidinones on the other hand (*exo*-oxazolidinone deuteration of 12 % after 12 hours, *cf.* over 50 % after 0.5 hours in the case of propionaldehyde). Therefore, the time slot for studying the temporary enamine stabilization is substantially widened for isobutyraldehyde: First, the thermodynamic and/or kinetic O-D stabilization of the enamine is expected to prevail and then, the slow oxazolidinone deuteration should lead to a steady reduction of the enamine ratio. These expectations are fully met by the experimental observations: The concentration-time-curve of the isobutyraldehyde-derived proline enamine is characterized by an increase over about 2.5 hours (see Figure 4.10A, chapter 4.1), followed by a slow, but steady decline till the end of the observation period after 15 hours. The maximum enamine ratio in the equilibrium with the oxazolidinones after 2.5 hours asymptotically reaches 4.8 % while the deuteration of the *exo*-oxazolidinone is below 2.5 % at that point in time. Along with the eventual deuteration of the oxazolidinones to 15 % after 15 hours (determined for the *exo* isomer), however, the enamine ratio drops to 3.7 %. Compared to the enamine ratio of 1.0 % in the deuterium-free case (chapter 3.2),[58] this overall constitutes a substantial stabilization of the isobutyraldehyde-derived enamine by the O-D bond.

Conclusion

In summary, we have presented the results of a deuteration study on the reaction mixture of 3-methyl-butyraldehyde with 100 mol% of L-proline in DMSO-d_6 with up to 2 vol% of D_2O. We could thereby reveal that the exchange of the enamine carboxylic proton against a deuteron causes a significant temporary stabilization of the proline enamine in solution. However, further consideration and experimentation will be necessary to identify thermodynamic and kinetic contributions to this phenomenon and to draw conclusions on structural and mechanistic issues of the proline enamine formation and stabilization. In any case, our findings again highlight the importance of the carboxylic proton for the overall stabilization and detectability of proline enamines in solution.

3.4.2 Stabilization of Proline Enamine Carboxylates by Amine Bases

Introduction

A rather different approach for the stabilization of proline enamines is their deprotonation to the enaminocarboxylates. This principle was outlined by Seebach, Eschenmoser, and coworkers who created enaminocarboxylates by the addition of DBU (1,8-diazabicyclo[5.4.0]-undec-7-en) to the corresponding oxazolidinones in tetrahydrofurane (THF).[33] The idea was recently exploited by Mayr and coworkers in acetonitrile and THF for the kinetic proof of the neighboring group participation in proline enaminocarboxylate catalysis[57] and by Blackmond, Armstrong, and coworkers for the reversal of enantioselectivity in the proline-catalyzed α-amination of aldehydes in dichloromethane.[59] At first glance, the stabilization of proline enamines by deprotonation seems to conflict with the above-mentioned rationalization of proline enamine stabilization by the stabilization of the carboxylic proton. But as postulated for the explanation of the reverse enantioselectivity of proline/DBU in contrast to proline,[59] this seeming contradiction may be solved by the assumption of ion pairs between the enaminocarboxylate and the protonated base and the accompanied stabilization of the former carboxylic proton in a salt bridge. However, only a few investigations on the impact of tertiary amine additives upon proline enamine catalysis have been reported so far[45,59,60] and no systematic studies on the potential of amine bases to stabilize proline enaminocarboxylates are available as yet.

Results and Discussion

Model Systems. To fill this gap, we performed NMR spectroscopic studies on the influence of basic amine additives on the amount of proline enamines derived from 3-methylbutyraldehyde **I-^{i}Pr**. For that purpose, reaction mixtures of **I-^{i}Pr** (c = 50 mM) with 100 mol% of L-proline and one equivalent of different additives (Figure 3.23) were prepared in DMSO at 300 K and the impact of the additives on the enamine amounts and its NMR properties were studied. As tertiary amine additives of different basicities (see Figure 3.23), *N*-methyl-morpholine (NMM),[61] 4-dimethylaminopyridine (DMAP),[62] 1,4-diazabicyclo[2.2.2]octan (DABCO),[63] triethylamine (TEA),[62] and 1,8-diazabicyclo[5.4.0]-undec-7-en (DBU)[62] were selected. In addition, the secondary amine piperidine (PIP)[61] and the hardly basic sodium azide (NaN_3)[64] were employed. Moreover, the influence of urea derivatives was investigated on the examples of *N*,*N*´-diphenylurea (DPU) and 1-(2-(dimethylamino)ethyl)-3-phenylurea (DMAEPU, synthesized following a literature procedure[65] in a yield of 64 %).

Enamine Deprotonation. First, NMR spectroscopic evidence for the deprotonation of proline enamines by amine bases under our experimental conditions in DMSO was to be collected. Seebach, Eschenmoser, and coworkers had already proven the deprotonation of proline enamines by DBU in tetrahydrofurane via ^{13}C NMR and they could even isolate a salt of a proline enamine with Heinzer´s amine base from acetonitrile.[33] In principle,

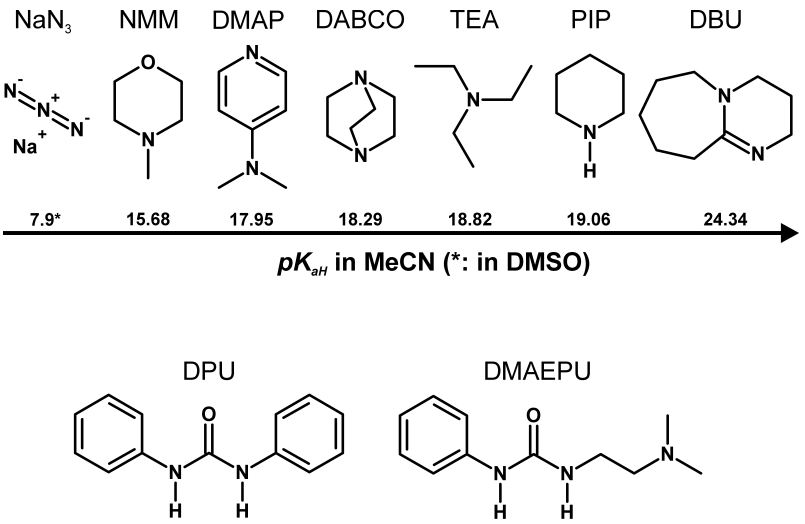

Figure 3.23: Amine and urea derivatives employed as additives to the proline enamine derived from 3-methyl-butyraldehyde **I-^{i}Pr**.

the carboxylic group COOH and the carboxylate group COO^- should differ significantly in their electronic properties and hence in their group electronegativities. Therefore, the reduced electron-withdrawing ability of the carboxylate group compared to the carboxylic group is expected to manifest itself in a lower deshielding of all atomic groups neighbouring the α-carbon atom (see Figure 3.25B for atom nomenclature). Namely, an NMR spectroscopic upfield shift of the α-proton resonance should be observed upon the deprotonation of the carboxylic group. Likewise, the nitrogen atom should gain in electron density which might, owing to the electronic conjugation of the enamine moiety, lead to an upfield shift also of the proton H2 of the aldehyde residue. To check if these effects could be verified experimentally, the proton chemical shifts of Hα and H2 of the enamine were evaluated for all the different proline/additive combinations and were related to the basicity of the amine additive (Figure 3.24A).

In fact, compared to the additive-free case, upfield shifts of the resonances of Hα and H2 of the proline enamine are observed for all amine additives whereas, for instance, the NMR resonance of H1 remains virtually unaffected by the basic additives. The upfield shifts of Hα and H2 increase with increasing basicity of the amine additive and reach $\Delta\delta$ values of 0.40 ppm and 0.17 ppm, respectively, when the strongest base of the series, DBU, is applied. The dependence of the chemical shifts of both Hα and H2 on the additive basicity can be described well by a sigmoidal correlation (Figure 3.24A) with an inflection point at pK_{aH} values between 18.5 and 19.0. Hence, these observations indicate that basic amine additives in fact cause the partial or complete deprotonation of proline enamines in DMSO. This interpretation is further backed by the experimental results for the addition of the urea derivatives DPU and DMAEPU: While the addition of DPU to the enamine does not alter the chemical shifts of Hα or H2, DMAEPU bearing a basic tertiary amine group causes a slight upfield shift of Hα (0.04 ppm) and of H2 (0.01 ppm).

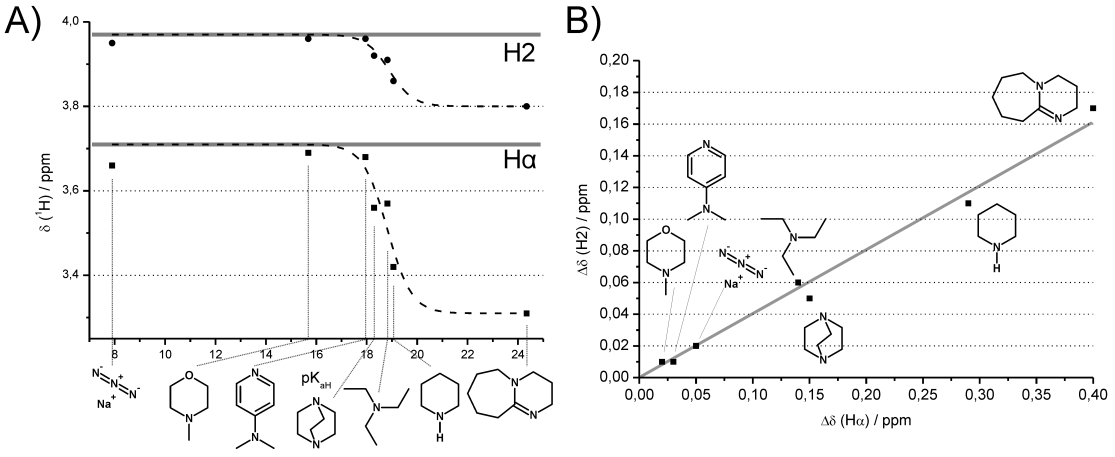

Figure 3.24: A) Sigmoidal dependence of the chemical shifts of the enamine resonances Hα (squares) and H2 (circles) on the basicity of amine additives (gray lines: additive-free reference values; dashed lines: sigmoidal fits); B) correlation between the upfield shifts of Hα (abscissa) and H2 (ordinate) for different amine additives.

It is furthermore most worthwhile to highlight the good correlation between the upfield shifts of Hα and H2 upon the enamine deprotonation (Figure 3.24B). This clearly shows that the impact of the deprotonation of the carboxylic group, *i.e.* the change of its group electronegativity, extends even onto the enamine moiety. Namely, the upfield shift of H2 is indicative of a higher electron density of the enamine moiety in the enaminocarboxylate than in the enamine carboxylic acid. To our knowledge, this is the first experimental evidence that the electron density of proline-derived enamines and hence their nucleophilic reactivity can be tuned by deprotonation (beyond the anchimeric assistance[57] of the carboxylate), *i.e.* by substituents of varying electronegativities in the α-position of the pyrrolidine ring. For instance, this may help to rationalize—on the basis of electronic arguments and beyond steric factors only—the different performances of diarylprolinol (ether) organocatalysts with different aryl substitution patterns (see also the discussion on diarylprolinol catalysts in chapter 6.2). In addition, further inspirations for the fine-tuning of organocatalysts with tailored properties can be expected from this experimental observation.

Enamine Stabilization. Next, the influence of the additives on the overall intermediate concentration (of the oxazolidinones **IV-^{i}Pr** and the enamine **V-^{i}Pr**) as well as on the ratio of the enamine in the equilibrium with the oxazolidinones was investigated in order to correlate these effects with the deprotonation trends. In general, these ratios can be described by the equilibria between the starting material and the oxazolidinones and between the oxazolidinones and the enamine (Figure 3.25A). The stabilizing role of basic additives is meant to be the deprotonation of the enamine, shown in Figure 3.25B, and hence the shift of the equilibria towards the enaminocarboxylate ion pair. Thus, in a very simplistic consideration, the enamine stabilization by basic additives may be described as

an acid-base reaction. Accordingly, again a sigmoidal dependence of the enamine ratio on the basicity of the additive can be expected. On the other hand, no clear-cut correlation between the overall intermediate concentration and the basicity of the additive can be predicted since there may be manifold interactions of the base not only with the intermediates but also with the starting material and the catalyst.

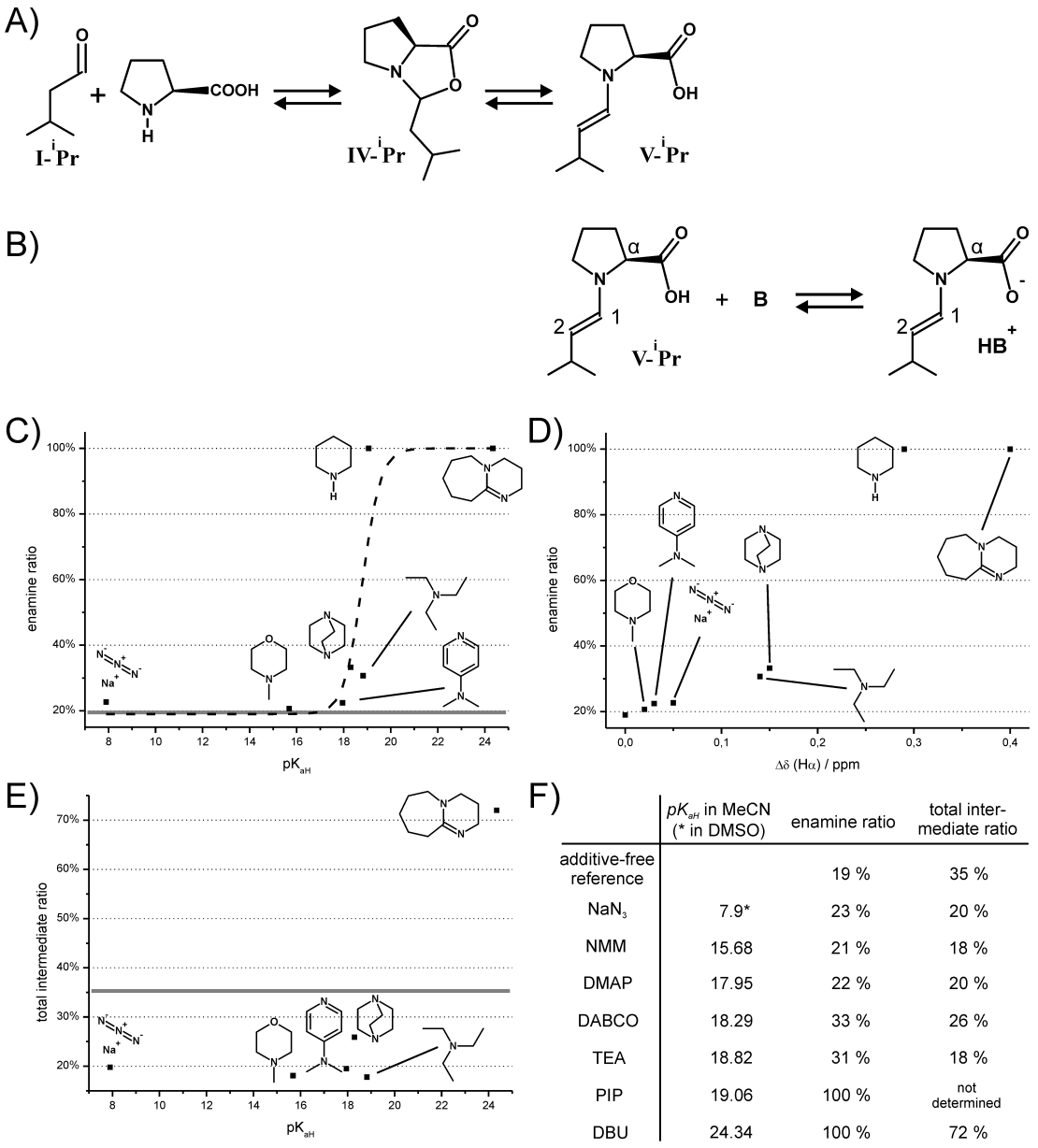

F)

	pK_{aH} in MeCN (* in DMSO)	enamine ratio	total intermediate ratio
additive-free reference		19 %	35 %
NaN_3	7.9*	23 %	20 %
NMM	15.68	21 %	18 %
DMAP	17.95	22 %	20 %
DABCO	18.29	33 %	26 %
TEA	18.82	31 %	18 %
PIP	19.06	100 %	not determined
DBU	24.34	100 %	72 %

Figure 3.25: A) Equilibrium between starting material and intermediates; B) base-induced deprotonation of the enamine; C) sigmoidal dependence of the enamine ratio on the additive basicity (gray line: additive-free reference value; dashed line: sigmoidal fit); D) correlation plot between the enamine ratio and the upfield shift of Hα; E) correlation plot between the total intermediate concentration and the additive basicity (gray line: additive-free reference value): F) basicities of the amine additives, total intermediate ratio and enamine ratio thereof.

For the additive-free reference sample, an initial total intermediate concentration of 35 % (related to all **I-^{i}Pr**-derived species in the first spectrum) and an enamine ratio of 19 % were found in this study, which is in good agreement with the previously reported data (chapter 3.2, Figure 3.25F).[58] The weaker bases of the series NaN_3, NMM, and DMAP do not significantly stabilize the enamine species (ratios up to 23 % only) while stronger bases like DABCO and TEA lead to an increase of the enamine ratio to 30-35 %. The strongest bases investigated, PIP and DBU lead to the exclusive detection of the enamine and totally suppress the observation of the oxazolidinones.[c] Overall and as outlined above, a sigmoidal relationship between the enamine ratio and the basicity of the additive may be indeed assumed on the basis of this data (Figure 3.25C). Interestingly, just like for the sigmoidal δ-pK_{aH}-curves (Figure 3.24A), the inflection point of this sigmoidal enamine ratio-pK_{aH}-curve is again found at pK_{aH} values between 18.5 and 19.0. Moreover, the enamine ratio and the upfield shift of the enamine proton Hα (likewise H2) qualitatively correlate reasonably well: the larger the upfield shift of Hα, the larger the enamine ratio (Figure 3.25D). Together, these correlations between the deprotonation of the enamine and the increase of the enamine ratio strongly suggest an underlying causal relationship in terms of an enamine stabilization by deprotonation to the enaminocarboxylate.

In contrast, the effect of the additives on the total intermediate concentration is by far not uniform. While the weak bases from NaN_3 up to TEA cause a decrease of the overall intermediate amount (18-26 % compared to 35 % in the additive-free case), the strong base DBU leads to a drastic increase in the intermediate ratio (72 %, Figure 3.25E). For DBU the high intermediate concentration has to be fully ascribed to the enaminocarboxylate (see again Figure 3.25C). Thus, one may argue that the stabilization of the enaminocarboxylate is so profound that even the equilibria of Figure 3.25A are strongly shifted to the right by the deprotonation of the enamine species. On the other hand, we can only speculate about the origin of the decrease of the total intermediate concentration by the addition of weaker bases than DBU. One may, for instance, consider salt formation between the catalyst proline and amine bases as a source of effective catalyst deactivation.

As a further class of additives, the urea derivatives DPU and DMAEPU (Figure 3.23) were employed and their impact on the overall intermediate concentration and on the enamine ratio was studied. While DPU is predestined only for hydrogen-bonding interactions with the intermediate species, DMAEPU combines the H-bonding ability of urea derivatives with the basicity of tertiary amines and should therefore allow to study potential cooperative effects of these two structural motifs. The enamine ratio in the case of DPU as the additive is found to be 18 % which is in the same range as in the additive-free case (19-20 %). Likewise in the case of DMAEPU, the enamine ratio was 19 %. In contrast, concerning the overall intermediate amounts, the performances of DPU and DMAEPU are

[c] Note: In the case of PIP addition, the enamine formation between 3-methyl-butyraldehyde and PIP is by far predominant and the proline enamine accounts for only 3% of the PIP enamine. It can hence not be excluded that proline oxazolidinones are actually present, but cannot be detected because of spectral overlap or severe line broadening. In addition, the determination of the total proline-intermediate ratio was not feasible because of the competition of proline and PIP for the aldehyde.

different: While DPU yields intermediate amounts of 34 % (*cf.* 35 % without additives), DMAEPU leads to a reduction of the total intermediate concentration to 19 %. The results for DPU show that pure H-bond donor additives influence neither the position of the equilibrium between the starting material and the intermediates (Figure 3.25A) nor the degree of protonation of the proline enamine (Figure 3.25B). In addition, the lack of enamine stabilization in the case of DMAEPU indicates on the basis of the above-mentioned amine additive studies that the basicity of its tertiary amine moiety is insufficient to deprotonate the enamine carboxylic group. On the other hand, by comparison with DPU, it becomes evident that the basic properties of DMAEPU must account for the observed reduction of the total intermediate concentration. This parallels the above-mentioned reduced intermediate amounts upon addition of amine bases.

Altogether, the ratio of proline enamines in their equilibrium with the oxazolidinones is evidenced to increase with increasing basicities of amine additives which can be interpreted as an indication that the deprotonation of proline enamines in DMSO leads to their stabilization. In contrast, pure H-bond donor additives, such as urea derivatives do not bear the potential to stabilize proline enamines in DMSO. The overall concentration of proline-aldehyde adducts is furthermore shown to be reduced by weak to moderate amine bases while it is drastically increased by strong amine bases such as DBU.

Ion Pair Formation. Since the deprotonation of proline enamines is now evidenced experimentally as a source of enamine stabilization, we wondered whether we could also prove the formation of ion pairs between the enaminocarboxylate and the protonated amine bases in solution. As the ion pair formation would imply the involvement of the former carboxylic proton in a salt bridge, this would reconcile the seemingly conflicting postulations of enamine stabilization either by stabilizing the carboxylic proton (*e.g.* by H-bond acceptor solvents or by deuteration, see above) or by deprotonation. In principle, the formation of ion pairs in solution can be evidenced by NMR with the help of DOSY or NOESY experiments. In the DOSY approach, the slower diffusion of the enaminocarboxylate compared to the enamine carboxylic acid would indicate ion pair formation. However, as surprisingly small diffusion coefficients are observed for enamine carboxylic acids (which was attributed to the formation of a stabilizing solvent shell, chapter 3.2),[58] changes of the diffusion coefficient upon deprotonation may be tiny and are certainly hard to interpret reliably. Therefore, in this experimental system, the detection of intermolecular NOEs between the counterions was considered the best method for the proof of ion pair formation. Since for this NOESY approach, sufficiently high enamine concentrations are indispensable, the combination of 3-methyl-butyraldehyde **I-^{i}Pr** and DBU (c = 50 mM in DMSO, each) was chosen as the model system for the NOESY analysis (mixing time 700 ms) because it provides the highest amounts of enaminocarboxylates (see above).

In this experimental setup, indeed a network of weak intermolecular NOEs between the enaminocarboxylate and protonated DBU is observed (Figure 3.26B). This strongly suggests the formation of ion pairs in DMSO and one may expect that the ion pair forma-

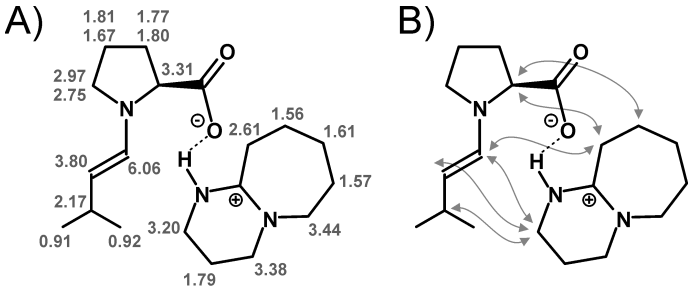

Figure 3.26: A) ^{1}H resonance assignment of the enaminocarboxylate/DBUH$^+$ ion pair in DMSO-d$_6$ at 300 K; B) the network of weak intermolecular NOEs between the enaminocarboxylate and protonated DBU in DMSO-d$_6$.

tion is even stronger in less polar solvents than DMSO. Thus, the enamine stabilization by strong amine bases in solution is achieved by deprotonation of the enamine and ion pair formation with the protonated amine base so that the former carboxylic proton is stabilized in a salt bridge. This ion pair formation is accompanied by a loss of the bifunctionality of the proline enamines since the activating and directing function of the carboxylic group is not maintained. In contrast, the association of the counterion may have an effect similar to the *O*-protecting group in diarylprolinol ether organocatalysts.[59] Accordingly, our study experimentally supports the previously suggested rationalization for the reversal of enantioselectivity in the proline-catalyzed aldehyde α-amination upon addition of basic amine additives.[59]

Stabilizing Underprivileged Enamines with DBU. The outstanding property of DBU to stabilize enamines in DMSO in the form of ion pairs inspired us to also test its ability to throw open the door to enamine species inaccessible as yet. So far the detection of proline enamines has failed completely in solvents such as MeOH or MeCN, but has been accomplished only in DMSO and DMF, *i.e.* in dipolar aprotic solvents with strong H-bond acceptor abilities (chapter 3.2).[58] While reasonable enamine amounts were thereby observed for α-unbranched aldehydes in DMSO, only tiny enamine quantities were detected for isobutyraldehyde and no ketone-derived proline enamines have been found *in situ* at all. To explore the scope of enamine stabilization by DBU, we first investigated the established 3-methyl-butyraldehyde/proline/DBU combination in other solvents than DMSO, namely in MeCN, $CDCl_3$, and PhMe. Next, we studied different carbonyl substitution patterns in DMSO on the examples of isobutyraldehyde and acetone.

In the solvent variation study, it is observed that the solvent properties are less critical for the detection of proline enaminocarboxylates of DBU than for enamine carboxylic acids. In all solvents investigated (DMSO-d$_6$, MeCN-d$_3$, $CDCl_3$, PhMe-d$_8$), the enaminocarboxylate is the only intermediate species detected and no oxazolidinones are observed at all. The overall enamine concentration (with respect to all aldehyde-derived species in the first spectrum), however, decreases from DMSO (72 %) over MeCN (68 %) to $CDCl_3$ (20 %). For PhMe, the initial enamine ratio after 10 minutes is below 4 %, but increases steadily

and reaches 13 % after 16 hours (presumably still rising at that point in time). This solvent study hence shows that the relative stabilization of the enamine within the ion pair with DBU, compared to the oxazolidinones, does not depend on H-bond acceptor properties of the solvent as was the case for enamine carboxylic acids. The decrease of the overall enamine amount from DMSO over MeCN and $CDCl_3$ to PhMe can be explained by the decreasing polarities of these solvents: The most polar DMSO ($\epsilon = 46.5$)[47] is most prone to the solvatization of ionic species and this ability decreases with decreasing solvent polarities (MeCN: 35.9, $CDCl_3$: 4.8, PhMe: 2.4).[47] In the case of PhMe, the slow buildup of the enamine amount over time might be accounted for by the slow solubilization of the catalyst proline, but this certainly necessitates further experimental confirmation.

However, their DBU-induced stabilization makes aldehyde-derived proline enamines now accessible to conformational studies in a variety of solvents. In addition, the high enamine amounts observed with the help of DBU allow for the characterization of less populated proline enamine configurations in solution. In particular, *Z*-configured proline enamines were detected for the first time (though their unambiguous identification has not been accomplished yet): Characteristically broadened doublets (presumably quartets of doublets) with coupling constants of 9.8 Hz each are observed at 5.57 ppm in DMSO-d_6 and at 5.65 ppm in MeCN-d_3, indicating H1 as the underlying proton.[66] In addition, the NOESY spectrum in DMSO reveals the spatial proximity of this H1 to a proton resonating at 3.44 ppm, presumably Hα of the pyrrolidine ring. The ratio of these putative *Z*-enamines of the total enamine amounts are 0.4 % in DMSO and 0.3 % in MeCN, which is in good agreement with the ratios observed for the putative *Z*-enamine of 3-methylbutyraldehyde and diphenylprolinol methyl ether (0.4 % in DMSO, chapter 6.2).

Next, we explored the potential of DBU to stabilize proline enamines derived from carbonyl species with different substitution patterns. For isobutyraldehyde, which had shown a ratio of only 1 % in its equilibrium with the oxazolidinones in DMSO without additives, now a ratio of more than 80 % is found (A more precise value cannot be given because the oxazolidinone quantification is hampered by resonance overlap.). The fact that for isobutyraldehyde the oxazolidinone is detected, too, and the enaminocarboxylate is not the only intermediate species formed, again suggests that the relative stabilization of the enamine with respect to the oxazolidinone is less pronounced for α-branched aldehydes because of the unfavorable allylic strain. On the other hand, for acetone as a typically employed ketone in organocatalytic reactions, the detection of the proline enamine was not feasible even after the addition of DBU. However, in contrast to the DBU-free case, the oxazolidinone was not observed either. This may be interpreted either in terms of a general reduction of the adduct formation tendency of proline and ketones by DBU or in terms of a conversion of the oxazolidinone into the enaminocarboxylate whose detection cannot be accomplished because of spectral overlap. Further investigations will be necessary to address this issue.

Conclusion

In summary, we could show that basic amine additives can deprotonate proline enamines in solution and, on the example of DBU in DMSO, the formation of ion pairs in solution is evidenced experimentally by NOESY analyses. This ion pair formation is also strongly suggested to be the origin of the relative stabilization of the enamine with respect to both the starting material and the oxazolidinones, which leads to the drastic increase of the enamine amounts observed. The enamine amounts are shown to depend on the polarity of the solvent, but significant quantities are also observed for solvents of moderate polarity ($CDCl_3$ and PhMe) as well as for structurally less privileged α-branched aldehydes. Owing to the high enamine amounts in DMSO and MeCN, the first proline-derived *Z*-enamines are detected in solution. The finding of ion pairs in solution supports the recently raised explanation for the reversal of enantioselectivity of proline-catalyzed reactions upon the addition of basic amine additives.[59] Moreover, the observed deprotonation of the carboxylic group of proline enamines is shown to have an impact on the electron density and hence on the nucleophilicity of the enamine moiety. This knowledge should allow for the fine-tuning of organocatalysts, for instance, of diarylprolinol ethers by the variation of the aryl substitution pattern.

3.4.3 *In Situ* Detection of an α-Oxy-Aldehyde-Derived Proline Enamine

α-Oxygenated aldehydes represent a further class of excellent reaction partners in proline-catalyzed aldol reactions; their use is moreover of synthetic value since, for instance, they allow facile access to monosaccharides in two-step syntheses.[67,68] The detection and characterization of α-oxy-aldehyde-derived proline enamines would hence contribute substantially to the understanding both of organocatalytic reaction mechanisms and of the stabilization of enamine intermediates by substitution effects.[69] Therefore, the potential to detect and characterize proline enamines of α-oxy-aldehydes was explored on the example of α-benzyloxy-acetaldehyde **9** (Figure 3.27B). In analogy to the study on aldehyde alkyl substitution effects (chapter 3.2),[58] a reaction mixture of **9** and L-proline (30 μmol) in 0.6 mL DMSO-d_6 at 300 K was investigated by continuously recording proton spectra.

This preliminary study showed that the starting material **9** is consumed very rapidly and that the self-condensation of **9** to **12** proceeded within two hours (Figure 3.27B). From the proton spectra, an oxazolidinone **10**, presumably the *exo* isomer, was found to be the majorily formed product in the beginning of the reaction; in contrast, the *endo* isomer could not be identified. This may be accounted for by the size of the BnO-substituent that causes severe steric conflicts if placed in the *endo*-position of the oxazolidinone. In addition, the existence of the enamine intermediate **11** was suggested by two doublets at 6.13 ppm and 5.66 ppm with a coupling constant of 11.1 Hz (Figure 3.27A). This coupling constant indicates an *E*-configuration of **11** since oxygen-substituents of C=C double bonds are known to reduce $^3J_{H,H}$,[70] (*cf.* the $^3J_{H,H}$ of 13.7 Hz in the case of the propionaldehyde-derived *E*-enamine). Furthermore, the ratio between oxazolidinone and enamine was determined

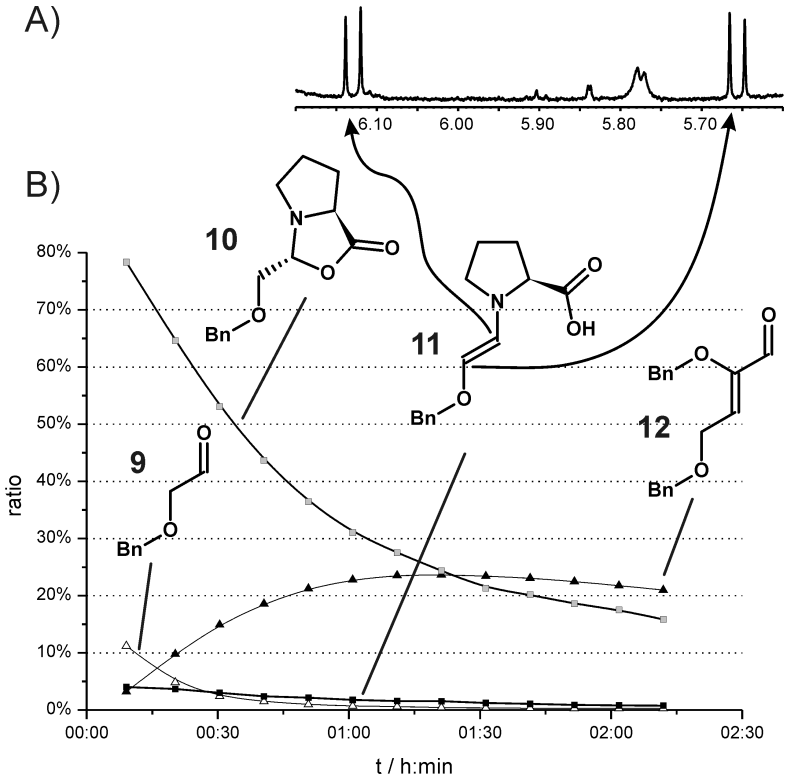

Figure 3.27: A) Section of a 1D ^{1}H spectrum of a reaction mixture of **9** and proline in DMSO-d_6 at 300 K revealing the existence of an enamine intermediate; B) reaction profile of the species identified in the reaction mixture of A.

as 95:5; this reveals that the relative enamine stabilization by one α-oxy substituents is weaker than by one α-alkyl substituent (*cf.* the ratio oxazolidinones:enamine of 91:9 in the case of propionaldehyde). Despite these reduced enamine amounts, the straightforward NMR observation of an α-oxy-aldehyde-derived proline enamine in DMSO over more than two hours is expected to allow for more detailed spectroscopic investigations, for instance, aiming at proving the enamine constitution, at disclosing conformational aspects, and at elucidating the enamine formation pathway. In addition, it should set in motion further studies on enamine stabilization by heteroatom substituent effects.

3.4.4 *In Situ* Detection of an Aldehyde-Derived Tripeptide Enamine

Encouraged by the outstanding properties of DMSO to stabilize aldehyde-derived proline enamines in solution, we next turned our interest towards the detection of enamines formed by proline-based peptidic organocatalysts of the type investigated in chapter 2.2.[71] The so far unaccomplished detection of peptide enamine intermediates in solution would certainly open up new options to conformationally investigate peptide enamines in order to elucidate the origin of stereoinduction by peptidic organocatalysts. By thus establishing structure-selectivity/reactivity-relationships, the directed optimization and design of catalysts should become feasible. For that purpose, a sample of H-(L)-Pro-▼-(L)-Pro-OBn, that had been utilized earlier for the tripeptide studies (chapter 2.2) was reused for enam-

ine studies in analogy to those presented above. Because of the eventual degradation of the tripeptide over the time of storage, the quality of the sample was not optimal any more; but it was judged to be still sufficient to prove the principle of peptide enamine detection and to gain first insights into potential routes for further investigations. The same experimental conditions that had successfully been applied for the detection of proline enamines were used for the tripeptide sample: Freshly distilled propionaldehyde (1 μL, 0.014 mmol) was added to a mixture of H-(L)-Pro-▼-(L)-Pro-OBn (approx. 0.004 mmol) and DMSO-d_6 (0.6 mL) and the ongoing events were monitored by one-dimensional proton spectra at 300 K (Figure 3.28).

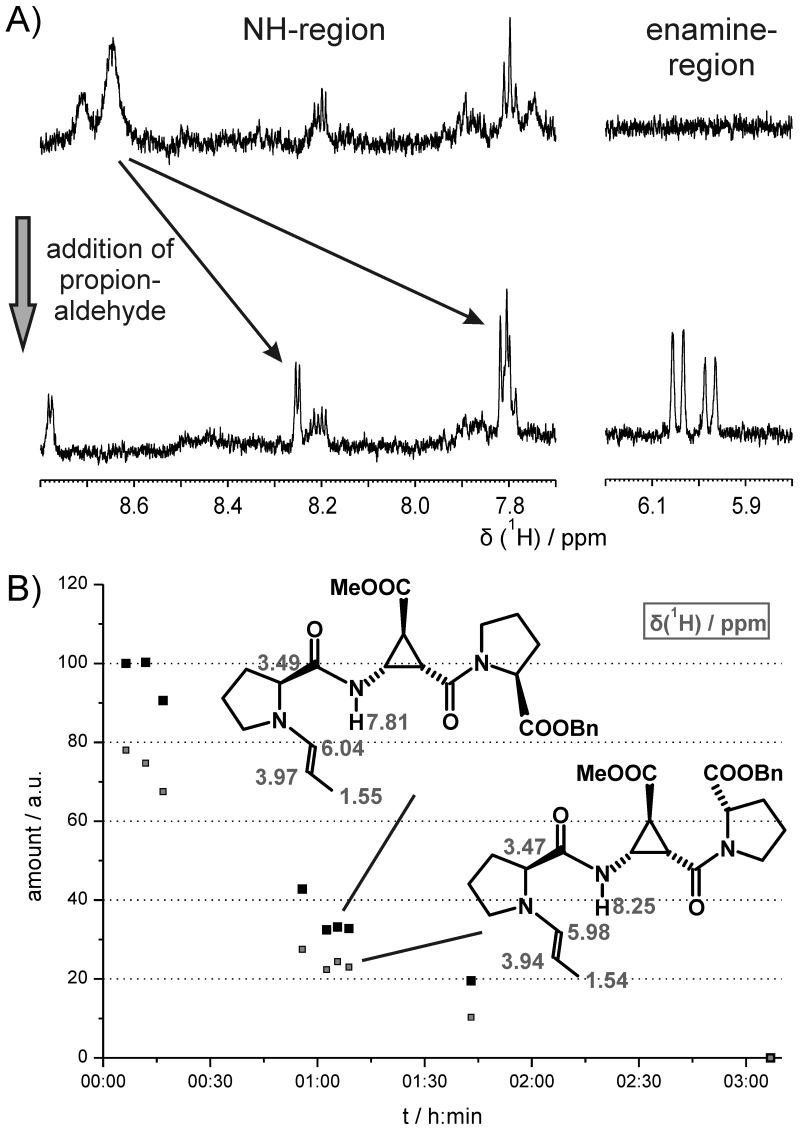

Figure 3.28: A) Proton spectra of H-(L)-Pro-▼-(L)-Pro-OBn in DMSO-d_6 before (top) and after (bottom) the addition of an excess of propionaldehyde; B) decrease of the amounts of enamine observed over time and fragmentary proton chemical shift assignment of the two enamines detected. (Note: Because of the poor sample quality, an absolute quantification of the enamine amount was not possible; the amount of the major isomer detected in the first spectrum was therefore set to 100 arbitrarily.)

The macroscopic solubility of the tripeptide in DMSO was rather poor, leading to a cloudy NMR sample. In addition, the broad lines of the amide proton resonances indicate spectroscopically that the dissolved tripeptide molecules are heavily aggregated. Upon the addition of an excess of propionaldehyde, two significant changes are observed in the 1D ^{1}H NMR spectra (Figure 3.28A). First, two doublets of 13.7 Hz each at 6.04 ppm and 5.98 ppm, respectively, as well as two doublets of quartets close to 4 ppm and two broad singlets at about 1.55 ppm are observed. These signals, agreeing excellently with the previously reported data for the propionaldehyde-derived proline enamine,[58] clearly evidence that two different *E*-configured enamine species (in a ratio of about 5:4) are formed from propionaldehyde and H-(L)-Pro-▼-(L)-Pro-OBn in DMSO. Following our earlier conformational studies on this tripeptide, one may well assume that these enamines are *cis*-*trans*-isomers with respect to the conformation of the ▼-(L)-Pro peptide bond (*cis*:*trans* ratio of the catalyst in chloroform: 1:4 at 240 K and 1:3 at 300 K).[72] Second, the formation of the enamines also has an impact on the spectral appearance of the amide proton resonances of ▼: The broad amide proton resonances of the tripeptide, at about 8.65 ppm in DMSO for both isomers, experience a significant upfield shift to 8.25 ppm and 7.81 ppm, respectively, in the enamine and turn into doublets of 8.2 Hz and 4.9 Hz. The well-defined multiplet pattern owing to the reduced linewidths indicate that (as anticipated earlier in chapter 2.4) the formation of the enamine is accompanied by the deaggregation of the tripeptide. Moreover, the comparison of the $^3J_{HN,H\beta}$ coupling constants with the value for the free tripeptide (8.9 Hz for the *trans*-isomer and 7.0 Hz for the *cis*-isomer, see chapter 2.2 and 2.4 clearly evidences that the enamine formation also leads to a drastic change in the backbone conformation of at least one of the two isomers. Accordingly, it can be concluded that conformational studies on peptide organocatalysis certainly need to be conducted on the enamine intermediates since the predictive power of free catalyst conformations for the actual reaction progress is limited. However, a long-term stabilization of the enamine species could not be achieved in this experimental system. After 3 hours, no enamine can be detected any longer (Figure 3.28B); instead, low amounts of the self-condensation product of propionaldehyde are observed. Still, the lifetime of the enamine species allowed for a rough conformational characterization by ^{1}H,^{1}H-NOESY analyses. The enamine resonances at 6.04 ppm and 5.98 ppm show cross-peaks to signals at 3.49 ppm and 3.47 ppm, most probably belonging to the Hα (Pro1) protons of the respective enamine species. Hence, this can be interpreted as a first evidence for the population of the s-*trans* conformation around the exocyclic N-C double bond; obviously, this conformation, that had been observed for proline enamines, is also preferred in the case of proline amide or peptide enamines. This constitutes a first preliminary insight into the stereoinduction exerted by proline amides[73] and *N*-terminal prolyl peptides[74] in asymmetric enamine organocatalysis. However, more detailed conformational studies will be necessary to elucidate further conformational features of the tripeptide enamines, such as the origin of the different $^3J_{HN,H\beta}$ coupling constants for the two enamines, of the change of the *cis*:*trans* ratio compared to the free catalyst, and of the upfield shift of the amide proton resonances.

3.4.5 Experiments towards Histidine Enamines

One of the intriguing findings of our study on substitution effects upon propionaldehyde-derived proline enamines was the observation that two-fold α-alkyl substitution reduces the amount of enamine in solution, compared to α-unbranched aldehydes. While enamines were readily observed for propionaldehyde, butyraldehyde, and 3-methyl-butyraldehyde, the amount of enamine was only tiny for isobutyraldehyde (see Figure 3.6). This was rationalized by the assumption that the stabilization of the enamine double bond by additional alkyl substitution is outperformed by the unfavorable allylic strain which is present in enamines derived from secondary amines, such as proline. Most interestingly, the reduced enamine amount of α-branched aldehydes corresponds very well with the predominant use of such aldehydes as aldol acceptors in proline-catalyzed reactions, but has on the other side largely impeded their employment as aldol donor species.[18,44,75] To overcome this limited applicability of α-branched aldehydes in organocatalyzed aldol reactions, Mahrwald and coworkers recently introduced histidine as a highly efficient and selective primary amine catalyst for crossed-aldol reactions.[76] Under histidine catalysis, isobutyraldehyde performed excellently as aldol donor species. Since in enamines derived from the primary amine histidine, the unfavorable allylic strain is expected to be much less pronounced than in those of the secondary amine proline (Figure 3.29), a more distinct inclination of histidine to form enamines may be assumed to rationalize this changed reactivity of isobutyraldehyde. To check this hypothesis, it was investigated whether higher isobutyraldehyde enamine equilibrium ratios are observed by NMR for histidine than for proline.

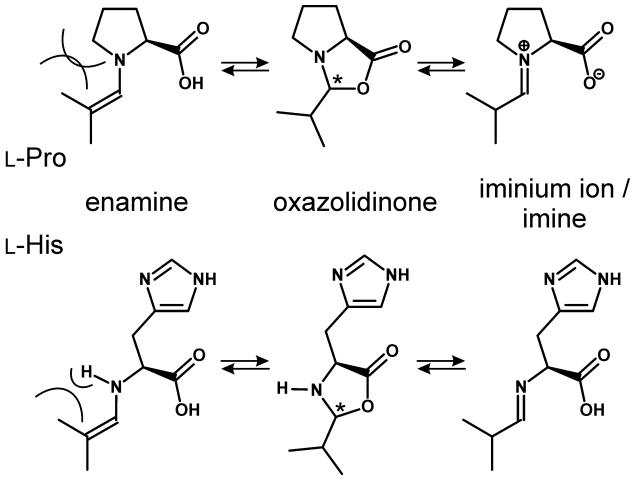

Figure 3.29: Intermediate equilibria of species derived from isobutyraldehyde and proline (top) or histidine (bottom).

For that purpose and in analogy to the proline enamine studies, equimolar amounts (30 μmol) of freshly distilled isobutyraldehyde and L-histidine were mixed in DMSO-d_6 or D_2O, respectively, and NMR spectra were recorded at 300 K. First, DMSO-d_6 was used as the solvent since this had allowed to detect *in situ* proline enamines for the first

time. However, the solubility of histidine in DMSO was so poor that no adducts formed from histidine and isobutyraldehyde could be detected. Next, in order to match the experimental conditions of histidine catalysis reported in the literature,[76] D_2O was applied as the solvent. In this case, histidine was well soluble and adduct formation between the aldehyde and the amino acid was observed. However, none of the characteristic enamine resonances could be detected in the proton spectra; therefore, no further efforts have been made to elucidate the nature of the adducts detected. Instead, more sophisticated experimental conditions (for instance, the addition of amine bases such as DBU) need to be applied to detect and characterize enamines derived from primary amine organocatalysts. This will be only the first step towards the elucidation of the intermediate equilibria effective in primary amine organocatalysis[77,78] (Figure 3.29, bottom), *e.g.* by histidine or by tryptophane that has recently been successfully applied, too.[79] The comparison with the intermediates of proline catalysis might then help to clarify the Janus-headed performance of α-branched aldehydes in amino acid-catalyzed crossed-aldol reactions.

3.5 References

[1] A. Berkessel, H. Gröger, *Asymmetric Organocatalysis - From Biomimetic Concepts to Applications in Asymmetric Synthesis*, Wiley-VCH, Weinheim, **2005**.

[2] *Chem. Rev.* **2007**, *107*, 12 (special issue on organocatalysis).

[3] *Ernst Schering Foundation Symposium Proceedings "Organocatalysis"* (Eds.: M. T. Reetz, B. List, S. Jaroch, H. Weinmann), Springer, Berlin, **2008**.

[4] *Asymmetric Organocatalysis, Vol. 291* (Ed.: B. List), **2010**.

[5] D. Seebach, U. Grošelj, D. M. Badine, W. B. Schweizer, A. K. Beck, *Helv. Chim. Acta* **2008**, *91*, 1999–2034.

[6] D. W. C. MacMillan, *Nature* **2008**, *455*, 304–308.

[7] J. Seayad, B. List, *Org. Biomol. Chem.* **2005**, *3*, 719–724.

[8] T. Akiyama, *Chem. Rev.* **2007**, *107*, 5744–5758.

[9] *Hydrogen Bonding in Organic Synthesis* (Ed.: P. M. Pihko), Wiley-VCH, Weinheim, **2009**.

[10] S. E. Denmark, G. L. Beutner, *Angew. Chem. Int. Ed.* **2008**, *47*, 1560–1638.

[11] U. Eder, G. Sauer, R. Wiechert, *Angew. Chem. Int. Ed.* **1971**, *10*, 496–497.

[12] Z. G. Hajos, D. R. Parrish, *J. Org. Chem.* **1974**, *39*, 1615–1621.

[13] B. List, R. A. Lerner, C. F. Barbas III, *J. Am. Chem. Soc.* **2000**, *122*, 2395–2396.

[14] S. Bertelsen, K. A. Jørgensen, *Chem. Soc. Rev.* **2009**, *38*, 2178–2189.

[15] B. List, *Chem. Commun.* **2006**, 819–824.

[16] P. Melchiorre, M. Marigo, A. Carlone, G. Bartoli, *Angew. Chem. Int. Ed.* **2008**, *47*, 6138–6171.

[17] A. Erkkilä, I. Majander, P. M. Pihko, *Chem. Rev.* **2007**, *107*, 5416–5470.

[18] S. Mukherjee, J. W. Yang, S. Hoffmann, B. List, *Chem. Rev.* **2007**, *107*, 5471–5569.

[19] B. List, *Acc. Chem. Res.* **2004**, *37*, 548–557.

[20] B. List, L. Hoang, H. J. Martin, *Proc. Natl. Acad. Sci. U. S. A.* **2004**, *101*, 5839–5842.

[21] C. Allemann, R. Gordillo, F. R. Clemente, P. H.-Y. Cheong, K. N. Houk, *Acc. Chem. Res.* **2004**, *37*, 558–569.

[22] S. Lakhdar, R. Appel, H. Mayr, *Angew. Chem. Int. Ed.* **2009**, *48*, 5034–5037.

[23] S. Lakhdar, T. Tokuyasu, H. Mayr, *Angew. Chem. Int. Ed.* **2008**, *47*, 8723–8726.

[24] A. L. Fuentes de Arriba, L. Simon, C. Raposo, V. Alcazar, J. R. Moran, *Tetrahedron* **2009**, *65*, 4841–4845.

[25] S. Bertelsen, M. Marigo, S. Brandes, P. Diner, K. A. Jørgensen, *J. Am. Chem. Soc.* **2006**, *128*, 12973–12980.

[26] U. Grošelj, D. Seebach, D. M. Badine, W. B. Schweizer, A. K. Beck, I. Krossing, P. Klose, Y. Hayashi, T. Uchimaru, *Helv. Chim. Acta* **2009**, *92*, 1225–1259.

[27] T. J. Peelen, Y. Chi, S. H. Gellman, *J. Am. Chem. Soc.* **2005**, *127*, 11598–11599.

[28] S.-I. Yamada, G. Otani, *Tetrahedron Lett.* **1969**, *10*, 4237–4240.

[29] X. Zhu, F. Tanaka, R. A. Lerner, C. F. Barbas III, I. A. Wilson, *J. Am. Chem. Soc.* **2009**, *131*, 18206–18207.

[30] H. Iwamura, S. P. Mathew, D. G. Blackmond, *J. Am. Chem. Soc.* **2004**, *126*, 11770–11771.

[31] H. Iwamura, J. Wells, D. H., S. P. Mathew, M. Klussmann, A. Armstrong, D. G. Blackmond, *J. Am. Chem. Soc.* **2004**, *126*, 16312–16313.

[32] F. Orsini, F. Pelizzoni, M. Forte, M. Sisti, G. Bombieri, F. Benetollo, *J. Heterocycl. Chem.* **1989**, *26*, 837–841.

[33] D. Seebach, A. K. Beck, D. M. Badine, M. Limbach, A. Eschenmoser, A. M. Treasurywala, R. Hobi, W. Prikoszovich, B. Linder, *Helv. Chim. Acta* **2007**, *90*, 425–471.

[34] C. Marquez, J. O. Metzger, *Chem. Commun.* **2006**, 1539–1541.

[35] C. Isart, J. Bures, J. Vilarrasa, *Tetrahedron Lett.* **2008**, *49*, 5414–5418.

[36] Y.-F. Hu, X. Lu, *Chinese J. Struct. Chem.* **2008**, *27*, 547–552.

[37] R. Mahrwald, B. Costisella, B. Gündogan, *Synthesis* **1998**, 262–264.

[38] A. B. Northrup, D. W. C. MacMillan, *J. Am. Chem. Soc.* **2002**, *124*, 6798–6799.

[39] A. Erkkilä, P. M. Pihko, *Eur. J. Org. Chem.* **2007**, 4205–4216.

[40] B. List, P. Pojarliev, C. Castello, *Org. Lett.* **2001**, *3*, 573–575.

[41] C. T. Wong, *Tetrahedron* **2009**, *65*, 7491–7497.

[42] D. A. Yalalov, S. B. Tsogoeva, T. E. Shubina, I. M. Martynova, T. Clark, *Angew. Chem. Int. Ed.* **2008**, *47*, 6624–6628.

[43] K. N. Rankin, J. W. Gauld, R. J. Boyd, *J. Phys. Chem. A* **2002**, *106*, 5155–5159.

[44] A. I. Nyberg, A. Usano, P. M. Pihko, *Synlett* **2004**, *11*, 1891–1896.

[45] P. M. Pihko, K. M. Laurikainen, A. Usano, A. I. Nyberg, J. A. Kaavi, *Tetrahedron* **2006**, *62*, 317–328.

[46] Y. Marcus, *Chem. Soc. Rev.* **1993**, *22*, 409–416.

[47] C. Reichardt, *Solvents and Solvent Effects in Organic Chemistry*, Wiley-VCH, Weinheim, **1988**.

[48] S. Protti, A. Mezzetti, J.-P. Cornard, C. Lapouge, M. Fagnoni, *Chem. Phys. Lett.* **2008**, *467*, 88–93.

[49] A. Douhal, M. Sanz, L. Tormo, J. A. Organero, *ChemPhysChem* **2005**, *6*, 419–423.

[50] V. I. Tomin, R. Javorski, *Opt. Spectrosc.* **2007**, *103*, 952–957.

[51] S. M. Bachrach, *J. Org. Chem.* **2008**, *73*, 2466–2468.

[52] R. M. Beesley, C. K. Ingold, J. F. Thorpe, *J. Chem. Soc. Trans.* **1915**, 1080–1106.

[53] T. F. Magnera, G. Caldwell, J. Sunner, S. Ikuta, P. Kebarle, *J. Am. Chem. Soc.* **1984**, *106*, 6140–6146.

[54] A. R. Ubbelohde, K. J. Gallagher, *Acta Cryst.* **1955**, *8*, 71–83.

[55] B. A. Krantz, A. K. Srivastava, S. Nauli, D. Baker, R. T. Sauer, T. R. Sosnick, *Nat. Struct. Mol. Biol.* **2002**, *9*, 458–463.

[56] V. Jaravine, F. Cordier, S. Grzesiek, *J. Biomol. NMR* **2004**, *29*, 309–318.

[57] T. Kanzian, S. Lakhdar, H. Mayr, *Angew. Chem. Int. Ed.* **2010**, *49*, 9526–9529.

[58] M. B. Schmid, K. Zeitler, R. M. Gschwind, *Angew. Chem. Int. Ed.* **2010**, *49*, 4997–5003.

[59] D. G. Blackmond, A. Moran, M. Hughes, A. Armstrong, *J. Am. Chem. Soc.* **2010**, *132*, 7598–7599.

[60] M. Amedjkouh, *Tetrahedron: Asymmetry* **2007**, *18*.

[61] K. T. Leffek, P. Pruszynski, K. Thanapaalasingham, *Can. J. Chem.* **1989**, *67*.

[62] I. Kaljurand, A. Kütt, L. Sooväli, T. Rodima, V. Mäemets, I. Leito, I. A. Koppel, *J. Org. Chem.* **2005**, *70*, 1019–1028.

[63] J. F. Coetzee, G. R. Padmanabhan, *J. Am. Chem. Soc.* **1965**, *87*, 5005–5010.

[64] C. D. Ritchie, R. E. Uschold, *J. Am. Chem. Soc.* **1967**, *89*, 1721–1725.

[65] S. L. Poe, A. R. Bogdan, B. P. Mason, J. L. Steinbacher, S. M. Opalka, D. T. McQuade, *J. Org. Chem.* **2009**, *74*, 1574–1580.

[66] Z. Rappoport, *The Chemistry of Enamines*, Wiley, New York, **1994**.

[67] A. B. Northrup, I. K. Mangion, F. Hettche, D. W. C. MacMillan, *Angew. Chem. Int. Ed.* **2004**, *43*, 2152–2154.

[68] A. B. Northrup, D. W. C. MacMillan, *Science* **2004**, *305*, 1752–1755.

[69] J.-F. Lin, C.-C. Wu, M.-H. Lien, *J. Phys. Chem.* **1995**, *99*, 16903–16908.

[70] E. Pretsch, T. Clerc, J. Seibl, W. Simon, *Tabellen zur Strukturaufklärung organischer Verbindungen mit spektroskopischen Methoden*, Springer, Berlin, **1990**.

[71] M. B. Schmid, M. Fleischmann, V. D'Elia, O. Reiser, W. Gronwald, R. M. Gschwind, *ChemBioChem* **2009**, *10*, 440–444.

[72] M. Schmid, Diploma Thesis, Universität Regensburg (Germany), **2007**.

[73] Z. Tang, F. Jiang, X. Cui, L.-Z. Gong, A.-Q. Mi, Y.-Z. Jiang, Y.-D. Wu, *Proc. Natl. Acad. Sci. U. S. A.* **2004**, *101*, 5755–5760.

[74] E. R. Jarvo, S. J. Miller, *Tetrahedron* **2002**, *58*, 2481–2495.

[75] P. M. Pihko, I. Majander, A. Erkkilä, *Top. Curr. Chem.* **2010**, *291*, 29–75.

[76] M. Markert, U. Scheffler, R. Mahrwald, *J. Am. Chem. Soc.* **2009**, *131*, 16642–16643.

[77] A. Bassan, W. Zou, E. Reyes, F. Himo, A. Córdova, *Angew. Chem. Int. Ed.* **2005**, *44*, 7028–7032.

[78] A. Cordova, W. Zou, I. Ibrahem, E. Reyes, M. Engqvist, W.-W. Liao, *Chem. Commun.* **2005**, 3586–3588.

[79] Z. Jiang, H. Yang, X. Han, J. Luo, M. W. Wong, Y. Lu, *Org. Biomol. Chem.* **2010**, *8*, 1368–1377.

4 The Mechanism of Proline Enamine Formation from Oxazolidinones

"A Selective 1D EXSY Study on the Oxazolidinone-Enamine Interconversion in Dipolar Aprotic Solvents: Urea and Amine Additives, Substituent and Isotope Effects"

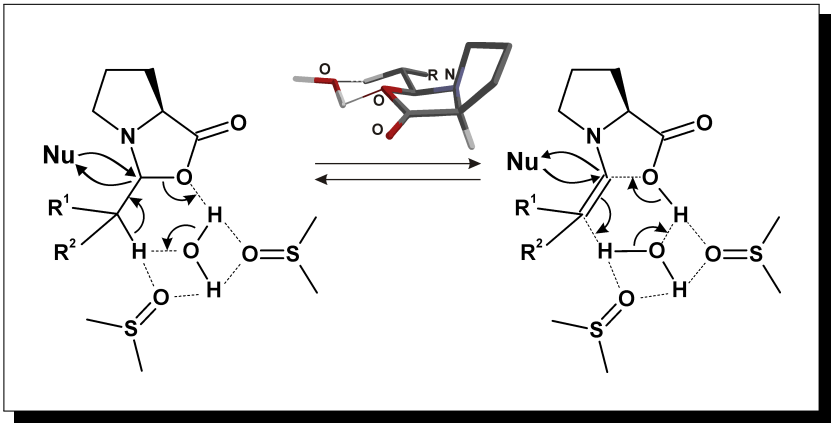

Markus B. Schmid, Kirsten Zeitler, and Ruth M. Gschwind

4.1 Direct Formation Pathway of Proline Enamines from Oxazolidinones

Introduction

Recently, we were able to detect by means of NMR spectroscopy the elusive proline enamine intermediate for the first time in solution. In addition, we could elucidate with the help of two-dimensional EXSY spectra that proline enamines are formed directly from the isomeric oxazolidinones in DMSO, but not via a dissociative pathway through central iminium intermediates (or a rapidly interconverting intermediate pool, chapter 3.2).[1] This surprising observation raises the question how the direct proline enamine formation from oxazolidinones proceeds mechanistically. Concerning this issue, so far only few proposals have been put forward in the literature. Seebach and Eschenmoser suggested an E2-elimination step under the influence of proline or oxazolidinones as bases.[2] On the other hand, McQuade and coworkers have claimed[3] that urea derivatives as H-bond donors may enhance the rate of enamine formation through intermolecular H-bonding interactions with the oxazolidinones.[a] In addition, theoretical calculations have proposed proton relay mechanism involving methanol or water for the enamine formation from carbinolamines[7] or from iminium zwitterions.[8] However, as yet, no experimental data on the suggested exchange mechanisms have become available. With our experience on studying proline enamines and oxazolidinones at the same time *in situ*, we therefore addressed the issue of the direct oxazolidinone-enamine interconversion NMR spectroscopically.

Here, we present our investigations on the exchange between enamines and oxazolidinones, formed from proline and 3-methyl-butyraldehyde in the dipolar aprotic solvents DMSO and DMF. With the help of a selective one-dimensional EXSY technique, the formation rates of the isomeric oxazolidinones from the enamine were studied experimentally, which can be correlated to the rates of the reverse reaction. In addition, urea derivatives as potential H-bond donors as well as different amines with varying basicities and nucleophilicities were employed as additives to the reaction mixtures in DMSO and their impact upon the interconversion rates was examined. Our results indicate that ureas mainly enhance the rate of the oxazolidinone-oxazolidinone interconversion, but that they affect the oxazolidinone-enamine interconversion only to a minor degree. In addition, most surprisingly our observations on amine additives suggest that not their basic, but rather their nucleophilic properties lead to a rate enhancement of the enamine formation from the oxazolidinones. This conclusion is further supported by a decelerating substitution effect on the enamine formation rate, for which also a deuterium isotope effect was observed. Altogether we interpret these findings as indicative of a proton relay mechanism for the direct proline enamine formation from oxazolidinones that is assisted by nucleophilic additives.

[a] Analogous interactions between proline and thioureas, being even stronger H-bond donors, have been postulated, too.[4,5] Even a proline-derived ketiminium zwitterion has been detected *in situ* with the help of a thiourea derivative, which was ascribed to the relative iminium stabilization through H-bonding interactions.[6]

Results and Discussion

Experimental Approach. NMR spectroscopy offers EXSY methods as a versatile tool for the investigation of chemical interconversion rates on the ms time scale.[9] EXSY experiments are based on the magnetization transfer between different nuclei through chemical exchange and are, despite different magnetization transfer mechanisms, performed similarly to the more common NOESY experiments. Hence, the buildup of EXSY cross-peaks as a function of the mixing time can be used as a measure for the rate of the underlying chemical exchange process, just like the linear section of the buildup of NOESY cross-peaks is converted into internuclear distances. This idea of EXSY studies is typically exploited to investigate the migration of exchangeable protons between different species. However, it may be also utilized to map isomerization processes, *i.e.* the interconversion of stable conformations and of chemically different species alike, with the help of non-exchangeable protons that resonate at different frequencies in the different isomers. Accordingly, EXSY experiments are in principle suited to study the exchange between proline enamines and oxazolidinones. However, recording EXSY buildup curves with the help of two-dimensional EXSY spectra is rather cumbersome and time-consuming. Therefore, a one-dimensional EXSY approach was applied in which a single resonance of one isomeric species is excited selectively (see Figure 4.1A) and the buildup of the corresponding resonances of the other isomers is observed as a function of the mixing time.

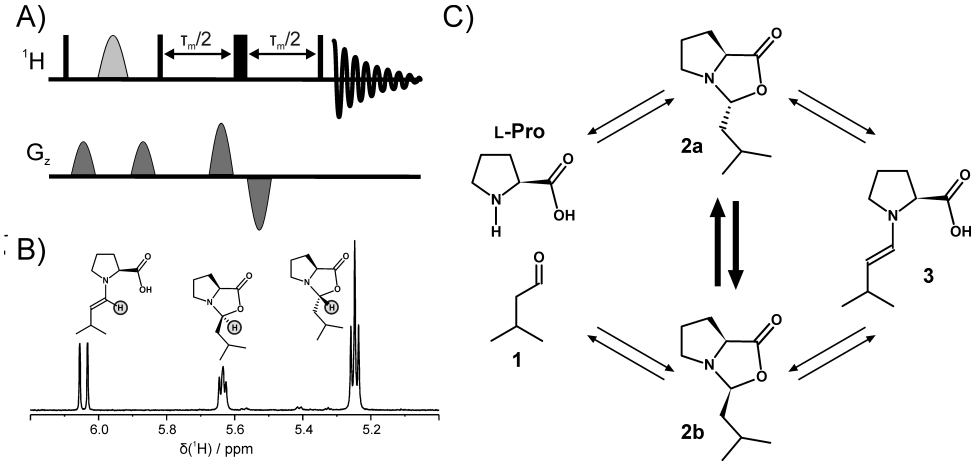

Figure 4.1: A) Pulse sequence of the selective 1D EXSY experiment ; B) section of the ^{1}H NMR spectrum of a reaction mixture of 3-methyl-butyraldehyde **1** and 100 mol% L-proline in DMSO-d_6 at 300 K; C) exchange cross-peak matrix between **1** and the corresponding proline-derived oxazolidinones **2a**,**b** and the enamine **3**, observed in a 2D EXSY spectrum in DMSO-d_6 at 300 K with a mixing time of 700 ms.

The selection of the species and resonance to be excited selectively is governed by the necessity to combine experimental simplicity and straightforward data interpretation. Since we had observed in our earlier EXSY studies (Figure 4.1C, chapter 3.2)[1] that the conversions of the oxazolidinones to the aldehyde and to the enamine are comparably fast, the competition between these two processes was considered to pose additional difficulties for

the data evaluation if one of the oxazolidinones was chosen for the selective excitation. For the enamine in contrast, neither the back-reaction of the enamine via the oxazolidinones to the aldehyde nor the forward C-C bond formation had been observed with a mixing time of 700 ms. Therefore, the enamine was chosen as the species to be selectively excited in the 1D EXSY studies. Proton H1 (highlighted in gray in Figure 4.1B) was identified as the proton of choice for the selective excitation (through selective refocusing) because of the optimal spectral dispersion of the protons H1 of the oxazolidinones **2a**,**b** and of the enamine **3** (Figure 4.1B). Still, this spectroscopic approach generally delivers information only on the oxazolidinone formation rate starting from the enamine. However, the impact of additives on the rate of the reverse reaction is of higher interest for our study on the mechanism of the direct enamine formation from oxazolidinones. In our experimental system, accelerations of the *oxazolidinone* formation by the presence of additives correspond to accelerations of the *enamine* formation unless the enamine ratio in the equilibrium with the oxazolidinones is decreased by the additive (Figure 4.2). However, as reported earlier (chapter 3.4), this prerequisite is fulfilled by all amines and ureas applied in this study so that increased oxazolidinone formation rates can be directly interpreted as increased enamine formation rates (right-hand side of Figure 4.2).

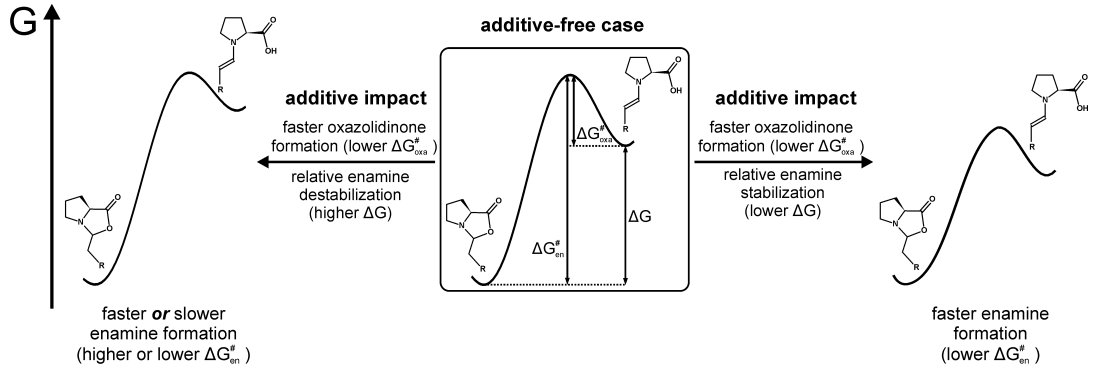

Figure 4.2: Scenarios for the correlation of experimentally observed accelerations of the *oxazolidinone* formation with the *enamine* formation rate depending on the additive impact upon the relative enamine stabilization.

Based on this spectroscopic approach, the experimental system consisting of an aldehyde, the catalyst proline, a suitable solvent, and a variety of additives was chosen in the following way. 3-Methyl-butyraldehyde **1** was selected as the aldehyde (c = 50 mM, if not stated otherwise) because it provides the highest enamine ratio and stable intermediate concentrations over at least one day (chapter 3.2).[1] In addition, for **1**, the spectral dispersion of H1 is maximum compared to other aldehydes (chapter 3.2).[1] 100 mol% of L-proline were applied to increase the intermediate amounts and hence to facilitate the NMR spectroscopic investigations. The dipolar aprotic solvents DMSO and DMF were used since they had allowed to detect proline enamines *in situ* (chapter 3.2).[1] Two urea derivatives as well as various amines of different basicities and nucleophilicities (100 mol% each, see also chapter 3.4) were utilized as additives and their influence on the oxazo-

lidinone formation rate was investigated by the 1D EXSY approach outlined above. For all experimental systems, the 1D EXSY spectra with selective enamine excitation were recorded with mixing times ranging from 200 ms to 2000 ms. The oxazolidinone buildup curves were obtained by integration of the H1 resonances of the intermediates **2a**,**b** and **3** and by subsequent calculation of their ratios of the total intermediate amount in each 1D EXSY spectrum. For the sake of better comparability of the different data sets, the oxazolidinone EXSY buildup curves were then normalized with respect to the oxazolidinone ratio in the thermodynamic equilibrium with the enamine, as determined from peak integration in standard 1D ^{1}H NMR spectra. The buildup curves are hence to be read as the degree to which the thermodynamic oxazolidinone-enamine equilibrium has been established at a given mixing time; accordingly the value of 100 % indicates the full establishment of the thermodynamic equilibrium.

Nevertheless, the following data evaluation and interpretation is based on a number of assumptions and is therefore of preliminary and qualitative character. First, differences in the relaxations of **2a**,**b** and **3** during the mixing time, potentially slightly distorting the results of the 1D integration, are neglected. Second, more severely, basically a two-site equally populated exchange is assumed, *i.e.* the different equilibrium ratios of the intermediates and the associated implications on the interconversion rates as well as further interconversion steps during the mixing time are not explicitly taken into account. Despite these shortcomings of the presently assumed exchange model, the results discussed in the following, based on rather large experimental effects, should also bear a more sophisticated data evaluation. Attempts in this direction are currently pursued.

Additive-Free Enamine-Oxazolidinone Exchange in DMSO and DMF. First, 3-methylbutyraldehyde **1** was mixed with 100 mol% of proline in DMSO-d_6 at concentrations of 50 mM and 10 mM, respectively, and in DMF-d_7 at a concentration of 50 mM while no additives were employed. Selective 1D EXSY spectra were recorded at 300 K to map the EXSY buildup curves of the oxazolidinones (Figure 4.3).

The EXSY buildup curves reveal that the thermodynamic equilibrium between the enamine and the oxazolidinones is not established within the mixing time of 2 seconds. In a 50 mM reaction mixture in DMSO (Figure 4.3B), used as the reference sample for the following investigations, the *exo*-oxazolidinone **2a** reaches almost 50 % of its equilibrium ratio within 2 seconds whereas the normalized amount of the *endo*-isomer **2b** does not exceed 40 % at that point in time. These different relative interconversion rates of the enamine **3** and the *exo*- or *endo*-oxazolidinone **2a**,**b**, respectively, agree well with the qualitative observation from 2D EXSY analyses in our previous report (chapter 3.2).[1] In addition, the different rates for the EXSY buildup of **2a**,**b** also reveal that, in the additive-free case, the interconversion of the isomeric oxazolidinones (which had been shown to be faster than the exchange with the aldehyde or with the enamine, Figure 4.1C and chapter 3.2)[1] is not fast enough to cause the complete thermodynamic equilibration of the

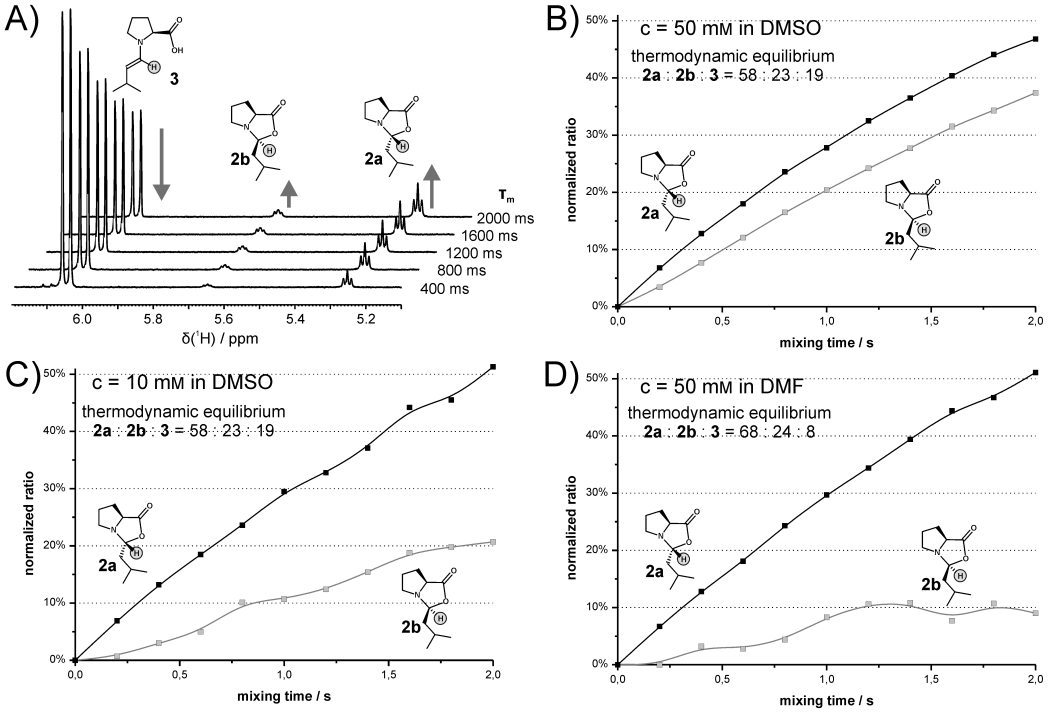

Figure 4.3: A) Stacked plot of selective 1D EXSY spectra with increasing mixing time (from bottom to top) of a 50 mM reaction mixture of 3-methyl-butyraldehyde **1** and 100 mol% proline in DMSO-d_6 at 300 K and B) the normalized EXSY buildup curve of the oxazolidinones derived thereof; C),D) EXSY buildup curves for a 10 mM reaction mixture in DMSO-d_6 (C) and for a 50 mM reaction mixture in DMF-d_7 (D).

oxazolidinones **2a**,**b**, once formed from the enamine within the mixing time. When the concentration of the reactants in DMSO is reduced to 10 mM (Figure 4.3C), the buildup of the normalized *exo*-oxazolidinone (**2a**) ratio appears to be slightly increased in the case of the higher dilution. In contrast, the buildup of the *endo*-isomer (**2b**) ratio is substantially decelerated and hardly exceeds 20 % within 2 seconds. For these deviations from the higher concentrated reaction mixture, two rationalizations may be put forward: On the one hand, considering the slight increase of the ratio buildup of **2a** as lying within the error range, the decelerated *endo*-oxazolidinone buildup may be taken as a hint that the interconversion of the enamine **3** and the *endo*-oxazolidinone **2b** depends on the overall amount of the catalyst proline, possibly being involved in the exchange process as a Brønsted acid, as a Brønsted base, or as a nucleophilic Lewis base. On the other hand, considering the slight increase of the ratio buildup of **2a** as relevant, this increase along with the decrease of the ratio buildup of **2b** can be interpreted as an indication that the equilibration between the isomeric oxazolidinones is decreased when the overall catalyst concentration is lowered, again suggesting that proline is involved in the exchange process between the oxazolidinones, playing one of the above-mentioned roles. These two lines of argument may also hold for the 1D EXSY data of a 50 mM reaction mixture in DMF (Figure 4.3D): Here, just like for the 10 mM reaction mixture in DMSO, the buildup of the normalized concentration of **2a** seems to be similarly fast as or even slightly faster

than in the reference sample in DMSO, while the amount of **2b** reaches only 10 % of the equilibrium ratio within a mixing time of 2 seconds. Again, this may indicate either a decelerated *endo*-oxazolidinone formation in DMF compared to DMSO or a decelerated interconversion of the isomeric oxazolidinones. Overall, the 1D EXSY approach in DMSO reveals that in principle information on the enamine-oxazolidinone interconversion and the oxazolidinone-oxazolidinone interconversion alike can be gathered. To shed more light on these issues, next the impact of additives on the oxazolidinone buildup curves was investigated.

Impact of Additives upon the EXSY Buildup Curves.

Urea Additives. First, two urea derivatives (Figure 4.4D), *N*,*N´*-diphenylurea (DPU) and 1-(2-(di-methylamino)ethyl)-3-phenylurea (DMAEPU) were tested as additives. The comparison of the two ureas offers the option to investigate the impact of the bifunctionality of DMAEPU (which has been argued to enhance the rate of enamine formation from the oxazolidinones in various solvents such as chloroform, ethyl acetate, and acetonitrile)[3] and of the stronger H-bond donor ability of DPU (owing to the -I-effect of the phenyl groups). The NMR experiments were performed with 50 mM reaction mixtures of the aldehyde **1** and 100 mol% of proline and the urea derivative, each, in DMSO-d_6 at 300 K (Figure 4.4).

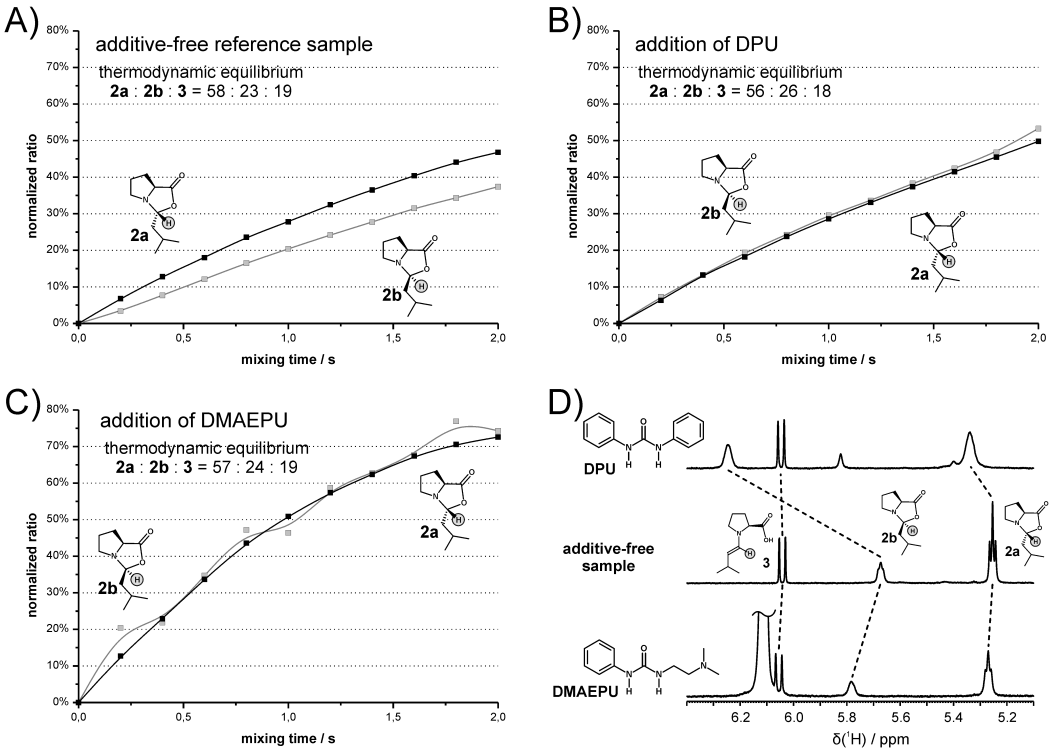

Figure 4.4: Normalized EXSY buildup curves of the oxazolidinones in the additive-free sample (A) and upon the addition of DPU (B) and DMAEPU (C) in DMSO-d_6 at 300 K; D) sections of ^{1}H NMR spectra of the additive-free reference sample (middle) and upon the addition of DPU (top) and DMAEPU (bottom).

Two significant changes with respect to the reference sample (Figure 4.4A) are observed in the 1D EXSY-derived buildup curves of **2a**,**b** upon the addition of the urea additives (Figure 4.4B,C). First, for both DPU and DMAEPU the buildup curves of the *exo*- and the *endo*-oxazolidinones **2a**,**b** are no longer different. This can be interpreted in terms of a relative acceleration of the formation of **2b**, in such a way that the formation rates of **2a**,**b** happen to coincide by chance. Alternatively, on may assume that the interconversion of **2a**,**b** is facilitated by the urea additives so that **2a**,**b** equilibrate after being formed from the enamine **3** within the mixing time. In fact, the latter rationalization is supported by the line-broadening of the oxazolidinone resonances in comparison to the additive-free case (Figure 4.4D). The second remarkable observation upon addition of the urea derivatives is the overall acceleration of the oxazolidinone formation. Most interestingly, however, the impact of DPU (50 % within 2 seconds) is a lot weaker than the one of DMAEPU (over 70 % and accordingly a much more pronounced saturation curve shape during 2 seconds). Since the stronger H-bond donor DPU causes the weaker acceleration, this indicates that H-bond donor additives only have a minor effect on the rate of the enamine-oxazolidinone interconversion in DMSO. On the other hand, on the example of the bifunctional DMAEPU it becomes evident that the presence of the Lewis basic, nucleophilic tertiary amine moiety is responsible for the drastic rate enhancement of the oxazolidinone-enamine exchange. As outlined above (Figure 4.2), since the relative thermodynamic stabilities of **2a**,**b** and **3** are essentially unchanged by DMAEPU (Figure 4.4C), the accelerated *oxazolidinone* formation from the enamine translates into an accelerated *enamine* formation from the oxazolidinones. Hence, we can provide experimental evidence for the recently postulated rate enhancement of enamine formation from oxazolidinones upon the addition of DMAEPU (Figure 4.5A).[3]

Intrigued by this finding, we investigated whether the interaction of **2a**,**b** and **3** with urea derivatives in solution could be verified NMR spectroscopically. In principle, this may be accomplished via different diffusion coefficients in DOSY experiments, via intermolecular magnetization transfer in NOESY experiments, or via chemical shift changes in 1D ^{1}H spectra. Yet, in our experimental system, containing rapidly interconverting species with *per se* varying diffusion coefficients (see chapter 3.2)[1] and in view of expected aggregation-deaggregation equilibria, DOSY measurements were not considered the method of choice. Instead, NOESY spectra were recorded in order to prove the proximity of the intermediates **2a**,**b** or **3** with the urea derivatives DPU or DMAEPU. However, no intermolecular NOEs could be detected. Thus, the ^{1}H chemical shifts of **2a**,**b** and **3** must be consulted to draw conclusions on potential intermolecular interactions (Figure 4.4D). Indeed, upon the addition of DPU or DMAEPU, significant downfield shifts of the resonances of H1 (less pronouncedly for Hα) of the oxazolidinones **2a**,**b** are observed whereas the resonances of the enamine remain virtually unaffected. Most notably, DPU causes more substantial deshieldings than DMAEPU; in addition, the *endo*-oxazolidinone **2b** is generally affected more strongly than the *exo*-isomer **2a** (Table 4.1).

proton		$\Delta\delta$ / ppm	
		DPU	DMAEPU
2a	Hα	0.03	0.00
	H1	0.09	0.02
2b	Hα	0.15	0.02
	H1	0.60	0.13

Table 4.1: Chemical shift changes of the protons Hα and H1 in the oxazolidinones **2a** and **2b** upon addition of DPU or DMAEPU in DMSO-d_6 at 300 K.

For the observed stronger downfield shifts caused by DPU two rationalizations may be considered in view of the structural difference between DPU and DMAEPU: On the one hand, ring current effects of the two phenyl rings and, on the other hand, the stronger H-bond donating properties of DBU compared to DMAEPU. Intermolecular ring current effects, however, seem rather unlikely as the main source of deshielding in view of the phenyl rings pointing away from the H-bonding site (Figure 4.5). In addition, simultaneous ring current-induced deshieldings at opposite faces of the oxazolidinone ring (as for H1 and Hα in the case of **2a**) are hardly possible by one DPU molecule. Moreover, DMAEPU, bearing one phenyl substituent, would be expected to deshield either H1 or Hα at least to a comparable degree as DPU, but this is not observed. And finally, in the case of such a tight coordination that intermolecular ring current effects are observed, the absence of intermolecular NOEs would be highly surprising. Instead of ring current effects, the H-bonding properties of DBU and DMAEPU may well account for the observed downfield shifts of H1 and Hα. H-bonding interactions with the lactone moiety of the oxazolidinone lead to a reduction of the electron density of the heterocycle and thus to a deshielding of the adjacent protons H1 and Hα. Since stronger H-bond donors intensify this effect, the hypothesis of H-bonding interactions between **2** and ureas rationalizes the stronger distinctness of the deshielding of H1 and Hα in the case of the stronger H-bond donor DPU.[b]

Moreover, this assumption also helps to explain the heavier impact on H1 in comparison to Hα. As has been shown recently,[6] strongly H-bond donating thioureas do not only withdraw electron density from the oxazolidinones, but they also stabilize proline ketiminium intermediates in their equilibrium with the isomeric oxazolidinones. To a less pronounced degree this may also be achieved by urea derivatives for aldiminium species (Figure 4.5B). However, in case the oxazolidinone-iminium interconversion is fast on the NMR time scale (as has been hypothesized previously in chapter 3.2 and as is also hinted at by the broadened resonances especially of **2b** upon urea addition),[1] only one averaged set of proton resonances is observed experimentally. The impact of this averaging on the chemical shift of individual resonances increases with increasing chemical shift differences of the interconverting resonances; therefore, for large chemical shift differences,

[b] Interestingly, the reciprocal correlation of the H1/Hα downfield shifts (DPU > DMAEPU) with the acceleration of the oxazolidinone-enamine exchange (DPU < DMAEPU) again emphasizes that H-bond donors and Lewis-bases exert different functions in this experimental system.

even small contributions of less populated species to the chemical equilibrium become detectable. Accordingly, since the ^{1}H chemical shift difference between the oxazolidinones and the iminium ions is expected to be the largest for the proton H1 (between 5.0 and 5.5 ppm in the oxazolidinones and between 8.0 and 9.0 ppm in the iminium species, *cf.* chapter 8.2 and literature data[10–12]) the averaging effect and hence the downfield shift is more distinct for H1 than for Hα. The hypothesis of a partial iminium stabilization as the origin of the downfield shifts of H1 and Hα is also in line with the aforementioned stronger effect of DPU in comparison to DMAEPU. The stronger H-bond donating ability of DPU results in a stronger iminium stabilization and hence in a higher iminium contribution to the observed averaged chemical shift.

Finally, the assumption of a partial iminium stabilization by urea additives also explains the hitherto unaddressed issue why the *endo*-oxazolidinone **2b** is affected so much more than the *exo*-isomer **2a** (Figure 4.4D). Ring opening of **2b** results in the favorable *E*-configured iminium species (Figure 4.5B) whereas **2a** is connected to the less favorable *Z*-configured iminium zwitterion. Therefore, the iminium contribution to the iminium-oxazolidinone equilibrium, enabled by stabilizing H-bonds to a urea derivative, is much more pronounced in the case of the *endo*-oxazolidinone **2b** than for the *exo*-oxazolidinone **2a**. Accordingly, the downfield shift of H1 is a lot stronger for **2b** than for **2a**.

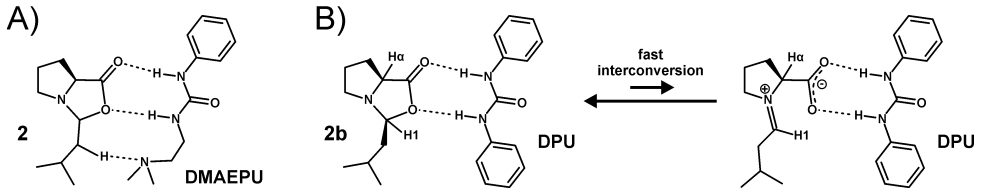

Figure 4.5: A) Previously postulated interactions between proline-derived oxazolidinones and DMAEPU;[3] B) potential oxazolidinone-iminium equilibrium, assisted by DPU.

Altogether, the H-bond donating abilities of urea derivatives are found to enhance the rate of the oxazolidinone-oxazolidinone interconversion significantly, but the one of the enamine-oxazolidinone exchange only to a minor degree. Moreover, intermolecular H-bonds are suggested to partially stabilize the iminium zwitterion in the equilibrium with the oxazolidinones. Further investigations will be necessary to address the question whether there is a causal connection between these two phenomena. In addition, the presence of a tertiary amine moiety is evidenced to enhance the enamine formation from the oxazolidinones. To clarify if its basic or rather its nucleophilic properties are responsible for this acceleration, next a variety of nitrogen-containing compounds was utilized as additives and their impact on the enamine-oxazolidinone interconversion was examined.

Amine Additives. Based on the study about the stabilizing influence of amines on proline enamine species (chapter 3.4), 4-dimethylaminopyridine (DMAP), *N*-methyl-morpholine (NMM), triethylamine (TEA), and 1,4-diazabicyclo[2.2.2]octan (DABCO) were employed as additives for the investigation of the enamine-oxazolidinone interconversion. The corre-

lation of their impact on the enamine-oxazolidinone interconversion rate with their different basicities and nucleophilicities was expected to allow conclusions on the underlying exchange mechanism. For that purpose, mixtures of 3-methyl-butyraldehyde **1** (c = 50 mM), 100 mol% L-proline and 100 mol% of one of the amine additives were prepared in DMSO-d_6 and NMR experiments were performed at 300 K (Figure 4.6).

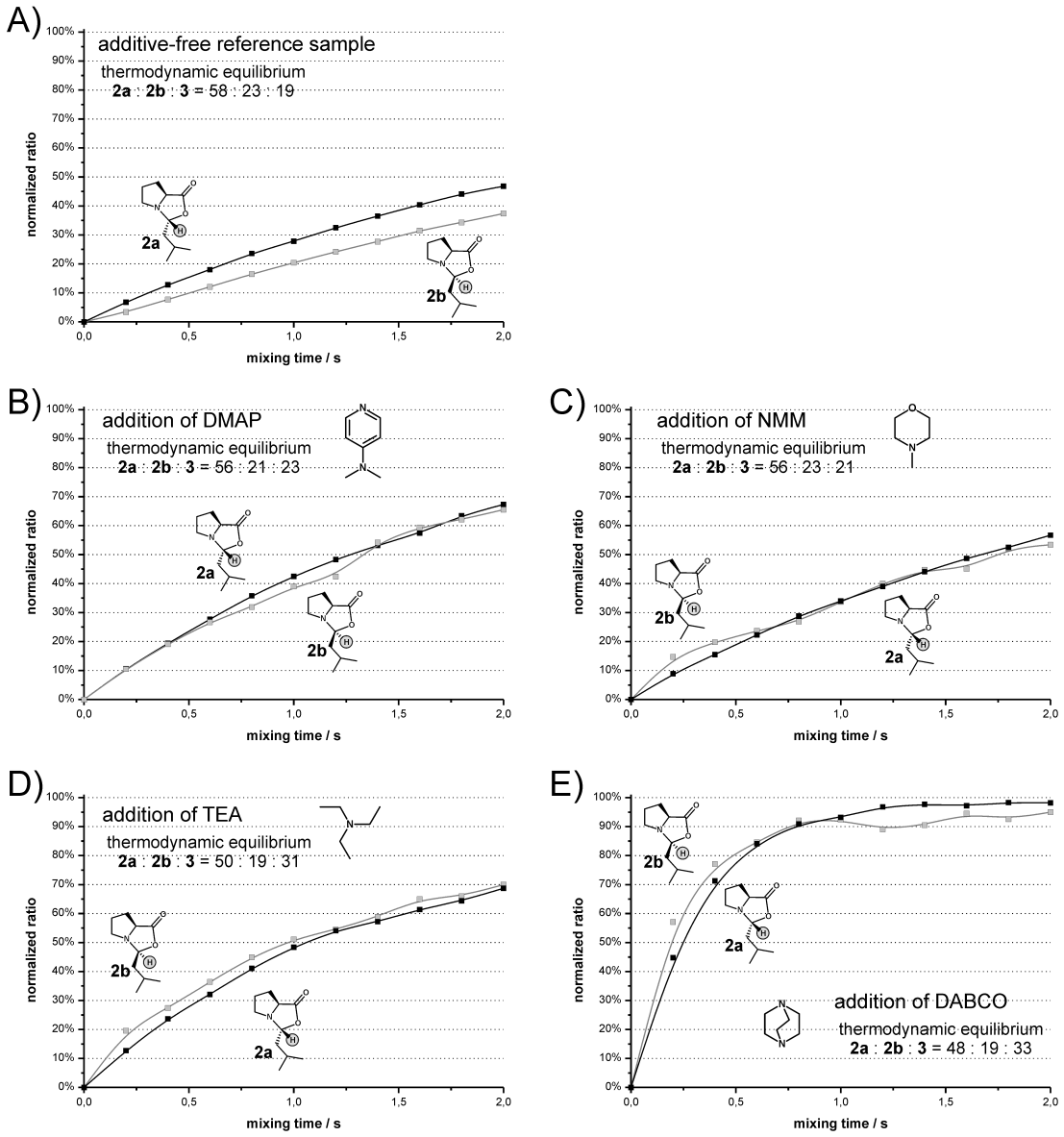

Figure 4.6: Normalized EXSY buildup curves of the oxazolidinones **2a**,**b** from the enamine **3** in the additive-free sample (A), with DMAP (B), with NMM (C), with TEA (D), and with DABCO (E) in DMSO-d_6 at 300 K.

For all amine additives, just like for the urea additives discussed above, the discrepancy between the buildup curves of **2a** and **2b** that had been observed for the additive-free case (Figure 4.6A) is essentially eliminated. This may again be taken as a hint that the amine additives enhance the rate of oxazolidinone-oxazolidinone interconversion so that the equilibrium between **2a** and **2b** can be established within the mixing time. Beyond

this common feature of all amine additives, the respective oxazolidinone buildup curves show remarkable differences: While the rate enhancement compared to the additive-free case (normalized ratios of **2a**,**b** below 50 % @ 2000 ms) is moderate in the case of NMM (about 55 % @ 2000 ms, Figure 4.6C), it is more pronounced for DMAP and TEA (65-70 % @ 2000 ms, Figure 4.6B,D) and thereby on the order of the rate enhancement with DMAEPU (see Figure 4.4B). Most intriguingly, DABCO shows by far the highest acceleration of the oxazolidinone formation so that the thermodynamical equilibrium between the enamine **3** and the oxazolidinones **2a**,**b** is virtually fully established after a mixing time of only 1000 ms (Figure 4.6E).

With this experimental data at hand, we intended to rationalize the different performances of the amine additives by their particular molecular properties because we expected this to allow insights into the mechanism of the enamine-oxazolidinone interconversion. For instance, in the case of an E2 mechanism,[2] the basicities of the amine additives should be connected to the observed rate enhancements. On the other hand, in the case of DMAP and DABCO, their different nucleophilicities have been identified as the main reason for their different behaviours in organocatalysis.[13] To check these hypotheses, we correlated the buildup rate of the oxazolidinones to the basicities and the nucleophilicities of the amines. For that purpose, the slope of the initial linear part of the buildup curves of **2a** was used as a measure for the buildup rate in "%/s". For the quantification of the amine basicities, pK_{aH} values in acetonitrile for DMAP,[14] NMM,[15] TEA,[14] and DABCO[16] were taken from the literature (see also chapter 3.4). To rank the amine nucleophilicities, the Mayr scales[17,18] were consulted and the nucleophilicity parameter N in acetonitrile was used for the nucleophilic reactivity of DMAP (14.95),[19] NMM (16.80),[20] TEA (17.10),[20] and DABCO (18.80).[13] For the additive-free case, DMSO was assumed to be the most abundant relevant nucleophile (N = 11.30).[21] The results of this evaluation are depicted in Figure 4.7.

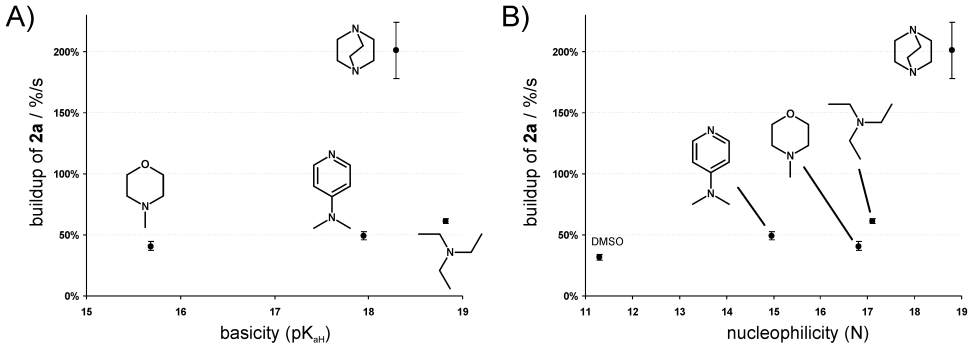

Figure 4.7: Correlation of the buildup of the amount of the oxazolidinone **2a** from the enamine **3** with the basicity (A) and the nucleophilicity (B) of the amine additive. (Error bars indicate the estimated preciseness of the linear fit to the buildup curves.)

The correlation plots show that there is no recognizable relationship between the rate of the oxazolidinone formation and the basicity of the amine additive (Figure 4.7A). As outlined earlier (Figure 4.2), this also implies that there is no acceleration of the enamine

formation from the oxazolidinones by basic additives; this is in contrast to the previously postulated E2 mechanism of proline enamine formation.[2] Instead, a certain correlation between the nucleophilicity of the amine additive and the oxazolidinone buildup can be stated: The stronger the nucleophile, the faster the oxazolidinone formation. Regarding the relative stabilization of the enamine **3** by TEA and DABCO (Figure 4.6), this trend should be even reinforced concerning the rate of the back-reaction, *i.e.* of the enamine formation (see again Figure 4.2 for the rationalization). This highly striking observation suggests a nucleophile-assisted, possibly an S_N2-type ring opening of the oxazolidinones; to our knowledge, such an involvement of nucleophilic species in the enamine-oxazolidinone exchange has not been considered so far.

To support this hypothesis experimentally, we next utilized 100 mol% sodium azide NaN_3 as an additive to our reference conditions. NaN_3 is characterized by a high nucleophilicity (N = 20.50 in DMSO),[22] but possesses virtually no basic properties ($pK_{aH} = 7.9$ in DMSO).)[23] Based on our postulation of a nucleophilic assistance in the enamine-oxazolidinone interconversion, a significant rate enhancement of the oxazolidinone buildup is therefore expected upon the addition of NaN_3. Indeed, the 1D EXSY data reveal that the buildup of the oxazolidinones from the enamine is significantly accelerated in the presence of NaN_3 (Figure 4.8B) and reaches almost the rate of the DABCO addition. Hence, we take this as an additional indication that there is in fact a nucleophilic assistance to the enamine-oxazolidinone interconversion.

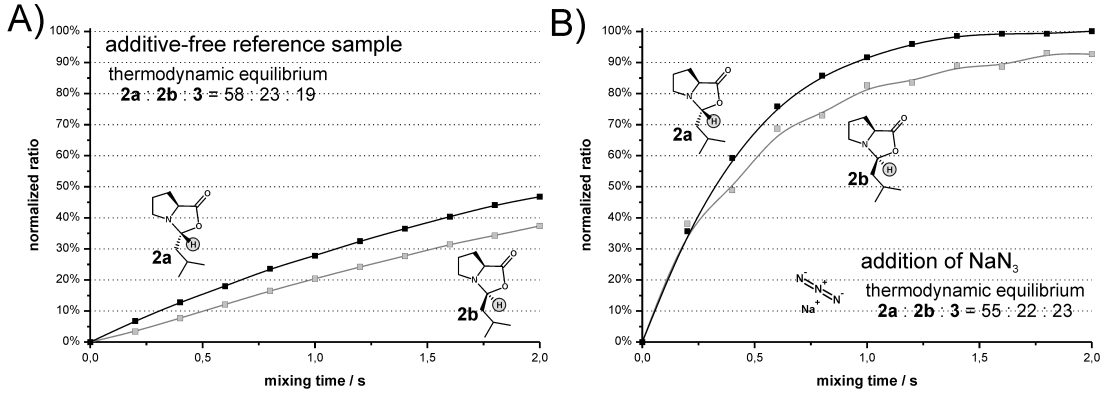

Figure 4.8: Normalized EXSY buildup curves of the oxazolidinones **2a**,**b** from the enamine **3** in the additive-free sample (A) and with NaN_3 (B) in DMSO-d_6 at 300 K. The lower values for **2b** than for **2a** in the presence of NaN_3 (B) are ascribed to the severe line broadening of the H1 resonance of **2b**.

Substitution Effects. If the direct formation of proline enamines from the corresponding oxazolidinones is really assisted by nucleophilic species in an S_N2-type ring opening mechanism, one may expect distinct substituent effects for this process. This is due to the well-known fact that S_N2 reaction are sensitive to steric hindrance so that, for instance, bimolecular nucleophilic substitution pathways in neopentyl positions are hardly viable.[24] However, since a neopentyl substituted oxazolidinone, derived from pivalalde-

hyde, cannot isomerize to the enamine, isobutyraldehyde was selected as the test aldehyde with increased steric hindrance in proximity to the ring closing site. Yet, the proline enamine amount, formed by isobutyraldehyde in DMSO, is only tiny (chapter 3.2) so that the selective 1D EXSY approach is hardly applicable. Nevertheless, we speculated that the decelerating substituent effect might be pronounced to such a degree that it causes the delayed buildup of the enamine equilibrium concentration in the reaction mixture. Therefore, to check this hypothesis, a 1D ^{1}H NMR reaction monitoring was performed on a mixture of isobutyraldehyde (c = 50 mM) with 100 mol% of L-proline in DMSO-d_6 at 300 K (Figure 4.9).

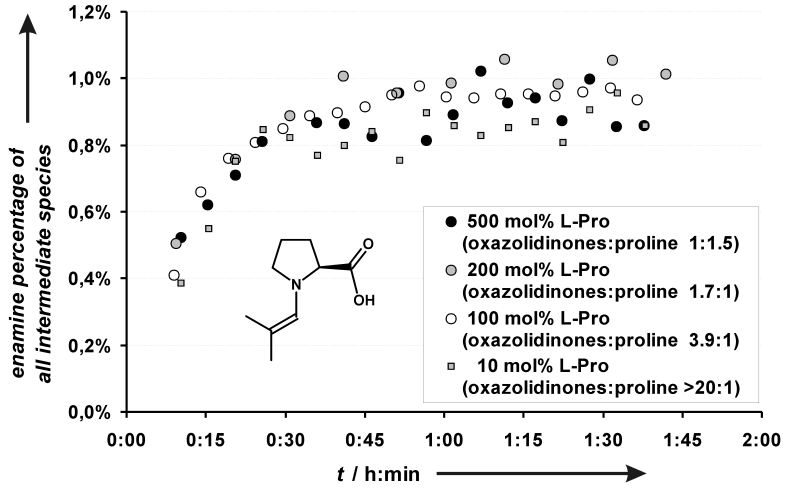

Figure 4.9: Increase of the enamine percentage of the overall oxazolidinone/enamine concentration in the case of isobutyraldehyde: The retarded establishment of the equilibrium seems (within the error range) independent of the amount of proline offered. (Oxazolidinone-proline ratios, given in brackets, were determined from the first ^{1}H spectra recorded; no exact quantification of proline was possible when applying only 10 mol%.)

Most interestingly and in striking contrast to all α-unbranched aldehydes, the equilibrium between the isobutyraldehyde-derived proline enamine and the oxazolidinones is in fact not fully established after a few minutes (*i.e.* in the first ^{1}H NMR spectrum recorded). Instead, the relative concentration of the enamine with respect to the oxazolidinones asymptotically increases over a period of approximately one hour to its equilibrium amount (Figure 4.9). We ascribe this to a decelerated formation of the enamine from the oxazolidinones. The delayed enamine buildup in the case of isobutyraldehyde hence indicates that the transition state for the formation of the enamine from the oxazolidinones is energetically more unfavorable in the case of α-branched aldehydes than in the case of aldehydes with monosubstituted α-carbon atoms. This substituent effect may thus possibly originate from the steric repulsion of the nucleophile assisting in the oxazolidinone ring opening. Nevertheless, besides the 1D EXSY approach applied above, this 1D ^{1}H NMR-observable enamine buildup now constitutes a further tool to straightforwardly study changes of the oxazolidinone-enamine interconversion rate.

For instance, the delay of the enamine formation should be altered by changing the amount of proline in case the oxazolidinone-enamine interconversion is an "concerted E2-type opening of the oxazolidinone ring by the action of an external base", as proline itself or a proline-derived oxazolidinone have been claimed previously to act as the base.[2] This is due to the fact that in both cases two proline-derived species participate in the bimolecular elimination so that the rate of enamine formation should depend on the amount of proline offered. Likewise, the addition of DBU as an external base should influence the enamine formation rate.[2] To investigate this, reaction mixtures of isobutyraldehyde with varying proline amounts, ranging from 500 mol% to 10 mol%, and with 100 mol% of proline and DBU each were prepared in DMSO. However, with all proline quantities offered, the decelerated increase of the enamine ratio was well reproduced (Figure 4.9). Likewise, the addition of 100 mol% of DBU did not alter the shape of the concentration-time curve of the enamine significantly (an increase over about 50 minutes was observed, data not shown). From these observations, we conclude again that there is no noticeable influence of bases on the interconversion rate of oxazolidinones to enamines. This rules out an E2 elimination as the enamine formation pathway from oxazolidinones.

In addition, with the help of the slow enamine formation in the case of isobutyraldehyde, the theoretically postulated proton relay pathways[7,8] can now be tested for their plausibility also in the oxazolidinone-enamine exchange. This option is based on the fact that a concerted proton relay mechanism in our experimental system is expected to include water. In such a model, the enamine formation from oxazolidinones comprises the cleavage and formation of O-H bonds and thus the eventual increase of the isobutyraldehyde-derived enamine depends—among others—on the ease of these bond cleavages and formations. Accordingly, isotope effects may be expected upon the replacement of H_2O by D_2O. Since the oxazolidinone deuteration is negligible (below 2 %) in the time window of the enamine buildup, observed isotope effects must then be attributed to the participation of D_2O in the enamine formation. To study such effects, the reaction progress in a mixture of isobutyraldehyde with 100 mol% of proline in DMSO-d_6 with 0.5 vol% of D_2O was monitored by 1D ^{1}H spectra at 300 K (Figure 4.10A).

Indeed, the enamine buildup is significantly slower in the presence of 0.5 vol% of D_2O than in pure DMSO and the maximum enamine ratio is reached only after about 2.5 hours. Though it has not been ruled out yet experimentally that this is just a water effect rather than an isotope effect, we take this as an indication of an explicit participation of water in the enamine formation from oxazolidinones. This interpretation is furthermore supported by an observation in 1D ^{1}H NMR spectra on a reaction mixture of propionaldehyde and 100 mol% of proline in DMSO (Figure 4.10B). Here, two different broad, strongly downfield shifted ^{1}H resonances (between 12.3 ppm and 12.0 ppm) are detected that vanish in parallel to the intermediate species. These resonances hint at the presence of different strongly deshielded and rather rapidly exchanging OH protons as long as the intermediate enamine and oxazolidinone species exist. Altogether, these observations may suggest that a proton relay mechanism with the participation of water is actually operative in the oxazolidinone-enamine interconversion.

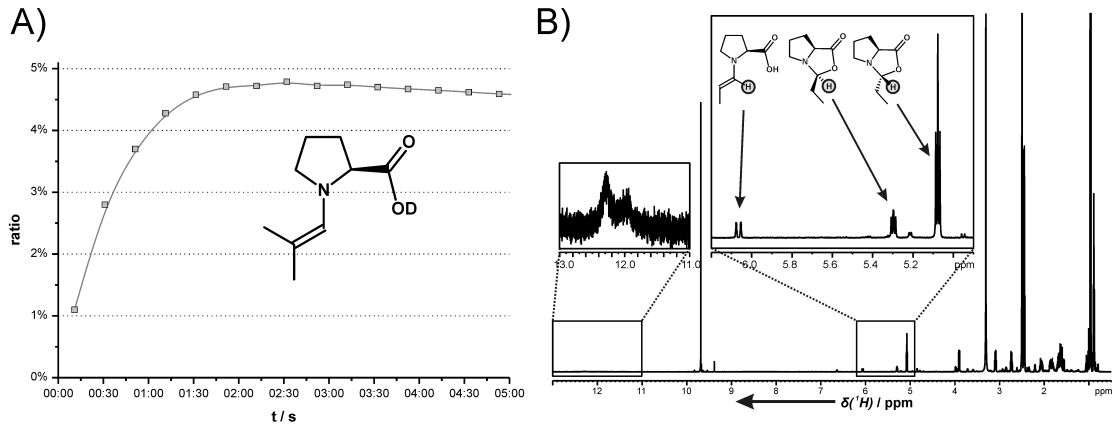

Figure 4.10: A) Increase of the enamine percentage of the overall oxazolidinone/enamine concentration in the case of isobutyraldehyde with 100 mol% of proline in DMSO-d_6 with 0.5 vol% of D_2O at 300 K; B) 1D ^{1}H NMR spectrum of a mixture of propionaldehyde and 100 mol% of proline in DMSO-d_6 at 300 K.

Mechanistic Proposal. Based on these results, along with the evidence for a nucleophilic assistance in this process and with the DOSY findings of the interaction between the enamine and DMSO molecules (chapter 3.2),[1] we propose the following mechanism for the direct formation of proline enamines from oxazolidinones in dipolar aprotic solvents. The enamine formation from oxazolidinones (ring-chain tautomerization) is assisted by nucleophiles and proceeds via a proton relay mechanism that is mediated by a cooperative H-bond network. This may be formed from solvent molecules with exclusive H-bond acceptor properties together with the carboxylic moiety of the enamine and water, being present as a product of the condensation step and/or as a solvent impurity. Our idea is exemplarily illustrated in Figure 4.11.

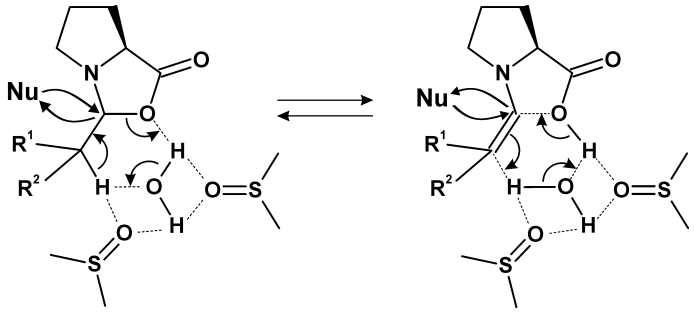

Figure 4.11: Mechanistic proposal for the oxazolidinone-enamine ring-chain tautomerization via a nucleophile-assisted proton relay mechanism within a cooperative H-bonded network formed from water, H-bond acceptor solvent molecules, and the carboxylic moiety of the enamine.

Our mechanistic proposal takes up the H-bonding interaction between the enamine and solvent molecules that had been used to rationalize the enamine stabilization in dipolar aprotic solvents and rationalizes the two strongly deshielded, broad proton resonances. It is furthermore basically in line with the theoretical studies on the proton relay mechanisms for the enamine formation from carbinolamines[7] and from iminium zwitterions.[8]

However, the additional assistance of an external nucleophile in our model helps to overcome the problems of the formal *syn*-eliminations in common proton relay pathways. The observed substituent effect in the case of isobutyraldehyde is accounted for by the fact that the nucleophilic assistance is hampered by steric shielding of the oxazolidinone carbon atom. In addition, assuming the ring-chain tautomerization to proceed via a six-membered transition state the isobutyraldehyde-enamine formation is expected to be additionally decelerated because the transition state suffers from one of the aldehyde methyl group being oriented in the stereoelectronically unfavorable axial position.

Conclusion

In summary, we have investigated the interconversion of proline enamines and oxazolidinones by a selective 1D EXSY technique. Urea derivates are evidenced to mainly accelerate the interconversion of the isomeric oxazolidinones. In addition, they are suggested to partially stabilize aldiminium zwitterions in solution through H-bonding interactions. In contrast, the enamine-oxazolidinone exchange is revealed to be accelerated by nucleophilic, but not by basic additives. If this nucleophilic assistance is hampered by steric crowding in the α-position, the enamine formation is drastically delayed and can be followed by 1D ^{1}H NMR reaction monitoring. In addition, a decelerating deuterium isotope effect on the buildup of the enamine concentration is observed. Based on these and earlier findings, a mechanistic proposal for the direct enamine formation from oxazolidinones in dipolar aprotic solvents is made: In this ring-chain tautomerization, a nucleophilically assisted proton relay mechanism through a cooperative H-bond network, comprising the carboxylic group of the enamine, water, and H-bond acceptor solvent molecules, is operative.

4.2 References

[1] M. B. Schmid, K. Zeitler, R. M. Gschwind, *Angew. Chem. Int. Ed.* **2010**, *49*, 4997–5003.

[2] D. Seebach, A. K. Beck, D. M. Badine, M. Limbach, A. Eschenmoser, A. M. Treasurywala, R. Hobi, W. Prikoszovich, B. Linder, *Helv. Chim. Acta* **2007**, *90*, 425–471.

[3] S. L. Poe, A. R. Bogdan, B. P. Mason, J. L. Steinbacher, S. M. Opalka, D. T. McQuade, *J. Org. Chem.* **2009**, *74*, 1574–1580.

[4] O. Reis, S. Eymur, B. Reis, A. S. Demir, *Chem. Commun.* **2009**, 1088–1090.

[5] X. Companyó, G. Valero, L. Crovetto, A. Moyano, R. Rios, *Chem. Eur. J.* **2009**, *15*, 6564–6568.

[6] N. El-Hamdouni, X. Companyó, R. Rios, A. Moyano, *Chem. Eur. J.* **2010**, *16*, 1142–1148.

[7] M. P. Patil, R. B. Sunoj, *J. Org. Chem.* **2007**, *72*, 8202–8215.

[8] A. Sharma, R. Sunoj, *Angew. Chem. Int. Ed.* **2010**, *49*, 6373–6377.

[9] A. D. Bain, *Prog. Nucl. Magn. Reson. Spectrosc.* **2003**, *43*, 63–103.

[10] S. Lakhdar, T. Tokuyasu, H. Mayr, *Angew. Chem. Int. Ed.* **2008**, *47*, 8723–8726.

[11] U. Grošelj, D. Seebach, D. M. Badine, W. B. Schweizer, A. K. Beck, I. Krossing, P. Klose, Y. Hayashi, T. Uchimaru, *Helv. Chim. Acta* **2009**, *92*, 1225–1259.

[12] I. Mager, K. Zeitler, *Org. Lett.* **2010**, *12*, 1480–1483.

[13] M. Baidya, S. Kobayashi, F. Brotzel, U. Schmidhammer, E. Riedle, H. Mayr, *Angew. Chem. Int. Ed.* **2007**, *46*, 6176–6179.

[14] I. Kaljurand, A. Kütt, L. Sooväli, T. Rodima, V. Mäemets, I. Leito, I. A. Koppel, *J. Org. Chem.* **2005**, *70*, 1019–1028.

[15] K. T. Leffek, P. Pruszynski, K. Thanapaalasingham, *Can. J. Chem.* **1989**, *67*.

[16] J. F. Coetzee, G. R. Padmanabhan, *J. Am. Chem. Soc.* **1965**, *87*, 5005–5010.

[17] H. Mayr, M. Patz, *Angew. Chem. Int. Ed.* **1994**, *33*, 938–957.

[18] H. Mayr, T. Bug, M. F. Gotta, N. Hering, B. Irrgang, B. Janker, B. Kempf, R. Loos, A. R. Ofial, G. Remennikov, H. Schimmel, *J. Am. Chem. Soc.* **2001**, *123*, 9500–9512.

[19] F. Brotzel, B. Kempf, T. Singer, H. Zipse, H. Mayr, *Chem. Eur. J.* **2007**, *13*, 336–345.

[20] J. Ammer, M. Baidya, S. Kobayashi, H. Mayr, *J. Phys. Org. Chem.* **2010**, *23*, 1029–1035.

[21] T. B. Phan, C. Nolte, S. Kobayashi, A. R. Ofial, H. Mayr, *J. Am. Chem. Soc.* **2009**, *131*, 11392–11401.

[22] T. B. Phan, H. Mayr, *J. Phys. Org. Chem.* **2006**, *19*, 706–713.

[23] C. D. Ritchie, R. E. Uschold, *J. Am. Chem. Soc.* **1967**, *89*, 1721–1725.

[24] R. Brückner, *Organic Mechanisms - Reactions, Stereochemistry and Synthesis* (Ed.: M. Harmata), Springer, Heidelberg, **2010**.

5 The Proline-Catalyzed Aldol Condensation

Article

"NMR Investigations on the Proline-Catalyzed Aldehyde Self-Condensation: Mannich Mechanism, Dienamine Detection, and Erosion of the Aldol Addition Selectivity"

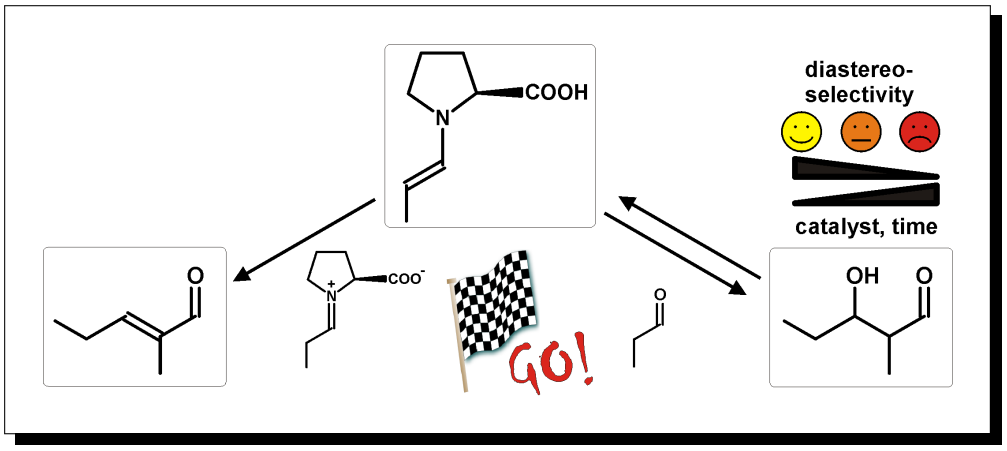

The synthesis of the aldol dimers **2a**,**b** was performed by Johannes Franz from the working group of Dr. Kirsten Zeitler.

Markus B. Schmid, Kirsten Zeitler, and Ruth M. Gschwind

J. Am. Chem. Soc. **2010**, *submitted for publication.*

5.1 Abstract

The proline-catalyzed self-condensation of aliphatic aldehydes in DMSO with varying amounts of catalyst was studied by *in situ* NMR spectroscopy. The reaction profiles and intermediates observed as well as deuteration studies reveal that the proline-catalyzed aldol addition and condensation are competing, but not consecutive reaction pathways. In addition, the rate determining step of the condensation is suggested to be the C-C bond formation. Our findings indicate the involvement of two catalyst molecules in the C-C bond formation of the aldol condensation, presumably by the activation of both the aldol acceptor and donor in a Mannich-type pathway. This mechanism is shown to be operative also in the oligomerization of acetaldehyde with high proline amounts, for which the first *in situ* detection of a proline dienamine was accomplished. In addition, the diastereoselectivity of the aldol addition is evidenced to be time-dependent since it is undermined by the retro-aldolization and the competing irreversible aldol condensation.

5.2 Manuscript

Introduction

Detailed insights into the mechanisms of both intended organic reactions and unwanted side reactions are of utmost importance for a better control and for the rational optimization of reaction conditions in synthetic organic chemistry. Nevertheless, such knowledge is often difficult to obtain since it is in many cases intimately connected to the detection of elusive reaction intermediates. Accordingly, in the growing field of asymmetric organocatalysis,[1–5] where the development of novel synthetic applications has been largely predominant over mechanistic investigations,[6–11] reaction optimization can often still be characterized as empirical rather than rational. For instance, the proline-catalyzed intermolecular aldol reaction,[12] archetypical for the concept of enamine catalysis by secondary amines in general,[13–18] has been reported right from its beginnings to be accompanied by the aldol condensation reaction;[12] yet, despite proline being an important bifunctional catalytic system of model character whose mechanistic features are still a matter of intensive theoretical[19–22] and experimental[6–11,23] studies, it has not be clarified unambiguously up to now whether the aldol addition and the aldol condensation must be regarded as *competing* or as *consecutive* reactions. However, such knowledge should help to rationally optimize reaction protocols for the suppression of the aldol condensation as an unwanted side reaction in asymmetric aldol addition reactions.[24] On the other hand, based on a better mechanistic understanding of the ongoing reactions, one may improve the outcome of organocatalytic carbonyl condensations. The potential of this modern route for the generation of versatile α,β-unsaturated carbonyl compounds has been recognized and successfully exploited recently.[25,26] Concerning the mechanistic understanding of the amine-catalyzed aldol condensation, it has been shown that α,β-unsaturated ketones are not obtained from the corresponding aldol products by treatment with proline in acetone/chloroform.[27] In addition, from a kinetic study on the pyrrolidine-catalyzed aldehyde-aldehyde condensation in chloroform, evidence has been reported that the reaction is of second order in the catalyst concentration.[25] A second-order pathway for the C-C bond-forming step was also suggested by kinetic studies on the acetaldehyde-condensation in aqueous and salt solution with high catalyst concentrations.[28] Based on these experimental findings, Mannich-like mechanisms for the proline-catalyzed aldol condensation have been proposed in contrast to the presumably more intuitive pathway of aldol addition and subsequent dehydration. Nonetheless, comprehensive mechanistic studies were not possible so far, in particular since more detailed investigations have been impeded for a long time by the inability to detect and characterize proline enamines *in situ*. Only recently could this key intermediate of most of the mechanistic proposals be snared *in situ* by means of NMR spectroscopy.[9] It should now allow access to more detailed insights into the underlying reaction mechanism.

Here, we present our mechanistic studies on the proline-catalyzed self-condensation of aliphatic aldehydes in DMSO. Starting from the monomeric aldehyde or from the aldol dimer, online-NMR spectroscopy was applied to monitor the aldol addition, the aldol condensation and the retro-aldolization, which were shown to proceed in parallel within our samples. This was achieved with the help of characteristic well-resolved resonances of the different species (see Figure 5.11 in the Supporting Information, chapter 5.3). Based on the reaction profiles obtained and the intermediates observed, we can now thoroughly interpret the ongoing events in the reaction mixtures with regard to the formation pathway of the condensation product. Furthermore, a deuteration study by adding small amounts of D_2O to the reaction mixtures allowed us to follow the progress of the α-deuteration via the reaction intermediates and to track the accumulation of deuterium in the reaction products. The observed reaction profiles and the degrees of deuteration rule out the existence of an aldol addition-dehydration pathway for the formation of the condensation product under proline-catalysis in DMSO. Instead, a Mannich-like mechanism, most probably via a double aldehyde-activation, is evidenced for the proline-catalyzed self-condensation of aliphatic aldehydes in DMSO. In addition, the first detection of a proline-derived dienamine is presented. In the context of parallel activation and reaction pathways, we demonstrate that the selectivity of the aldol addition reaction is dependent on the reaction time because of the competition between the reversible aldol addition and the irreversible aldol condensation.

Results and Discussion

Model Reaction and General Mechanistic Considerations. As a model system for our investigations on the proline-catalyzed self-condensation of aliphatic aldehydes, propionaldehyde **1a** was selected as the starting material (c = 50 mM), 100 mol% of L-proline as the amine catalyst and DMSO-d_6 at 300 K as the solvent (Figure 5.1A). This choice was based on our recent study that had allowed us to detect *in situ* the elusive proline enamine and further intermediate species in the intermolecular aldol reaction for the first time.[9] By thus presenting new options for the interpretation of reaction profiles, these experimental conditions were expected to also bring forward the mechanistic understanding of the proline-catalyzed aldehyde-condensation reaction.

As a first simplistic issue, the relationship between the proline-catalyzed aldol addition and the aldol condensation should be addressed, *i.e.* whether the aldol addition and aldol condensation are consecutive (Figure 5.1B) or competing (Figure 5.1C) reaction steps. More detailed considerations on the potential pathways of the proline-catalyzed aldehyde self-condensation have led to the three basic mechanistic pathways, proposed in the literature (Figure 5.2A).[25,27,29–35] They can be classified by the nature of the species that are involved in the C-C bond forming steps into an aldol pathway (I), a Mannich pathway (II), and a double-activation Mannich-type pathway (III).

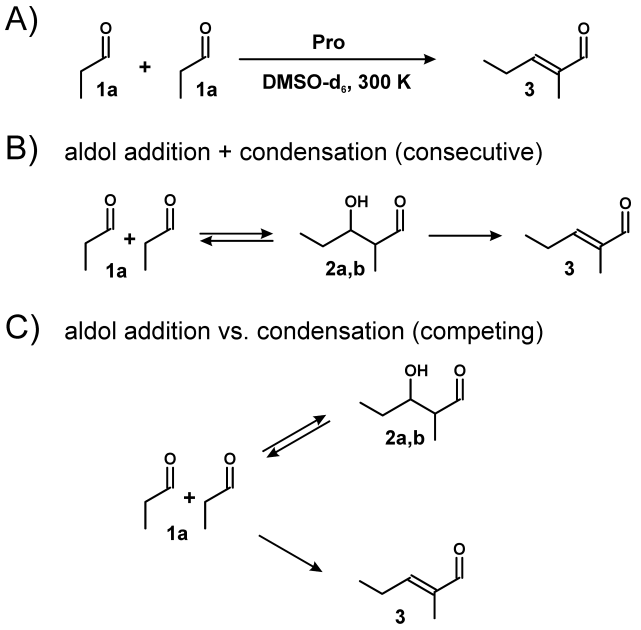

Figure 5.1: A) The model reaction investigated: the proline-catalyzed self-condensation of propionaldehyde **1a**; B) and C) the aldol condensation as a process that is consecutive or competing with the aldol addition, respectively.

Pathway I initially constitutes the commonly accepted mechanism of the proline-catalyzed intermolecular aldol reaction; it is characterized by the addition of the catalyst-derived enamine **4d** of the donor aldehyde to the acceptor aldehyde molecule **1a** and is completed by hydrolysis and dehydration (or *vice versa*), like the classical aldol condensation reaction.[31–33] Pathway II corresponds to a textbook Mannich mechanism, in which the enol tautomer **1b** of the donor aldehyde adds to the iminium ion **4a**, formed from the acceptor aldehyde and the amine catalyst, followed by elimination of the catalyst.[27,29,30] A third mechanistic alternative, described by pathway III,[25,34,35] has been pointed out recently: It resembles the Mannich pathway II, but comprises the simultaneous activation of both the donor and the acceptor aldehyde as an enamine **4d** and an iminium ion **4a**, respectively, and subsequent elimination and hydrolysis steps.[a]

Forward Aldol Addition and Condensation. To distinguish between the three proposed mechanisms, we employed our recently gained knowledge on the observation of intermediates in proline-catalyzed aldol reactions.[9] On this basis, a very simple kinetic consideration should help to obtain first insight into potential condensation reaction pathways: Whatever the exact underlying mechanism of the formation of the enal **3** may be, a certain correlation between the concentration of the intermediates involved in the rate determining step and the formation rate of **3**, *i.e.* the slope of its NMR-derived concentration-time-curve, should be expected. To apply this criterion to the different potential reaction pathways,

[a] A similar dual activation of carbonyl species by proline has recently been proposed for the organocatalytic homodimerization of enones.[36]

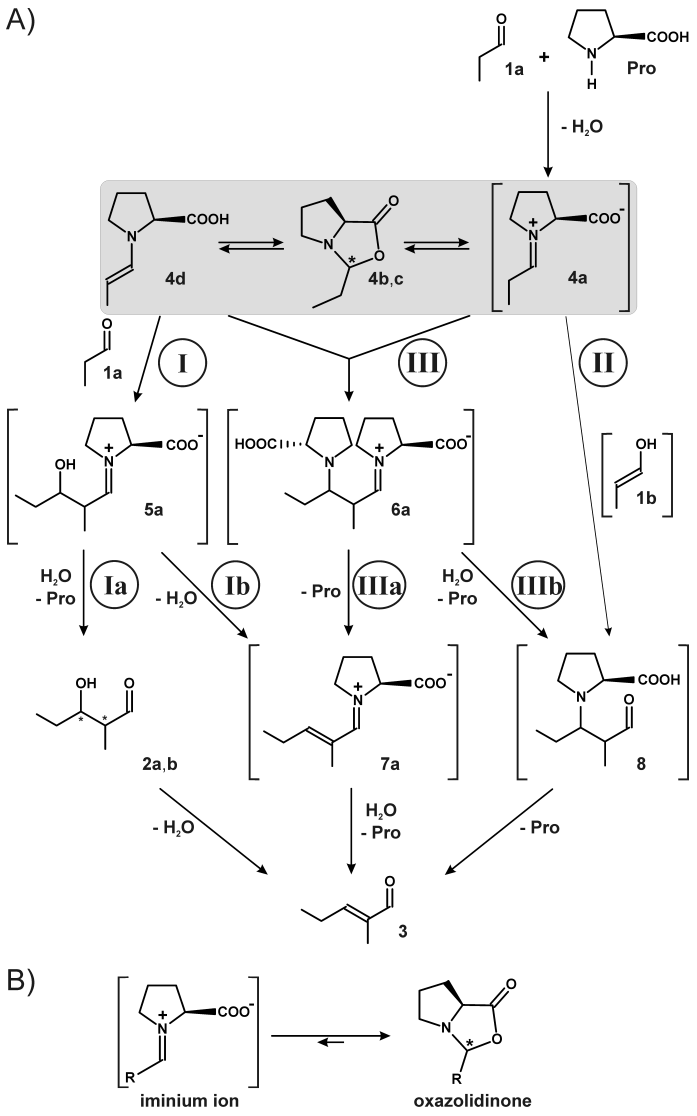

Figure 5.2: A) Possible mechanistic pathways for the process of Figure 5.1A, proposed in the literature.[25,27,29–35] (Note: Species that could not be detected in this study are shown in brackets.) B) The commonly proposed iminium-oxazolidinone-equilibrium.

we conducted the self-aldolization/condensation of propionaldehyde with different amounts of L-proline (100, 50, 20, and 10 mol%) in DMSO-d_6 at 300 K inside an NMR tube and monitored the progress of the reactions by one-dimensional proton spectra. For all the different proline concentrations applied as well as for butyraldehyde as the starting material with 100 mol% of proline, very similar characteristic features of the reaction progress were monitored. (Exemplary results for 100 mol% of proline are shown in Figure 5.3; see Figures 5.10 and 5.12 in the Supporting Information, chapter 5.3, for the results of the other experimental setups.) First, the consumption of the starting material **1a** and the steady decrease of the concentration of the proline-derived propionaldehyde intermediates (the enamine **4d** and the isomeric oxazolidinones **4b**,**c**; Figure 5.3A) are observed. In addition, the formation of two product oxazolidinones **5b**,**c** (among others) and of the

aldol dimers **2a**,**b** is evidenced as well as their disappearance (Figure 5.3B; maximum concentrations of **5b**,**c** after about 100 and 200 minutes and of **2a**,**b** after about 70 and 100 minutes, respectively). Finally, the aldehyde self-condensation product **3** is formed irreversibly (Figure 5.3C) in about 90 % yield after 12 hours (The molar ratio on the y axis refers to the initial concentration of the aldehyde **1a**; see the Supporting Information, chapter 5.3, for observations about aldehyde substitution effects on the reactivity and the enal E/Z selectivity).

In a previous study on a crossed-aldolization/-condensation of aldehydes,[25] the constant ratio of the aldol and the condensation product throughout the reaction time could be interpreted as an indication of the competition between the two reaction pathways. However, in the case of our self-aldolization/-condensation this argument cannot be applied since **3** is the only product of the reaction, while **2a**,**b** vanish again, either because of dehydration or because of retro-aldolization (Figure 5.1B and 5.1C). Thus, the issue whether the aldol addition and the aldol condensation are consecutive or competing reaction steps must be addressed by other means. In view of the reaction profile of Figure 5.3, it is highly striking that the maximum concentration of the aldol dimers **2a**,**b** (after 75 and 105 minutes, respectively, Figure 5.3B) does not at all coincide with the maximum slope of the concentration-time-curve of the condensation product **3**, *i.e.* with its rate of formation (right at the beginning of the reaction, Figure 5.3C). According to the criterion outlined above, reaction pathway Ia (the aldol addition-hydrolysis-dehydration sequence in Figure 5.2A) can hence clearly be ruled out as the major pathway for the formation of enal **3**. Accordingly, the decrease of the concentration of the aldol dimers **2a**,**b** must be due to retro-aldolization rather than due to dehydration. In analogy, reaction pathway Ib (the aldol addition-dehydration-hydrolysis sequence, Figure 5.2A) can be analyzed with regard to its plausibility. For the formation of enal **3** from the product iminium **5a** via its dehydrated analog **7a** in this pathway, the elimination of water should be rate determining since we could show previously by cross-peak evaluation in EXSY spectra[9] that the hydrolysis of iminium ions/oxazolidinones to the corresponding aldehydes is a fast process and that, in contrast, the dehydration of aldol dimers is significantly slower (see also the next paragraph). Accordingly, in case pathway Ib were operative, the maximum formation rate of **3** would be expected to correlate with the maximum concentration of the hypothetical iminium ion **5a** (undetected in this study) and thus with the concentration of the well observed isomeric oxazolidinones **5b**,**c**, as suggested by the commonly proposed iminium-oxazolidinone equilibrium (Figure 5.2B).[9] Under these premises, the observed discrepancy between the maximum of the concentration-time-curves of **5b**,**c** and the maximum rate of formation of **3** (*cf.* Figure 5.3B and 5.3C) again indicates that pathway Ib is not the main route of the proline-catalyzed aldehyde self-condensation, either. Instead, as the formation of **3** is the faster the higher the concentration of the reactant intermediates **4b**,**c**,**d** is (*cf.* Figure 5.3A and 5.3C), processes involving these intermediates in the rate determining step are suggested by the monitored concentration-time-curves. Altogether, as a first result and in agreement with a previous study on the pyrrolidine-catalyzed alde-

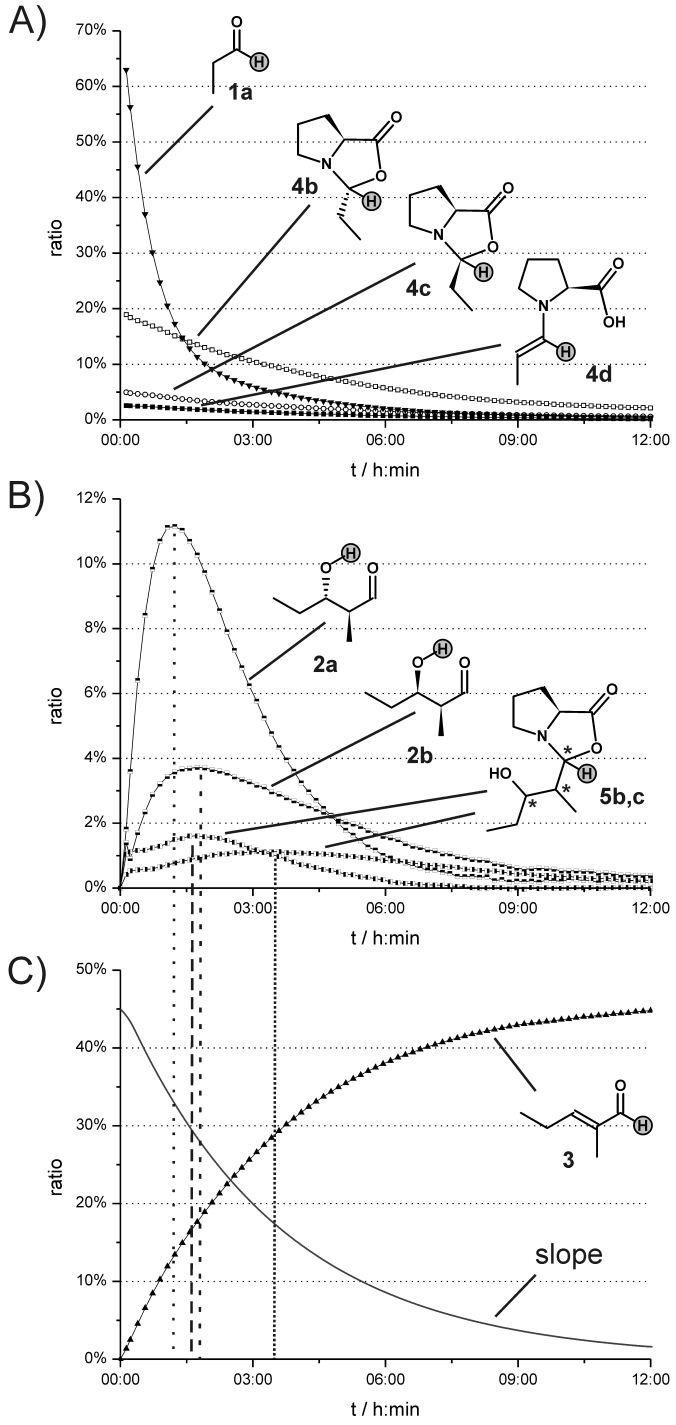

Figure 5.3: Reaction profile of the proline-catalyzed self-aldolization/condensation of propionaldehyde **1a** with 100 mol% L-proline in DMSO-d_6 at 300 K: A) starting material and intermediates derived thereof; B) aldol dimers and related oxazolidinones; C) condensation product and the slope (displayed in arbitrary units) of its buildup curve, which corresponds to the formation rate of **3**. (Those protons whose resonances were used for the monitoring, are highlighted in gray, see Figure 5.11 in the Supporting Information, chapter 5.3; note: The total amount of C_3 moieties stemming from propionaldehyde, detected in the first spectrum, was set to 100 %. Times of concentration maxima of **2a**,**b** and **5b**,**c** are marked with vertical dotted lines.)

hyde self-condensation,[25] the kinetic profile of an equimolar reaction mixture of proline and propionaldehyde **1a** in DMSO evidences that the proline-catalyzed intermolecular aldol addition and aldol condensation are not consecutive, but rather competing reaction pathways (Figure 5.1C).

Formal Dehydration of Aldoldimers via Retro-Aldolization. To corroborate this finding, we investigated in more detail whether the condensation product **3** could be generated from the aldol products **2a**,**b** under our experimental conditions. For that purpose, the aldol addition dimers **2a**,**b** were synthesized,[37] isolated as a mixture of diastereomers, dissolved in DMSO-d_6 inside an NMR tube, and exposed to benzoic acid or proline as potentially dehydrating additives. The events in the reaction mixtures were then again monitored by one-dimensional proton NMR spectra. First, we studied the influence of Brønsted acid addition: However, 100 mol% of benzoic acid, a previously employed co-catalyst in organocatalytic aldehyde self-condensations,[25,30] virtually did not effectuate any dehydration of the aldol dimers **2a**,**b** over 15 hours (data not shown). We conclude from this that the proline-catalyzed aldehyde condensation is not a Brønsted acid-catalyzed dehydration of aldol addition products. As a next approach, we added 100 mol% of L-proline to **2a**,**b** in DMSO-d_6. The concentration curves of the observed species in the reaction mixture are summarized in Figure 5.4.

In contrast to an early report on a similar approach in acetone/chloroform starting from a β-hydroxy-ketone,[27] we could easily detect the formal dehydration of the β-hydroxy-aldehydes **2a**,**b** in DMSO-d_6 under the influence of 100 mol% of proline: The concentrations of the aldol dimers **2a**,**b** decrease over time (Figure 5.4A), while the amount of the condensation product **3** increases in turn (Figure 5.4C). However, the monomeric propionaldehyde **1a**, and—in agreement with our previous EXSY findings[9]—the corresponding oxazolidinones **4b**,**c** and the enamine **4d** (Figure 5.4B) are observed in the reaction mixture, too, being indicative of the readily occurring retro-aldol reaction under our experimental conditions. Thus, to clarify whether the condensation product **3** results from **2a**,**b** via a direct dehydration (Figure 5.1B) or rather from a sequence of retro-aldol reaction and Mannich-type condensation (Figure 5.1C), the above-mentioned argumentation needs to be applied once more: In concordance with the findings for the forward aldol condensation (Figure 1), the maximum formation rate of **3** (Figure 5.4C), starting from the aldol dimers **2a**,**b**, does not coincide with the highest concentration of **2a**,**b** (at the very beginning of the reaction, Figure 5.4) or the product-oxazolidinones **5b**,**c**. This confirms that the major formation pathway of **3** is not the direct dehydration of **2a**,**b** (pathway Ia in Figure 5.2A). Instead, the formation rate of **3** shows an induction period, its maximum is reached only after 4-5 hours. Most interestingly, it is correlated to the maximum concentration of the intermediates **4b**,**c**,**d**. This supports the hypothesis that these species are involved in the rate determining step of the proline-catalyzed aldehyde condensation.

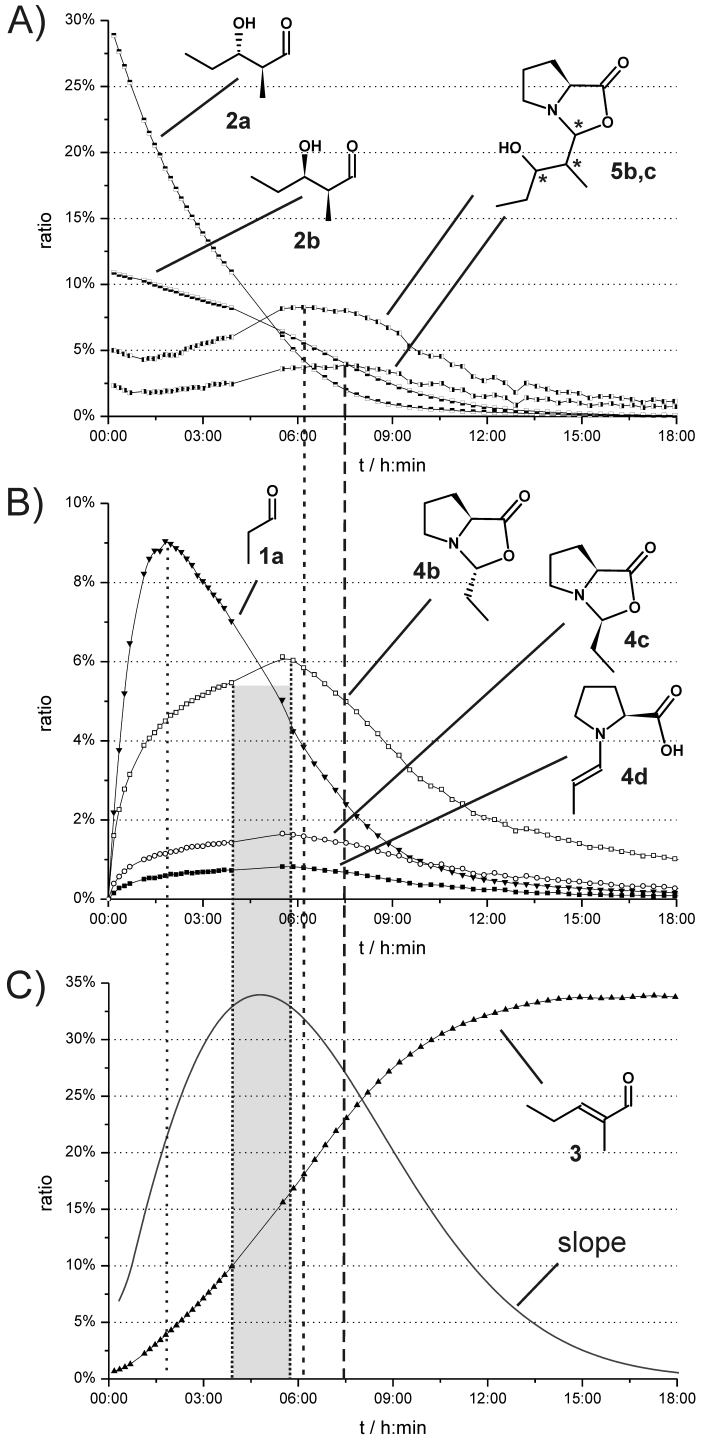

Figure 5.4: Reaction profile of the proline-catalyzed formal dehydration of the aldol addition dimers **2a**,**b** in DMSO-d_6 at 300 K under proline catalysis (100 mol%): A) aldol dimers and related oxazolidinones; B) propionaldehyde and intermediates derived thereof; C) condensation product and the slope (displayed in arbitrary units) of its buildup curve, which corresponds to the formation rate of **3**. (Notes: The total amount of C_3 moieties stemming from propionaldehyde, detected in the first spectrum, was set to 100 %. Times of concentration maxima of **1a** and **4b**,**c**,**d** are marked with vertical dotted lines. The kinks in some of the curves are due to the temporary removal of the sample from the NMR spectrometer and the associated disturbances, resulting in a larger error range for the maximum concentration of **4b**,**c**,**d**.)

Deuteration Experiments. Further evidence for the observed competition between the proline-catalyzed aldol addition and aldol condensation was collected from a deuteration study on the above-mentioned formal dehydration of the aldol dimers **2a**,**b**. In the case of a consecutive aldol condensation (Figure 5.5A, left), the degree of α'-deuteration of **3** is determined by the degree of α'-deuteration of **2a**,**b** (α' and β' refer to the α and β position of the former aldol acceptor moiety within the dimers **2a**,**b** and **3**, see Figure 5.5A), whereas in the case of a competing condensation pathway (Figure 5.5A, right), it is determined by the degree of α'-deuteration of the aldol acceptor species (*i.e.* **1a** or **4a** in Figure 5.2A). The latter case implies that there is not necessarily a causal relationship between the degrees of α'-deuteration of **2a**,**b** and **3** so that the degree of α'-deuteration of **3** may well exceed the one of **2a**,**b**. In contrast, for our experimental approach starting from non-deuterated **2a**,**b**, the consecutive condensation pathway (Figure 5.5A, left) does not allow for a higher degree of α'-deuteration of **3** compared to **2a**,**b** because it can be assumed, following well-known kinetic isotope effects,[38] that the dehydration of α'-deuterated **2a**,**b** is not faster than the one of non-deuterated **2a**,**b**. Hence, the observation of a higher degree of α'-deuteration of **3** compared to **2a**,**b** would provide further strong evidence for the aldol condensation being in competition with the aldol addition (Figure 5.1C). For these deuteration experiments, **2a**,**b** and 100 mol% of proline were mixed in DMSO-d_6, to which 1 vol% of D_2O had been added. Under otherwise identical experimental conditions, but in the absence of D_2O, we had observed the readily occurring retro-aldolization of **2a**,**b** as well as the presence of the rapidly interconverting[9] intermediates **4b**,**c**,**d** (Figure 5.4). Since both the retro-aldol reaction and the enamine-oxazolidinone exchange are associated with protonation in α-position of the carbonyl compound, the α-deuteration of propionaldehyde **1a** and the derivatives thereof could be expected to proceed with ease in the presence of D_2O. Accordingly, an accumulation of deuterons in α'-position of **2a**,**b** and **3** should be observed over time (Figure 5.5A) and the comparison of the deuteration of the different species observed should provide insights into the actual formation pathway of **3**. To be able to connect this increasing degree of α'-deuteration, *i.e.* the ratio of ^2H in α'-position, to the formation pathway of **3**, the direct α'-deuteration of the reaction products **2a**,**b** and **3** must be ruled out first. For **2a**,**b**, the lack of CH-acidity generally prevents α'-deuteration. In the case of **3**, direct vinylogous α'-deuteration was excluded by treating non-deuterated **3** with proline in DMSO/1 vol% D_2O for more than one day: No α'-deuteration was observed (data not shown), which proves at the same time the irreversibility of the condensation under our experimental conditions. Thus, the degree of α'-deuteration of **3** must be really caused by the degree of deuteration of the reaction intermediates involved.

To distinguish between the two fundamental reaction schemes (Figure 5.5A), the degrees of deuteration of the reaction products **2a**,**b** and **3** were evaluated. For **2a**,**b**, the loss of signal intensities of the α'-protons over time, compared to the aldehyde proton resonance, was ascribed to the deuteration and was hence used as a measure for the degree of α'-deuteration. In the case of **3**, the β'-methyl proton resonance of the aldol acceptor moiety was used as a probe for the deuteration in the neighboring α'-position. On the

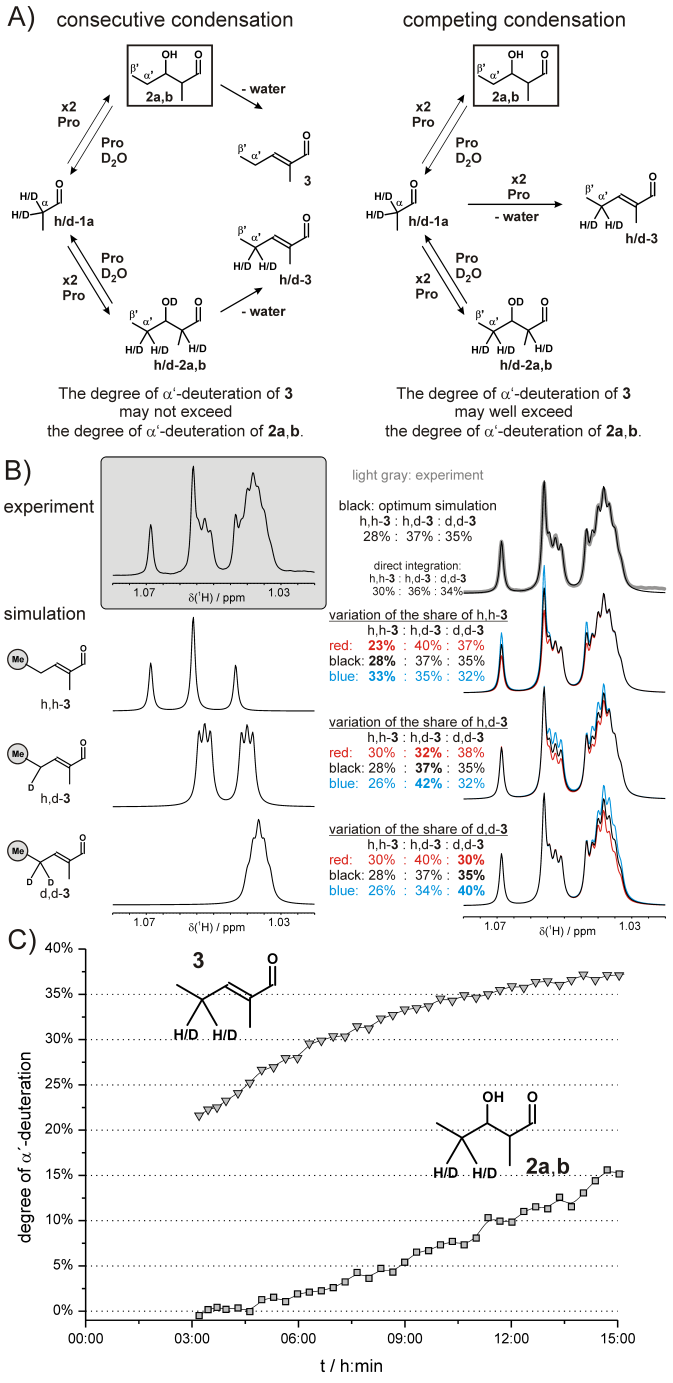

Figure 5.5: A) Possible relationships of the aldol condensation with the aldol addition, with different implications for the relative degrees of α'-deuteration of **2a**,**b** and **3**; B) exemplary deconvolution of overlapping NMR resonances of differently deuterated species of the condensation product **3**. Displayed are the experimental spectral section (left top) as well as the underlying simulated spectra of the non-, mono- and di-deuterated compounds (left rows 2 to 4). For an estimation of the error range, the experimental spectrum and simulated spectra with varying ratios of the differently deuterated species are presented (right); C) experimentally determined degrees of α'-deuteration in the course of the formal dehydration of **2a**,**b** to **3** under catalysis of 100 mol% proline in DMSO-d_6 with 1 vol% of D_2O at 300 K, supporting the general reaction scheme on the right hand side of A). (Note: Data points for the first 3 hours are not depicted because the amounts of **3** are so tiny, *cf.* Figure 2C, that an evaluation of the degree of deuteration is not reasonable.)

basis of isotope-induced chemical shift changes of the β' resonance, the amounts of h,h-**3**, h,d-**3** and d,d-**3** and hence the degree of α'-deuteration can be calculated after direct integration of the different branches of the β' resonance (see Figure 5.5B for an exemplary deconvolution of the experimental spectrum). The resulting degree of deuteration agrees very well with an exemplary simulation of the peak structure (Figure 5.5B, right top). The accuracy of this direct integration approach was furthermore supported by peak simulation with deviating shares of h,h-**3**, h,d-**3** and d,d-**3**, respectively, (see Figure 5.5B, right rows 2 to 4): Variations of the individual shares on the order of 5 percentage points would be easily detected despite the multiple resonance overlap. Accordingly, the error range of the degrees of deuteration of **3**, determined by this approach, can be estimated to be below 5 percentage points. On the basis of this good correspondance of the integration and the simulation, the more convenient integration method was used for the determination of the degrees of deuteration of **3**. The results of the evaluation of the degrees of deuteration of **2a**,**b** and **3** are shown in Figure 5.5C.

The comparison of the degrees of α'-deuteration of **2a**,**b** and **3** reveals substantially higher values for **3** than for **2a**,**b** throughout the reaction time observed. According to our above-mentioned argumentation, pathway I (Figure 5.2A) can definitely be ruled out as the formation pathway of **3**. From this observation we can conclude that the proline-catalyzed condensation of aliphatic aldehydes does not proceed via the aldol addition and a consecutive dehydration step, but rather represents a reaction pathway that competes with the aldol addition.

For the differentiation between pathways II and III, the rate determining step of the aldol condensation should be clarified first. For the proline-catalyzed aldol addition, the C-C bond formation has been shown to be rate determining.[8,38,39]b Our experimental findings suggest the same for the aldol condensation: On the one hand, EXSY analyses[9] revealed that the formation of the enamine from the aldehyde via the oxazolidinones is a fast process (opposite to a study on the amino acid-catalyzed acetaldehyde self-condensation in aqueous and salt solution[28]). In contrast, neither the aldol addition nor the aldol condensation product formation could be traced beyond the enamine by EXSY. On the other hand, the inability to detect species of type **6**, **7**, and **8** may be taken as an additional hint that the final elimination and hydrolysis steps are relatively rapid in comparison to the C-C bond formation. For the hydrolysis, this is covered experimentally by our EXSY findings[9] and also the elimination is unlikely to be rate limiting.[25] Together with the above-mentioned correlation of the maximum formation rates of **3** with the maximum concentrations of **4b**,**c**,**d**, these experimental findings suggest that the C-C bond formation is rate determining in pathways II and III. Since both these pathways of the aldol condensation share the same aldol acceptor species, a correlation of the concentration

[b] Interestingly, the rate limiting step of the proline-catalyzed *intra*molecular Hajos-Parrish-Eder-Sauer-Wiechert[40,41] aldol reaction has been shown to precede the C-C bond formation.[42] However, this may be attributed to the acceleration of the C-C bond formation by the "apparent concentration effect in the intramolecular case".[8]

of **4a** to the formation rate of **3** is expected. To check this and hence to further support the assumption that the C-C bond formation is the rate determining step in the proline-catalyzed aldol condensation, the progress of the aldol condensation was investigated for a sample of propionaldehyde **1a** and 100 mol% proline in DMSO-d_6 with 0.5 vol% of D_2O at 300 K (Figure 5.6A). The concentration of the oxazolidinone **4b** was employed once more as a measure for the concentration of the aldol acceptor iminium ion **4a** (see above and Figure 5.2B) and the slope of the concentration-time-curve of **3** was again used as a measure for the formation rate of **3**. The beneficial effect of the addition of D_2O was an increase of the information density of our investigation, in that three different aldol acceptors (h,h-**4b**, h,d-**4b**, d,d-**4b**) and three different condensation products (h,h-**3**, h,d-**3**, d,d-**3**) could be studied in parallel by using only one sample. The results of this experiment are depicted in Figure 5.6.

In the beginning of the reaction, h,h-**4b** is the only oxazolidinone present (Figure 5.6B). Then, the deuterated isotopologues h,d-**4b** and d,d-**4b** appear quite rapidly, reaching their maximum concentrations after about 20 minutes and 1 hour, respectively (Figure 5.6C,D). Likewise, h,h-**3** is the only condensation product formed in the beginning (Figure 5.6B), whereas the formation of h,d-**3** and d,d-**3** is retarded by an induction period (Figure 5.6C,D). In view of the convoluted proton spectra of the differently deuterated species and the associated deconvolution for the quantitative evaluation (see Figure 5.5B and Figure 5.14 in the Supporting Information, chapter 5.3), it is highly striking how well the maxima of the concentration of **4b** and of the slope of **3** coincide in the cases of all three isotopologues (Figure 5.6B,C,D). This suggests according to the above-mentioned reasoning that the hypothetical iminium ion **4a** (represented in its concentration-time-curve by **4b**) is in fact involved in the rate determining step of the formation of **3** in our experimental system. Thus, the C-C bond formation should be the crucial and rate determining step in the proline-catalyzed aldol condensation of aldehydes in DMSO.

Variation of the Catalyst Amount. With the knowledge that the proline-catalyzed aldol addition and aldol condensation are competing reactions and based on the experimentally supported assumption that the C-C bond formation is rate determining both in the condensation and in the addition pathway,[8,38,39] there is now a possibility to differentiate between pathway II and pathway III: This option is due to the fact that both the aldol addition reaction and pathway II of the aldol condensation comprise one catalyst molecule in the rate determining step, either as the enamine **4d** or as the iminium ion **4a**. But in contrast, following pathway III, two catalyst molecules (**4a** and **4d**) are involved in the rate determining step of the aldol condensation.[25,34,35] Thus, changes in the amount of catalyst should not have a significant impact on the competition between the aldol addition and the aldol condensation if the aldol condensation proceeds via pathway II. In contrast, if pathway III is operative for the aldol condensation reaction, lower catalyst amounts should initially favor the aldol addition whereas higher catalyst amounts should

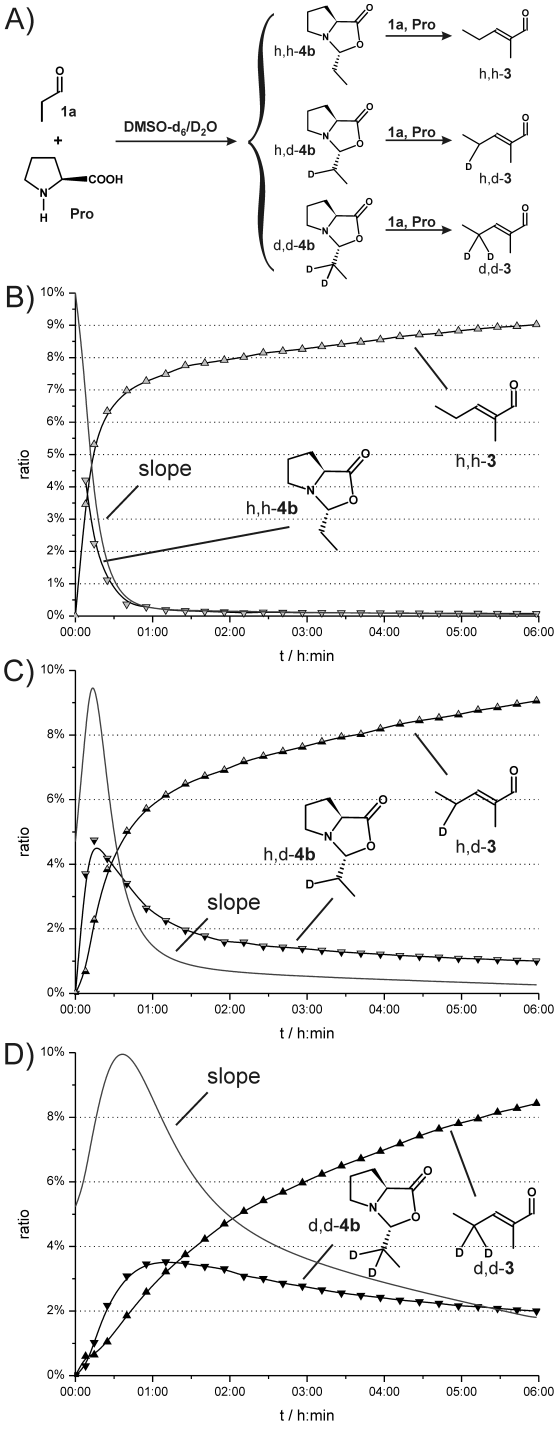

Figure 5.6: A) Hypothetical formation of differently deuterated species of **3** via differently deuterated aldol acceptors (The oxazolidinone **4b** is shown as a representative for the typically postulated, yet undetected iminium ion **4a**.); B)-D) concentration curves of selected species in a reaction mixture of propionaldehyde with 100 mol% L-proline in DMSO-d_6 with 0.5 vol% of D_2O at 300 K: B) non-deuterated **4b** and **3**; C) monodeuterated **4b** and **3**; D) di-deuterated **4b** and **3** and, in each single case, the slope (displayed in arbitrary units) of the buildup curve of **3**, which corresponds to its formation rate. (Note: The total amount of C_3 moieties stemming from propionaldehyde, detected in the first spectrum, was set to 100 %.)

increase the extent of the aldol condensation relative to the aldol addition. The revelation of such different trends for the addition/condensation rate dependences on the catalyst amount would thereby qualitatively confirm the detailed kinetic studies that have already proven the aldol condensation to be of higher order in the catalyst concentration.[8,25,28]c To check this influence of the catalyst amount on the relative reaction rates of the aldol addition and condensation, different amounts of proline (10, 20, 50 and 100 mol%) were offered to propionaldehyde **1a** in DMSO-d_6 at 300 K and the progress of the reactions was followed by one-dimensional proton spectra. Mathematical curves were fit to the concentration curves of the aldol dimers **2a**,**b** and of the condensation product **3**. The slope of the curves was then determined by differentiation and the initial value was taken as a measure of the initial formation rates of **2a**,**b** and **3**, respectively (Figure 5.7). (Note: Retro-aldolization is expected to be negligible at early stages of the reaction.).

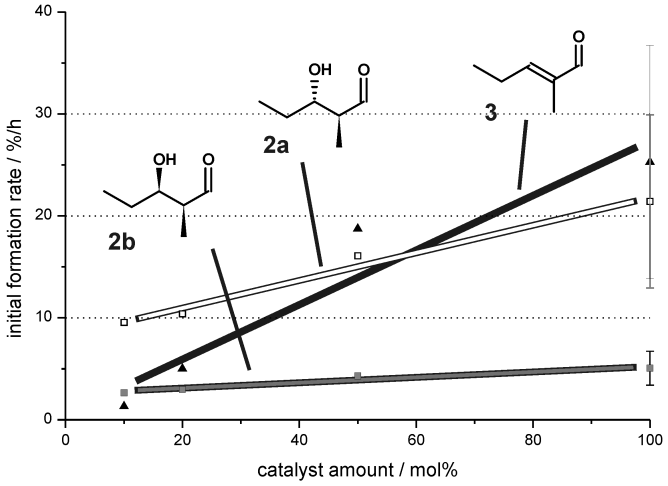

Figure 5.7: Initial formation rates of the aldol products **2a**,**b** and of the condensation product **3** in DMSO-d_6 at 300 K with varying amounts of proline offered. (For 100 mol%, the mean value of six independent experiments is displayed and the standard deviation is indicated by error bars. Inserted lines are meant as a guide to the eye.)

For all three dimer species, an increase in the initial formation rate is found with increasing amounts of proline. Without a doubt, another tendency becomes obvious from Figure 5.7 concerning the relative rates of the aldol addition and condensation: While the condensation product **3** is formed more slowly than the addition products **2a**,**b** at low catalyst concentrations (10 mol%), its formation is the fastest at high catalyst loadings (50 and 100 mol%). This observation is unimpaired by the *quantitatively* rather large error range of the data with 100 mol% of catalyst. On the contrary, it is even supported by

[c]Unfortunately, in our experimental system with complex reversible and competing reaction pathways, comparably elaborate analyses of the reaction order in proline were not practicable. This was partially also due to rather large error ranges of quantitative evaluations which we assign to the poor reproducibility of sample mixing within the NMR tube, to the potential influence of water on the reaction rates (see Figure 5.15 in the Supporting Information, chapter 5.3), to the eventual solubilization of proline, and to imperfections in fitting curves to the experimental data. We therefore concentrated on revealing meaningful qualitative trends that confirm the already reported kinetic studies.

the *qualitatively* well reproducable formation rate ranking that was obtained with varying amounts of water in the samples (Figure 5.15 in the Supporting Information, chapter 5.3). In addition, it is confirmed by the comparison of the initially formed quantities of **2a**,**b** and **3** (*cf.* Figure 5.10C and 5.10D in the Supporting Information, chapter 5.3): While **2a**,**b** exceeds **3** in early stages of the aldol addition/condensation with low catalyst loadings (10 and 20 mol%), the formation of **3** is preferred over the one of **2a**,**b** right from the beginning if higher amounts of catalyst (50 and 100 mol%) are used. These qualitatively different acceleration tendencies of the aldol addition and aldol condensation indicate that different amounts of catalyst-derived species are involved in the rate determining steps of these reactions. Therefore, as elaborated above, pathway II can be ruled out as the pathway for the aldol condensation since, just like the aldol addition, it requires one catalyst molecule in the C-C bond forming step. In contrast, pathway III of the aldol condensation is associated with two catalyst-derived molecules in the rate determining step. Thus, this pathway can well explain the stronger acceleration effect of the aldol condensation in comparison to the aldol addition upon increasing amounts of proline.

Hence we can provide further evidence that the proline-catalyzed aldol condensation of aldehydes proceeds via a double activation of both the aldol donor and the aldol acceptor molecule (pathway III in Figure 5.2A). Since the enamine **4d** is readily detected in our study, there can be little doubt that it is involved as the aldol donor species in the formation of the condensation product **3**. On the other hand, the iminium ion **4a** has been typically proposed as the electrophilic aldol acceptor species. However, since the existence of this intermediate iminium zwitterion in solution has not been proven experimentally in proline-catalyzed reactions under our experimental conditions, one may well speculate about different electrophilically activated species acting as aldol acceptors, for instance, the carbinolamines (likewise undetected in our study) or the readily observed oxazolidinones. Further experimental and theoretical approaches will be necessary to shed more light on this unsolved issue of the proline-catalyzed aldol reaction. Likewise, more investigations will be necessary to clarify whether the aldol condensation proceeds via pathway IIIa or IIIb. We cannot further address this issue here since we have not been able to detect any of the intermediates of type **6**, **7**, or **8**.

Detection of an Acetaldehyde-Derived Proline Dienamine. Nevertheless, the observation that high proline loadings favor the Mannich-type aldehyde self-condensation over the aldehyde self-aldolization is supported by our findings on the proline-catalyzed self-aldolization/-condensation of acetaldehyde **9**. As reported earlier,[9] the detection of the acetaldehyde-derived proline enamine was not feasible because of the rapid progress of the proline-catalyzed self-aldolization reaction of acetaldehyde in DMSO. While this had largely impeded the use of acetaldehyde **9** as a nucleophilic reaction partner in amine-catalyzed crossed-aldol, Mannich or Michael reactions until recently,[43–48] the proline-catalyzed asymmetric self-aldolization of **9** could be exploited synthetically to generate

the triketide 5-hydroxy-2-hexenal **12**.[31] For this acetaldehyde trimerization, an aldol-Mannich cascade (Figure 5.8A, top)[31] as well as a Mannich-aldol sequence (Figure 5.8A, middle) are possible. In contrast, **13**, the condensation product of the trimerization of **9**, must be formed by two subsequent Mannich-type condensations (Figure 5.8A, bottom). Accordingly, while the formation of the triketide **12** was predominant at proline loadings on the order of 1 mol%,[31] the condensation product **13** should be favored at higher proline amounts. To check this hypothesis, a reaction mixture of acetaldehyde **9** (c = 50 mM) and 100 mol% L-proline was prepared in DMSO-d_6 at 300 K and the progress of the reaction was monitored by 1D ^{1}H NMR spectra (Figure 5.8B).

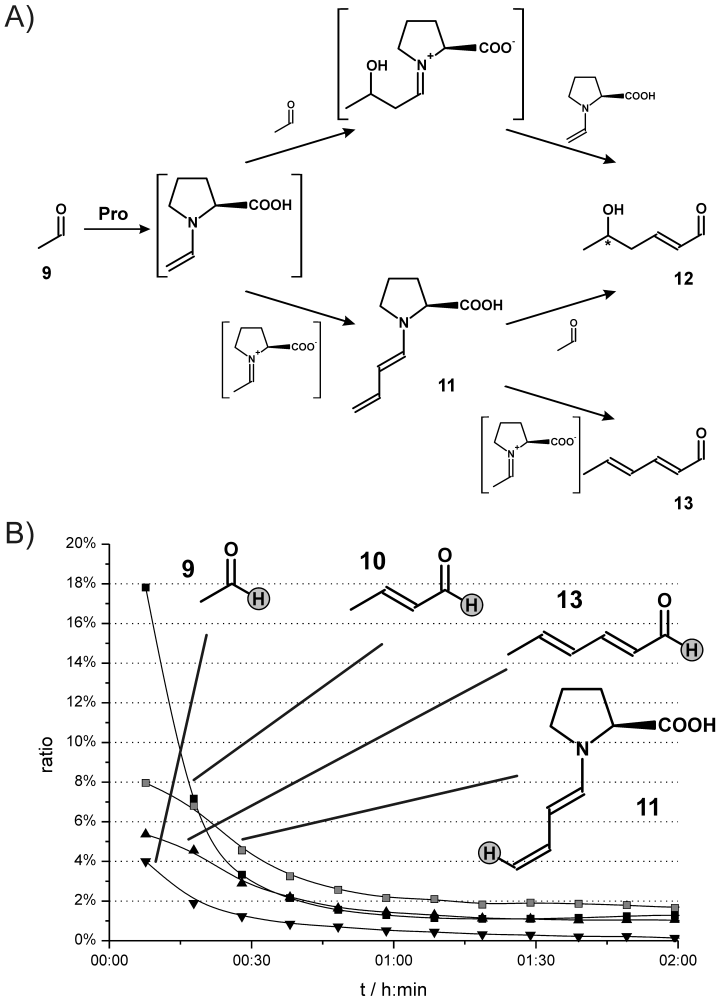

Figure 5.8: A) Potential formation mechanisms of **12** via an aldol-Mannich[31] or via a Mannich-aldol cascade and of **13** via a Mannich-Mannich sequence; B) reliably assignable intermediates in the reaction mixture and the development of their concentrations over time as well as their ^{1}H chemical shift assignments (in ppm). (Those protons whose resonances were used for the monitoring, are highlighted in gray, see Figure 5.16 in the Supporting Information, chapter 5.3; note: The total amount of C_2-units stemming from **9**, detected in the first spectrum, was set to 100 %. However, because of the incomplete characterization of the whole of the reaction mixture, the actual ratios may be substantially lower.)

Despite the complexity of the *in situ* NMR spectra of the reaction mixture, various rapidly vanishing species could be identified (because of the short lifetimes of all theses species more detailed investigations could not be performed and their assignments are based on ^{1}H NMR data, see Figure 5.16 in the Supporting Information, chapter 5.3). Among them, two condensation products, the dimeric enal **10** and the trimeric **13** (Figure 5.8B) could be assigned reliably owing to their characteristic ^{1}H chemical shifts and multiplet patterns and in comparison with literature data.[49] Additionally, a butadienyl unit was recognized that can be assigned to **11**, the proline dienamine derived from **9**. In contrast, neither aldol dimers of **9** nor the triketide **12** were detected. Hence, the presence of the condensation dimer **10** and the absence of aldol dimers of **9** can be interpreted such that, for monomeric **9**, the Mannich-type condensation is favored over the aldol addition reaction when 100 mol% of proline are applied. The same conclusion can be drawn for the formation of trimers starting from **10**: The dienamine **11** should, as the common intermediate, in principle allow for the aldol addition to the triketide **12** and for the condensation to **13**. But only **13** is detected experimentally. Altogether, this preliminary study of the proline-catalyzed self-aldolization/-condensation in DMSO corroborates our finding that high proline loadings favor the aldol condensation over the competing aldol addition and that hence a Mannich-type mechanism with a two-fold substrate activation underlies the condensation reaction. In addition, these investigations unearth the first *in situ* proline dienamine. Thus, they should moreover guide the way towards the elucidation of mechanistic issues of the growing field of dienamine catalysis.[50–57]

Time-Dependence of the Diastereoselectivity of the Aldol Addition. Another interesting finding of our studies, closely associated with the competitive nature of aldol addition and aldol condensation, concerns an issue that has not been addressed so far to our knowledge: the time-dependence of the diastereoselectivity of proline-catalyzed intermolecular aldol reaction of aldehydes. As can be seen from Figure 5.3B and 5.4A, the time-dependent appearance and vanishing is qualitatively different for the diastereomeric aldol products **2a** and **2b** in DMSO and in DMF alike (Figure 5.17 in the Supporting Information, chapter 5.3). In addition, Figure 5.10C (Supporting Information, chapter 5.3) reveals that these differences depend on the catalyst amount, too. As a synopsis of the experimental approaches discussed above, the ratio of the two aldol products **2a** and **2b**, hence the diastereoselectivity of the reaction, is depicted in Figure 5.9A.

For all catalyst amounts sampled, ranging from 10 to 100 mol%, a decrease of the ratio of **2a**:**2b** over time is observed. The more catalyst is employed, the steeper is this decay, for instance, with 100 mol% of proline, the diastereomeric ratio drops within 3 hours from 4:1 to 2:1. We attribute this effect to the different rates of the retro-aldolization of the aldol dimers **2a** and **2b** together with the competition of the aldol addition and the aldol condensation for the monomeric species (Figure 5.9B): The condensation withdraws the monomeric aldehyde(**1a**)-derived species of type **4** irreversibly from the equilibrium

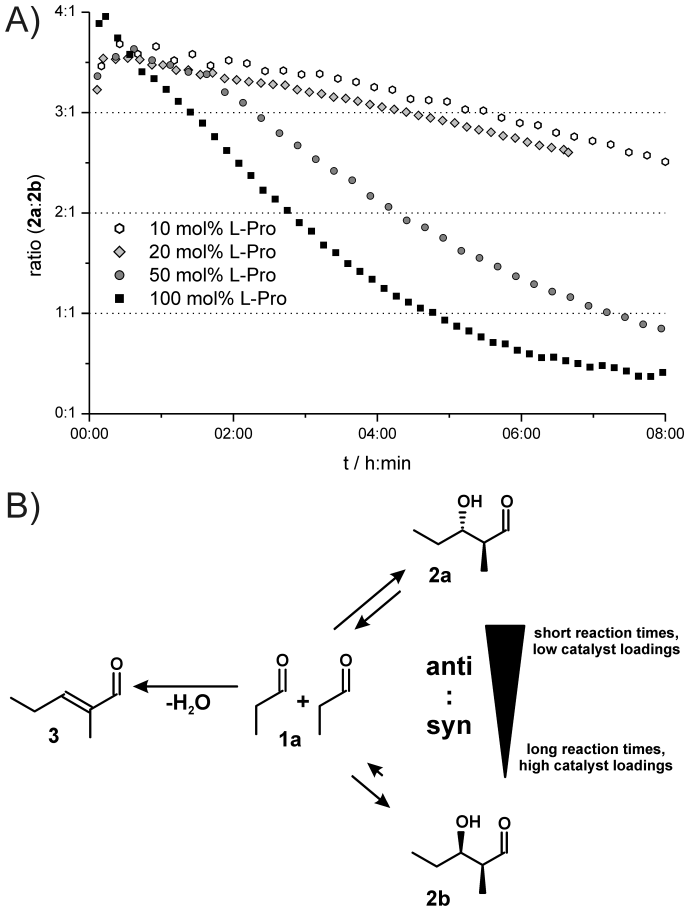

Figure 5.9: A) Dependence of the product ratio **2a**:**2b** of the proline-catalyzed self-aldolization of **1a** on the reaction time and on the amount of proline offered; B) graphical summary of the parameters and reaction pathways influencing the diastereoselectivity of the proline-catalyzed aldol addition of **1a**.

between aldolization and retro-aldolization. However, the retro-aldol reaction is obviously significantly faster for **2a** than for **2b** (see Figure 5.4A). Thus, a faster disappearance of the mainly formed **2a** is observed, which leads to a decrease in the diastereomeric ratio of the aldol products. Since the rates of both the aldol addition (thus most probably also of the retro-aldol reaction) and the aldol condensation are enhanced by higher catalyst amounts (see Figure 5.7), the steeper decays in the selectivity-time-curves with 50 and 100 mol% (Figure 5.9A) are readily rationalized. In summary, this study demonstrates that, in the mechanistically complex field of amine catalysis, unwanted competing side reactions may deteriorate the results of seemingly well planned synthetic strategies. Therefore, such potential effects on the stereochemical outcome should be taken into account when choosing appropriate reaction conditions for amine-catalyzed intermolecular aldol reactions. In particular, based on our results on the erosion of the diastereoselectivity of the aldol addition, it is therefore highly advisable to optimize catalyst loadings as well as reaction times in order to find the optimum balance between conversions and selectivities in proline-catalyzed

aldol reactions. This is another illustrative example that it is not always quantity (in terms of reaction times and catalyst loadings) that counts in catalysis, but quality (in terms of precise reaction design and control). Since the time-dependence of the diastereoselectivity in our case originates from two competing reactions with different mechanisms and hence reversibility properties, proline may be regarded here as a bifunctional model system for amine catalysts with dual activation modes. With respect to the growing field of organocatalytic domino reactions,[58–60] typically comprising manifold alternating activation modes, too, our study hence urges caution when designing the reaction cascade. On the other hand, depending on the catalyst and substrate structures, the time-dependence of the diastereoselectivity may also be assumed to be positive under certain circumstances and hence to be converted into a welcome tool. Altogether, our study outlines that, by rapid sampling of the diastereoselectivity of an organocatalytic reaction at distinct points in time, such detrimental or desired effects can be prevented or exploited, respectively.

Conclusion

We have presented our NMR spectroscopic study on the proline-catalyzed self-condensation of aliphatic aldehydes in DMSO. By a detailed interpretation of the NMR-monitored reaction profiles of the condensation, starting from the monomeric aldehyde and from the aldol dimers, respectively, we have provided evidence that the aldol addition and the aldol condensation are *competing*, but not *consecutive* reaction pathways. This was deduced from the observation that the maximum formation rate of the condensation product does not correspond to the maximum concentration of the aldol addition products, but to the one of the aldehyde-proline adducts. This result was confirmed by the formal dehydration of the aldol dimers in the presence of proline and D_2O for which a higher degree of α'-deuteration of the condensation product was found in comparison to the aldol dimers. Additionally, it was observed that the acceleration of the aldol condensation by increasing the catalyst loading is more pronounced than for the competing aldol addition. Thus, it is concluded that two catalyst molecules are involved in the rate determining step of the aldol condensation which is suggested by our experimental findings to be the C-C bond formation. Accordingly, a Mannich-type reaction pathway, including the activation of both the aldol acceptor and the aldol donor, is indicated for the proline-catalyzed self-condensation of aldehydes. This can also rationalize the preference of the aldol condensation over the aldol addition when high amounts of catalyst are applied in the proline-catalyzed oligomerization of acetaldehyde. In this reaction mixture, the first *in situ* detection of a proline dienamine was accomplished. Finally, we could demonstrate the time-dependence of the stereoselectivity of the aldol addition, resulting from the competitive nature of the aldol addition and condensation. Altogether, by recommending careful choices of catalyst loadings and reaction times, in particular in the case of amine catalysts with more than one potential activation mode, our findings can be expected to aid in optimizing synthesis protocols for both organocatalyzed aldol additions and aldol condensations.

5.3 Supporting Information

Experimental Section

All monitored reactions were conducted inside standard 5 mm NMR tubes by adding freshly distilled aldehyde **1a** or a mixture of **2a**,**b** or **3** (30 μmol, each) to a suspension of L-proline (10, 20, 50 or 100 mol%) in 0.6 mL of DMSO-d_6 (optionally with 0.5 or 1 vol% of D_2O). The NMR tube was transferred to the spectrometer immediately after the mixing of all reacting components.

NMR measurements were performed at 300 K on a Bruker Avance DRX 600 (600.13 MHz) and on a Bruker Avance III 600 (600.25 MHz) spectrometer, the latter equipped with a TCI cryoprobe. NMR data were processed and evaluated with Bruker´s TOPSPIN 2.1, the included DAISY software was used for the simulation of NMR spectra. The concentration-time-curves of the observed aldol addition and condensation products were fit and its slope was calculated with the help of Origin 6.0.

The aldol dimers **2a**,**b** were synthesized according to a slightly modified literature procedure of MacMillan and coworkers.[37]

Additional Information

Proline-Catalyzed Self-Aldolization/-Condensation of 1a with Different Amounts of Catalyst

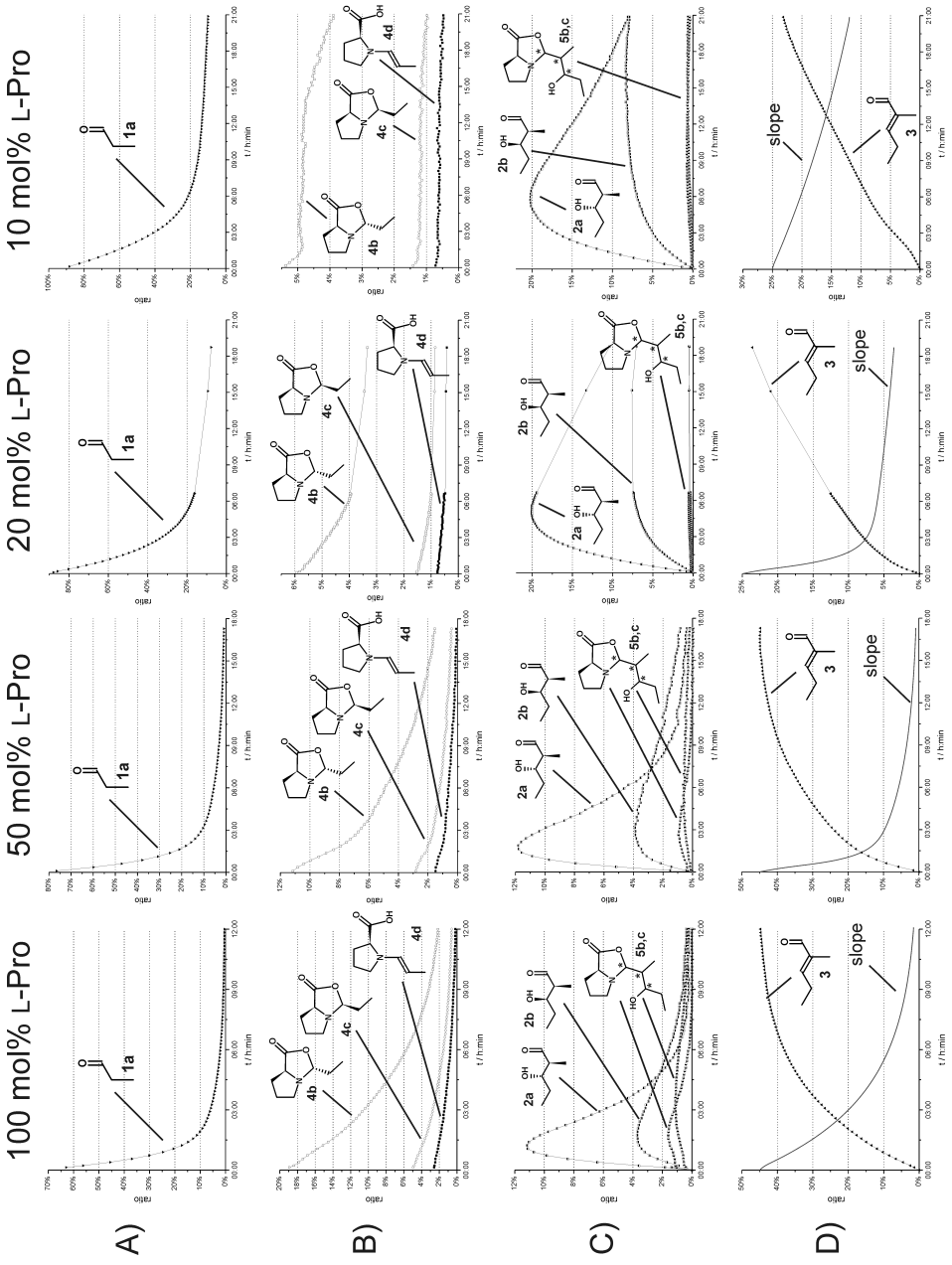

Figure 5.10: Reaction profiles of the proline-catalyzed self-aldolization/condensation of propionaldehyde with 100 mol% (1st column), 50 mol% (2nd column), 20 mol% (3rd column), and 10 mol% (4th column) of L-proline in DMSO-d_6 at 300 K: A) starting material, B) intermediates derived thereof, C) aldol dimers and related oxazolidinones, and D) condensation product and the slope (displayed in arbitrary units) of its buildup curve, which corresponds to the formation rate of **8**. (Note: The total amount of C_3 moieties stemming from propionaldehyde, detected in the first spectrum, was set to 100 %.)

NMR Spectrum and NMR Characterization of the Propionaldehyde-Derived Species

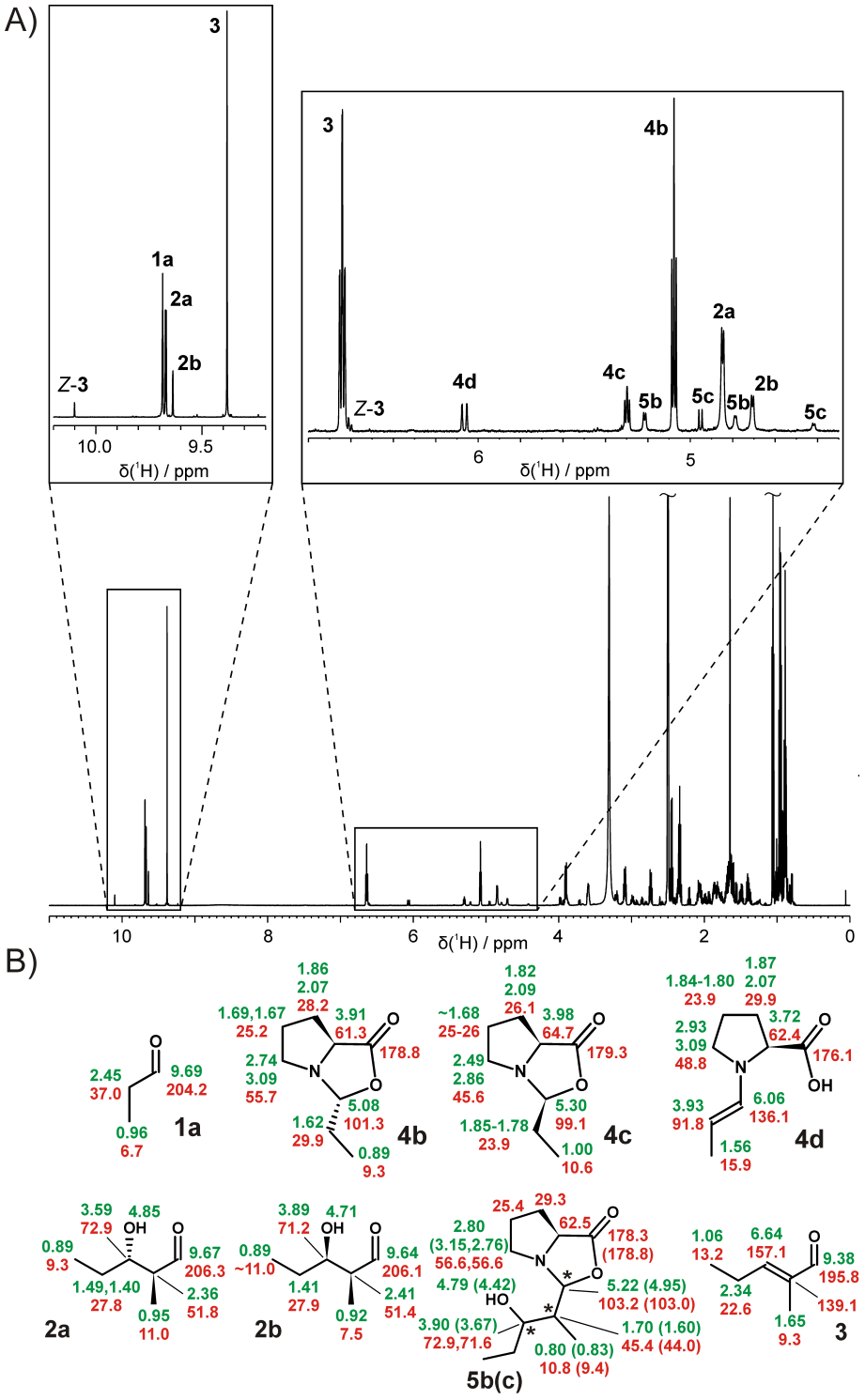

Figure 5.11: a) NMR spectrum of a reaction mixture of propionaldehyde with 100 mol% of L-proline in DMSO-d_6 at 300 K after 100 minutes; B) ^{1}H (green) and ^{13}C (red) assignment of the **1a**-derived species (referenced to the solvent residual peak).

Proline-Catalyzed Self-Aldolization/-Condensation of Butyraldehyde

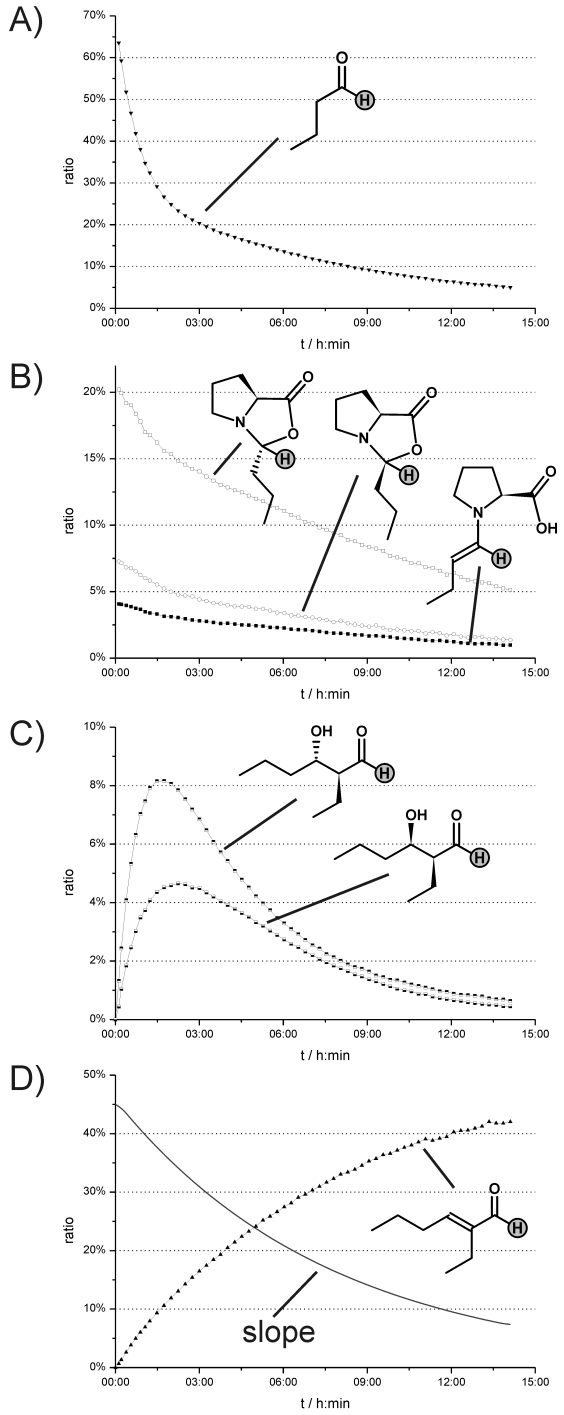

Figure 5.12: Reaction profile of the proline-catalyzed self-aldolization/condensation of butyraldehyde with 100 mol% of L-proline in DMSO-d_6 at 300 K: A) starting material, B) intermediates derived thereof, C) aldol dimers (related oxazolidinones not detected), and D) condensation product and the slope (displayed in arbitrary units) of its buildup curve, which corresponds to its formation rate. (Those protons whose resonances were used for the monitoring, are highlighted in gray, see Figure 5.13; note: The total amount of C_4 moieties stemming from butyraldehyde, detected in the first spectrum, was set to 100 %.)

NMR Spectrum of the Butyraldehyde-Derived Species

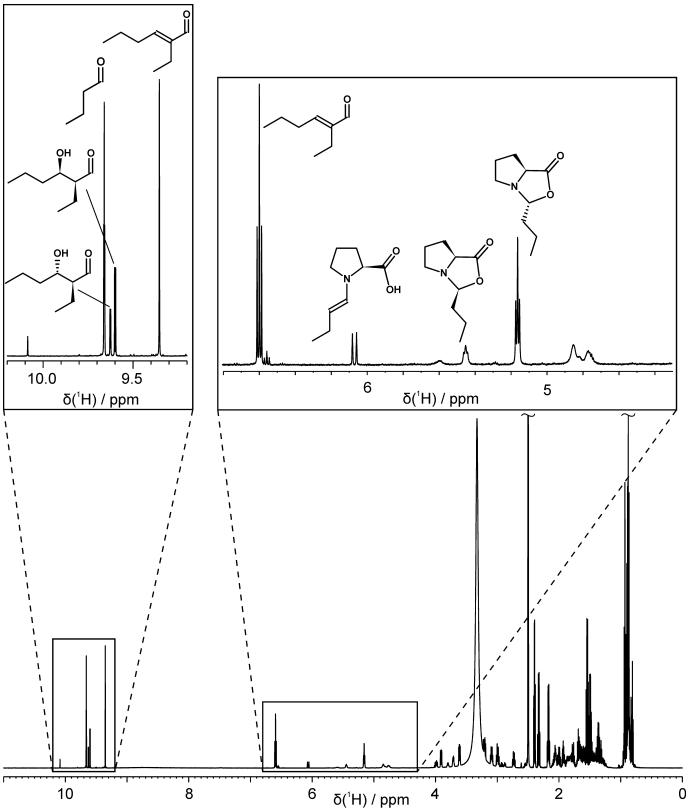

Figure 5.13: NMR spectrum of a reaction mixture of butyraldehyde with 100 mol% of L-proline in DMSO-d_6 at 300 K after 3 hours (referenced to the solvent residual peak).

Observations on Aldehyde Substitution Effects on the Reactivity and on the Enal *E*/*Z* Selectivity

As depicted in Figure 5.3 for propionaldehyde **1a** and in Figure 5.12 for butyraldehyde, the conversion of the monomeric aldehyde to the self-condensation product was found to be in the range of 80-90 % after 12 hours with 100 mol% of L-proline in DMSO at 300 K. In contrast, the self-condensation of 3-methyl-butyraldehyde hardly exceeded 7 % after 24 hours under identical experimental conditions (data not shown). This is in good agreement with a previous report on the reduced reactivity of β-branched aldehydes in amine-catalyzed self-condensation reactions.[25]

Concerning the stereochemistry of the enals, formed from aldehyde-self-condensation, the *E*-isomers were largely preferred above the *Z*-isomers. For propionaldehyde **1a**, the fraction of *Z* was below 4 % throughout the reaction time observed, for butyraldehyde below 7 %. In addition, a decrease of the absolute concentration of the *Z*-isomers was observed in both cases, which might be rationalized by their isomerization to the thermodynamically more stable *E*-configured enal. For 3-methyl-butyraldehyde in contrast, the *Z* fraction was in the range of 40 % and no decrease of this value, indicating the conversion to the *E*-isomer, was detected.

Analysis of Resonance Overlap of Differently Deuterated Species

For the distinction between h,h-**4b**, h,d-**4b** and d,d-**4b**, the methyl proton resonances were used as a probe. In this case, the separation of the different branches of the signal was too poor to allow for a reliable direct integration approach (Figure 5.12A). Therefore, for the first two hours of observation, the experimental methyl signal was approximated manually by overlapping the individual simulated spectra for h,h-**4b**, h,d-**4b** and d,d-**4b** in varying ratios until optimum congruence with the experimental spectrum. After two hours, the shares of h,h-**4b**, h,d-**4b** and d,d-**4b** were constant for the remaining time of investigation. From these simulated ratios, the absolute amounts of h,h-**4b**, h,d-**4b** and d,d-**4b** were obtained with the help of the easily accessible total amount of **4b**. Again, the accuracy of this simulation approach was confirmed by purposefully varying the individual amounts of the differently deuterated species of **4b** within the simulations (Figure 5.12B): Variations of 5 percentage points from the optimum simulation values lead to noticeable deviations of the simulated from the experimental spectra.

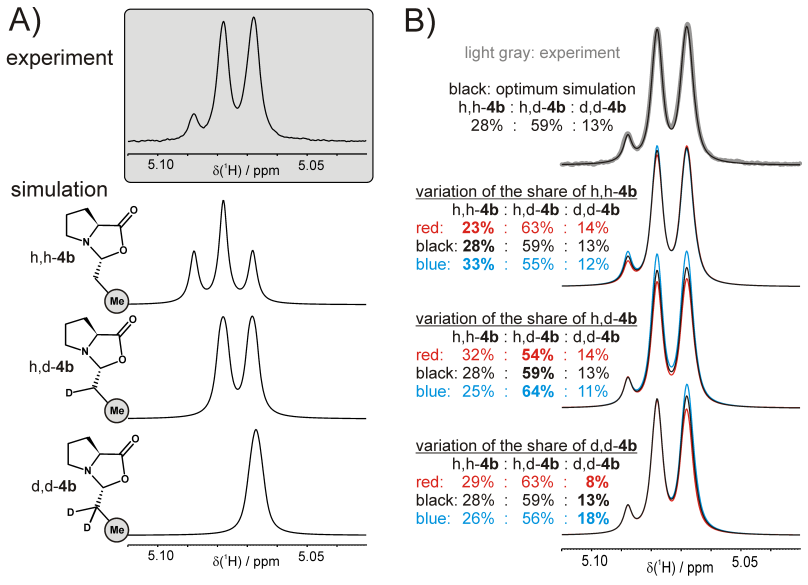

Figure 5.14: Exemplary deconvolution of overlapping NMR resonances of differently deuterated species of the *exo*-oxazolidinone **4b**. Displayed are the experimental spectral section (A, top) as well as the underlying simulated spectra of the non-, mono- and di-deuterated compounds (A, rows 2 to 4). For an estimation of the error range, the experimental spectrum and simulated spectra with varying ratios of the differently deuterated species are presented (B).

Dependence of Initial Formation Rates on the Water Content of the Sample

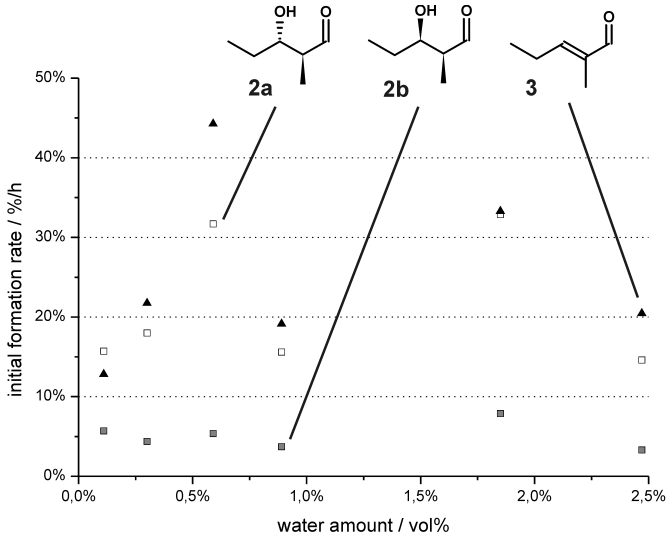

Figure 5.15: Dependence of the initial formation rate of **2a**,**b** and **3** on the water content of the sample. No clear tendency is discernible in contrast to the previously reported retardation of an organocatalyzed Mannich condensation.[25] The scattering of the data must be attributed to the poor reproducibility of sample mixing within the NMR tube, to the eventual solubilization of proline, and to imperfections in fitting curves to the experimental data and determining their initial slopes.

NMR Spectrum and NMR Characterization of the Acetaldehyde-Derived Species

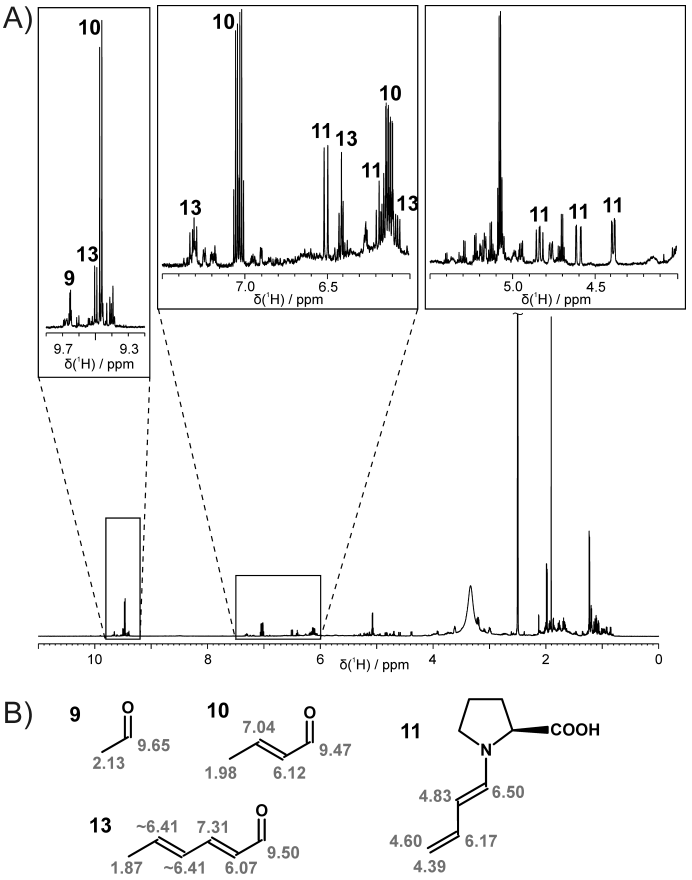

Figure 5.16: A) NMR spectrum of a reaction mixture of acetaldehyde with 100 mol% of L-proline in DMSO-d_6 at 300 K after 8 minutes; B) ^{1}H assignment of the acetaldehyde-derived species (referenced to the solvent residual peak).

Time-Dependent Diastereoselectivity of the Aldol Addition of 1a in DMF

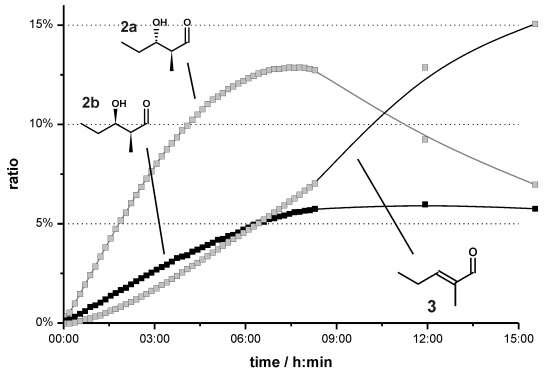

Figure 5.17: Concentration-time curves of the aldol and condensation dimers in the proline-catalyzed self-aldolization/condensation of propionaldehyde with 100 mol% of L-proline in DMF-d_7 at 300 K. (Note: The total amount of C_3 moieties stemming from propionaldehyde, detected in the first spectrum, was set to 100 %.)

5.4 Additional Experimental Findings

5.4.1 The Impact of Amine Additives on the Aldehyde Dimerization

DBU and DABCO have proven outstanding performances in the stabilization of enaminocarboxylates (chapter 3.4) and in the oxazolidinone-enamine conversion (chapter 4), respectively. Since it had already been shown that the proline-catalyzed aldol reaction is basically insensitive to basic additives,[61] we were thus mainly interested in to what extent the particular features of these amines have an impact on the competition of the proline-catalyzed self-aldolization and Mannich-type self-condensation of aliphatic aldehydes in DMSO. To address this issue, reaction mixtures of propionaldehyde **1a** (c = 50 mM) with 20 mol% of L-proline and 20 mol% of one of the additives DBU or DABCO were prepared in DMSO-d_6 and the reaction progresses were monitored by 1D ^{1}H NMR spectra. The additive-free sample (chapter 3.2) was used as the reference for this study (see Figures 5.18A and 5.19A).

The strongly basic additive DBU has been shown (chapter 3.4) to deprotonate proline enamines quantitatively and to increase their amounts by stabilizing them in the form of ion pairs. Since the enamine intermediate is believed to participate in the rate determining steps of both the aldol addition and condensation, significant changes in the absolute and relative rates of these reactions upon the addition of DBU may be expected.

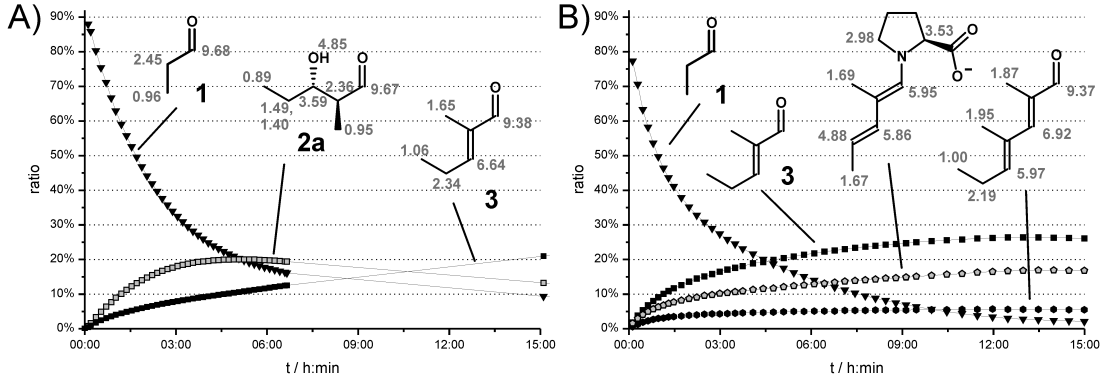

Figure 5.18: Reaction profiles of mixtures of propionaldehyde **1** with 20 mol% L-proline without (A) and with (B) 20 mol% of DBU in DMSO-d_6 at 300 K. ^{1}H NMR assignments are given in gray (in ppm). (Note: The total amount of **1**-derived species in the first spectra was set to 100 %.)

When DBU is applied as an additive in the proline-catalyzed self-aldolization/condensation of propionaldehyde **1**, the aldol addition dimers are observed only in tiny amounts (below 1 %), but in turn, the aldol condensation is by far predominant in the reaction mixture (Figure 5.18B). The *in situ* yield of the condensation dimer, the enal **3**, exceeds 40 % already after 5 hours (*cf.* after about 14 hours without DBU, Figure 5.18A), which indicates that the condensation reaction is accelerated substantially by DBU. In addition, the high tendency of the reaction mixture towards the aldol condensation is also reflected by the straightforward observation of the condensation trimer, a dienal, in an *in situ*

yield of about 15 % (Figure 5.18B). As intermediates of these condensation steps, the enaminocarboxylate of propionaldehyde is detected (data not shown) and moreover the deprotonated proline enamine derived from the enal **3** (Figure 5.18B). This first detection of a dienaminocarboxylate again highlights the outstanding ability of DBU to stabilize less privileged enamine species by the formation of ion pairs in solution (chapter 3.4).

These experimental observations can be explained in terms of a disfavoring of the aldol addition on the one hand and a favoring of the aldol condensation on the other hand on the basis of the recently evidenced deprotonation and stabilization of proline enamines by DBU[7,11] (see also chapter 3.4). In the List-Houk model of the intermolecular proline-catalyzed aldol reaction,[6,62] the electrophilic aldol acceptor is directed and also activated by an H-bond to the carboxylic proton of the proline enamine carboxylic acid. However, in the presence of DBU, the enamine is virtually fully deprotonated so that this Brønsted acid-type activation of the electrophile is hardly possible. Thus, the aldol addition should be largely impeded under these conditions. In this respect, the performance of the enamine/DBU ion pair again parallels the catalytic properties of diarylprolinol silyl ethers which are also known to be poor catalysts for homo-aldol reactions[15] (see also chapter 7.4). On the other hand, beyond its detrimental effect on the aldol addition, DBU can be argued to enhance the rate of the competing aldol condensation. In contrast to the aldol addition reaction, the proline-catalyzed aldol condensation proceeds via a Mannich-type mechanism (chapter 5.2) in which the electrophilic aldol acceptor is not activated through an H-bond to the carboxylic group of the enamine, but instead as an iminium ion. This iminium activation is fairly insensitive to the deprotonation of the enamine so that the aldol condensation should not be hampered by the presence of DBU (as is the aldol addition). On the contrary, one may in fact speculate that the electrostatic attraction between the iminium ion and the DBU-stabilized enaminocarboxylate actually facilitates the aldol condensation reaction.[63] Moreover, even without this speculative Coulombic attraction, the enaminocarboxylate can be expected to react in general more vividly than the carboxylic acid because of the anchimeric assistance of the negatively charged carboxylate group.[11] Altogether, the deprotonation of the enamine by DBU hence impedes the aldol addition by eliminating the carboxylic proton as the source of electrophile activation, but accelerates the aldol condensation owing to favorable electrostatic attractions and to the anchimeric assistance of the carboxylate group. In addition to the enamine deprotonation, DBU increases the overall concentration of proline-aldehyde adducts by forming stable ion pairs with the enaminocarboxylate in solution (chapter 3.4). At the same time, it provides steady supplies of the iminium species, as is evidenced by the EXSY-detected vivid exchange between the aldehyde and the enamine (data not shown), for which the iminium ion is commonly assumed as an intermediate. On this basis and with the knowledge that higher concentrations of proline-aldehyde intermediates in solution in principle favor the Mannich-type aldol condensation over the aldol addition (see chapter 5.2), we can thus state that DBU promotes the aldol condensation reaction also by increasing the amounts of proline-aldehyde adducts in solution. In summary, the ability of DBU to deprotonate

proline enamines and to increase their amounts by ion pair formation has a drastic impact on the competition between the proline-catalyzed aldol addition and condensation in that it hampers the aldol addition on the one hand and accelerates the aldol condensation on the other hand.

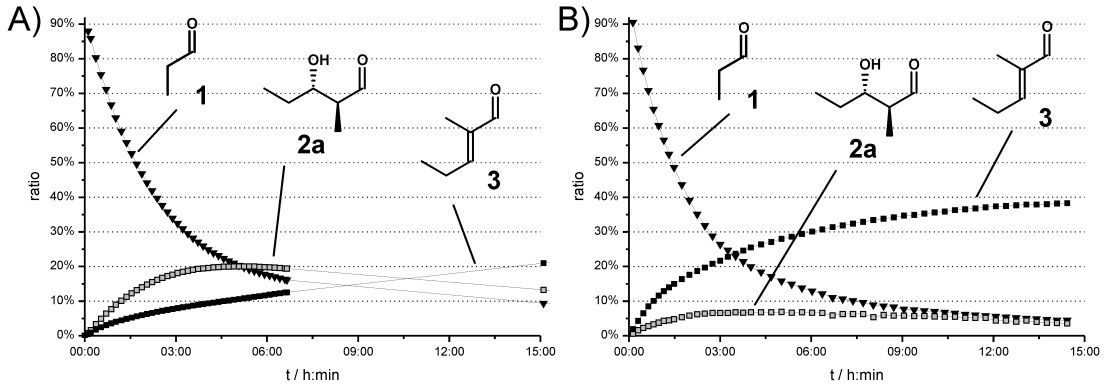

Figure 5.19: Reaction profiles of mixtures of propionaldehyde **1** with 20 mol% L-proline without (A) and with (B) 20 mol% of DABCO in DMSO-d_6. (Note: The total amount of **1**-derived species in the first spectra was set to 100 %.)

In contrast to the more basic DBU, the amine additive DABCO does not fully deprotonate proline enamines in DMSO and does not lead to an increase of their concentrations (chapter 3.4). Instead, because of its higher nucleophilicity,[64] DABCO can accelerate the formation of enamines from the isomeric oxazolidinones (chapter 4). However, since the enamine formation is presumably not the rate determining step of the aldol addition or condensation,[8,38,39] remarkable changes of the absolute and relative ratios of the two competing reaction pathways should be attributed rather to the moderate basicity of DABCO than to its exquisite nucleophilicity. When DABCO is added to the proline-catalyzed propionaldehyde self-aldolization/condensation, the reaction rates of the competing addition and condensation are reversed compared to the additive-free case (Figure 5.19). While the concentration of the *anti* aldol dimer **2a** exceeds the one of the condensation product **3** for about 10 hours in the absence of DABCO, the amount of **3** is higher than the one of **2a** throughout the reaction progress in the presence of DABCO, similarly to the case of DBU. Still, in contrast to the additive DBU, DABCO does not suppress the aldol addition onto a marginal level and, on the other hand, the condensation is not predominant to such a degree that higher condensed oligomers are observed. Overall, these trends that are observed upon the addition of DABCO correspond well to the ones from the DBU-addition, but they are a lot less pronounced, presumably because of the lower basicity of DABCO. Accordingly, the rationalization of the effects of DABCO addition may be in principle based on the argumentation outlined above for DBU: The partial deprotonation of the enamine intermediate by DABCO should bias the competition between the aldol addition and condensation towards the condensation as the aldol addition is hampered by enamine deprotonation and as the condensation is favored through electrostatic attraction and the anchimeric assistance of the carboxylate group. These effects are, however, weaker in the

case of DABCO than of DBU because of its lower basicity. The decrease of the overall proline intermediate concentration by DABCO (chapter 3.4) thereby constitutes an additional moderating factor since low intermediate concentrations favor the aldol addition over the condensation (chapter 5.2).

In summary, we investigated the influence of the basic amine additives DABCO and DBU on the proline-catalyzed dimerization of propionaldehyde in DMSO. For both amines, an acceleration of the Mannich-type aldol condensation at the expense of the competing aldol addition is observed. This effect is stronger for DBU than for DABCO, which can be ascribed to the higher basicity of DBU: The deprotonation of the enamine intermediate by amine bases hampers the aldol addition since it eliminates the Brønsted acidity of the enamine that is hypothesized in the List-Houk model to activate the aldol acceptor species. On the other hand, the aldol condensation is accelerated owing to favorable electrostatic interactions between the enaminocarboxylate and the iminium ion and owing to the assistance of the carboxylate group in the rate determining C-C bond formation. For this amine base-induced bias of the competition aldol addition *vs.* condensation in favor of the condensation, the change of the overall concentration of proline-aldehyde adducts may act either as a moderating factor (as DABCO decreases the intermediate concentration) or as an amplifying factor (as DBU increases the intermediate concentration).

5.4.2 Is there a Particular Role of DMSO in Proline Enamine Catalysis?

The exquisite role of DMSO and DMF in stabilizing proline-derived enamines in solution raises the question what role the solvent properties of DMSO and DMF in general or individual DMSO or DMF molecules in particular play for the progress of the proline-catalyzed intermolecular aldol reaction. Despite the well-known explicit participation of DMSO molecules in the Swern oxidation[65] and of DMF molecules in the Vilsmeyer-Haack formylation,[66] to our knowledge, this issue has not been addressed so far in the field of organocatalysis. To shed some light on a potential solvent participation in proline enamine catalysis, the residual solvent ^{1}H NMR signal was investigated for potential changes in the course of the intermolecular aldol reaction. First, an equimolar reaction mixture of L-proline and propionaldehyde (50 mM each) in DMSO-d_6 at 300 K was studied. Thereby, the chemical shift of the residual DMSO-d_5 remained unchanged in the course of the reaction. In contrast, a decrease of the signal intensity of DMSO-d_5 by about 20 % over 2 hours was found in spectra that had been recorded by 30° pulse excitation with 8 scans and a relaxation delay of 3 seconds. In view of the concentration difference of the reactants (50 mM each) and of DMSO (about 14 M) by a factor of 280, the magnitude of the solvent signal reduction is highly striking. However, as soon as single scan spectra were recorded, this decrease of the DMSO-d_5 signal intensity was not observed any longer (see Figure 5.20). Accordingly, the signal intensity decay must be ascribed to a deceleration of the longitudinal relaxation of DMSO-d_5 throughout the progress of the proline-catalyzed aldehyde self-aldolization, *i.e.* to an increase of the relaxation time constant T_1.

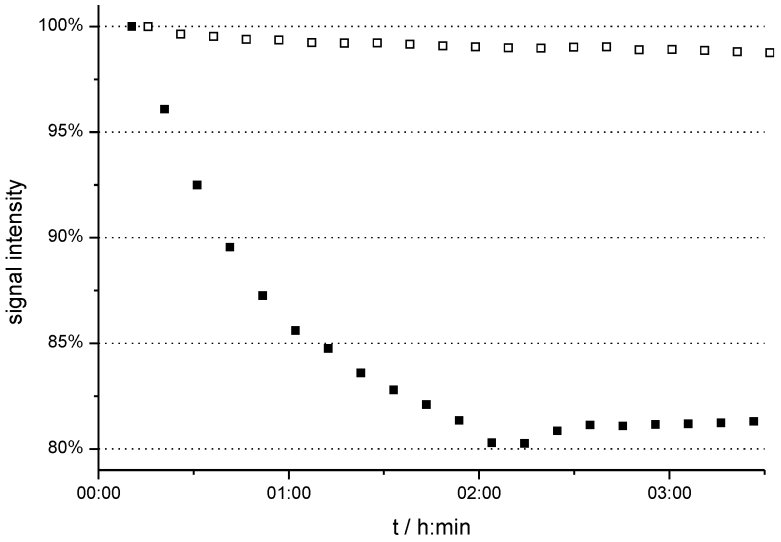

Figure 5.20: Signal intensities of residual DMSO-d_5 in a reaction mixture of 50 mM propionaldehyde and 100 mol% L-proline in DMSO-d_6 at 300 K. Intensities with open squares are extracted from single scan spectra, those with filled squares from spectra recorded with 30° pulses, 8 scans and 3 seconds relaxation delay. (Note: The two sets of intensities are scaled to the first points of their series individually.)

To gather more information on the origin of this highly surprising observation, the influence of the catalyst amount, of the solvent, and of different carbonyl species on this phenomenon was investigated by studying the impact on the signal reduction of the solvent. First, the amount of proline present in the reaction mixtures with propionaldehyde was varied from 100 mol% over 50 mol% and 20 mol% to 10 mol%. In all the cases, the amplitude of the signal decay of DMSO was between 20 and 25 %, but the rate of the signal decay, *i.e.* the extension of the T_1 relaxation time constant, was found to be the faster the higher the amount of proline was. However, no clear-cut connection of the signal decay to the presence of certain intermediates or to certain reaction steps could be elucidated by the comparison of the reaction profiles with the signal decays of DMSO-d_5.

Next, the influence of solvent variations on the T_1 extension was studied with 100 mol% of proline. The intensity loss of DMSO-d_5 in reaction mixtures of proline and propionaldehyde was insensitive to the addition of up to 10 vol% of water. An analogous decrease of other solvent peak intensities was only detected for DMF, though it was pronouncedly slower than for DMSO (25-30 % intensity loss over 15 hours). In contrast, the signal intensity of acetonitrile as the solvent was not affected. Interestingly, also for methanol, no signal intensity decay was observed. By comparison with the solvent dependence of the enamine stabilization (chapter 3), it is worthwhile to note that the extension of the T_1 relaxation time constant in reaction mixtures of proline and aldehydes corresponds rather to the abilities of solvents to stabilize proline enamines than to their performance in promoting the proline-catalyzed self-aldolization/condensation of aldehydes.

Since enamine detection had proven to strongly depend on the carbonyl species, the influence of different substitution patterns on the T_1 extension of DMSO-d_5 was investigated, too. No signal intensity loss of DMSO was observed in the equimolar reaction mixture of proline with acetone. Likewise, isobutyraldehyde did not lead to a reduction of the residual solvent peak in the presence of proline. In contrast, reaction mixtures of proline with butyraldehyde and 3-methyl-butyraldehyde brought about a similar effect on the DMSO signal intensity as propionaldehyde (26 % intensity loss within 200 minutes). The fact that the self-aldolization/condensation of 3-methyl-butyraldehyde proceeds extremely slowly, indicates that the prolongation of the T_1 relaxation time constant of DMSO cannot be explained by temperature changes within the sample owing to the reaction heat of the aldol addition/condensation. Instead, just like for the solvent dependence, a certain correlation between the proline enamine stabilization and the solvent signal reduction is observed.

In our earlier communication on proline enamine stabilization (chapter 3), we had already established a relationship between the presence of proline enamines in solution and the particular solvent properties of DMSO (and DMF): On the basis of DOSY data and of the solvent dependence of enamine detection, DMSO was argued to stabilize proline enamines by its excellent hydrogen-bond acceptor ability through a favorable interaction with the enamine carboxylic proton. Now having indication for a correlation between the presence of enamines and DMSO properties (namely T_1) from a different context, we were highly interested to check whether a particular impact of the enamine carboxylic proton on the DMSO signal attenuation could be proven. Therefore, reaction mixtures of propionaldehyde with prolinol as well as with diphenylprolinol methyl and silyl ethers (c = 50 mM each) were prepared in DMSO-d_6. As will be discussed later (see chapter 6), under these conditions, prolinol ethers show substantially higher enamine amounts than proline or prolinols, but, in contrast, they do not possess an exchangeable carboxylic or hydroxylic proton. On this basis, one should be able to nicely differentiate between the general presence of an enamine species and the particular presence of a carboxylic/hydroxylic enamine proton as the potential origins of DMSO signal reduction. For that purpose, the 1D ^{1}H reaction monitoring was evaluated with respect to the DMSO-d_5 signal intensity. The prolinol ether mixtures showed high enamine ratios, but no impact on the DMSO signal intensity was observed. In contrast, only low enamine amounts were detected for prolinol, but a significant decrease of the DMSO resonance was observed although it was less pronounced than for proline (only about 10 % within 5 hours). This striking finding indicates that it may be indeed the carboxylic/hydroxylic proton of the enamine species that interacts with DMSO, thereby leading to the stabilization of the enamine on the one hand and to the initially accelerated longitudinal relaxation of DMSO on the other hand. This interpretation is also backed by the observation that no DMSO signal intensity loss can be monitored in the presence of the proline enaminocarboxylate, formed with DBU.

Yet, as stated above, no straightforward correlation between the mere presence of a proline/prolinol enamine and the change in the DMSO longitudinal relaxation could be

established. Also, such a simplistic interpretation is not covered by the observation of a signal intensity reduction of DMSO-d_5 when the aldol dimer of propionaldehyde is used as the starting material. One may thus, for instance, speculate that the sum and nature of all potentially H-bond donating species cause the changes in the longitudinal relaxation of the H-bond acceptor solvent DMSO. To check this hypothesis in more detail, first, the NMR experimental approach should be optimized in terms of relaxation delays and sample concentrations (possibly also by using NMR spectrometers of different field strengths ω_0, see Figure 5.21A and discussion below) and may be complemented by direct T_1 measurements. This should allow to gather more information on the rate and on the extent of T_1 changes of the solvent. On this basis, the influence of various catalysts with different acidities and hence H-bond donating properties on the relaxation behaviour of the solvent can be studied and the experimental setup may be even extended onto other solvents than DMSO or DMF. With more experimental data at hand, one may then explore whether the observation of T_1 changes of the solvent bears the potential to act as a sensitive tool for monitoring the presence and impact of H-bond networks in solution. This may be possible because the T_1 relaxation originates, just like the nuclear Overhauser effect, from dipolar interactions. These are strongly affected by tiny changes in the rotational correlation time τ_c (see Figure 5.21B), *i.e.* by changes in the size of the molecular aggregates. Variations of T_1 relaxation times can therefore in principle be used as a sensor to visualize variations in molecular sizes, for instance, induced by H-bonding interactions. Finally, this may lead to the development of a new method to study the impact of the H-bonding properties of organocatalysts in various solvents and might be correlated to the catalytic performances of organocatalyst-solvent combinations.

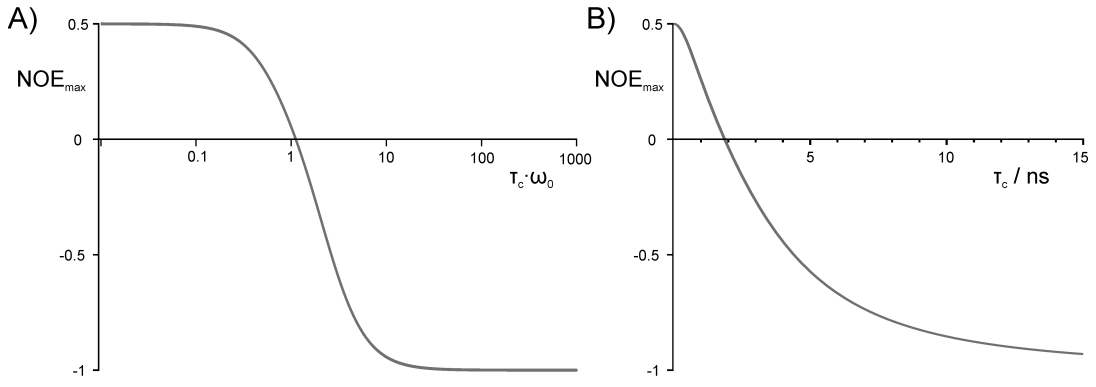

Figure 5.21: Maximum theoretical steady-state NOE as a function of molecular tumbling, *i.e.* A) $\tau_c \cdot \omega_0$ (logarithmic scale), B) τ_c (for a given spectrometer observation frequency of 600 MHz).

Altogether, more detailed considerations and experimentation will be necessary to address the origin of the solvent T_1 extension observed and to clarify whether this effect can be exploited with regard to a better understanding of proline enamine catalysis.

5.4.3 Parasitic at last? Aromatic Aldehydes in Proline Catalysis

Previously, the observed formation of oxazolidinones from proline and carbonyl compounds had been ascribed to a so-called parasitic equilibrium[6] that reduces the amount of the active enamine species within the catalytic cycle and therefore diminishes the reaction rate of proline-catalyzed aldol and Mannich reactions. In contrast to this early hypothesis, we could recently show for aliphatic aldehydes as aldol donors that proline enamines are formed directly from the isomeric oxazolidinones[9] so that the term "parasitic" seems inadequate in this respect. However, there is a potential further role of oxazolidinones in proline-catalyzed aldol reactions for which the attribute "parasitic" may well be justified: Oxazolidinones formed from proline and the aldol acceptor carbonyl species may deteriorate the reaction rates and yields either by reducing the available amounts of proline and the aldol acceptor or, even more severely, by inducing unwanted side reactions which irreversibly deactivate the catalyst. The latter is, for example, pointed out by the observation that adducts of proline and aromatic aldehydes can undergo decarboxylation to the azomethine ylide, followed by 1,3-dipolar cycloaddition to 1-oxapyrrolizidines.[38,67,68]

To study such potential parasitic influences, a reaction mixture of equimolar amounts of propionaldehyde **1** and benzaldehyde **9** with 100 mol% of L-proline in DMSO-d_6 at 300 K was prepared within an NMR tube. Besides the crossed-aldol addition/condensa-tion of **1** and **9** (Figure 5.22A), the self-aldolization/condensation of **1** (Figure 5.22B) as well as the irreversible formation of the 1-oxapyrrolizidines **14a**,**b** (Figure 5.22C) via the azomethine ylide **13** were expected in this experimental setup. The progress of these reactions was monitored by 1D ^{1}H NMR spectra and the obtained kinetic profiles were checked for parasitic species and parasitic effects associated with the addition of the aromatic aldol acceptor aldehyde **9**. By comparison with the spectroscopic data presented above and in the literature,[38] the compounds in Figure 5.23 could be identified tentatively. (Their unambiguous spectroscopic verification has not been accomplished yet.)

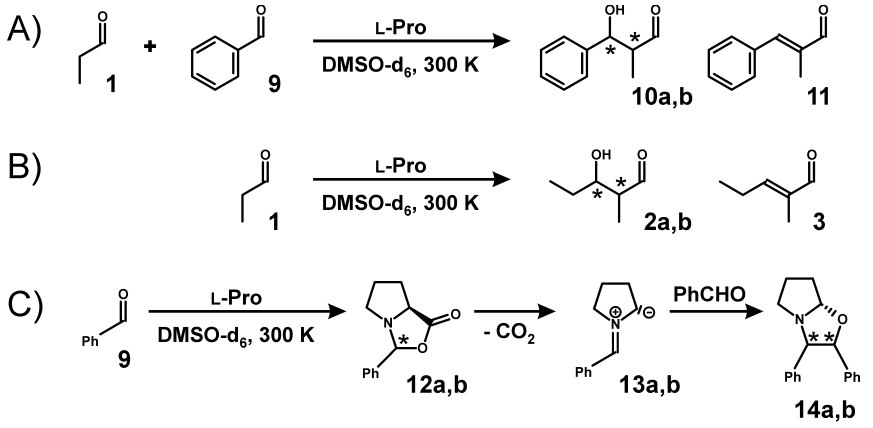

Figure 5.22: Reaction pathways in a mixture of **1** and **9** with 100 mol% L-proline in DMSO-d_6 at 300 K: A) crossed-aldol addition/condensation between **1** and **9**; B) self-aldolization/condensation of **1**; C) decarboxylative formation of **14a**,**b** from L-proline and two equivalents of **9**.

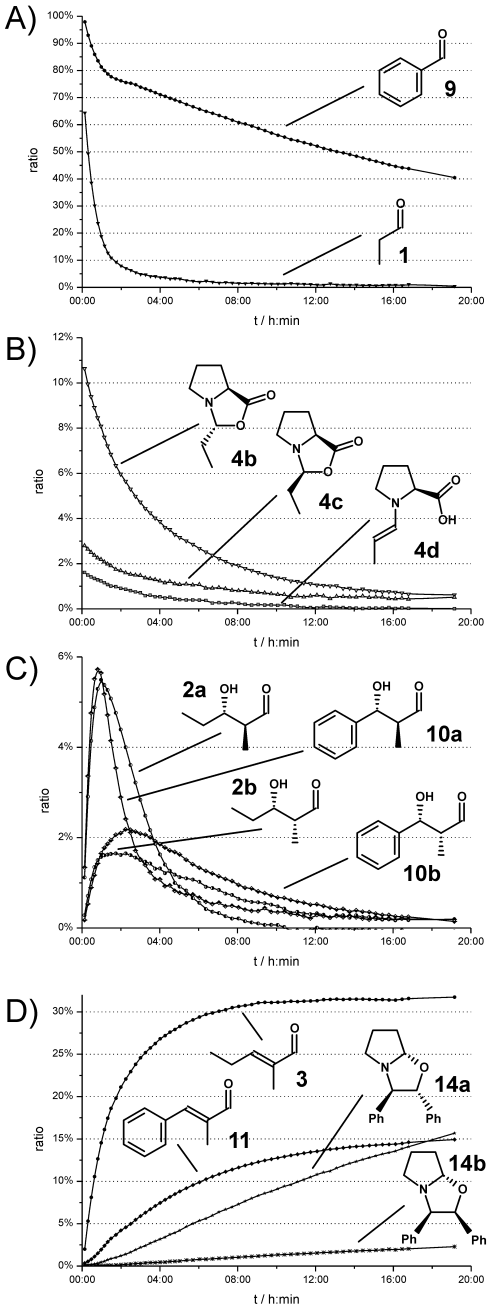

Figure 5.23: Reaction profile of a mixture of **1** and **9** (c = 50 mM, each) with 100 mol% L-proline in DMSO-d_6 at 300 K: A) starting material; B) intermediates formed from proline and **1**; C) intermediate products of self- and crossed-aldol addition; D) self- and crossed-aldol condensation products and products of decarboxylative proline deactivation by aromatic aldehydes according to Figure 5.22C. (Note: The total amount of **9**-derived species detected in the first spectrum was set to 100 %.)

The aliphatic aldol donor **1** and the aromatic aldol acceptor **9** are both consumed in the course of the reaction, but **1** vanishes a lot faster than **9** (Figure 5.23A). In addition, as intermediates, the enamine **4b** and the oxazolidinones **4c**,**d** are detected (Figure 5.23B) and their concentrations decrease in parallel (*cf.* chapter 3). Most notably, the concentration of the enamine key intermediate is below 2 % in the presence of **9** while it had been found

to be between 2.5 % and 3.5 % in reaction mixtures of **1** and proline without **9**, but under otherwise identical experimental conditions. Furthermore, in early stages of the reaction, the homo- and crossed-aldol addition products (**2a**,**b** and **10a**,**b**, respectively) are formed (Figure 5.23C). However, in line with our previous finding on the competition between aldol addition and aldol condensation (chapter 5), they disappear with increasing reaction times and the homo- and crossed condensation products **3** and **11** are formed in turn (Figure 5.23D). Besides these aldol addition and condensation pathways, the slow, yet steady and irreversible formation of the 1-oxapyrrolizidines **14a**,**b** is monitored (Figure 5.23D).

The more rapid consumption of **1** in comparison to **9** can be rationalized by its involvement **1** in both the crossed-aldol addition and condensation with **9** and in its rapid self-aldolization/condensation (Figure 5.23C,D). On the other hand, besides by the crossed-aldol reaction, the consumption of **9** is driven only by the slow formation of the 1-oxapyrrolizidines **14a**,**b**. For the latter reaction pathway (Figure 5.22), the putative intermediates, the oxazolidinones **12a**,**b** and the azomethine ylides **13a**,**b**, could not be detected in contrast to an earlier report.[38] This may be due to the slightly different reaction conditions in our case, *i.e.* due to the residual water in the sample and due to the differing nature of the aromatic residue.[38] Nevertheless, the formation of **14a**,**b** clearly evidences the existence of an adduct between proline and the aromatic aldehyde **9**, be it an oxazolidinone or an iminium ion, that allows for decarboxylation and subsequent cycloaddition with another molecule of **9** (Figure 5.22C). The observation that **14a**,**b** is formed in parallel to **10a**,**b** and **11** (see Figure 5.23D), furthermore teaches that adducts of proline and **9** exist in the reaction mixture right from the beginning. Hence, the aldol donor **1** and the aldol acceptor **9** in fact compete for the catalyst proline. This competition may well be termed "parasitic" for two reasons: First, it compromises the yield of the reaction since the unwanted side reaction of **9** to **14a**,**b** irreversibly consumes one crossed-aldol reaction partner. Second, it is also expected to reduce the rate of the crossed-aldol reaction since it eventually deactivates the catalyst irreversibly and keeps catalyst molecules from forming the reactive enamine intermediate **4d** of the aldol donor **1**, as evidenced experimentally by the lower enamine concentration in the presence of **9** than in its absence.

In summary, this preliminary study shows that the formation of oxazolidinones from proline and carbonyl compounds may indeed have parasitic character in proline-catalyzed aldol and Mannich reactions in DMSO. This is due to the fact that the aldol acceptor competes with the aldol donor for the catalyst in an unproductive way that reduces the amount of active aldol donor enamine intermediates. Moreover, in the case of aromatic aldehydes, decarboxylation of the proline-aldehyde-adduct and follow-up reactions irreversibly remove aldol acceptor molecules from the reaction mixture and furthemore eventually deactivate the catalyst. However, further investigations, for instance using different aromatic aldehydes and different reactant ratios, are expected to shed more light on the parasitic behavior of proline-derived oxazolidinones.

5.4.4 Towards an Understanding of the C-C Bond Forming Step

Since we had been able for the first time to detect and characterize an enamine intermediate in the proline-catalyzed intermolecular aldol reaction,[9] we then turned our experimental interest to the mode of action through which this enamine intermediate is involved in the C-C bond forming step of the catalytic aldol reaction cycle. In principle, two major mechanistic proposals for the transition state of this decisive stereogenic reaction step have been proposed in the literature. The List-Houk model[20] suggests that the s-*trans* enamine activates and at the same time directs the aldol acceptor molecule through an H-bond between the carboxylic proton of the enamine and the carbonyl oxygen of the incoming aldol acceptor. In contrast, the Seebach-Eschenmoser model[7] assumes that a deprotonated s-*cis* enamine performs the nucleophilic attack to the aldol acceptor under participation of the carboxylate group, thereby directly forming the more stable product oxazolidinone. Indeed, Mayr and coworkers could recently provide kinetic evidence for the anchimeric assistance of the carboxylate group of a deprotonated proline enamine in the attack to an electrophile.[11] In case one would be able to prove the deprotonation of the enamine species under typical catalytic conditions in solution, this would hence fill the catalytic cycle of proline-catalyzed intermolecular aldol reactions with the final missing piece of experimental evidence. The cycle would then consist of the condensation of proline and the aldol donor to the oxazolidinone, the conversion to the enamine, the deprotonation of this enamine, the nucleophilic attack to the aldol acceptor under carboxylate assistance, and finally the hydrolysis of the product-proline-adduct.

As the formation of the enamine is so fast that it can be followed by EXSY, it does most probably not comprise the rate determining step of the reaction. Likewise, the hydrolysis of oxazolidinones, formed from proline and aldehydes, has been shown by EXSY to proceed rather rapid.[9] In the hypothetical catalytic cycle outlined above, either the deprotonation of the enamine or the C-C bond forming step should be rate determining. The latter was suggested by kinetic studies; however, a certain participation of the carboxylate group in the rate determining step was indicated by isotope effects, too.[8] Notably, the deprotonation of the enamine species and the C-C bond formation may be part of a concerted process. Now having at hand the possibility to generate and stabilize detectable amounts of enamine intermediates,[9] the potential to observe isotopic effects in proline-catalyzed intermolecular aldol reactions was to be explored. For that purpose, a stable proline enamine was to be generated with either a protonated or a deuterated carboxylic group. Upon addition of an electrophile, the rate of the addition reaction was to be monitored NMR spectroscopically. Therefore, 3-methyl-butyraldehyde **15** was mixed with 50 mol% of L-proline (in order to reduce the amount of free catalyst for unwanted side reactions) in DMSO-d_6 and 1 vol% of H_2O or D_2O was added, respectively. In order to guarantee their thermodynamic equilibration, these two reaction mixtures were stored at room temperature for one hour so that comparable amounts of protonated or deuterated enamines, respectively, were present *in situ*.

The choice of **15** thereby assured a low tendency for self-aldolization and thus a rather constant enamine concentration over a sufficiently long period of time. Then 0.5 equivalents of *para*-nitro-benzaldehyde **16** as a good aldol acceptor for the crossed-aldol reaction were added to the mixtures and the progress of the reactions was monitored by 1D ^{1}H spectra at 300 K (Figure 5.24). Furthermore, the addition of H_2O was expected to suppress the irreversible decarboxylation of proline with 2 equivalents of **16**.

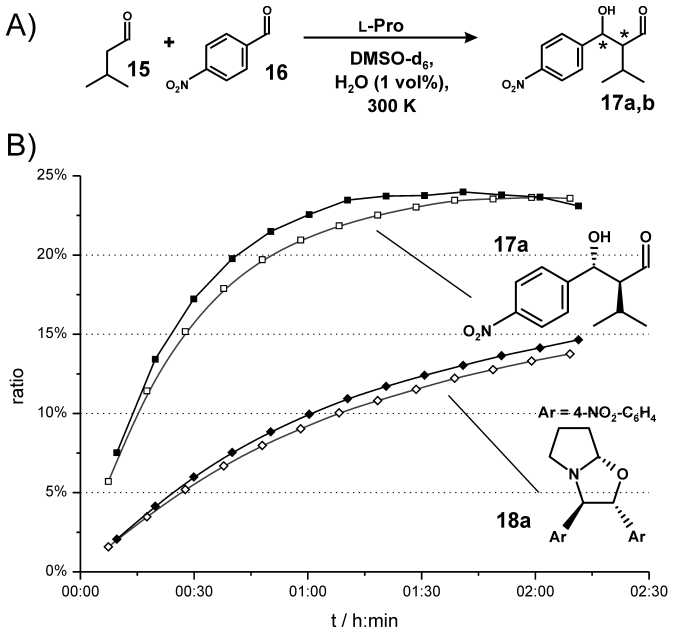

Figure 5.24: A) Proline-catalyzed crossed-aldol reaction between **15** and **16**; B) buildup curves for the crossed-aldol product **17a** and the decarboxylative adduct **18a** of proline and two equivalents of **16**. Results starting from deuterated enamine are represented by filled symbols, those from protonated enamine by open symbols. (Note: The total amount of **16**-derived species detected in the first spectrum was set to 100 %.)

Two major reaction pathways were observed in the prepared mixtures (Compounds were again assigned tentatively on the basis of 1D ^{1}H spectra with the help of literature data and our own experience.). First, the expected crossed-aldol reaction was observed, yielding the products **17a**,**b**. Second, the irreversible decarboxylative reaction of proline with two molecules of the aromatic aldehyde **16** was found to proceed as the addition of 1 vol% of water and of a two-fold excess of **15** were not sufficient to totally suppress this undesired side reaction (see again Figure 5.22C in the previous section for the proposed mechanism; in the case of **16**, a transient singlet at 6.44 ppm may even be attributed to the presence of **16**-derived proline oxazolidinone.) However, as becomes evident from Figure 5.24, neither for the crossed-aldol reaction nor for the catalyst deactivation pathway was an isotope effect detected. Still, on the basis of the findings on the proline-catalyzed intermolecular aldol reaction obtained so far and despite the complexity of interpreting isotope effects, further experiments addressing the issue of isotope effects for the understanding of the reaction mechanism should be feasible.

5.5 References

[1] A. Berkessel, H. Gröger, *Asymmetric Organocatalysis - From Biomimetic Concepts to Applications in Asymmetric Synthesis*, Wiley-VCH, Weinheim, **2005**.

[2] *Enantioselective Organocatalysis: Reactions and Experimental Procedures* (Ed.: P. I. Dalko), Wiley-VCH, Weinheim, **2007**.

[3] *Chem. Rev.* **2007**, *107*, 12 (special issue on organocatalysis).

[4] *Ernst Schering Foundation Symposium Proceedings "Organocatalysis"* (Eds.: M. T. Reetz, B. List, S. Jaroch, H. Weinmann), Springer, Berlin, **2008**.

[5] *Asymmetric Organocatalysis, Vol. 291* (Ed.: B. List), **2010**.

[6] B. List, L. Hoang, H. J. Martin, *Proc. Natl. Acad. Sci. U. S. A.* **2004**, *101*, 5839–5842.

[7] D. Seebach, A. K. Beck, D. M. Badine, M. Limbach, A. Eschenmoser, A. M. Treasurywala, R. Hobi, W. Prikoszovich, B. Linder, *Helv. Chim. Acta* **2007**, *90*, 425–471.

[8] N. Zotova, L. J. Broadbelt, A. Armstrong, D. G. Blackmond, *Bioorg. Med. Chem. Lett.* **2009**, *19*, 3934–3937.

[9] M. B. Schmid, K. Zeitler, R. M. Gschwind, *Angew. Chem. Int. Ed.* **2010**, *49*, 4997–5003.

[10] D. A. Bock, C. W. Lehmann, B. List, *Proc. Natl. Acad. Sci. U. S. A.* **2010**, *107*, 20636–20641.

[11] T. Kanzian, S. Lakhdar, H. Mayr, *Angew. Chem. Int. Ed.* **2010**, *49*, 9526–9529.

[12] B. List, R. A. Lerner, C. F. Barbas III, *J. Am. Chem. Soc.* **2000**, *122*, 2395–2396.

[13] B. List, *Chem. Commun.* **2006**, 819–824.

[14] S. Mukherjee, J. W. Yang, S. Hoffmann, B. List, *Chem. Rev.* **2007**, *107*, 5471–5569.

[15] P. Melchiorre, M. Marigo, A. Carlone, G. Bartoli, *Angew. Chem. Int. Ed.* **2008**, *47*, 6138–6171.

[16] S. Bertelsen, K. A. Jørgensen, *Chem. Soc. Rev.* **2009**, *38*, 2178–2189.

[17] P. M. Pihko, I. Majander, A. Erkkilä, *Top. Curr. Chem.* **2010**, *291*, 29–75.

[18] M. Nielsen, D. Worgull, T. Zweifel, B. Gschwend, S. Bertelsen, K. A. Jørgensen, *Chem. Commun.* **2011**, *47*, 632–649.

[19] S. Bahmanyar, K. N. Houk, *J. Am. Chem. Soc.* **2001**, *123*, 11273–11283.

[20] S. Bahmanyar, K. N. Houk, H. J. Martin, B. List, *J. Am. Chem. Soc.* **2003**, *125*, 2475–2479.

[21] L. Hoang, S. Bahmanyar, K. N. Houk, B. List, *J. Am. Chem. Soc.* **2003**, *125*, 16–17.

[22] A. Sharma, R. Sunoj, *Angew. Chem. Int. Ed.* **2010**, *49*, 6373–6377.

[23] D. G. Blackmond, A. Moran, M. Hughes, A. Armstrong, *J. Am. Chem. Soc.* **2010**, *132*, 7598–7599.

[24] B. M. Trost, C. S. Brindle, *Chem. Soc. Rev.* **2010**, *39*, 1600–1632.

[25] A. Erkkilä, P. M. Pihko, *Eur. J. Org. Chem.* **2007**, 4205–4216.

[26] K. Zumbansen, A. Döhring, B. List, *Adv. Synth. Catal.* **2010**, *352*, 1135–1138.

[27] B. List, P. Pojarliev, C. Castello, *Org. Lett.* **2001**, *3*, 573–575.

[28] B. Nozière, A. Córdova, *J. Phys. Chem. A* **2008**, *112*, 2827–2837.

[29] M. Arend, B. Westermann, N. Risch, *Angew. Chem. Int. Ed.* **1998**, *37*, 1044–1070.

[30] T. Ishikawa, E. Uedo, S. Okada, S. Saito, *Synlett* **1999**, *1999*, 450–452.

[31] A. Córdova, W. Notz, C. F. Barbas III, *J. Org. Chem.* **2002**, *67*, 301–303.

[32] J. Casas, H. Sundén, A. Córdova, *Tetrahedron Lett.* **2004**, *45*, 6117–6119.

[33] M. B. Smith, J. March, *March's Advanced Organic Chemistry: Reactions, Mechanisms, and Structure, Sixth Edition*, John Wiley & Sons, Inc., Hoboken, NJ, USA, **2006**.

[34] B.-C. Hong, M.-F. Wu, H.-C. Tseng, J.-H. Liao, *Org. Lett.* **2006**, *8*, 2217–2220.

[35] A. Erkkilä, P. M. Pihko, *J. Org. Chem.* **2006**, *71*, 2538–2541.

[36] V. Guidi, S. Sandoval, M. A. McGregor, W. Rosen, *Tetrahedron Lett.* **2010**, *51*, 5086–5090.

[37] A. B. Northrup, D. W. C. MacMillan, *J. Am. Chem. Soc.* **2002**, *124*, 6798–6799.

[38] N. Zotova, A. Franzke, A. Armstrong, D. G. Blackmond, *J. Am. Chem. Soc.* **2007**, *129*, 15100–15101.

[39] N. Zotova, A. Moran, A. Armstrong, D. Blackmond, *Adv. Synth. Catal.* **2009**, *351*, 2765–2769.

[40] U. Eder, G. Sauer, R. Wiechert, *Angew. Chem. Int. Ed.* **1971**, *10*, 496–497.

[41] Z. G. Hajos, D. R. Parrish, *J. Org. Chem.* **1974**, *39*, 1615–1621.

[42] H. Zhu, F. R. Clemente, K. N. Houk, M. P. Meyer, *J. Am. Chem. Soc.* **2009**, *131*, 1632–1633.

[43] B. Alcaide, P. Almendros, *Angew. Chem. Int. Ed.* **2008**, *47*, 4632–4634.

[44] P. García-García, A. Ladépêche, R. Halder, B. List, *Angew. Chem. Int. Ed.* **2008**, *47*, 4719–4721.

[45] Y. Hayashi, T. Okano, T. Itoh, T. Urushima, H. Ishikawa, T. Uchimaru, *Angew. Chem. Int. Ed.* **2008**, *47*, 9053–9058.

[46] Y. Hayashi, T. Itoh, S. Aratake, H. Ishikawa, *Angew. Chem. Int. Ed.* **2008**, *47*, 2082–2084.

[47] Y. Hayashi, T. Itoh, M. Ohkubo, H. Ishikawa, *Angew. Chem. Int. Ed.* **2008**, *47*, 4722–4724.

[48] Y. Hayashi, S. Samanta, T. Itoh, H. Ishikawa, *Org. Lett.* **2008**, *10*, 5581–5583.

[49] SDBSWeb, `http://riodb01.ibase.aist.go.jp/sdbs/`.

[50] S. Bertelsen, M. Marigo, S. Brandes, P. Diner, K. A. Jørgensen, *J. Am. Chem. Soc.* **2006**, *128*, 12973–12980.

[51] B.-C. Hong, M.-F. Wu, H.-C. Tseng, G.-F. Huang, C.-F. Su, J.-H. Liao, *J. Org. Chem.* **2007**, *72*, 8459–8471.

[52] N. Utsumi, H. Zhang, F. Tanaka, C. F. Barbas III, *Angew. Chem. Int. Ed.* **2007**, *46*, 1878–1880.

[53] R. M. de Figueiredo, R. Fröhlich, M. Christmann, *Angew. Chem. Int. Ed.* **2008**, *47*, 1450–1453.

[54] K. Liu, A. Chougnet, W.-D. Woggon, *Angew. Chem. Int. Ed.* **2008**, *47*, 5827–5829.

[55] B. Han, Y.-C. Xiao, Z.-Q. He, Y.-C. Chen, *Org. Lett.* **2009**, *11*, 4660–4663.

[56] E. Marqués-López, R. P. Herrera, T. Marks, W. C. Jacobs, D. Könning, R. M. de Figueiredo, M. Christmann, *Org. Lett.* **2009**, *11*, 4116–4119.

[57] G. Bencivenni, P. Galzerano, A. Mazzanti, G. Bartoli, P. Melchiorre, *Proc. Natl. Acad. Sci. U. S. A.* **2010**, doi: 10.1073/pnas.1001150107.

[58] D. Enders, C. Grondal, M. R. M. Hüttl, *Angew. Chem. Int. Ed.* **2007**, *46*, 1570–1581.

[59] A.-N. Alba, X. Companyo, M. Viciano, R. Rios, *Curr. Org. Chem.* **2009**, *13*, 1432–1474.

[60] C. Grondal, M. Jeanty, D. Enders, *Nat. Chem.* **2010**, *2*, 167–178.

[61] P. M. Pihko, K. M. Laurikainen, A. Usano, A. I. Nyberg, J. A. Kaavi, *Tetrahedron* **2006**, *62*, 317–328.

[62] C. Allemann, R. Gordillo, F. R. Clemente, P. H.-Y. Cheong, K. N. Houk, *Acc. Chem. Res.* **2004**, *37*, 558–569.

[63] S. Lakhdar, R. Appel, H. Mayr, *Angew. Chem. Int. Ed.* **2009**, *48*, 5034–5037.

[64] M. Baidya, S. Kobayashi, F. Brotzel, U. Schmidhammer, E. Riedle, H. Mayr, *Angew. Chem. Int. Ed.* **2007**, *46*, 6176–6179.

[65] K. Omura, D. Swern, *Tetrahedron* **1978**, *34*, 1651–1660.

[66] A. Vilsmeier, A. Haack, *Chem. Ber.* **1927**, *60*, 119–122.

[67] F. Orsini, F. Pelizzoni, M. Forte, R. Destro, P. Gariboldi, *Tetrahedron* **1988**, *44*, 519 –541.

[68] T. Kano, J. Takai, O. Tokuda, K. Maruoka, *Angew. Chem. Int. Ed.* **2005**, *44*, 3055–3057.

6 Formation and Stability of Prolinol (Ether) Enamines

Article

"Formation and Stability of Prolinol and Prolinol Ether Enamines by NMR: Delicate Selectivity and Reactivity Balances and Parasitic Equilibria"

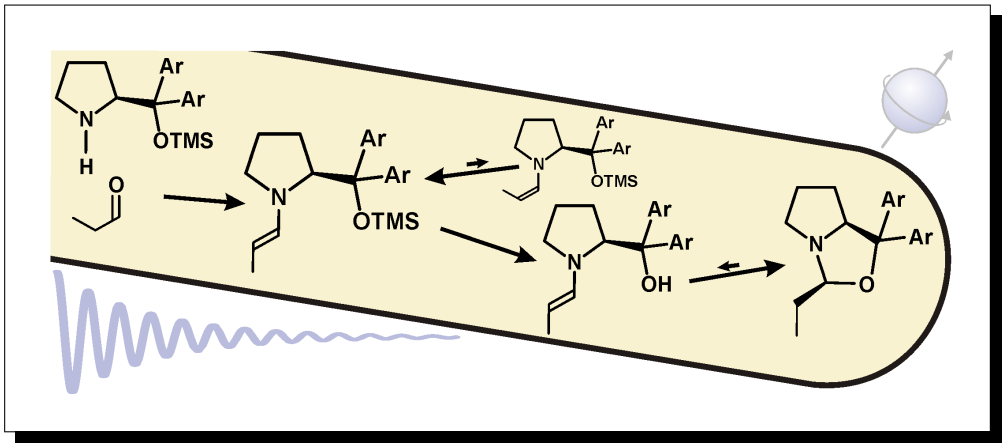

Markus B. Schmid, Kirsten Zeitler, and Ruth M. Gschwind

J. Am. Chem. Soc. **2010**, *submitted for publication.*

6.1 Abstract

Enamine key intermediates in organocatalysis, derived from aldehydes and Jørgensen/ Hayashi-type prolinol or prolinol ether catalysts, were generated in different solvents and investigated by NMR spectroscopy. Depending on the catalyst structure, trends for their formation and amounts are elucidated. For prolinol catalysts, the first enamine detection *in situ* is presented and the rapid cyclization of the enamine to the oxazolidine ("parasitic equilibrium") is monitored. In the case of diphenylprolinol, this equilibrium is fully shifted to the kinetic *endo*-oxazolidine ("dead end") by the two geminal phenyl rings most probably because of the Thorpe-Ingold-effect. With bulkier and electron-withdrawing aryl rings, however, the enamine is stabilized relative to the oxazolidine allowing for the parallel detection of the enamine and the oxazolidine. In the case of prolinol ethers, the enamine amounts decrease with increasing sizes of the aryl *meta*-substituents and the *O*-protecting group. In addition, for small aldehyde alkyl chains, *Z*-configured enamines are observed for the first time in solution. Prolinol silyl ether enamines are evidenced to undergo slow desilylation and subsequent rapid oxazolidine formation in DMSO. For unfortunate combinations of aldehydes, catalysts, solvents, and additives, the enamine formation is drastically decelerated, but can be screened for by a rapid and facile NMR approach. Altogether, especially by clarifying the delicate balances of catalyst selectivity and reactivity, our NMR spectroscopic findings can be expected to substantially aid synthetically working organic chemists in the optimization of organocatalytic reaction conditions and of prolinol (ether) substitution patterns for enamine catalysis.

6.2 Manuscript

Introduction

Detailed knowledge on the formation and the stability of intermediate species is essential for an improved understanding and hence control of organic reactions. Especially in the increasingly important and still rapidly growing field of modern asymmetric organocatalysis,[1–5] detailed mechanistic insights into intermediate properties should largely facilitate the development of novel catalytic systems and the optimization of reaction conditions. As one of the most successfully and widely applicable principles of modern organocatalysis, enamine catalysis by secondary amines, typically originating from the chiral pool,[6–11] has emerged to an extension of the original proline catalysis[12–14] in recent years. Among a variety of different catalyst scaffolds, in particular Jørgensen/Hayashi-type prolinol ethers[15–20] have demonstrated excellent performances in asymmetric enamine organocatalysis and, though a lot less pronouncedly, prolinol-type organocatalysts[21] have also found applications based on enamine intermediates.[22–25]

Still, in view of the vast number of synthetic applications, studies on the mechanistic understanding of enamine catalysis must be termed insufficient. Accordingly, knowledge on the appearance of active reaction intermediates is often poor. Only recently could we detect and characterize *in situ* the first enamine intermediate[26] in the archetypical proline-catalyzed intermolecular aldol reaction.[14] At the same time, the first crystal structure of an enamine intermediate in an aldolase antibody was reported.[27] Nevertheless, to our knowledge, not a single prolinol-derived enamine in solution has been reported so far. For prolinol silyl ether-type organocatalysts on the other hand, two enamines could be isolated and characterized,[28,29] but *in situ* only one dienamine intermediate[30] and one product enamine[31] have been observed. Hence, very little is known about the formation trends and the stabilities of prolinol- and prolinol ether-derived enamines even though this information should be highly appreciated by synthetically working organic chemists for the optimization of organocatalytic reaction conditions.

To fill this gap, we designed *in situ* NMR studies on reactive prolinol and prolinol ether enamines. In this article, we present the first detailed study on the formation and stability of enamines, derived from aldehydes and prolinol(ether)-type organocatalysts, by means of NMR spectroscopy in solution. Our findings by ^{1}H NMR reaction monitoring reveal trends for the formation rates of such enamines depending on the catalyst structure and for the amounts of enamine formed. Furthermore information on the enamine resistance against cleavage of the hydroxyl protecting group and against ring closure to the isomeric oxazolidines ("dead ends") is provided.

Results and Discussion

Model Enamines. Following the experience from our earlier investigations on proline enamines,[26] mixtures of prolinol(ether)-type organocatalysts and α-unbranched aldehy-

des (Figure 6.1) in DMSO were envisaged as the best conditions for achieving the enamine stabilization. Thereby, the observation of prolinol (ether) enamines was furthermore expected to be aided by the well-known fact that, in contrast to proline, prolinol(ether)-type organocatalysts do not promote aldehyde self-aldolizations as readily.[8] Various secondary amines (**3**-**9**),[15–17] derived from proline, that are typically and very successfully used as organocatalysts for enamine catalysis, were selected for our studies. They were mixed with two different aldehydes, 3-methyl-butyraldehyde **1** and propionaldehyde **2**. Especially **1** was chosen for the enamine formation study as we had found earlier that in this case the unwanted aldehyde self-aldolization is minimized even under proline catalysis;[26] therefore, the superimposition of enamine formation and the potentially subsequent aldol reaction is expected to be less problematic for **1**. By comparison with **2**, the impact of the size of the aldehyde alkyl chain was to be studied. DMSO was used predominantly as the solvent in order to achieve the maximum amounts and stabilities of the enamines, especially in the case of prolinol-type catalysts;[26] the obtained results were then verified for selected other solvents (methanol, acetonitrile, chloroform, dichloromethane, and toluene). All experiments mentioned hereafter (if not stated otherwise) were performed within NMR tubes by mixing equimolar amounts of aldehyde and catalyst in perdeuterated solvents to obtain concentrations of 50 mM each and NMR spectra were recorded at 300 K (see Experimental Section, chapter 6.3, for details).

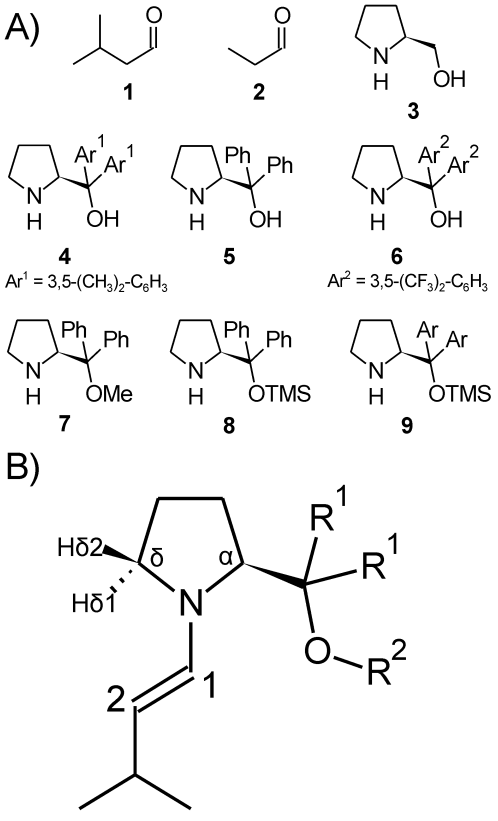

Figure 6.1: A) Aldehydes and organocatalysts examined in this study; B) general atom nomenclature used for enamines derived thereof.

Enamine Formation and NMR Characterization. Overall 14 different enamines formed from the aldehydes **1**-**2** and the organocatalysts **3**-**9** (designated as "catalyst-number.aldehyde-number", i.e. as **3.1**-**9.2**; Figure 6.2) were obtained in different solvents and investigated *in situ* (see Figure 6.9 and 6.10 in the Supporting Information, chapter 6.3, for the NMR assignments).

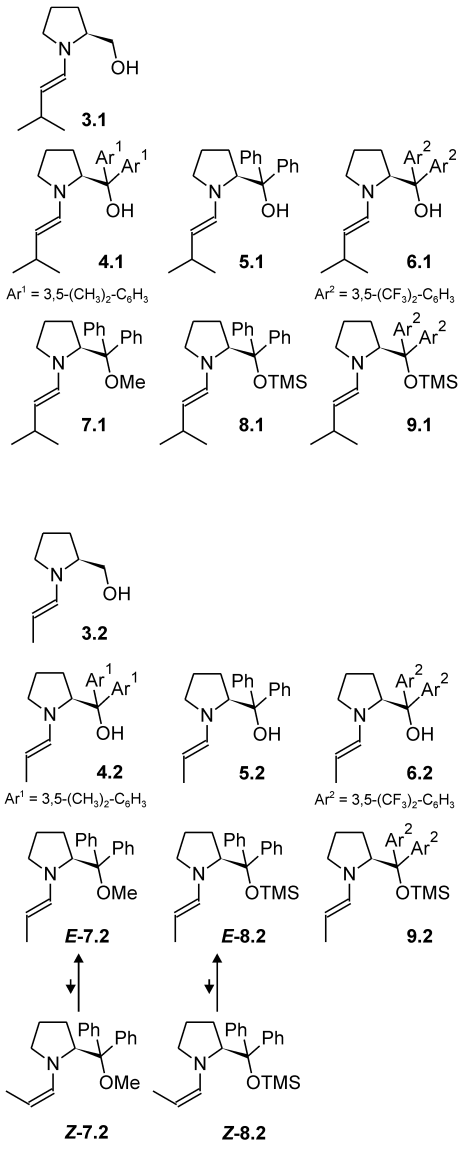

Figure 6.2: Overview on the investigated enamines derived from aldehydes **1** and **2** and catalysts **3**-**9**. All enamines are displayed in the (more stable) s-*trans* conformation with respect to the exocyclic N-C bond.

The detection of the ene-moiety of the enamines was straightforwardly accomplished on the basis of its characteristic resonances in one-dimensional ^{1}H spectra;[26] in particular the doublet for H1 proved to be characteristic and easily recognizable because of its appearance in the non-crowded spectral region between 6.3 ppm and 5.9 ppm. (Only the H1-resonances of the diarylprolinol enamines derived from **4**, **5**, and **6** appeared between 5.42 ppm and 5.20 ppm because of ring current effects, chapter 7.) For all aldehyde-amine

combinations, the major conformer was evidenced to be *E*-configured at the enamine double-bond by the scalar coupling constant $^{3}J_{H1,H2}$ of 13.5 – 13.9 Hz.[32] In addition, for **7.2** and **8.2**, *i.e.* for enamines formed in high amounts and bearing a relatively small alkyl chain, the *Z*-configured isomers were detected for the first time besides the *E*-isomers in solution. They are characterized by their upfield shifted (about 0.2 – 0.3 ppm relative to the *E*-enamines) H1 doublets of about 8.8 Hz,[32] but accounted for only about 1.5 % of the total enamine amount in DMSO, MeCN, and PhMe. (A putative *Z*-enamine of **6.1**, amounting to only 0.4 % of the enamine concentration in DMSO, could not be verified unambiguously.) Because of their low concentrations, the *Z*-enamines could not be investigated further so far so that we can only speculate whether their presence may actually compromise the selectivity of prolinol ether enamine catalysis. Our experimental detection of the favoring of the *E*-configuration over the *Z*-configuration agrees with other experimental findings reported earlier: the detection of the *E*-configuration for isolated prolinol ether enamines by NMR in solution and by X-ray analyses in the crystal[28,29] and for an *in situ* prolinol ether dienamine.[30] Our *in situ* NMR findings on a substantial preference of the *E*-configuration are moreover in good agreement with an empirical estimation of the relative stability of enamine *E*/*Z*-isomers[33] and also with the results from theoretical calculations.[29,30,34–36] Nevertheless, on the examples of **7.2** and **8.2**, we could show that also a small amount of *Z*-configured enamines, derived from aldehydes and amine organocatalysts, is present in solution. For the *E*-enamines, comprehensive homo- and heteronuclear NMR experiments were performed on the example of **8.2** (see Figure 6.12B in the Supporting Information, chapter 6.3). Thereby, in analogy to our previous investigations,[26] the covalent connection of the ene-unit to the pyrrolidine ring of the catalyst was proven via the ^{1}H,^{13}C-HMBC by crosspeaks from H1 to Cα and Cδ and *vice versa* from Hα and Hδ1 to C1, obviously conflicting with a previously calculated enol mechanism.[37] This finding was confirmed by $^{4,5}J_{H,H}$ long-range couplings from H1 and H2 to Hδ1,2, observed in the ^{1}H,^{1}H-COSY spectrum.

Enamine Stability, Formation, and Degradation.

Prolinol Enamines. The employment of *O*-unprotected prolinol derivatives[21] in enamine organocatalysis is a lot less common than of the corresponding methyl or silyl ethers since, *e.g.* in combination with aldehydes, considerable amounts of the catalysts are said to be irreversibly removed from the catalytic cycle by formation of stable oxazolidines (frequently also referred to as hemiaminals).[34] Accordingly, only a few superior applications of prolinol enamines have been reported so far.[22–25] To shed some light on the properties and the behaviour of prolinol enamines, we investigated the formation and stability of enamines derived from **1** or **2** and the (diaryl)prolinols **3**-**6**, respectively, *i.e.* **3.1**, **3.2**, **4.1**, **4.2**, **5.1**, **5.2**, **6.1**, and **6.2**. Similarly to the proline-derived enamines,[26] prolinol enamines could not be detected in MeOH-d_4, MeCN-d_3, $CDCl_3$ or PhMe-d_8, but only in the dipolar aprotic solvent DMSO-d_6 as was tested on the example of diphenylprolinol **5**. This again underlines

our previous statement that the stabilizing interaction between solvent molecules with exclusive hydrogen-bond acceptor properties and the carboxylic/hydroxylic proton of the enamine intermediate may be crucial for the detectability of proline/prolinol enamines in the equilibrium with their cyclized oxazolidinone/oxazolidine tautomers.[26] First, by comparison of prolinol **3** and diphenylprolinol **5**, we investigated the general influence of the two geminal phenyl rings on the formation and stability of prolinol enamines. The evolution of the amounts of enamines in the reaction mixtures of aldehydes **1** or **2** and catalysts **3** or **5**, respectively, in DMSO-d_6 is depicted in Figure 6.3A and 6.3B.

For diphenylprolinol **5**, only low amounts of the enamines **5.1** and **5.2** (below 20 % of all aldehyde-derived species) can be detected in the reaction mixture and their observation by NMR is temporally restricted to the first 1.5 hours since their amounts decrease rapidly and the isomeric oxazolidine is in fact formed almost quantitatively (Figure 6.3A and 6.3B).[34] Only the kinetic cyclization product, the thermodynamically less favorable *endo*-oxazolidine (with the proline side-chain and the aldehyde alkyl chain in the same halfspace of the oxazolidine ring; see Figure 6.3C) is observed;[a] this is in agreement with previous findings on the preferred oxazolidine formation of diphenylprolinol **5**.[38,39] For prolinol **3** on the other hand, the enamines **3.1** and **3.2** and the corresponding kinetic *endo*-oxazolidines are found in the beginning, too, but the enamines do not disappear in favor of the *endo*-oxazolidines during the time interval observed. Instead, the *endo*-oxazolidine and the enamine amounts decrease in parallel at a constant ratio of about 6:1 in the case of **1** and of about 11:1 in the case of **2** (after an induction period of about 30 minutes) throughout the observation period. In turn, along with the vanishing of the *endo*-oxazolidine and the enamine, the thermodynamically favorable *exo*-oxazolidine appears, its molar ratio increases over time and approaches asymptotically a constant value of about 60 % in the case of **1**. Thereby, the formation rate of the *exo*-oxazolidine (Figure 6.3A) is the highest when the concentration of the *endo*-oxazolidine and the enamine is the highest, *i.e.* in the beginning of the reaction. Similarly for propionaldehyde **2**, the eventual formation of the *exo*-oxazolidine is observed, but its amount increases substantially slower than in the case of **1**.

For prolinol **3**, the parallel decay of the concentrations of the *endo*-oxazolidines and the corresponding enamines indicates that there is a rapid equilibration between these tautomeric species (possibly via the commonly proposed iminium ions, Figure 6.3C)[34] and that the oxazolidine formation is hence reversible (similarly to the enamine-oxazolidinone equilibrium in the case of proline catalysis).[26] This interpretation is backed experimentally by an EXSY cross-peak from the *endo*-oxazolidine, formed from **3** and **2**, to the enamine **3.2** (data not shown). Most notably, however, in striking contrast to the direct enamine formation from oxazolidinones in proline catalysis in DMSO,[26] the vanishing of the diphenylprolinol-derived enamines **5.1** and **5.2** in favor of the *endo*-oxazolidines (Figure 6.3A and 6.3B) clearly reveals that the enamines are not formed directly from the ox-

[a] In the case of propionaldehyde **2**, the transformation into the *endo*-oxazolidine is not quantitative, mainly because of the formation of the product-oxazolidine.

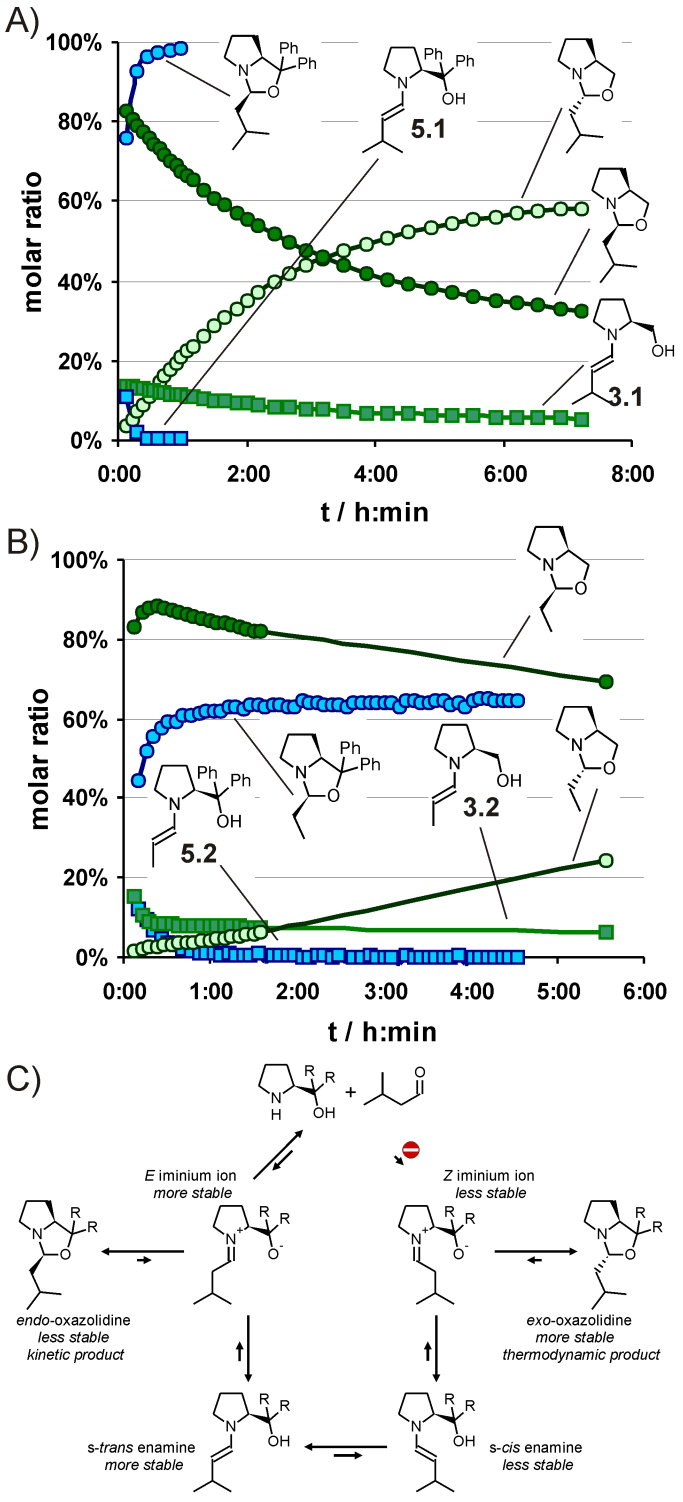

Figure 6.3: A), B) Evolution of the amounts of enamines and oxazolidines derived from the aldehydes **1** (A) and **2** (B) and the prolinol-type organocatalysts **3** (green) and **5** (blue) in DMSO-d_6 over time as monitored by 1D ^{1}H NMR spectroscopy (Note: The total amount of aldehyde-derived species, detected in the first spectrum, was set to 100 %.); C) proposed equilibria[34] between the starting material, iminium ions, enamines and oxazolidines.

azolidines. Hence, the commonly postulated equilibria including the hypothetical iminium ions (Figure 6.3C)[34] may well be justified in the case of diarylprolinol-aldehyde adducts. Comparing the enamines **3.1** and **3.2** in their equilibria with the *endo*-oxazolidines, the lower ratio *endo*-oxazolidine:enamine in the case of **1** may be rationalized thermodynamically by the steric destabilization of the *endo*-oxazolidine and the inductive stabilization of the enamine owing to the larger aldehyde alkyl chain present in **1** (isopropyl residue) than in **2** (methyl residue). Starting from this rapid exchange between the *endo*-oxazolidine and the enamine in the case of **3**, the thermodynamic equilibrium between these two species and the *exo*-oxazolidine is slowly established. For this eventual formation of the thermodynamic *exo*-oxazolidine, the iminium ion E/Z isomerization (Figure 6.3C) has to occur either directly, via the starting aldehyde, via putative carbinolamines, or via the s-*cis* s-*trans* isomerization of the enamine species. However, in our reaction mixture of **3** and aldehydes in DMSO, neither iminium ions nor carbinolamines were detected and only tiny amounts of the free aldehyde (far below 1 %) so that these species can hardly be expected to provide sufficient amounts of the thermodynamically unfavorable Z-iminium ion for the substantial formation of the *exo*-oxazolidine. Instead, the enamines are readily observed and the maximum concentration of **3.1** corresponds well to the maximum formation rate of the *exo*-oxazolidine. Moreover, in a parallel study, we could evidence on the example of **3.2** for the first time a significant population of the s-*cis* enamine conformation (chapter 7). In addition, the s-*trans* s-*cis* equilibration must be fast since only one enamine signal set is observed NMR spectroscopically (chapter 7). Altogether, these findings strongly suggest that the thermodynamic *exo*-oxazolidine is formed from its kinetic *endo*-isomer via ring opening to the enamine, s-*cis* s-*trans* isomerization on the enamine stage and subsequent ring closure. On this basis, the faster formation of the *exo*-isomer in the case of aldehyde **1**, may be explained by the stronger steric repulsion in the *endo*-oxazolidine of **1** compared to **2** which facilitates the ring opening reaction to the enamine.

In contrast to **3**, for diphenylprolinol **5**, the enamines **5.1** and **5.2** rapidly vanish in favor of the *endo*-oxazolidine and no *exo*-oxazolidines are detected. Considering the small structural difference between **5** and **3**, the strikingly higher stability of the *endo*-oxazolidine derived from **5** is rather surprising. The experimental discrepancies between catalysts **3** and **5** must hence be attributed to the impact of the two geminal phenyl rings present in the diphenylprolinol **5** only, namely to their steric demand and to the well-known Thorpe-Ingold effect.[40,41] In line with our assumptions in a previous study on proline enamines,[26] this structural motif promotes the ring closure to the kinetic *endo*-oxazolidine and moreover stabilizes the oxazolidine ring, once formed, thermodynamically, as evidenced by the absence of the enamines **5.1** and **5.2** after more than 1.5 hours. The inability to detect the thermodynamically favorable *exo*-isomer in the case of **5** suggests, in combination with the low ability of DMSO to stabilize anions,[42] that this effect is so strong that the lifetime of the open-chain species (iminium ion and enamine) and/or the extent of the oxazolidine ring opening are insufficient to allow for an isomerization process between the oxazolidines; this might also be reflected by the inability to detect iminium species in our study. Thus,

the conversion of the kinetic *endo*-oxazolidine to the thermodynamically more stable *exo* form is unfeasible for **5**, since it would have to proceed via an open-chain intermediate. In contrast, the *endo*-oxazolidine derived from **1** or **2**, respectively, and **3**, being devoid of the geminal phenyl rings, is less stabilized and thus opens more easily. This leads to the enamine for which, because of the lower steric demand of the CH_2OH-moiety in **3**, the thermodynamic preference of the s-*trans* enamines over the s-*cis* enamines (likewise the preference of the *E*- over the *Z*-iminium ion) is lower than in the case of **5**.[28–30,34–36] This allows the easy population of the s-*cis* conformation (chapter 7) and hence the formation of the *exo*-oxazolidines. Most interestingly, the *in situ* observation of higher enamine concentrations in the case of **3** in comparison to **5** as well as the suggested s-*cis* s-*trans* isomerization of the enamine are also in good agreement with the typical performances of **3** and **5** in enamine catalysis: Higher reactivities are reported for **3**, but better selectivities for **5**.[43–46]

However, the overall performance of **5** as an organocatalyst for aldol reactions is very poor. This can now be rationalized for the first time on an experimental basis by the lack of reasonable amounts of enamine over a sufficiently long time. In contrast, different diarylprolinol organocatalysts with substituted phenyl rings, for instance the di-*meta*-methyl- or di-*meta*-trifluoromethyl-substituted analogs **4** and **6**, have demonstrated substantially better catalytic properties in promoting aldol reactions.[24,25] Most interestingly, reaction times of several days are reported for these prolinol-catalyzed reactions, which is in seeming contradiction to the disappearance of the diphenylprolinol enamines **5.1** and **5.2** within less than two hours in DMSO. To shed more light on this issue of prolinol enamine catalysis, the formation and stability of enamines derived from the aldehydes **1** and **2** and the diarylprolinols **4**-**6** were investigated. The choice of **4** and **6** with phenyl substituents of similar sizes (CH_3 and CF_3), but with different electron demands (electron release by CH_3 and electron withdrawal by CF_3) should, by comparison with **5**, allow to identify and to distinguish steric and electronic contributions to the relative enamine stabilization with respect to the isomeric *endo*-oxazolidines. On the one hand, the increased size of the aryl substituents in **4** and **6** (referred to as Ar^1 and Ar^2, respectively, in the following) compared to **5** may destabilize the *endo*-oxazolidine because of unfavorable steric repulsions. Owing to the similar sizes of Ar^1 (=3,5-$(CH_3)_2C_6H_3$) and Ar^2 (=3,5-$(CF_3)_2C_6H_3$), this effect should be comparable for catalysts **4** and **6**. On the other hand, the electronic contributions of the electron-releasing CH_3 and the electron-withdrawing CF_3 groups in **4** and **6**, respectively, should be inverse and should also have opposite effects on the enamine amounts with respect to **5** as the reference catalyst. These electronic influences may impact on the enamine stability either by influencing the enamine π system or by changing the H-bond donor ability of the hydroxylic group of the enamine that has been suggested to be essentially involved in the enamine stabilization (see the solvent dependence of prolinol enamines above and our previous study on proline enamines[26]). However, such influences should be observable straightforwardly with the help of ^1H NMR chemical shifts as sensors for local electron densities.

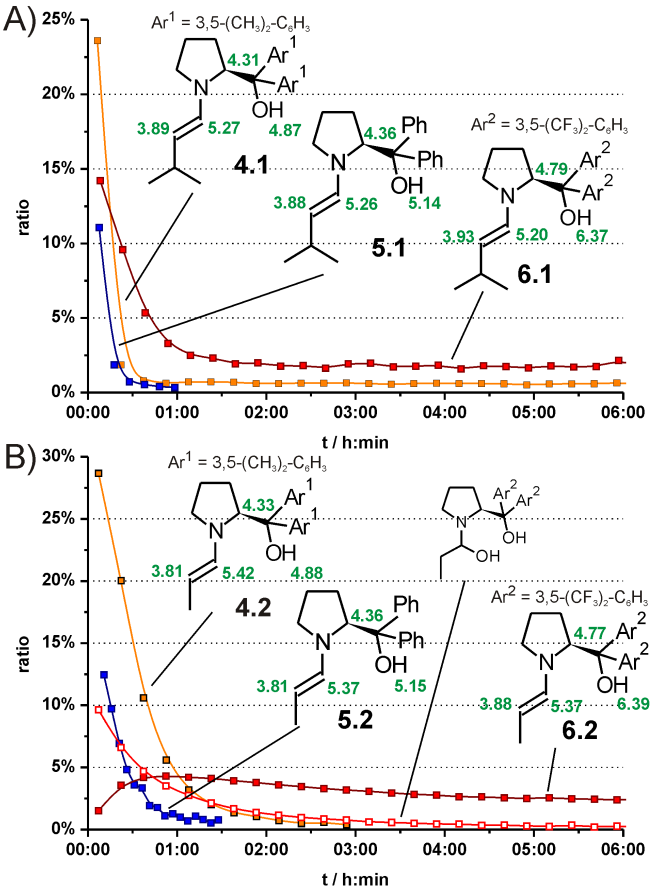

Figure 6.4: A), B) Evolution of the amounts of enamines derived from the aldehydes **1** (A) and **2** (B) and the diarylprolinol-type organocatalysts **4** (orange), **5** (blue), and **6** (red) in DMSO-d_6 at 300 K over time as monitored by 1D ^{1}H NMR spectroscopy. (Note: The total amount of aldehyde-derived species, detected in the first spectrum, was set to 100 %.) Relevant ^{1}H chemical shifts (in ppm) are given in green.

The results of the 1D ^{1}H reaction monitoring in DMSO-d_6 as well as the relevant chemical shifts of the enamines formed from **1** and **2** with **4**-**6** are summarized in Figure 6.4. Enamine species were detected transiently or permanently in all samples investigated. Concerning the enamine ^{1}H chemical shifts, one distinct trend becomes obvious: From **4** via **5** to **6**, *i.e.* with stronger electron-withdrawing properties of the aryl rings, downfield shifts of the protons OH (from 4.87/4.88 ppm to 6.37/6.39 ppm with aldehydes **1**/**2**), Hα (from 4.31/4.33 ppm to 4.79/4.77 ppm with **1**/**2**), and also of H2 (from 3.89/3.81 ppm to 3.93/3.88 ppm with **1**/**2**) are observed. On the other hand, the low influence of the catalyst substituents on the chemical shift of H1 indicates that all diaryl prolinol enamines adopt basically the same conformation around the exocyclic C-C bond (chapter 7). In all cases, the enamines were predominantly converted into the *endo*-oxazolidines and again the *exo*-oxazolidines were not observed at all (see Figure 6.11 in the Supporting Information, chapter 6.3). However, the degree and the rate of this conversion are largely dependent on the nature of the aryl substituents. For the dimethyl-substituted catalyst **4**, the formation of the *endo*-oxazolidine from the enamines with both aldehydes is similarly fast as

for diphenylprolinol **5**, but the amounts of the enamines of **4** are significantly higher than for **5**: With propionaldehyde **2**, the enamine **4.2** can be detected for about three hours in solution, while for 3-methyl-butyraldehyde **1**, the enamine **4.1** does not disappear during more than 12 hours, but rather coexists with the *endo*-oxazolidine in a constant ratio of 0.6:99.4 (after an induction period). On the other hand, the concentrations of the enamines **6.1** and **6.2**, derived from the trifluoromethyl-substituted catalyst **6**, decrease remarkably more slowly than the ones of **5.1** and **5.2**. In addition, **6.1** and **6.2** are detected easily throughout the observation time of more than six hours (**6.1** was observed even after more than 3 days) and show constant ratios with the oxazolidines of 3.6:96.4 in the case of **6.1** (after an induction period) and of 2:98 (asymptotically decreasing to this value) in the case of **6.2**. In the case of **6.2**, not only the conversion of the enamine into the oxazolidine is significantly decelerated, but also the formation of the enamine itself. This may be rationalized by the detection of an additional intermediate species that was tentatively identified on the basis of its ^{1}H chemical shifts as a carbinolamine of **6** and **2** (Figure 6.4B; to our knowledge, the detection of a prolinol-derived carbinolamine has not been reported before; see Figure 6.12A in the Supporting Information, chapter 6.3, for the ^{1}H chemical shift assignment).

For the rationalization of the different enamine amounts observed with the different catalysts **4**, **5**, and **6**, steric and electronic effects of the phenyl substituents must be taken into account. The common observation of higher enamine amounts with both aldehydes for the CH_3- and CF_3-substituted catalysts **4** and **6** than for the unsubstituted **5** indicates the common increase of the steric bulk as one of the contributions to the relative enamine stabilization. This may be caused by the increased steric repulsion and the associated destabilization of the isomeric *endo*-oxazolidine. The even increased enamine amounts with catalyst **6** in comparison to **4** furthermore suggest that the enamine π system is stabilized by electron-withdrawing *N*-substituents. The impact of electronegativity changes of the pyrrolidine α-substituent on the enamine π system is also evidenced by the slight downfield shift of the proton H2 from catalyst **4** to **6**. This relative enamine stabilization in **6.1** and **6.2** is in line with the long-standing observation that enamine-imine tautomeric equilibria are shifted towards the enamine by electron-accepting *N*-substituents and that this effect is most pronounced in polar solvents.[47] In addition, one may speculate that the higher OH acidity of enamines derived from **6** than of **4** or **5**, as evidenced by the downfield shift of the OH resonance, is accompanied by a higher H-bond donor ability. This may lead to a stronger intramolecular H-bond to the enamine nitrogen (chapter 7) and to more favorable interactions with dipolar aprotic solvents such as DMSO and thereby cause an additional relative stabilization of the enamine species. The explanation of the influence of the aldehyde substitution pattern on the enamine amounts is in parallel to our previous study on proline enamines:[26] The higher enamine amounts for **1** than for **2** can be accounted for by the stronger stabilizing +I- and hyperconjugation effects in the enamine and by the stronger steric destabilization of the *endo*-oxazolidine by the *iso*-propyl group in **1**.

In contrast to the amounts of enamines, the different rates of their formation and formal cyclization to the oxazolidines depending on the catalyst structure cannot be explained as straightforwardly at this stage of our investigations. Hence, we cannot yet give a conclusive rationale why the formation of the oxazolidine is so much faster for 3-methylbutyraldehyde **1** than for propionaldehyde **2**. Likewise, the origin of the stabilization of the carbinolamine by catalyst **6** and the reason for the slow establishment of the enamine-oxazolidine equilibrium in the case of **6** will be addressed in a separate, more comprehensive study on this issue. However, on the basis of the amounts and lifetimes of the enamines observed for the different diarylprolinol catalysts **4**-**6**, *i.e.* with the help of their "parasitic equilibria" with the isomeric oxazolidines, we can now explain the better conversions in prolinol enamine-catalyzed reactions by **6** than by **4** or **5** as well as the required long reaction times[24,25] on an experimental basis. Accordingly, prolinol enamine catalysis appears to be successful only in the case of sufficient enamine equilibrium concentrations over a reasonably long period of time, as is illustrated most impressively by the results of the Hayashi group on the prolinol enamine-catalyzed crossed-aldol reaction of acetaldehyde (Figure 6.5).[24]

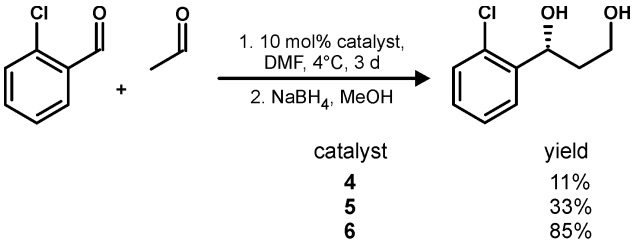

Figure 6.5: Performances of diarylprolinol organocatalysts **4**-**6** in a direct crossed-aldol reaction of acetaldehyde according to Hayashi *et al.*.[24]

Prolinol Ether Enamines. By analogy with the study on prolinol enamines and in order to reveal trends concerning formation, stability, and degradation of organocatalytically more relevant enamines, we investigated mixtures of **1** with the diarylprolinol ether organocatalysts **7**-**9**[8,18,19] in different solvents. This choice was due to the fact that such *O*-protected diarylprolinol derivatives are more broadly applicable and more successfully used for enamine catalysis particularly as they cannot fall victim to parasitic deactivation by oxazolidine ring closure. Accordingly, enamines of **7**-**9** were readily formed (*in situ* yields in DMSO-d_6 between 70 %[b] and 90 % for **7** and **8**, *cf.* less than 30 % for **3**-**6**) and, in contrast to the enamines of **3**-**6**, they were detected with ease even in solvents other than the dipolar aprotic DMSO (see Figure 6.10 in the Supporting Information, chapter 6.3). On the example of **7.2**, which had shown the highest enamine quantities, a rapid screening for the solvent dependence of the enamine amount was performed. While

[b]The significantly lower absolute enamine concentration of **8.2** in comparison to **8.1** is partially attributed to the higher amount of residual water present within the sample.

7.2 accounted for 85 % of the **2**-derived species after half an hour in DMSO-d_6, this ratio was only 30 % in PhMe-d_8, 22% in MeCN-d_3, 16 % in $CDCl_3$ and 15 % in MeOH-d**4**.[c] Hence, just like for prolinol enamines, DMSO provides the best conditions for the stabilization of prolinol ether enamines, too. Most of the experiments mentioned hereafter were therefore performed in DMSO-d_6 as the solvent. The time-dependent evolution of the enamine amounts in the reaction mixtures of aldehydes and prolinol ether catalysts in DMSO-d_6 is depicted in Figure 6.6.

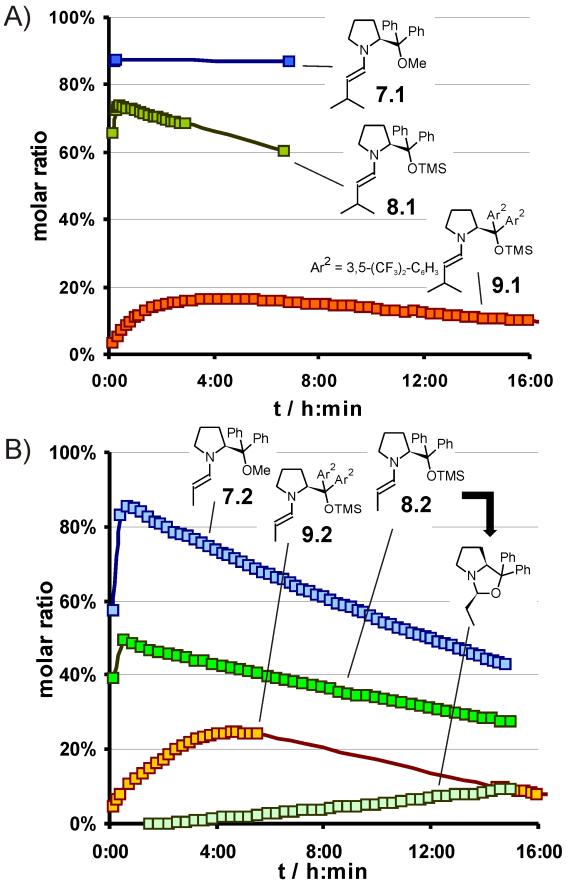

Figure 6.6: Evolution of the amounts of enamines derived from **1** (A) and **2** (B) and the prolinol ether-type organocatalysts **7**-**9** in DMSO-d_6 over time as monitored by 1D ^{1}H NMR spectroscopy. Also shown is the increase of the *endo*-oxazolidine concentration formed from **8.2** upon desilylation (B). (Note: The total amount of aldehyde-derived species in the first spectrum was set to 100%.)

Two trends are clearly visible therein: First, the absolute amount of enamine decreases depending on the catalyst structure from **7** over **8** to **9**. While the equilibrium between the enamine (and water) and the starting materials **1**,**2** and **7**-**9** is shifted almost completely towards the enamine in the case of the diphenylprolinol methyl ether **7**, the sterically more demanding TMS (trimethylsilyl) moiety of **8** causes lower amounts of the enamine and substitution of the phenyl ring by the even bulkier Ar^2 in **9** further reduces the

[c] In MeOH-d_4, about 80 % of the initial amount of **2** was found by 1D ^{1}H spectra in a species that must be assigned as either the hemiaminal of **2**, **7**, and water or the hemiaminal ether of **2**, **7**, and methanol.

concentration of the enamine significantly.[d] From a thermodynamical point of view, this reveals that the relative stability of the enamine with respect to the starting material decreases with increasing bulkiness of the α-substituent of the pyrrolidine ring. This in turn indicates that the effective shielding of one face of the enamine by the bulky α-substituent, desired for high stereoselectivities of the catalyst, comes along with unfavorable steric interactions between the "obese" substituent and the aldehyde alkyl chain that lead to a certainly undesired reduction of the active enamine intermediate concentration. The fact that this trend is brought about by enlarging the *O*-protecting group as well as the *meta*-substituents on the phenyl ring is in line with the finding from our conformational investigations on such enamines that both of these groups interact with the enamine moiety and play a role for the stereoselection in enamine catalysis by prolinol(ether)-derivatives (chapter 7).

Second, the nature of the *O*-protecting group and the phenyl *meta*-substituents of the catalysts **7**-**9** also have an impact on the formation rate and the persistence of the corresponding enamines. The enamine **7.1** is formed within minutes in DMSO-d_6 and proved to be stable over the period of time observed. The enamines **7.2**, **8.1**, and **8.2** appear rapidly, too, however their amounts decrease over time. In the case of **7.2**, this is due to the consumption of the enamine by unproductive reactions, but not due to the demethylation of the catalyst moiety. In contrast, for **8.1** and **8.2** and likewise for **9.1** and **9.2**, the loss of the TMS-protecting group is observed and the subsequent cyclization to the oxazolidine (see above) is mainly responsible for the decrease of the enamine concentration.[e] This cleavage of the silyl ether has already been alluded to in the literature,[29,48,49] but is monitored here experimentally for the first time (Figure 6.6B). Hence, according to our findings in DMSO-d_6, the replacement of TMS by Me to increase the stability of the catalyst against cleavage of the *O*-protecting group and hence to facilitate, for instance, mechanistic investigations[50] seems well justified.

In addition, by comparison with **8.1** and **8.2**, the formation rates of the enamines **9.1** and **9.2** in DMSO-d_6 are drastically reduced so that their maximum concentrations are reached only after more than 4 hours. Certainly, a reduced rate of enamine formation might be a critical point for the application of prolinol ether-type organocatalysts in enamine catalysis. To understand and to avoid this potentially detrimental effect, we searched for different experimental conditions which either promote or prevent the delayed enamine formation: Interestingly, the enamine formation is not slowed down in DMSO-d_6 when the substituents Ar^2 of **9** are replaced by Ph (see **8.1** and **8.2** in Figure 6.6). Likewise,

[d] Notably, the steric destabilization of the prolinol ether enamine by Ar^2 thereby seems to exceed the electron-withdrawing stabilization by Ar^2 that was observed for prolinol enamines. This can be explained in the context of the different enamine conformations of prolinols and prolinol ethers observed in our parallel enamine conformation study. Note: These differences in the amounts of enamines cannot be accounted for by different amounts of residual water within the samples since the 1D ^{1}H NMR integration indicates that the amount of water was the highest in the sample with **7** and the lowest in the sample with **9**.

[e] Interestingly, the desilylation of prolinol silyl ethers seems to be most critical in DMSO. The results of more detailed studies on this issue will be reported in due course.

the delayed enamine buildup is not observed for **9** and **2** if the solvent is changed from DMSO-d_6 to PhMe-d_8 (see Figure 6.7A). On the other hand, the enamine formation *is* decelerated when **8** is used in DMSO-d_6 together with K_2CO_3 as an additive (see Figure 6.7B). These observations lead us to the conclusion that unfortunate combinations of catalysts, additives, and solvents (with regard to Figure 6.4 also of aldehydes) can cause delayed enamine formations in solution. Interestingly, distinct experimental observations and parameters are connected to the decelerated enamine formation: On the one hand, in the case of the prolinol enamine **6.2**, a carbinolamine as a further intermediate on the way to the enamine seems to be stabilized, which can delay the enamine formation (see Figure 6.4B). A similar species, possibly the prolinol ether **8**-derived analog, was observed in the case of **8**/K_2CO_3 as the catalytic system in DMSO (data not shown). On the other hand, a deceleration of the NH proton exchange was observed for prolinol ethers (see below). This may be caused by steric crowding in proximity to the pyrrolidine nitrogen atom and solvent and/or additive molecules that are H-bonded to the NH proton. Such an effective shielding of the nitrogen of the prolinol ether catalyst may hamper the enamine formation with the aldehyde: In the case of the sterically crowded catalyst **9**, DMSO as the solvent may be assumed to block the nitrogen whereas in the case of the less crowded **8** an additional small and multiple H-bond acceptor such as the carboxylate ion can exert this effect.

If this hypothesis is true, one should be able to prove the steric shielding of the nitrogen atom experimentally by a reduced exchange rate of the nitrogen-bound proton HN. For instance, such reduced exchange rates can be evidenced NMR spectroscopically by the observation of homonuclear scalar couplings to the exchangeable proton or by identical diffusion coefficients of exchangeable and non-exchangeable protons within the same molecule. Indeed, both of these NMR spectroscopic features were observed on the level of catalyst/additive solvent combinations only in those cases, for which decelerated enamine formation was observed, too, *i.e.* for **9** in DMSO-d_6 and for **8**/K_2CO_3 (likewise for **8**/Na_2CO_3) in DMSO-d_6, but most notably not for **8** with other basic additives such as acetates (NaOAc, KOAc) or NEt_3. First, the hampered HN exchange manifests itself in the appearance of scalar proton-proton couplings $^3J_{H,H}$ between HN and the adjacent protons Hα and Hδ1,2 in the one-dimensional ^{1}H spectra (see Figure 6.7C). Secondly, the slow HN exchange is also evidenced from DOSY investigations (data not shown): For **8**/K_2CO_3 in DMSO-d_6, identical diffusion coefficients are observed for HN and the non-exchangeable protons of the catalyst **8**. In contrast, in the absence of K_2CO_3 the diffusion of HN appears to be a lot faster than the one of the non-exchangeable protons of **8** because of the exchange of HN with the faster diffusing residual water in the sample during the diffusion period of 50 ms. Both the $^3J_{H,H}$ scalar couplings to HN and the diffusion coefficients of HN indicate a substantially slower exchange of the nitrogen-bound proton HN for **9** or **8**/K_2CO_3 in DMSO than in all the other cases and are therefore in line with our hypothesis of a combination of steric crowding and H-bonding interactions at the nitrogen atom that compromises the tendency of the nitrogen to form enamines.

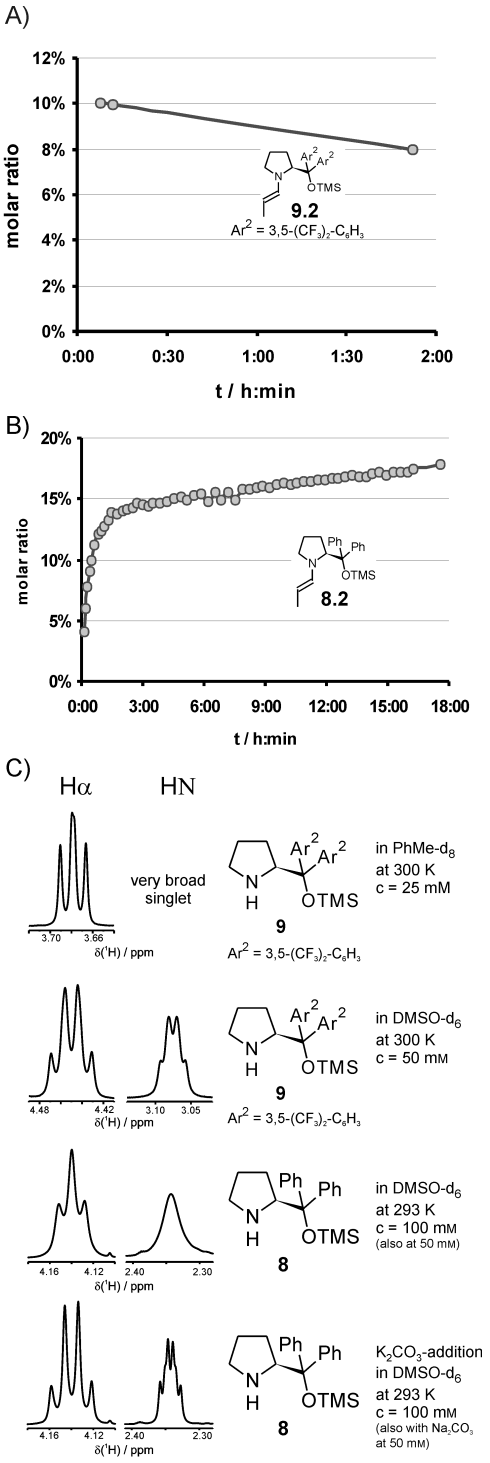

Figure 6.7: Evolution of the amounts of enamine derived A) from **2** and the diarylprolinol ether **9** in PhMe-d_8 and B) from **2** and the diphenylprolinol ether **8** with 100 mol% K_2CO_3 in DMSO-d_6 over time as monitored by 1D ^{1}H NMR spectroscopy. (Note: The total amount of aldehyde-derived species in the first spectrum was set to 100 %.); C) ^{1}H NMR resonances of Hα (left column) and HN (right column) of **9** in PhMe-d_8 (1^{st} row), of **9** in DMSO-d_6 (2^{nd} row), of **8** in DMSO-d_6 (3^{rd} row) and of **8** in DMSO-d_6 with 100 mol% K_2CO_3 (4^{th} row): Additional resonance splittings of the signals for **9** and **8**/K_2CO_3 in DMSO-d_6 are indicative of the presence of $^3J_{H,H}$ couplings to HN.

These two NMR spectroscopic characteristics may hence be regarded as a very simple and rapid method to check catalyst/additive/solvent combinations for the delayed enamine formation with aldehydes (see Figure 6.8 for a graphical summary of this screening method and Figure 6.13 and 6.14 in the Supporting Information, chapter 6.3, for the NMR assignments of the catalysts). This may help to avoid resulting, potentially disadvantageous effects in diarylprolinol silyl ether catalysis, for instance, one may speculate that the delayed enamine formation is one of the reasons for the inferior performance of **9** in DMSO than in other solvents[51] and for the even more detrimental effect of K_2CO_3 than of other basic additives (NaOAc and NEt_3) to **8** in DMSO.[52]

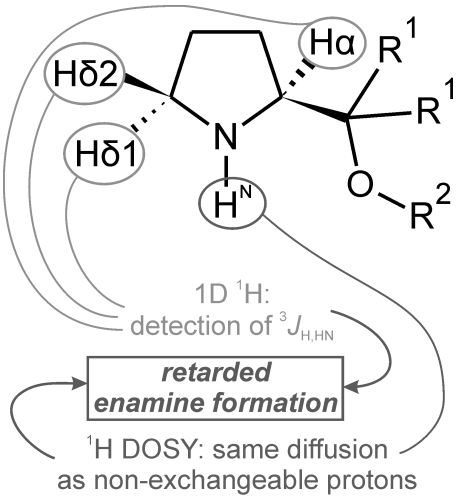

Figure 6.8: Graphical summary of the screening methods for the decelerated formation of prolinol (ether) enamines on the early level of the catalyst/additive solvent combination.

Conclusion

In summary, we have investigated the formation and stability of enamines derived from prolinol(ether)-type organocatalysts with two different aldehydes in various solvents by means of NMR spectroscopy. In all enamines studied, the *E*-configuration is adopted predominantly. For prolinol ether enamines with small aldehyde alkyl chains, we could evidence for the first time the presence of the *Z*-isomer besides the *E*-enamine in solution.

For prolinol-derived catalysts, the first *in situ* detection of enamine intermediates is presented. Similarly to proline enamines, they can be observed only in the dipolar aprotic solvent DMSO, but not in methanol, acetonitrile, chloroform, or toluene. In contrast to proline, however, these prolinol enamines are shown to coexist in a "parasitic equilibrium" with the isomeric oxazolidines since they rapidly undergo cyclization. In the case of prolinol, the oxazolidine formation is easily reversible and the thermodynamic equilibrium between the enamine and both oxazolidines is slowly established. In diphenylprolinol, the geminal phenyl rings shift this equilibrium, presumably through the Thorpe-Ingold effect, virtually completely towards the exclusively detected kinetic *endo*-oxazolidine which is then appropriately termed a "dead end" of prolinol enamine catalysis. Yet, this state can

be overcome by destabilizing the *endo*-oxazolidine and by stabilizing the prolinol enamine with the help of bulkier and electron-withdrawing aryl substituents. In this context, also the first prolinol-derived carbinol amine was detected *in situ*.

Diarylprolinol ether enamines are detected readily *in situ*. Their amounts decrease with increasing sizes of the aryl rings and of the *O*-protecting group probably owing to steric conflicts with the enamine moiety. Methyl ether enamines are more robust than silyl ethers as, for the latter, we could monitor the desilylation and subsequent cyclization to the oxazolidine in DMSO. A drastically delayed formation of the prolinol ether enamines is observed for unfortunate combinations of aldehydes, catalysts, solvents, and additives, possibly caused by the stabilization of carbinolamines and/or by the steric shielding of the nitrogen atom. Based on its concordance with a reduced exchange rate of the nitrogen protons, a rapid and facile 1D ^{1}H- or DOSY-based screening method on the level of the catalytic systems themselves is presented for this potentially detrimental effect.

On the examples of prolinol- and prolinol ether-derived enamines, we illustrate the impact of the size and the electronic properties of the pyrrolidine substituent on the delicate interplay between intermediate selectivities and reactivities in terms of the conformational preferences (s-*cis*/s-*trans*) of enamines, their amounts, and their robustness. Our results hence provide a broad experimental basis for an improved understanding of enamine catalysis by diarylprolinol(ether)s. They should also inspire to further studies on the elucidation of the prolinol (ether) enamine formation pathway, including the role of oxazolidines and carbinolamines therein and the issue of the enamine formation rate. Likewise, they are expected to pave the way for conformational investigations aiming at the origin of stereoselection exerted by prolinol (ether) organocatalysts. From a more practical point of view, helpful advice for the optimization of reaction conditions is provided for synthetically working organic chemists. Despite their tremendous success in enamine catalysis, there is still sufficient space for improving the scaffolds of prolinol ether organocatalysts, for instance, by avoiding *O*-deprotection in solution or too long reaction times, caused by low enamine amounts and formation rates. In this context, our rapid screening method may facilitate the future optimization of the prolinol (ether) catalyst scaffold by substituent variations. On this basis, also the fine-tuning of the selectivity-reactivity balance for prolinol catalysts ("parasitic equilibrium") should be facilitated and might help to expand the scope of prolinol derivatives for enamine catalysis.

6.3 Supporting Information

Experimental Section

Enamines were created *in situ* inside a standard 5 mm NMR tube by adding freshly distilled aldehydes **1** or **2** (30 μmol, if not stated otherwise) to a solution of one equivalent of the organocatalysts **3**-**9**, respectively, in 0.6 mL of deuterated solvent. The NMR tube was transferred to the spectrometer immediately after the mixing of all reacting components.

NMR measurements were performed at 300 K on a Bruker Avance DRX 600 (600.13 MHz) and on a Bruker Avance III 600 (600.25 MHz) spectrometer, the latter equipped with a TCI cryoprobe with z-gradient (53.5 G/cm). Reaction monitoring by 1D ^{1}H-NMR spectra was employed to identify appropriate time slots for more detailed 2D NMR spectroscopic investigations: ^{1}H,^{1}H-COSY, ^{1}H,^{1}H-NOESY/EXSY (mixing time 700 ms), ^{1}H,^{13}C-HSQC and ^{1}H,^{13}C-HMBC spectra were recorded for the characterization of the observed species if information from 1D NMR spectra proved to be insufficient. NMR data were processed and evaluated with Bruker´s TOPSPIN 2.1.

Additional Information

NMR Characterization of Enamines

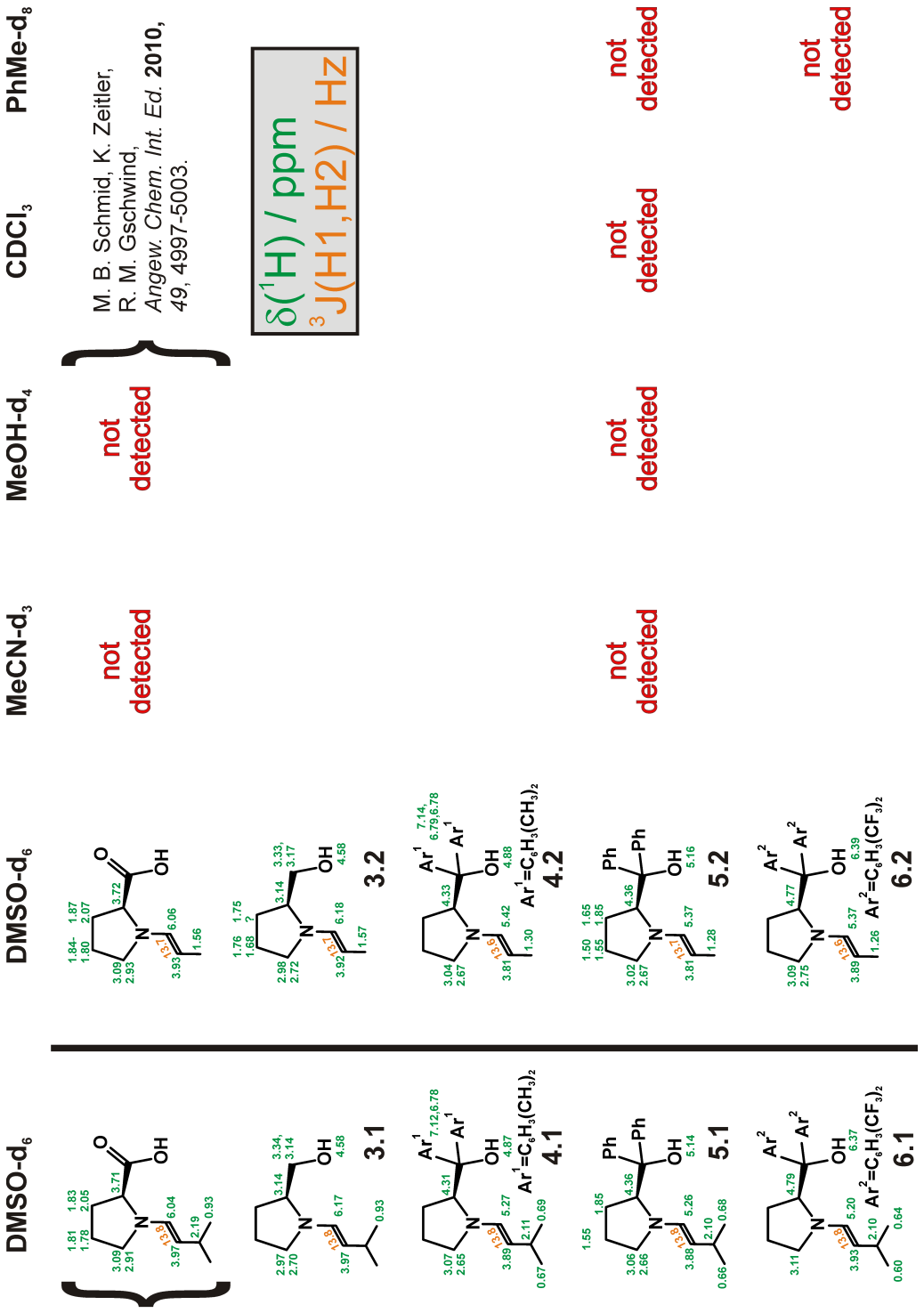

Figure 6.9: Overview of the prolinol enamines, relevant ^{1}H chemical shifts and coupling constants. (Note: Chemical shifts of Hβ1, Hγ1 and Hδ1 are listed below those of Hβ2, Hγ2, Hδ2.)

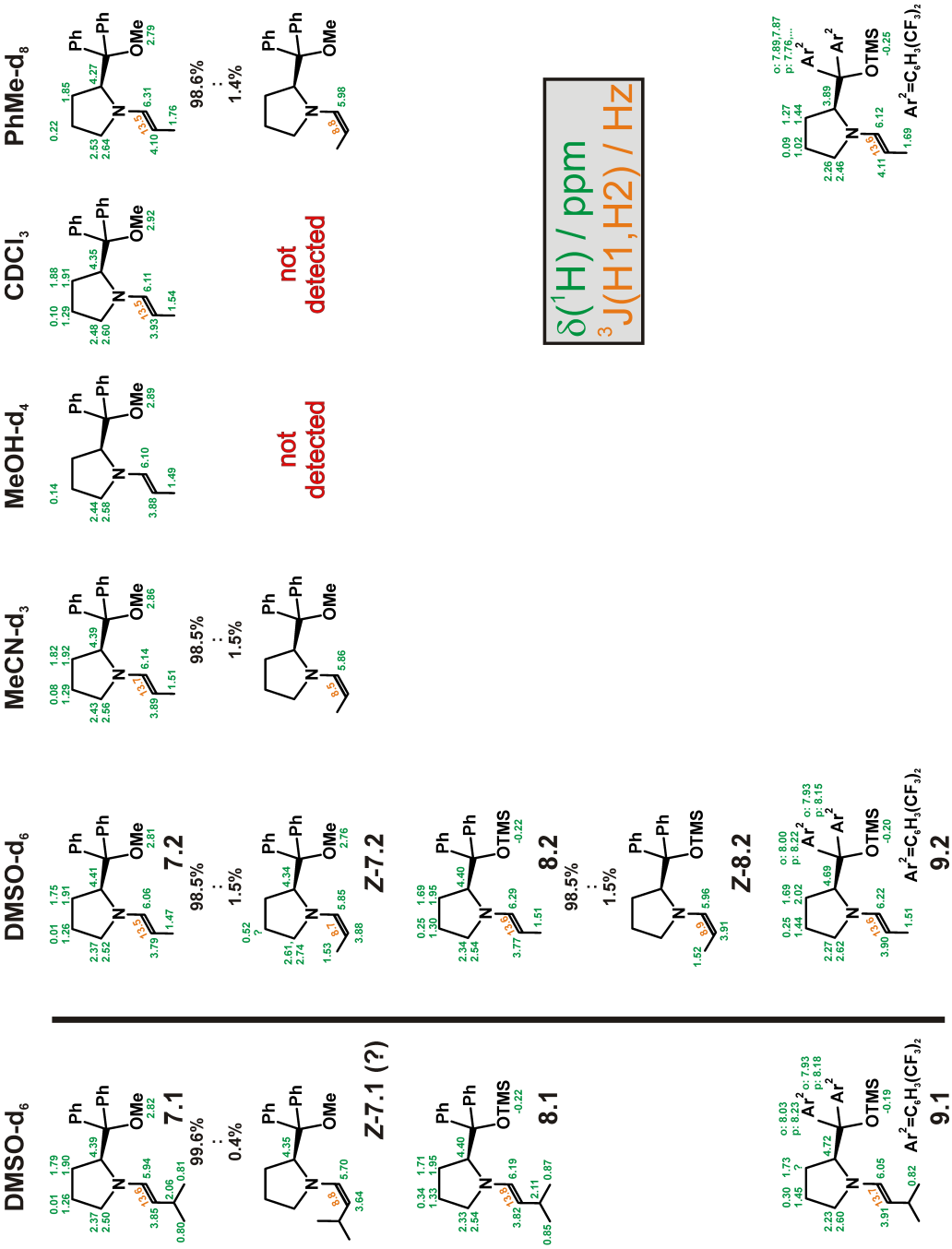

Figure 6.10: Overview of the prolinol ether enamines, relevant ^{1}H chemical shifts and coupling constants. (Note: Chemical shifts of Hβ1, Hγ1 and Hδ1 are listed below those of Hβ2, Hγ2, Hδ2.)

Oxazolidine Formation

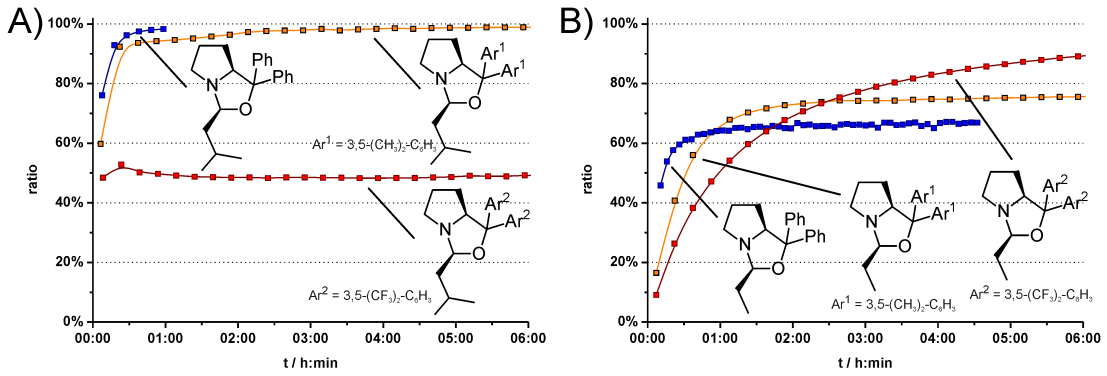

Figure 6.11: Buildup curves of oxazolidines derived from aldehydes **1** (A) or **2** (B) and prolinol catalysts **4**-**6** in DMSO-d_6 at 300 K. In the case of **2** (B), the self-aldolization of the aldehyde was observed so that the oxazolidine formation is not quantitative. In the case of **1** and **6** (red curve in A), a not yet identified unproductive side-reaction prevented the formation of higher amounts of the oxazolidine.

NMR Characterization of a Carbinolamine and an Exemplary Enamine Intermediate

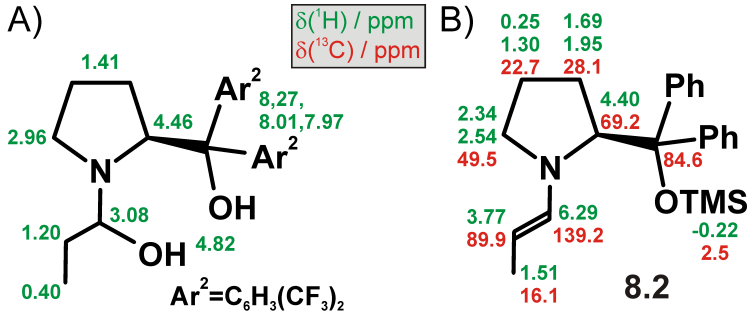

Figure 6.12: A) Fragmentary ^{1}H NMR assignment of a carbinolamine derived from propionaldehyde **2** and catalyst **6** (in DMSO-d_6); B) complete NMR assignment of the enamine **8.2**, accomplished by 2D NMR methods in DMSO-d_6. (The phenyl rings could not be assigned without ambiguities because of severe spectral overlap. Note: Chemical shifts of Hβ1, Hγ1 and Hδ1 are listed below those of Hβ2, Hγ2, Hδ2.)

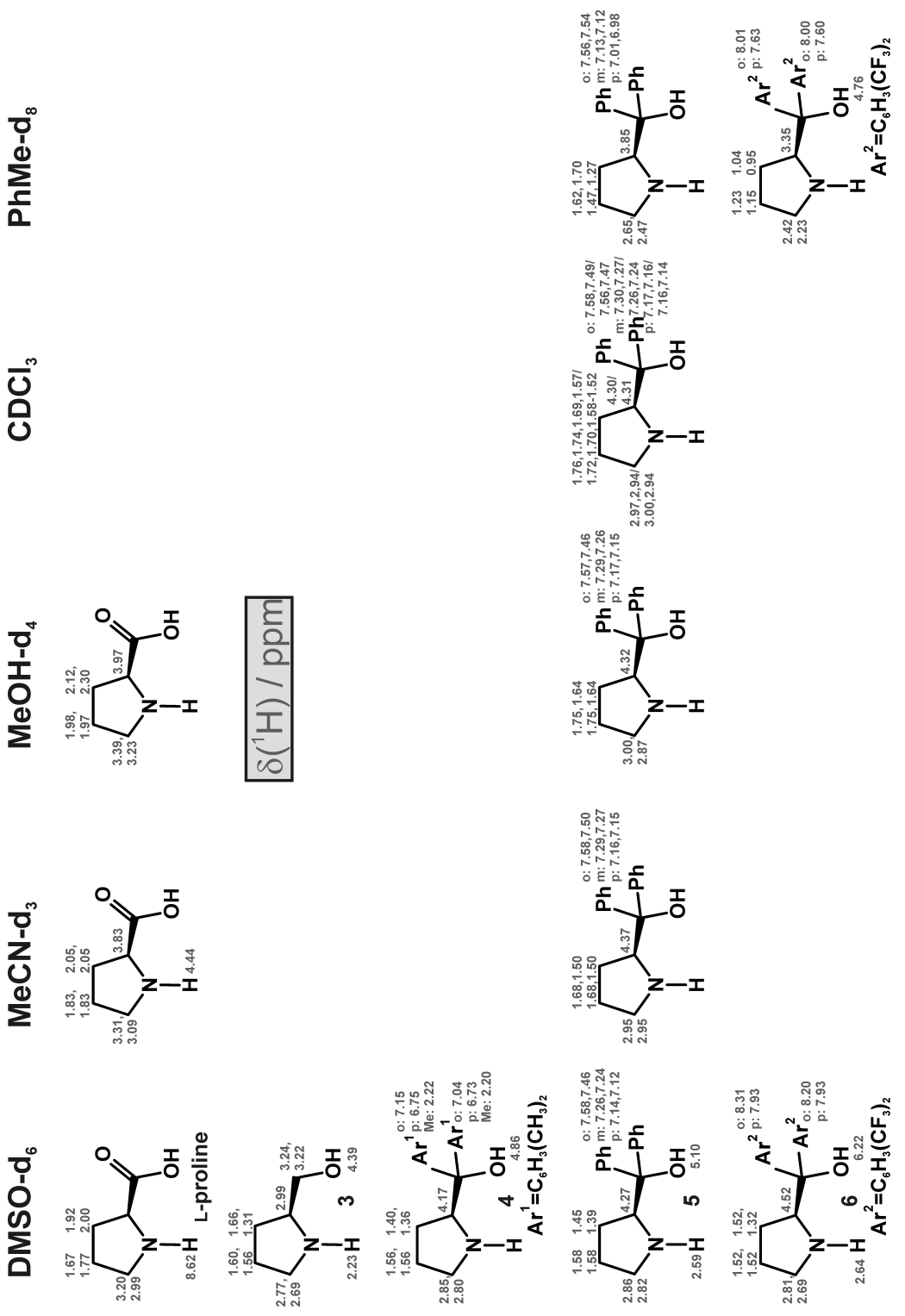

Figure 6.13: ^{1}H chemical shift assignment and relevant coupling constants of the prolinol organocatalysts. (Note: Chemical shifts of Hβ1, Hγ1 and Hδ1 are listed below those of Hβ2, Hγ2, Hδ2.)

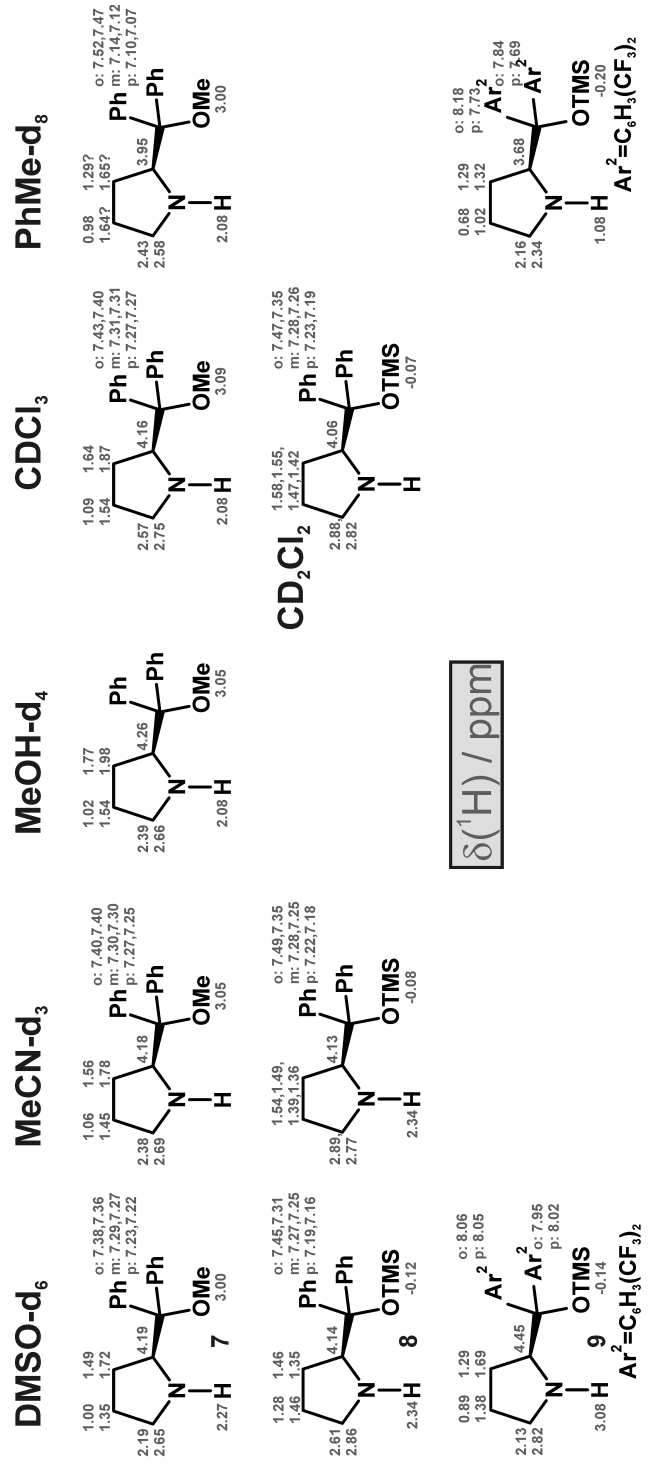

Figure 6.14: ^{1}H chemical shift assignment and relevant coupling constants of the prolinol ether organocatalysts. (Note: Chemical shifts of Hβ1, Hγ1 and Hδ1 are listed below those of Hβ2, Hγ2, Hδ2.)

6.4 References

[1] A. Berkessel, H. Gröger, *Asymmetric Organocatalysis - From Biomimetic Concepts to Applications in Asymmetric Synthesis*, Wiley-VCH, Weinheim, **2005**.

[2] *Enantioselective Organocatalysis: Reactions and Experimental Procedures* (Ed.: P. I. Dalko), Wiley-VCH, Weinheim, **2007**.

[3] *Chem. Rev.* **2007**, *107*, 12 (special issue on organocatalysis).

[4] *Ernst Schering Foundation Symposium Proceedings "Organocatalysis"* (Eds.: M. T. Reetz, B. List, S. Jaroch, H. Weinmann), Springer, Berlin, **2008**.

[5] *Asymmetric Organocatalysis, Vol. 291* (Ed.: B. List), **2010**.

[6] B. List, *Chem. Commun.* **2006**, 819–824.

[7] S. Mukherjee, J. W. Yang, S. Hoffmann, B. List, *Chem. Rev.* **2007**, *107*, 5471–5569.

[8] P. Melchiorre, M. Marigo, A. Carlone, G. Bartoli, *Angew. Chem. Int. Ed.* **2008**, *47*, 6138–6171.

[9] S. Bertelsen, K. A. Jørgensen, *Chem. Soc. Rev.* **2009**, *38*, 2178–2189.

[10] P. M. Pihko, I. Majander, A. Erkkilä, *Top. Curr. Chem.* **2010**, *291*, 29–75.

[11] M. Nielsen, D. Worgull, T. Zweifel, B. Gschwend, S. Bertelsen, K. A. Jørgensen, *Chem. Commun.* **2011**, *47*, 632–649.

[12] U. Eder, G. Sauer, R. Wiechert, *Angew. Chem. Int. Ed.* **1971**, *10*, 496–497.

[13] Z. G. Hajos, D. R. Parrish, *J. Org. Chem.* **1974**, *39*, 1615–1621.

[14] B. List, R. A. Lerner, C. F. Barbas III, *J. Am. Chem. Soc.* **2000**, *122*, 2395–2396.

[15] Y. Chi, S. H. Gellman, *Org. Lett.* **2005**, *7*, 4253–4256.

[16] M. Marigo, T. C. Wabnitz, D. Fielenbach, K. A. Jørgensen, *Angew. Chem. Int. Ed.* **2005**, *44*, 794–797.

[17] Y. Hayashi, H. Gotoh, T. Hayashi, M. Shoji, *Angew. Chem. Int. Ed.* **2005**, *44*, 4212–4215.

[18] C. Palomo, A. Mielgo, *Angew. Chem. Int. Ed.* **2006**, *45*, 7876–7880.

[19] A. Mielgo, C. Palomo, *Chem. As. J.* **2008**, *3*, 922–948.

[20] L. W. Xu, L. Li, Z. H. Shi, *Adv. Synth. Catal.* **2010**, *352*, 243–279.

[21] A. Lattanzi, *Chem. Commun.* **2009**, 1452–1463.

[22] G. Zhong, J. Fan, C. F. Barbas III, *Tetrahedron Lett.* **2004**, *45*, 5681–5684.

[23] D. Enders, S. Chow, *Eur. J. Org. Chem.* **2006**, *2006*, 4578–4584.

[24] Y. Hayashi, T. Itoh, S. Aratake, H. Ishikawa, *Angew. Chem. Int. Ed.* **2008**, *47*, 2082–2084.

[25] Y. Hayashi, S. Samanta, T. Itoh, H. Ishikawa, *Org. Lett.* **2008**, *10*, 5581–5583.

[26] M. B. Schmid, K. Zeitler, R. M. Gschwind, *Angew. Chem. Int. Ed.* **2010**, *49*, 4997–5003.

[27] X. Zhu, F. Tanaka, R. A. Lerner, C. F. Barbas III, I. A. Wilson, *J. Am. Chem. Soc.* **2009**, *131*, 18206–18207.

[28] D. Seebach, U. Grošelj, D. M. Badine, W. B. Schweizer, A. K. Beck, *Helv. Chim. Acta* **2008**, *91*, 1999–2034.

[29] U. Grošelj, D. Seebach, D. M. Badine, W. B. Schweizer, A. K. Beck, I. Krossing, P. Klose, Y. Hayashi, T. Uchimaru, *Helv. Chim. Acta* **2009**, *92*, 1225–1259.

[30] S. Bertelsen, M. Marigo, S. Brandes, P. Diner, K. A. Jørgensen, *J. Am. Chem. Soc.* **2006**, *128*, 12973–12980.

[31] S. Lakhdar, T. Tokuyasu, H. Mayr, *Angew. Chem. Int. Ed.* **2008**, *47*, 8723–8726.

[32] Z. Rappoport, *The Chemistry of Enamines*, Wiley, New York, **1994**.

[33] R. Knorr, *Chem. Ber.* **1980**, *113*, 2441–2461.

[34] J. Franzén, M. Marigo, D. Fielenbach, T. C. Wabnitz, K. A. Jørgensen, *J. Am. Chem. Soc.* **2005**, *127*, 18296–18304.

[35] P. Dinér, A. Kjærsgaard, M. A. Lie, K. A. Jørgensen, *Chem. Eur. J.* **2008**, *14*, 122–127.

[36] J.-Q. Zhao, L.-H. Gan, *Eur. J. Org. Chem.* **2009**, *2009*, 2661–2665.

[37] C. T. Wong, *Tetrahedron* **2009**, *65*, 7491–7497.

[38] Y. Okuyama, H. Nakano, H. Hongo, *Tetrahedron: Asymmetry* **2000**, *11*, 1193–1198.

[39] G. Zuo, Q. Zhang, J. Xu, *Heteroat. Chem.* **2003**, *14*, 42–45.

[40] R. M. Beesley, C. K. Ingold, J. F. Thorpe, *J. Chem. Soc. Trans.* **1915**, 1080–1106.

[41] S. M. Bachrach, *J. Org. Chem.* **2008**, *73*, 2466–2468.

[42] T. F. Magnera, G. Caldwell, J. Sunner, S. Ikuta, P. Kebarle, *J. Am. Chem. Soc.* **1984**, *106*, 6140–6146.

[43] K. Juhl, K. A. Jørgensen, *Angew. Chem. Int. Ed.* **2003**, *42*, 1498–1501.

[44] P. Melchiorre, K. A. Jørgensen, *J. Org. Chem.* **2003**, *68*, 4151–4157.

[45] N. Halland, A. Braunton, S. Bachmann, M. Marigo, K. A. Jørgensen, *J. Am. Chem. Soc.* **2004**, *126*, 4790–4791.

[46] E. Reyes, J. L. Vicario, D. Badía, L. Carrillo, *Org. Lett.* **2006**, *8*, 6135–6138.

[47] H. Ahlbrecht, S. Fischer, *Tetrahedron* **1970**, *26*, 2837–2848.

[48] M. C. Varela, S. M. Dixon, K. S. Lam, N. E. Schore, *Tetrahedron* **2008**, *64*, 10087–10090.

[49] E. Alza, M. A. Pericàs, *Adv. Synth. Catal.* **2009**, *351*, 3051–3056.

[50] I. Mager, K. Zeitler, *Org. Lett.* **2010**, *12*, 1480–1483.

[51] Q. Zhu, Y. Lu, *Org. Lett.* **2008**, *10*, 4803–4806.

[52] D. Enders, C. Wang, J. Bats, *Angew. Chem. Int. Ed.* **2008**, *47*, 7539–7542.

7 Conformational Preferences of Prolinol (Ether) Enamines

Article

"Distinct Conformational Preferences of Prolinol and Prolinol Ether Enamines in Solution Revealed by NMR"

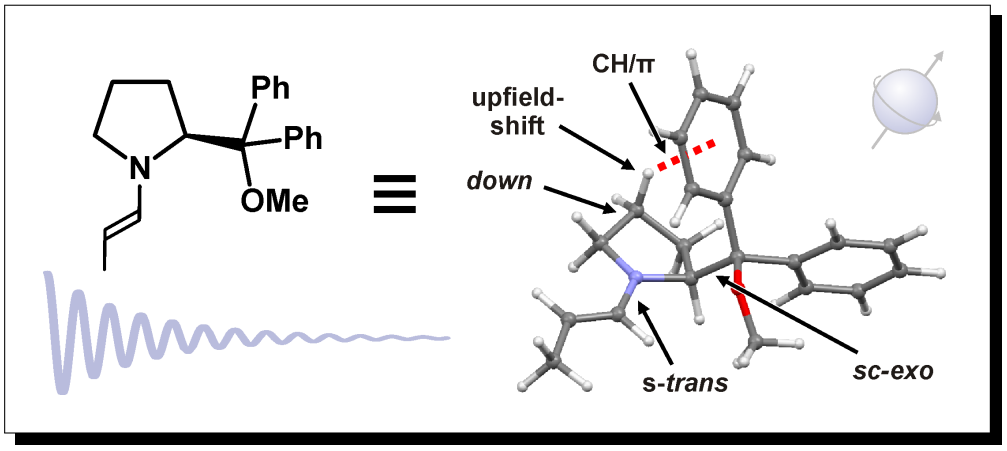

Markus B. Schmid, Kirsten Zeitler, and Ruth M. Gschwind

J. Am. Chem. Soc. **2010**, *submitted for publication.*

7.1 Abstract

Enamine key intermediates in organocatalysis, derived from aldehydes and Jørgensen/ Hayashi-type prolinol or prolinol ether catalysts, were investigated conformationally in different solvents by means of NMR spectroscopy in order to provide an experimental basis for a better understanding of the origin of stereoselectivity. Owing to the bulkiness of the pyrrolidine α-substituent, the enamines of diarylprolinol (ether) catalysts exist exclusively in the s-*trans* conformation, while a prolinol enamine is shown for the first time to partially populate the s-*cis* conformation in solution. In all enamines studied and in contrast to the free catalysts, the pyrrolidine ring is found to adopt the *down* conformation. In the case of diarylprolinol ether enamines, exclusively the sc-*exo* conformation around the exocyclic Cα-Cϵ bond is observed, which is stabilized by CH/π interactions. In contrast, diarylprolinol enamines adopt the sc-*endo* conformation allowing for an OH$\cdots$N hydrogen bonding and a CH/π interaction. A rapid conformational screening method for these conformational enamine features was developed and applied to show their generality for various catalyst, aldehyde, and solvent combinations. Thus, by revealing unexpectedly pronounced conformational preferences of prolinol and prolinol ether enamines in solution, our study provides for the first time an experimental basis for discussing the previously controversial questions of s-*cis*/s-*trans* and *sc-endo*/*sc-exo* conformation of prolinol and prolinol ether enamines. The presented conformational preferences are in agreement with the experimental results from synthetic organic chemistry. Our results are therefore expected to have a significant impact for future theoretical calculations and synthetic optimizations of asymmetric prolinol (ether) enamine catalysis.

7.2 Manuscript

Introduction

In-depth studies on intermediate species are highly important for a better understanding of the mechanistic principles that underlie organic reactions. In particular, conformational analyses of active intermediates may guide towards the origin of stereocontrol in asymmetric reactions and are therefore highly valuable for the directed optimization of already existing and the design of novel high-performance catalysts in the important and ever growing field of stereoselective catalysis. Modern asymmetric organocatalysis has contributed substantially to this research area throughout the last years,[1–5] with its many different concepts and activation modes[6,7] such as non-covalent catalysis via phase transfer[8] or hydrogen bonding[9–11] and covalent catalysis via Brønsted acids[12,13] or Lewis bases.[14] By typically making use of compounds originating from the chiral pool, catalysis by secondary amines[15–17] through enamine,[5,18] iminium,[19,20] or SOMO[21–23] activation has emerged as one of the most successfully and widely applicable principles. Especially proline[24–26] as well as Jørgensen/Hayashi-type prolinol ethers[27–32] have proven remarkable performances in asymmetric iminium and enamine organocatalysis. Though a lot less pronouncedly, prolinol-type organocatalysts[33] have also found applications based on enamine intermediates,[34–37] but are majorily employed for iminium catalysis.

Yet, regarding the vast number of synthetic applications, conformational studies on enamine intermediates, especially on the origin of stereoselection in enamine catalysis are rather scarce and experimental studies in solution are missing as yet. This can be partially attributed to the limited number of relevant enamines in solution reported so far: Only two prolinol silyl ether-type enamines have been isolated and characterized[38,39] and only one dienamine intermediate[40] and one product enamine[41] have been observed *in situ*. Accordingly, the conformations of such enamine intermediates in solution have been largely unknown and conformational information has been limited to theoretical calculations[39,40,42–44] and crystal structure analyses.[38,39] However, the respective shortcomings of these approaches such as potential vacuum calculation artifacts and crystal packing effects, for instance, had to be put up with so that "wishful thinking" (as stated by Seebach, Uchimaru *et al.*[39]) could not be totally eliminated from conformational considerations. Different results concerning the conformational preference of both the exocyclic N-C bond[38–40,42–44] and the exocyclic C-C bond[39,40,42–44] of diarylprolinol ether enamines have therefore been put forward in the literature. Only recently could we expand the available pool of enamines in solution by various aldehyde-derived prolinol ether enamines (chapter 6), and, in addition, by the first enamine intermediates derived from proline[45] and prolinols (chapter 6). Thus, the foundation stone is laid for more detailed conformational studies on such enamine intermediates in solution that should help to understand the origin of stereoselection and hence to tailor optimized organocatalysts.

To fill this gap, we designed *in situ* NMR studies on reactive prolinol and prolinol ether enamines. In this article, we present the first detailed experimental investigations on the conformations of enamines, derived from aldehydes and prolinol(ether)-type organocatalysts, by means of NMR spectroscopy in different solvents. ^{1}H,^{1}H-NOESY spectra reveal the preference of the enamine s-*trans* arrangement owing to the steric influence of the pyrrolidine α-substituent. In addition, the pyrrolidine ring is shown by scalar coupling constants to predominantly adopt the *down* conformation which allows for intramolecular CH/π interactions between pyrrolidine protons and the aryl groups of the "obese" α-substituent. In the case of diarylprolinol ether enamines exclusively the *sc-exo* conformation for the exocyclic Cα-Cϵ bond was observed which is stabilized by two CH/π interactions. For diarylprolinol-derived enamines in contrast, only the *sc-endo* conformation was found which allows for both an OH$\cdots$N hydrogen bond and one CH/π interaction. In addition, a rapid and facile 1D ^{1}H NMR-based screening approach for this conformational feature, which plays a key role in the shielding of one face of the enamine and hence in the stereocontrol effectuated by the organocatalyst, is presented.

Results and Discussion

Model Enamines. Our recent studies on proline enamines[45] and on the formation and stability of prolinol (ether) enamines (chapter 6) in solution provided the basis for our conformational enamine investigations: Various typical secondary amine catalysts (Figure 7.1: **3**-**9**)[27–29] were selected as the organocatalysts of interest for our study. Two different aldehydes, 3-methyl-butyraldehyde **1** and propionaldehyde **2** (Figure 7.1), were chosen as representatives of aldehydes with alkyl chains of different sizes, to suppress the unwanted self-aldolization (**1**)[45] and to provide a substantial relevance for organocatalytic applications (**2**). Since DMSO was the only solvent that allowed for the detection of prolinol enamines (chapter 6), we predominantly used it as the solvent of choice for our conformational investigations to facilitate the comparison of the results of prolinol and prolinol ether enamines. For the prolinol ether enamines, the obtained results were then verified for selected other solvents (methanol, acetonitrile, chloroform, dichloromethane, and toluene).

All experiments mentioned hereafter (if not stated otherwise) were performed within NMR tubes by mixing equimolar amounts of aldehyde and catalyst in perdeuterated solvents to obtain concentrations of 50 mM each and NMR spectra were recorded at 300 K (see Experimental Section, chapter 7.3 for details). Overall 14 different enamines formed from the aldehydes **1**-**2** and the organocatalysts **3**-**9** (designated as "catalyst-number.aldehyde-number", *i.e.* as **3.1**-**9.2**; Figure 7.2) were obtained *in situ* and investigated in different solvents. The detection and characterization as majorily *E*-configured enamines has been reported recently (chapter 6.2, see also Figure 7.9 and 7.10 in the Supporting Information, chapter 7.3, for the NMR assignments).

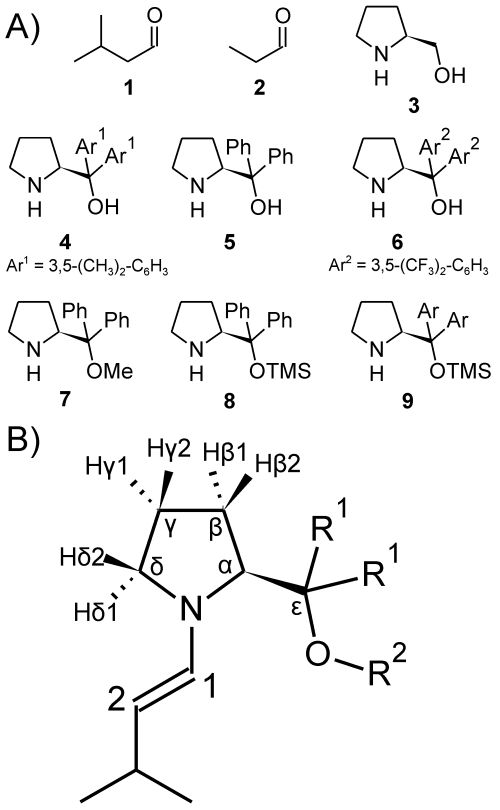

Figure 7.1: A) Aldehydes and organocatalysts examined in this study; B) general atom nomenclature used for enamines derived thereof.

Enamine Conformations. Besides the already reported aspects concerning the stability, formation, and degradation of enamine intermediates (chapter 6), knowledge on how the stereoselectivity is controlled in the bond-forming step is of utmost importance for the understanding of organocatalyzed asymmetric reactions. On the basis of theoretical calculations[39,40,42–44] and crystal structure analyses[38,39] and in agreement with experimental results, it is generally assumed that the methanol(ether)-substituent of the pyrrolidine ring secures both the s-*trans* arrangement of the enamine and the effective shielding of one face of the enamine π system, thereby directing incoming electrophiles to the opposite side.[39] In the following, we present the results of our conformational investigations of the prolinol (ether) *E*-enamines **3.1**-**9.2** in solution by NMR spectroscopy, mainly based on ^{1}H,^{1}H-NOESY spectra, which provide the first detailed insights into the conformations of these reactive intermediates in organocatalysis concerning the conformation of the pyrrolidine ring as well as the conformations around the exocyclic N-C1 and Cα-Cϵ bonds.

s-*cis*- and s-*trans*-Enamines: Conformation of the exocyclic N-C1 bond. One of the two supposed functions of the (diaryl)methanol(ether) substituent in the organocatalysts **3**-**9** is the shift of the equilibrium between the two enamine intermediate conformations (s-*cis* and s-*trans* of the N-C1 single bond with partial double bond character) towards

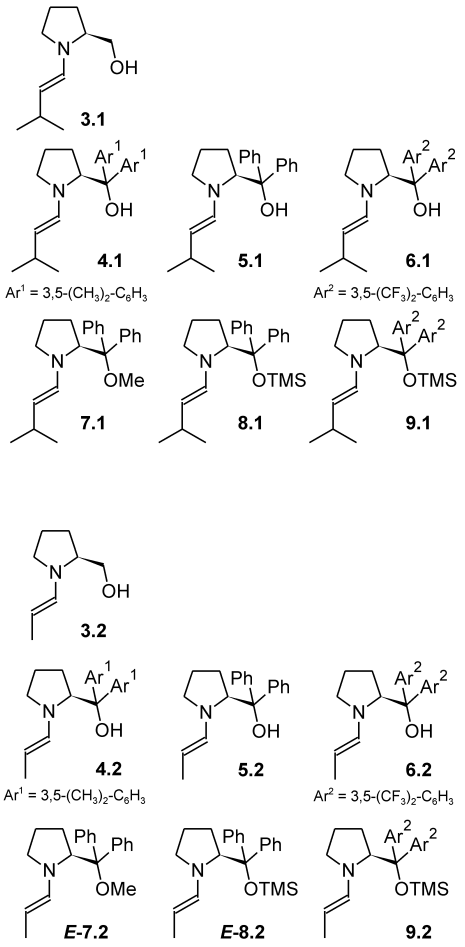

Figure 7.2: Overview on the investigated *E*-enamines derived from aldehydes **1** and **2** and catalysts **3**-**9**. All enamines are displayed in the (more stable) s-*trans* conformation around the exocyclic N-C bond.

the s-*trans* conformation, most likely by unfavorable steric repulsion.[39] Likewise, a correlation of the s-*cis* and s-*trans* enamine stabilities to the preference of the corresponding isomeric *E*-iminium ion over the *Z*-isomer can be assumed as both biases are thought to originate from the same steric effect (Figure 7.3A).[39] The guarantee of this basic conformational feature of the enamine key intermediate by the bulky α-substituent is believed to be essential for the stereochemical outcome of prolinol(ether)-catalyzed reactions. For instance, the stereochemical implication of the s-*cis* s-*trans* enamine equilibrium for the formation of the isomeric oxazolidines by prolinol catalysts has been pointed out by us recently (chapter 6). The predominance of the s-*trans* enamine for proline was proposed by calculations[46] and experimentally proven by our NMR studies in solution[45] and exclusively s-*trans* proline enamines are detected in crystal structures.[47] Accordingly, also for prolinol ether enamines, the s-*trans* conformation is observed in crystal structures[38,39] and its energetic preference has been calculated thoroughly.[38–40,42–44] Interestingly, the generally accepted assumption that s-*trans* enamines of diarylprolinol silyl ethers are a lot more stable than the s-*cis* enamines has recently been challenged by two theoretical studies

that predict similar energies and hence similar populations of the s-*trans* and the s-*cis* conformation by gas-phase calculations.[39,43] To clarify this issue, we analyzed ^{1}H,^{1}H-NOESY spectra of the enamines **3.2**-**9.2** (Exemplary sections of these spectra are shown in Figure 7.3B.). We thereby considered the relative intensities of the NOEs between H1 and the protons Hα or Hδ1,2, respectively, as a suitable probe for the differentiation between the s-*trans* and the s-*cis* conformation (Figure 7.3A). While for the s-*trans* conformation, a stronger NOE between H1 and Hα is expected, a stronger NOE between H1 and Hδ1,2 would be indicative of the predominant population of the s-*cis* conformation. As an additional criterion, ^{1}H,^{13}C-HMBC cross-peak intensities between H1 and Cα or Cδ, respectively, can be used since $^{3}J_{H,C}$ couplings are known to be larger in an antiperiplanar than in a synperiplanar arrangement.[48] Accordingly, a larger HMBC cross-peak H1-Cδ is indicative of the s-*trans* conformation whereas the s-*cis* conformation is revealed by a larger H1-Cα cross-peak.

In our experiments, significantly more intensive cross-peaks from H1 to Hα than to Hδ1,2 were observed for all the enamines investigated by NOESY spectra, *i.e.* for **3.2**, **5.2**, **7.2**-**9.2** as well as for **5.1**, **7.1** and **8.1** in DMSO-d_6 and, in addition, for **7.2** in $CDCl_3$ and for **9.2** in PhMe-d_8. This indicates that the s-*trans* conformation is indeed preferably populated by enamines derived from different aldehydes in both polar and non-polar solution. This finding is confirmed by the ^{1}H,^{13}C-HMBC spectrum of **8.2**: The more intensive cross-peak between H1 and Cδ in comparison to H1 and Cα (Figure 7.3B, right) evidences a larger $^{3}J_{H,C}$ coupling between H1 and Cδ and thus indicates the preferred adoption of the s-*trans* conformation of the enamine, too.

We furthermore studied to what extent the methanol (ether) substituent has an impact on the actual position of the s-*cis* s-*trans* equilibrium by quantitative analyses of NOESY cross-peak volumes (The results are summarized in Table 7.1). For this purpose, the volume of the NOESY cross-peak between H1 and Hα was compared to the sum of the cross-peak volumes between H1 and Hδ1,2: The larger the ratio NOE(H1-Hα):NOEs(H1-Hδ1,2), the larger is the contribution of the s-*trans* conformation to the s-*cis* s-*trans* equilibrium in solution. The theoretical ratio NOE(H1-Hα):NOEs(H1-Hδ1,2) for a pure s-*trans* enamine conformation was calculated on the basis of internuclear distances from DFT-optimized s-*trans* prolinol ether enamine structures provided in the literature.[43,44] Following this calculation, the maximum NOE ratio is about 9:1 for the pure s-*trans* conformation and can accordingly not be exceeded further (Table 7.1, two columns on the right).

From the experimental NOESY cross-peak integration of enamine **3.2** (Table 7.1), it becomes obvious that in the case of catalyst **3** the theoretical value of about 9:1 for the pure s-*trans* enamine conformation is not reached. This indicates the partial adoption of the s-*cis* conformation by **3.2** and hence represents the first experimental evidence that the s-*cis* conformation contributes significantly to the conformational ensemble of a prolinol enamine in solution. This interpretation is also supported by the observed slow equilibration between the isomeric prolinol oxazolidines via the s-*trans*-s-*cis* isomerization of the

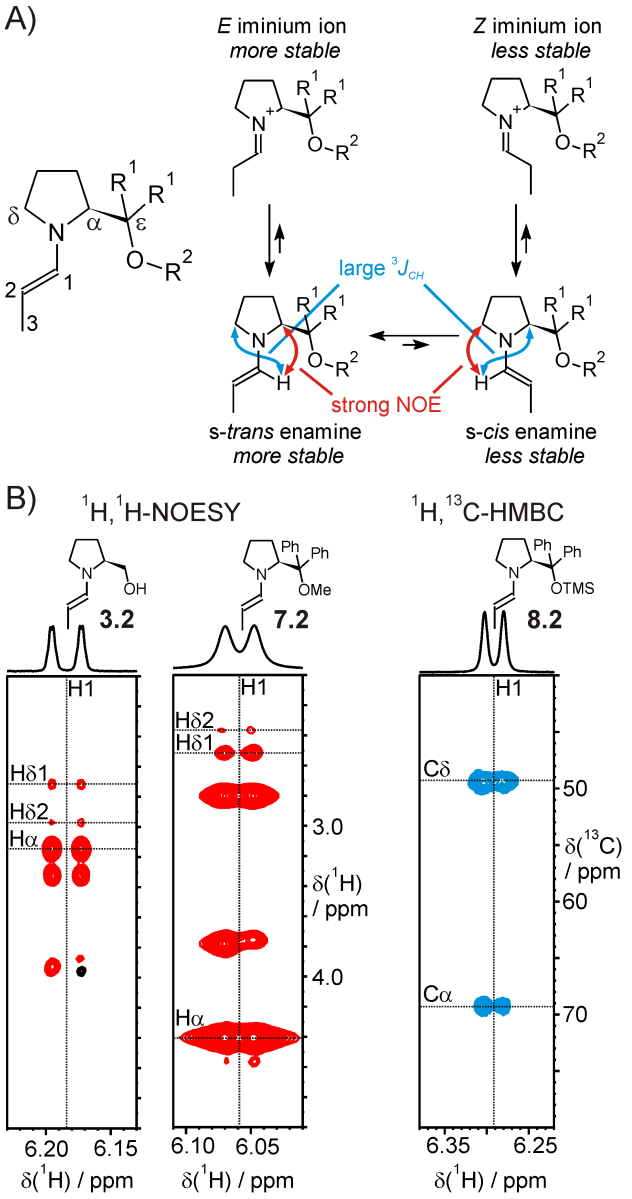

Figure 7.3: A) left: nomenclature used; right: equilibrium between enamine conformations, their connection to iminium ions, and distinctive NOEs; B) sections of ^{1}H,^{1}H-NOESY spectra of **3.2** (left) and **7.2** (middle) and of a ^{1}H,^{13}C-HMBC spectrum on **8.2** (right) in DMSO-d$_6$ at 300 K each.

enamines (chapter 6). In contrast, the increasing size of the pyrrolidine substituents in the catalysts **6-8** leads to an increase in the H1-Hα NOESY cross-peak intensity relative to the H1-Hδ1,2 cross-peak volumes from less than 8:2 to more than 9:1. This in turn can be interpreted as an evidence that more "obese" catalyst substitution patterns indeed enforce a stronger preference of the s-*trans* enamine conformation. However, interestingly, there is no significant additional increase in the NOESY cross-peak ratio visible by enlarging either the pyrrolidine substituent (from **7.2** over **8.2** to **9.2**) or the aldehyde alkyl chain (compare entries for **7.1** and **8.1**). In all these cases, the congruence of the experimental NOE ratios

	normalized NOESY cross-peak volumes				
	experimental values			theoretical values (s-*trans* enamines)	
NOE pair	**3.2**	**7.2**,**8.2**,**9.2**	**7.1**,**8.1**	**8.2**[44]	**9.2**[43]
H1-Hα	$\leq$79[b]	91-94	90-91	88	92
H1-Hδ1 + H1-Hδ2	$\geq$21[b]	6-9	9-10	12	8

[a]The NOESY investigations were hampered for the diphenylprolinol enamines **5.1** and **5.2** by their short lifetimes which allowed only poor spectral resolution and made meaningful peak integration impossible.
[b]The spectrum of **3.2** suffers from peak overlap of Hα and one of the diastereotopic methanol protons Hϵ. Taking into account the overlap of the NOESY cross-peak H1-Hα with H1-Hϵ, the ratio of 8:2 must be taken as a drastically overestimated upper limit so that the actual increase in the cross-peak ratio from **3.2** to **7.2**-**9.2** should be even significantly higher.

Table 7.1: Experimental NOESY crosspeak volumes for different enamines[a] and theoretical values based on calculated[43,44] s-*trans* enamines structures.

with the theoretical values for the pure s-*trans* conformation (about 9:1 experimentally and theoretically) suggests that this "saturation" of the NOESY cross-peak ratio and accordingly of the corresponding s-*cis* s-*trans* population ratio can be understood in terms of an almost exclusive adoption of the s-*trans* conformation for all diarylprolinol (ether) enamines studied. In addition, this postulation of a negligible s-*cis* population of diarylprolinol ether enamines is also in line with our observations on the exclusive formation of the kinetic *endo*-oxazolidines by diarylprolinol catalysts (chapter 6).

***up* and *down*: Conformation of the pyrrolidine ring.** To our knowledge, no attention has been paid to the potential influence of the puckering of the pyrrolidine ring on the overall conformation of enamines derived from prolinol-based organocatalysts. Only for proline-derivatives has the pyrrolidine conformation in aldol transition states been studied theoretically.[49] This previous lack of interest is striking in view of the fact that the pyrrolidine ring is known to be a privileged structure[26,50,51] since proline as an organocatalyst has been found to provide significantly better yields and stereoselectivities than related catalysts with four- or six-membered rings. Accordingly, in the context of diarylprolinol ether enamines, only one single comment on the pyrrolidine conformation has become known to us from an X-ray study which states that "the puckering of the pyrrolidine ring varies from structure to structure".[38] However, to our mind, one should consider conformational preferences of the pyrrolidine ring in more detail for two reasons: First, pyrrolidine hydrogen atoms may potentially participate in stabilizing CH/π interactions[52–54] with the phenyl rings in diarylprolinol (ether) enamines; these weak interactions have proven to have important implications not only in biochemistry,[55,56] but also in molecular recognition and organic chemistry.[57–60] Secondly, in general, different pyrrolidine ring conformations may well be associated with different reactivities[61] and also catalytic performances of the underlying compounds.[49,62] In particular, in diarylprolinol ether enamines the pyrrolidine *up* conformation in combination with the known slight pyramidality of the enamine ni-

trogen atom[38–40,42–44,49] creates a concave surface for the attack of the electrophile (the convex surface is supposed to be shielded by the "obese" α-substituent, Figure 7.4A, left), which is known to be a sterically highly unfavorable situation. In contrast, in the *down* conformation the enamine surface opposite to the "obese" substituent is convex and hence wide-open for the electrophilic attack towards the enamine.

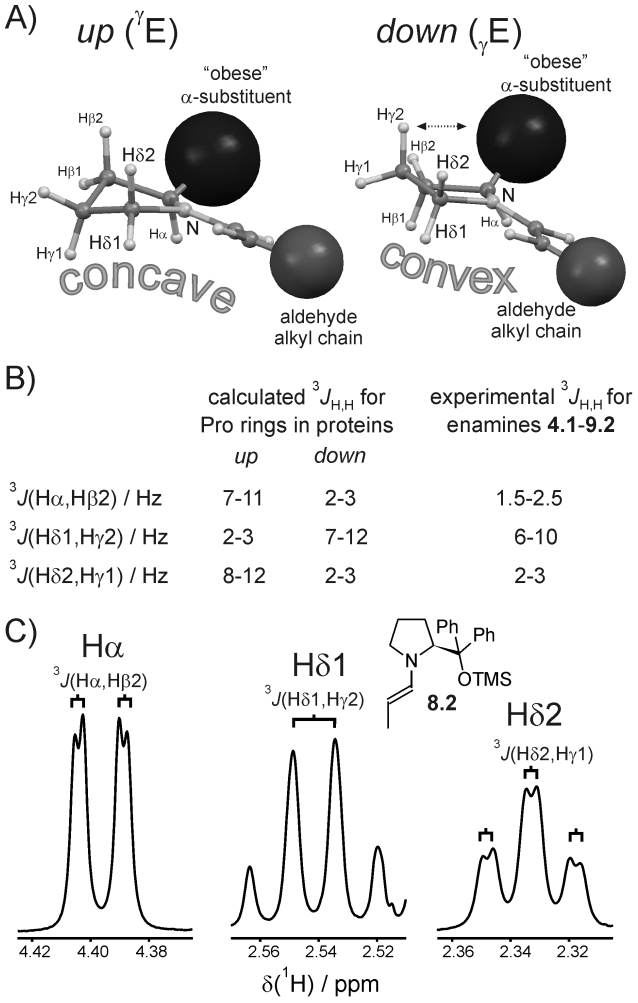

Figure 7.4: A) The two low-energy pyrrolidine conformations "*up*" and "*down*"; B) distinguishing calculated $^3J_{H,H}$ coupling constants for *up* and *down* of proline rings in proteins[63] and the experimental range for the enamines investigated; C) sections of the 1D ^{1}H NMR spectrum of **8.2** in DMSO-d_6 at 300 K showing the typical multiplet patterns for Hα, Hδ1 and Hδ2 observed in diarylprolinol (ether) enamines.

To study experimentally the pyrrolidine conformation in prolinol (ether) derivatives, the extensive conformational investigations on proline side-chain conformations were used as a basis. For proline it has been established that two distinct puckered pyrrolidine envelope conformations are preferentially adopted in proteins and peptides, commonly designated as "*up*" and "*down*" (Figure 7.4A). This simple model of two main conformations for the pyrrolidine ring in proline should be readily transferable onto the pyrrolidine ring in prolinol (ether) enamines since, in particular, planarity may be assumed for both the amide

group in peptides and the enamine moiety in organocatalytically reactive intermediates, as a first approximation on the basis of the prolinol ether enamine crystal structures[38,39] and DFT calculations[39,40,42–44] available. In addition, the J criteria established for proline side-chain conformations in proteins were found to be applicable also to diarylprolinol and diarylprolinol (ether) enamines since, for the free catalysts, proline and **4**-**9**, no systematic shift of the $^3J_{H\alpha,H\beta 1/2}$, owing to the different Cϵ-substitution patterns, was observed (see Figure 7.11 and 7.12 in the Supporting Information, chapter 7.3). Experimentally, the two different conformations *up* and *down* can be distinguished by NMR via their characteristic $^3J_{H,H}$ scalar coupling constants,[63] which are easily extracted from well-resolved ^{1}H resonance multiplet patterns. Accordingly, small $^3J_{H\alpha,H\beta 2}$ and $^3J_{H\delta 2,H\gamma 1}$ indicate the population of the *down* conformation while small $^3J_{H\delta 1,H\gamma 2}$ are indicative of the *up* conformation.[a] The two conformations *up* and *down* as well as associated theoretical and the experimentally observed coupling constants are summarized in Figure 7.4.

For all diarylprolinol (ether) enamines **4.1**-**9.2**, unless signal overlap disturbed the observation of these multiplets, small vicinal couplings of 1.5-2.5 Hz and 2-3 Hz, respectively, were found for $^3J_{H\alpha,H\beta 2}$ and $^3J_{H\delta 2,H\gamma 1}$, (not only in DMSO-d$_6$, but also in MeCN-d$_3$, CDCl$_3$ and PhMe-d$_8$, see Figure 7.9 in the Supporting Information, chapter 7.3); in contrast, values between 6 Hz and 10 Hz were detected for $^3J_{H\delta 1,H\gamma 2}$, which leads to the characteristic multiplet patterns depicted on the example of **8.2** in Figure 7.4C. (Unfortunately, coupling constants could not be extracted for **3.1** and **3.2** due to spectral overlap and higher order NMR signals.) The experimental values for $^3J_{H\alpha,H\beta 2}$ and $^3J_{H\delta 2,H\gamma 1}$ equal those expected for the pure *down* conformation.[63] This indicates the *down* conformation of the pyrrolidine ring in diarylprolinol (ether) enamines in solvents ranging from DMSO over MeCN to CHCl$_3$ and PhMe. In addition, these small coupling constants of $^3J_{H\alpha,H\beta 2}$ and $^3J_{H\delta 2,H\gamma 1}$ show that conformations with large coupling constants, *i.e.* the *up* conformation, do not contribute significantly to the conformational ensemble and can be taken as a hint for a conformationally rather stable structure.[64][b] In contrast, in the free catalysts **4**-**9** both $^3J_{H\alpha,H\beta 1/2}$ are larger than 7 Hz, which is indicative of a dynamic equilibrium of *up* and *down* conformations (see Figure 7.11 and 7.12 and also the exemplary Hα multiplets in Figure 6.7C of our previous report, chapter 6).

These experimental results show that the enamine formation is essential for the adoption of a conformational preference of the pyrrolidine ring. This means that the approximate planarity of the enamine moiety (including the NRR´-group) in combination with the "obese" substituent imposes conformational constraints on the pyrrolidine ring to such a degree that exclusively one pyrrolidine conformation is observed. As a first assumption, this may be rationalized by the different steric repulsion modes of the two enve-

[a] Since the evaluation of $^3J_{H,H}$ coupling constants was not feasible for Hγ or Hβ because of severe resonance overlap, only the multiplet patterns of Hα, Hδ1 and Hδ2 could be used as probes for the conformational preferences of the pyrrolidine ring.

[b] Interestingly, for the aldol transition states of proline-derived catalysts, theoretical calculations suggested that only in the presence of substituents at the β-position of the pyrrolidine ring, the *down* conformation is significantly preferred.[49]

lope conformations *up* and *down* presented in Figure 7.4A. The *up* conformation may be destabilized by the detrimental steric repulsion between the "obese" substituent and the vicinal β protons as well as the δ protons, which is less disadvantageous in the preferred *down* conformation (Figure 7.4A; this hypothesis parallels the observed slight pyramidalization of the enamine nitrogen known from crystal structure analyses[38,39] and DFT calculations.[39,40,42–44,49]) Furthermore, for proline derivatives, the *down* conformation has been calculated to be compatible with less deviations of the enamine moiety from the favorable planarity than the *up* conformation.[49] In addition, it is only the *down* conformation which creates a sufficient spatial proximity of the methanol ether substituents and the Hγ2 of the pyrrolidine ring (Figure 7.4A) to potentially allow for stabilizing CH/π interactions (see below). Finally with regard to the reactivity and the stereoselection of the enamine, only in the *down* conformation can the attack of an electrophile occur in a sterically favorable manner to the unshielded and convex surface of the enamine.

***sc-exo*, *sc-endo*, and *ap*: Orientation of the diarylmethanol substituent by rotation around the exocyclic Cα-Cϵ bond.** The effective shielding of one face of the enamine π system, leading to the approach of the incoming electrophiles from the opposite side, is meant to be one important function of the diarylmethanol (ether) substituent in organocatalysts **4**-**9** for the stereochemical outcome of the enamine-catalyzed reaction.[39] However, beyond empirical experience on catalyst performances, only little is known about whether this shielding is brought about by the *O*-protecting group or the phenyl rings of the "obese" substituents of diarylprolinol(ether)-type organocatalysts. This issue, which is in particular highly important for theoretical calculations aiming at the understanding of stereoselection, is closely connected to the conformation of the exocyclic Cα-Cϵ bond. Rotation around this bond is supposed to be rather fixed by the geminal-diaryl effect.[38] Again, the available conformational information has been limited to crystal structure analyses[38,39] and to theoretical calculations.[39,40,42–44] But because of the lack of experimental data in solution, partially conflicting results were put forward, in particular whether the *sc-exo*[39,44] or the *sc-endo*[40,42,43] conformation of diarylprolinol ether enamines constitutes the better structural basis for intermediate and transition state calculations. This holds also true for (diaryl)prolinol-derived enamines, for which two opposite modes of stereoselection have been claimed: steric shielding of one face of the enamine by the aryl rings[35] on the one hand and direction of the electrophile to this face of the enamine via an H-bond[34,36] on the other hand. Here, knowledge on the rotation around the Cα-Cϵ bond should help to shed some light on this issue, too.

There are three different staggered conformations for the exocyclic Cα-Cϵ bond (Figure 7.5A), termed *sc-endo*, *sc-exo*, and *ap*. In general, the stereoelectronic preference of 1,2-electronegatively disubstituted ethane moieties (such as N-C-C-O) to adopt a synclinal conformation (commonly referred to as *gauche* effect)[65,66] is expected to favor the *sc-endo* and *sc-exo* over the *ap* conformation. To determine which of these conformations is really populated preferentially by prolinol (ether) enamines in solution, enamines

3.1-9.2 were investigated in different solvents by means of NMR spectroscopy. The *sc-endo*, *sc-exo*, and *ap* conformations can be in principle distinguished by their associated NOE intensity patterns obtained from ^{1}H,^{1}H-NOESY spectra, in particular as *gauche* oriented vicinal substituents should give rise to larger NOEs than *ap* oriented vicinal substituents. Thereby, especially the investigation of the NOEs of the OH/OR-substituent protons proved to be valuable to determine the preferred conformation at the Cα-Cϵ bond. Figure 7.5B exemplarily shows sections from ^{1}H,^{1}H-NOESY spectra of **5.2** (left) and **7.2** (right) in DMSO-d$_6$ at 300 K.

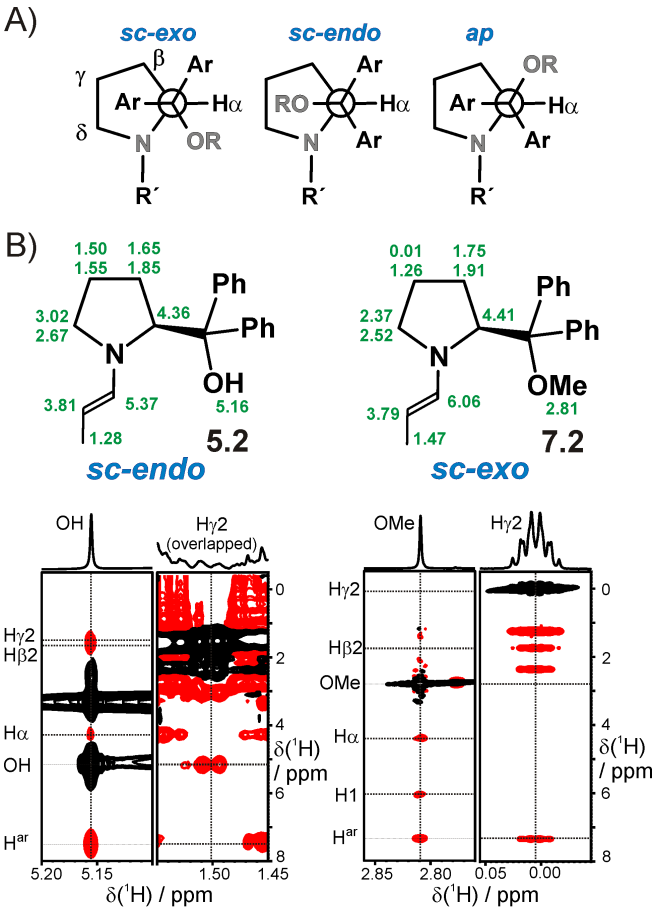

Figure 7.5: A) Staggered conformations of diarylprolinol (ether) enamines; B) ^{1}H NMR assignments of **5.2** (left) and **7.2** (right) (Note: Chemical shifts of Hβ1, Hγ1 and Hδ1 are listed below those of Hβ2, Hγ2, Hδ2.) and sections of their ^{1}H,^{1}H-NOESY spectra (bottom) in DMSO-d$_6$ at 300 K (Note: Intensities of the sections are scaled individually for optimum clarity.).

The spectral sections of **5.2** reveal significantly stronger NOEs from OH to Hβ2 and Hγ2 than to Hα and, in addition, a stronger NOE of Hγ2 to OH than to the aromatic protons of the phenyl rings (Figure 7.5B, left). This NOE pattern is best explained by an *sc-endo* conformation of the Cα-Cϵ bond in the case of **5.2**. In contrast, for **7.2**, the protons of OMe show pronouncedly stronger NOEs to H1 and Hα than to Hβ2 or Hγ2 and, *vice versa*, a stronger NOE from Hγ2 to the aromatic protons than to the protons

of OMe is observed (Figure 7.5B, right). These findings for **7.2** are indicative of an *sc-exo* conformation around the exocyclic Cα-Cϵ bond. In line with the *gauche* effect, the preferential adoption of the *ap* conformation, however, can be ruled out on the basis of these NOE intensity patterns in both cases.

Since the conformation of the exocyclic Cα-Cϵ bond is of high importance for the understanding of the stereocontrol exerted by diphenylprolinol (ether) organocatalysts, we intended to develop a facile and rapid way to screen enamines for the Cα-Cϵ conformation without the need to record and analyze NOESY spectra. In this context, we could observe that the two different preferred conformations of the Cα-Cϵ bond in **5.2** and **7.2** are also reflected in a very characteristic way by the ^{1}H chemical shifts: For the *sc-endo* conformation of **5.2** a significant upfield shift of H1 is found (δ = 5.37 ppm, $\Delta\delta$ = 0.81 ppm relative to **3.2**) whereas in the case of the *sc-exo* conformation of **7.2** the protons on the "upper" face of the pyrrolidine ring Hγ2 and Hδ2 are remarkably shielded (δ = 0.01 and 2.37 ppm, $\Delta\delta$ = 1.75 and 0.61 ppm relative to **3.2**, respectively; see the proton assignment in Figure 7.5B). The comparison of these characteristic chemical shifts of **5.2** and **7.2** to the corresponding values of **3.2** (6.18, 1.76, 2.98 ppm), being devoid of aromatic rings, suggests that the upfield shifts are in fact caused by ring current effects (Figure 7.6A). The observation of such shielded CH protons in the presence of aromatic rings is long-known in terms of the ASIS (aromatic solvent-induced shift)[67] and is rationalized by the Bovey model,[68] which predicts deshielding of protons outside the ring current, but shielding of those within. Upfield shifted proton resonances in the presence of aromatic moieties can therefore be interpreted as an indication of CH/π interactions.[52] This interpretation is in very good agreement with the other conformational findings presented so far, as shown by the structure models for **5.2** and **7.2** (Figure 7.6B): These geometric models (refined with molecular mechanics, MMFF force field) are based on the *down* conformation of the pyrrolidine ring, the s-*trans* arrangement of the enamine moiety, and the *sc-endo* or *sc-exo* conformation around the Cα-Cϵ bond, respectively. They reveal that the *sc-endo* conformation in **5.2** may be stabilized by an OH$\cdots$N hydrogen bond and, in addition, may be effortlessly accompanied by an H1-Ph interaction. In contrast, for the *sc-exo* conformation of **7.2**, an interaction between Hγ2 (also Hδ2) and Ph is achieved straightforwardly; all these CH/π interactions correspond well with the observation of the selectively upfield shifted proton resonances. It is moreover important to note that in the *sc-exo* conformation, the steric shielding of the "upper" face of the enamine is effectuated by both the aromatic ring (in particular its *meta*-substituent) and the *O*-protecting group.[38,39] The associated steric conflicts should—to a certain degree—destabilize the enamine and in fact, this is in striking correspondence with our observation on the decrease of the prolinol ether enamine amount by increasing the size of either the aryl *meta*-substituent or the *O*-protecting group (chapter 6). Hence, our different NMR spectroscopic findings concerning the various conformational aspects of diarylprolinol (ether) enamines show excellent consistency and indicate the conformations of Figure 7.6B as the preferred ones for **5.2** and **7.2** in DMSO-d$_6$.

In contrast to all enamines studied, neither the conformational fixation of the pyrrolidine ring (see above) nor the upfield shifts of individual protons are observed for the free catalysts **4**-**9** (see Figure 7.11 and 7.12 in the Supporting Information, chapter 7.3). One may thus assume that the predictive value of conformational studies on prolinol (ether) organocatalysts for the conformations of their enamine intermediates is rather limited. Instead, our investigations stress the importance of performing conformational studies on the actual intermediates of organocatalysis themselves. In addition, the simultaneous appearance of the conformational preferences of the pyrrolidine ring and around the Cα-Cϵ bond in prolinol (ether) enamine intermediates strongly suggest stabilizing interactions between the pyrrolidine ring and the methanol ether substituents (in agreement with the interactions discussed above and shown in Figure 7.6).

On the basis of their excellent correspondence with the *sc-endo* or *sc-exo* conformation around the exocyclic Cα-Cϵ bond, the upfield shifts of protons H1 or Hγ2 and Hδ2, respectively, in the enamine intermediates can be used as a facile method to rapidly screen diarylprolinol-derived organocatalysts for the orientation of the obese diarylmethanol substituent: In case the *ap* conformation can be ruled out as the major conformation, as revealed for all enamines studied (see below), upfield shifts of H1 to 5.20-5.42 ppm are indicative of the *sc-endo* conformation while upfield shifted Hγ2 and Hδ2 resonances in the ranges 0.00-0.35 ppm and 2.20-2.40 ppm, respectively, evidence the adoption of the *sc-exo* conformation.

As a first test for our screening method to deduce the conformation around the Cα-Cϵ bond, we investigated the generality of the conformational switch from *sc-endo* (**5.2**) to *sc-exo* (**7.2**) upon protection of the OH functionality of **5.2**. For that purpose, enamines **3.1**-**9.2**, derived from different aldehydes and different catalysts, were studied in DMSO-d$_6$ by NMR spectroscopy; subsequently, enamines **7.2** and **9.2** were investigated in other solvents, too. The 1D ^{1}H screening results were verified by NOESY analyses wherever possible (Table 7.2 and Table 7.3).

enamine	δ (^{1}H) / ppm			conformation acc. to NOESY spectra
	H1	Hγ2	Hδ2	
3.1 / **3.2**	6.17 / 6.18	1.75-1.45[a] / 1.76	2.97 / 2.98	n. ass.[b] / n. ass.[b]
4.1 / **4.2**	5.27 / 5.42	1.80-1.35[a] / 1.65-1.35[a]	3.07 / 3.04	n. det. / n. det.
5.1 / **5.2**	5.26 / 5.37	1.55 / 1.50	3.06 / 3.02	*sc-endo* / *sc-endo*
6.1 / **6.2**	5.20 / 5.37	1.75-1.30[a] / 1.65-1.35[a]	3.11 / 3.09	n. det. / n. det.
7.1 / **7.2**	5.94 / 6.06	0.01 / 0.01	2.37 / 2.37	*sc-exo* / *sc-exo*
8.1 / **8.2**	6.19 / 6.29	0.34 / 0.25	2.33 / 2.34	*sc-exo* / *sc-exo*
9.1 / **9.2**	6.05 / 6.22	0.30 / 0.25	2.23 / 2.27	n. det. / *sc-exo*

[a]Only chemical shift ranges can be given because of severe resonance overlap.
[b]Spectral overlap prevented determination of the conformation.
n. ass. = not assignable; n. det. = not determined

Table 7.2: Characteristic ^{1}H chemical shifts of enamines **3.1**-**9.2** in DMSO-d$_6$ and their correlations to the conformation around the exocyclic Cα-Cϵ bond.

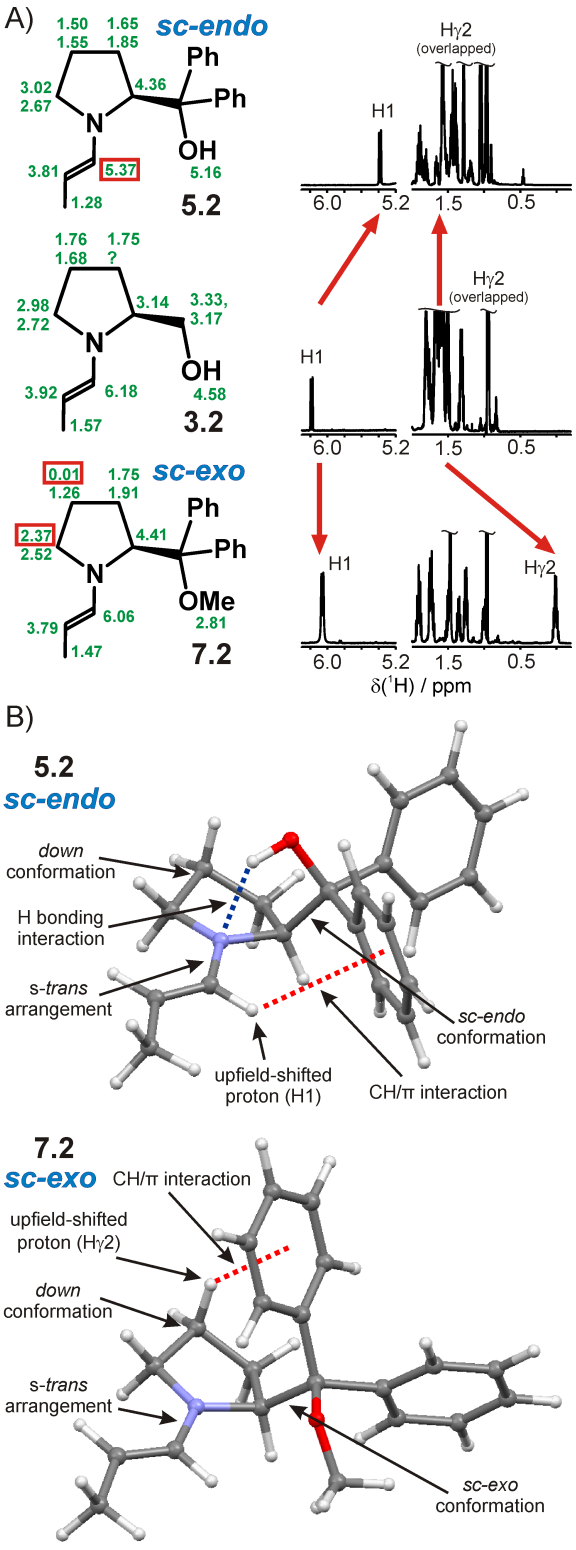

Figure 7.6: A) ^{1}H chemical shift assignments of **5.2**, **3.2**, and **7.2** in DMSO-d$_6$ with upfield shifted resonances highlighted in red (left; note: Chemical shifts of Hβ1, Hγ1 and Hδ1 are listed below those of Hβ2, Hγ2, Hδ2. The Cα-Cϵ conformation could not be determined for **3.2** unambiguously due to signal overlap.) and sections of the corresponding 1D ^{1}H NMR spectra (right); B) structure models (MMFF-refined geometries) of **5.2** and **7.2** based on the conformational findings from NMR investigations.

We first examined potential influences of the catalyst structure and the aldehyde alkyl chain on the Cα-Cϵ conformation (Table 7.2). By comparison to the ring current-free enamines **3.1** and **3.2**, upfield shifts of the H1-resonance in the *O*-unprotected **4.1**-**6.2** become evident as well as upfield shifts of the Hγ2/δ2-resonances of the *O*-protected enamines **7.1**-**9.2** (entries in Table 7.2 highlighted in gray). Again and as verified in most cases by NOESY analyses, these shifts are indicative of the *sc-endo* conformation for all the diarylprolinol enamines (**4.1**-**6.2**) and of the *sc-exo* conformation for all the diarylprolinol ether enamines (**7.1**-**9.2**), respectively. In addition, possible solvent effects on the preferred population of these conformations were investigated (Table 7.3). As the detection of prolinol enamines was successful only in DMSO-d_6, these solvent studies were performed only for diarylprolinol ether enamines on the examples of **7.2** and **9.2**: The characteristic upfield shifts of Hγ2/δ2 are found in all solvents applied, ranging from polar aprotic (DMSO-d_6, MeCN-d_3) over polar protic (MeOH-d_4) to nonpolar ($CDCl_3$) and aromatic solvents (PhMe-d_8), indicating that solvent properties do not play an important role for the conformation around the Cα-Cϵ bond of diarylprolinol ether enamines.

enamine	solvent	δ (^{1}H) / ppm			conformation acc.
		H1	Hγ2	Hδ2	to NOESY spectra
7.2	DMSO-d_6	6.06	0.01	2.37	*sc-exo*
	MeCN-d_3	6.14	0.08	2.43	n. det.
	MeOH-d_4	6.10	0.14	2.44	n. det.
	$CDCl_3$	6.11	0.10	2.48	*sc-exo*
	PhMe-d_8	6.31	0.22	2.53	n. det.
9.2	DMSO-d_6	6.22	0.25	2.27	*sc-exo*
	PhMe-d_8	6.12	0.09	2.26	n. det.

n. det. = not determined

Table 7.3: Characteristic ^{1}H chemical shifts of enamines **7.2** and **9.2** in different solvents and their correlations to the conformation around the exocyclic Cα-Cϵ bond.

Altogether, our straightforward ^{1}H NMR screening method, backed by NOESY analyses, shows that the protection of the hydroxylic group is the decisive factor for the conformational change observed from diarylprolinol to diarylprolinol ether enamines; in contrast, neither the nature of the protecting group (TMS or Me, *cf.* **7.x** and **8.x**) nor the nature of the aromatic rings (Ph or Ar, *cf.* **4.x.**, **5.x**, and **6.x** or **8.x** and **9.x**) nor the size of the aldehyde alkyl chain (iPr or Me, *cf.* **x.1** and **x.2**) seem to be of greater conformational importance. Moreover, the *sc-exo* conformation is preferred by diarylprolinol ethers independently of the solvent used. Thus, from a conformational point of view, etherification of the hydroxylic group of prolinols does not only have a significant impact on the stability of the corresponding enamines, as reported by us recently (chapter 6), but also on the orientation of the bulky α-substituent.

Our exclusive observation of *sc-exo* conformations of diarylprolinol ether enamines in solution by NMR is not only in agreement with the available enamine crystal structure,[38,39]

but also with the previously reported NMR data on comparable enamine intermediates:[39,40] Following our ^{1}H chemical shift criterion for the rapid screening of Cα-Cϵ bond conformations, the enamines **10**-**12** (Figure 7.7) are to be classified as *sc-exo*, too, as upfield shifts of aliphatic pyrrolidine resonances are observed, but no significant upfield shifts of H1.

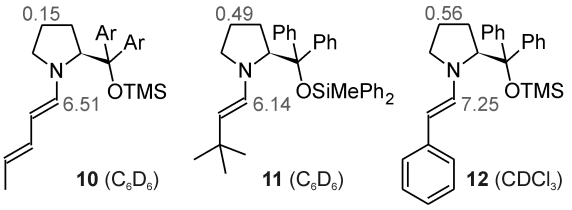

Figure 7.7: ^{1}H chemical shifts of diarylprolinol silyl ether enamines available in the literature so far: **10** was observed *in situ* by Jørgensen *et al.*,[40] **11** and **12** were isolated and investigated in Seebach´s group.[39] (Note: H1 of **11** and **12** had obviously been misassigned by accident in the literature.)

These results provide furthermore for the first time a broad experimental basis to comment on the recently presented conflicting results from theoretical calculations on the Cα-Cϵ bond conformation of diarylprolinol ether enamines. On the basis of our experimental data and in agreement with a comparative theoretical study performed in Seebach´s group,[39] the assumption of the *sc-exo* conformation for s-*trans* diarylprolinol ether enamines[39,44] seems more adequate for the calculation of intermediate structures than using the *sc-endo* conformation.[40,42,43]

Beyond the determination of intermediate structures, we believe our study to be relevant also for the calculation and investigation of organocatalytic transition states. Although transition states are of course inaccessible to NMR investigations and intermediate and transition state conformations are not necessarily identical, our conformational intermediate studies provide for the first time an extensive experimental basis for the future selection of appropriate enamine conformations as the basis for transition state calculations and for the evaluation of previously reported transition states. Interestingly, a very recent DFT calculation on the transition state for the asymmetric Michael addition of **7.2** to methyl vinyl ketone[69] features all the conformational properties of the enamine intermediate that we determined experimentally: the *E*-configuration of the enamine double-bond, the s-*trans* arrangement of the enamine, the *down* conformation of the pyrrolidine ring and the *sc-exo* conformation of the α-substituent around the Cα-Cϵ bond. Accordingly, the electrophilic attack of methyl vinyl ketone to the enamine occurs from the convex halfspace opposite to the "obese" diphenylmethoxymethyl substituent of **7.2**. This outstanding congruence of the conformational results of our experimental enamine intermediate study with those of this theoretical transition state calculation can be backed by evaluating the predictive value of intermediate conformations for the stereochemical outcome of organocatalytic reactions since the latter is determined by the transition state conformation only. As pointed out previously,[38,39] in the *sc-exo* conformation of diarylprolinol ether enamine intermediates, the steric shielding of one face of the enamine is provided by

both the *meta*-substituents of the aryl groups and the *O*-protecting group. If this enamine conformation was predominant also in the transition state, increasing stereoselectivities of asymmetric reactions should be obtained by enlarging both the aryl *meta*-substituent and the *O*-protecting group of the organocatalyst. Indeed, this effect has been reported regularly for increasing sizes of both the aryl *meta*-substituent[28,70–72] and the *O*-protecting group[27,72–75] and can now finally be rationalized on an experimental basis. In addition, our experimental finding of a stable *sc-exo* Cα-Cϵ conformation predicts that the enlargement of only one of the two phenyl rings should be sufficient to increase the shielding of one face of the enamine and hence to increase the stereoselectivity of the reaction. In fact, such an effect has been reported recently.[76] One may thus assume that the *sc-exo*[44] conformation and not the *sc-endo*[42–44] conformation is also predominant in transition states involving diarylprolinol ether enamines and our intermediate studies can therefore be expected to have an impact also on the calculation of organocatalytic transition states.

As the applicability of prolinol-based catalysts in enamine catalysis is rather limited, the relevance of conformational investigations on prolinol enamines seems a lot lower than on the prolinol ether enamines. Nevertheless also this first experimental conformation data on prolinol enamine intermediates might be a useful guide for further theoretical investigations on the origin of stereocontrol in enamine catalysis by diarylprolinol organocatalysts. Still, it is interesting to note, that for prolinol enamines two different types of stereocontrol in the bond-forming transition state have been postulated: While on the one hand, steric shielding of the "upper" enamine face by the bulky substituent has been postulated,[35] other findings were explained by an approach of the electrophile from this "upper" face because of a directing function of the hydroxylic group of the enamine via H-bonding interactions.[34,36,37,76] In principle, the *sc-endo* conformation around the Cα-Cϵ bond of diarylprolinol enamines that we observed in this study seems to allow for both an H-bond from the *sc-endo* hydroxylic group to an incoming electrophile and steric shielding by the *sc-exo* aryl ring. Thus, both interactions may indeed contribute as stereodirecting factors. Nevertheless, since the change of the *sc-endo* conformation in diarylprolinol enamines to the *sc-exo* conformation in diarylprolinol ether enamines is apparently triggered by the protection of the OH-functionality, a special role in the stabilization of the *sc-endo* conformation might be attributed to the OH group. As pointed out previously,[38] prolinol enamines may develop an N$\cdots$HO hydrogen bond only in the *sc-endo* conformation (Note: N is to be taken as a representative of the enamine π system as hydrogen bond acceptor.). In the case of our simple structure model of Figure 7.6B (d (N$\cdots$H) $\approx$ 2.1 Å, d (N$\cdots$O) $\approx$ 2.7 Å, $\angle$ (N$\cdots$H-O) $\approx$ 122°), this hydrogen bond in **5.2** is to be classified as weak to moderate,[77] but it might be sufficient to cause the preference of the *sc-endo* conformation. In solvents with lower H-bond acceptor abilities than DMSO, the favourable energetic contribution of this H-bond should be even more pronounced. Moreover, the upfield shift of the H1 resonance (see above) indicates an additional stabilizing CH/π contribution between H1 and one of the phenyl rings that also favors the *sc-endo* conformation (Figure 7.6B, top). Previously, for the explanation of the *sc-endo* conformation of

diarylprolinol derivatives, the stronger steric repulsion between the pyrrolidine hydrogens and the aryl rings compared to the OH-group was also consulted.[38] This would imply that the *sc-exo* conformation in diarylprolinol ether enamines should be changeable towards *sc-endo* either by reducing the size of the *O*-protecting group (Me instead of TMS) or by increasing the size of the aromatic rings (Ar instead of Ph); yet, in none of these cases did we observe a change of the preferred *sc-exo* conformation towards *sc-endo*. This makes us believe that steric clashes are of minor importance for the issue of conformational preferences around the Cα-Cϵ bond. Thus, weak conformation-stabilizing intramolecular interactions are highly probable to account for the observed preferences of the *sc-endo* and the *sc-exo* conformation of diarylprolinol enamines and diarylprolinol ether enamines, respectively. For diarylprolinol enamines, we found evidence for an N$\cdots$HO hydrogen bond and one CH/π interaction; in diarylprolinol ether enamines strong experimental evidence for two CH/π interactions is provided. It is worth mentioning that single separately upfield shifted pyrrolidine protons were also reported for diarylprolinol ether iminium salts,[39,41] which in combination with the crystallographic data,[38,39] may be interpreted in terms of similar CH/π interactions being operative and structure-determining in iminium ions, too. So far, little attention has been paid to the involvement of such weak CH/π interactions in the intramolecular stabilization of intermediate conformations in nucleophilic organocatalysis. More detailed experiments, calculations, and considerations might help to ultimately clarify the real impact and significance of the CH/π interactions in this conformational issue.

To summarize this section, our NMR study shows that diarylprolinol enamines adopt the *sc-endo* conformation around the Cα-Cϵ bond in solution because of a weak to moderate N$\cdots$HO hydrogen bond and an additional stabilizing contribution from a CH/π interaction between H1 and one aromatic ring. In contrast, for diarylprolinol ether enamines a preference for the *sc-exo* conformation is found in solution most probably owing to CH/π interactions between the pyrrolidine hydrogen atoms and the aromatic ring. Thus, for the first time, strong experimental evidence is provided for CH/π interactions to be the conformation-determining factor for enamine intermediates in organocatalysis.

Options for the Screening of Enamine Conformations. The crucial conformational aspects of diarylprolinol (ether) enamines, the orientation of the ene moiety, the pyrrolidine puckering, and the rotation of the bulky diarylmethanol substituent, can be screened for straightforwardly by means of NMR spectroscopy. For the sake of clarity, these approaches that have been outlined above are again summarized graphically in Figure 7.8.

Conclusion

In summary, we presented the first detailed conformational investigations on enamines derived from prolinol- and prolinol ether-type organocatalysts with two different aldehydes in various solvents by means of NMR spectroscopy. Concerning the exocyclic N-C

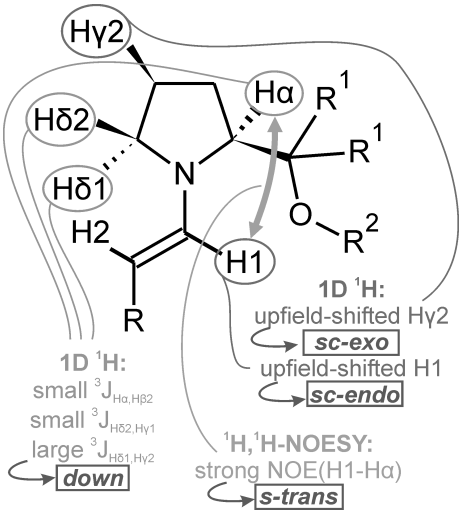

Figure 7.8: Graphical summary of the screening methods for the conformation of prolinol (ether) enamines.

bond, we present the first experimental proof by NOESY analysis that a prolinol-derived enamine partially exists in the s-*cis* conformation in solution. In diarylprolinol ether enamines in contrast, the bulkiness of the pyrrolidine α-substituent guarantees the nearly exclusive adoption of the enamine s-*trans* conformation in solution. In addition, for all enamines studied, the enamine formation is associated with a strong preference for the *down* conformation of the pyrrolidine ring. For the rotation around the exocyclic Cα-Cϵ bond, diarylprolinol enamines are found by NOESY analyses to be present in the *sc-endo* conformation while the diarylprolinol ether enamines adopt the *sc-exo* conformation. Strong experimental evidence is provided that the *sc-exo* conformation in diarylprolinol ether enamines is stabilized by CH/π interactions between aliphatic hydrogen atoms of the pyrrolidine ring in the *down* conformation and an aromatic π system of the bulky pyrrolidine α-substituent. In addition, a rapid conformational screening method, based on ^{1}H chemical shifts and backed by NOESY analyses, was developed and applied to show the generality of these conformational preferences for various catalyst, aldehyde, and solvent combinations.

The broad experimental basis provided in this study and our observation of exquisite conformational preferences of enamine intermediates in solution clarify experimentally the hitherto contradictory postulations and unsolved issues of s-*cis*/s-*trans* and *sc-endo*/*sc-exo* enamine conformations. In addition, the presented conformational features can help to explain the experimental performances of various catalysts used in organocatalytic reactions so that our data may promote the rationalization of the stereochemical outcome of organocatalytic reactions by diarylprolinol(ether)s. Altogether, our results are hence expected to have a significant impact for the understanding of enamine catalysis, they should inspire to further detailed experimental and theoretical investigations, and they can be helpful for the catalyst optimization process.

7.3 Supporting Information

Experimental Section

Enamines were created *in situ* inside a standard 5 mm NMR tube by adding freshly distilled aldehydes **1** or **2** (30 μmol, if not stated otherwise) to a solution of 100 mol% of the organocatalysts **3**, **4**, **5**, **6**, **7**, **8**, or **9** respectively, in 0.6 mL of deuterated solvent. The NMR tube was transferred to the spectrometer immediately after the mixing of all reacting components.

NMR measurements were performed at 300 K on a Bruker Avance DRX 600 (600.13 MHz) and on a Bruker Avance III 600 (600.25 MHz) spectrometer, the latter equipped with a TCI cryoprobe with z-gradient (53.5 G/cm). ^{1}H,^{1}H-NOESY spectra were recorded using a mixing time of 700 ms. NMR data were processed and evaluated with Bruker´s TOPSPIN 2.1.

Spartan ´06[78] was employed for the structure models displayed in Figure 7.6B. The structures were refined with the help of molecular mechanics conformer distribution calculations (MMFF force field).

Additional Information

NMR Characterization of Enamines

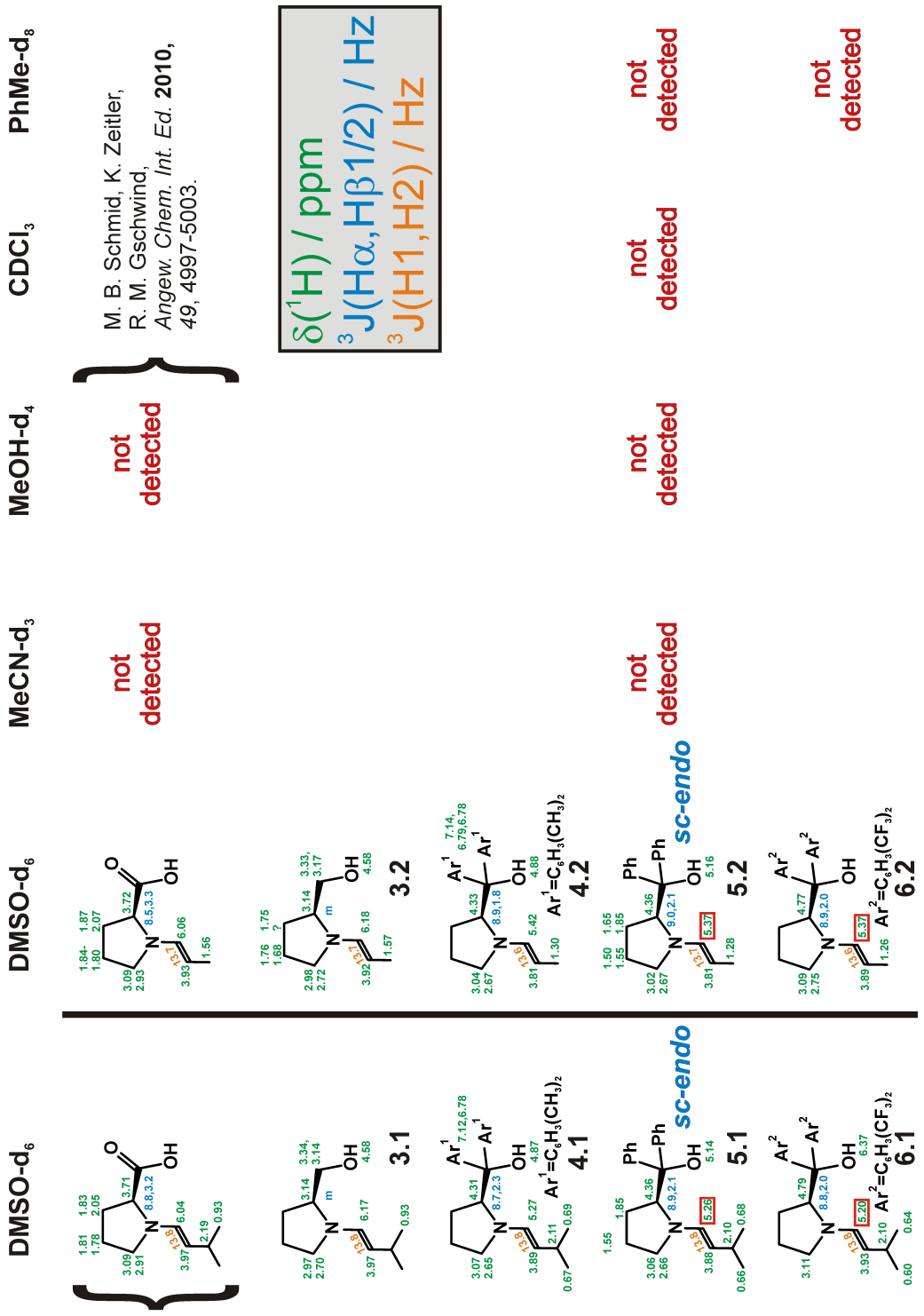

Figure 7.9: Overview of the prolinol enamines, relevant ^{1}H chemical shifts and coupling constants. (Note: Chemical shifts of Hβ1, Hγ1 and Hδ1 are listed below those of Hβ2, Hγ2, Hδ2.)

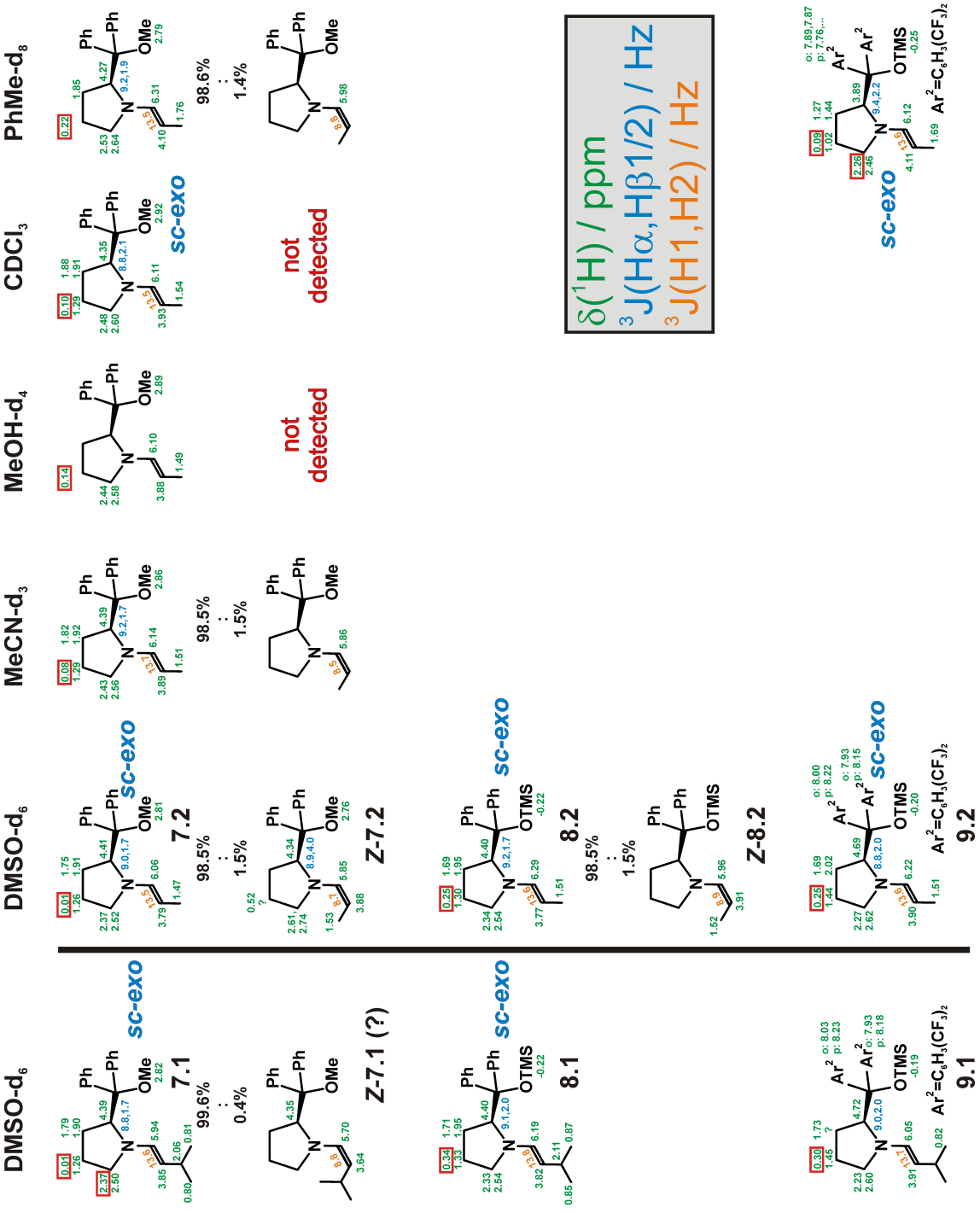

Figure 7.10: Overview of the prolinol ether enamines, relevant ^{1}H chemical shifts and coupling constants. (Note: Chemical shifts of Hβ1, Hγ1 and Hδ1 are listed below those of Hβ2, Hγ2, Hδ2.)

NMR Characterization of Organocatalysts

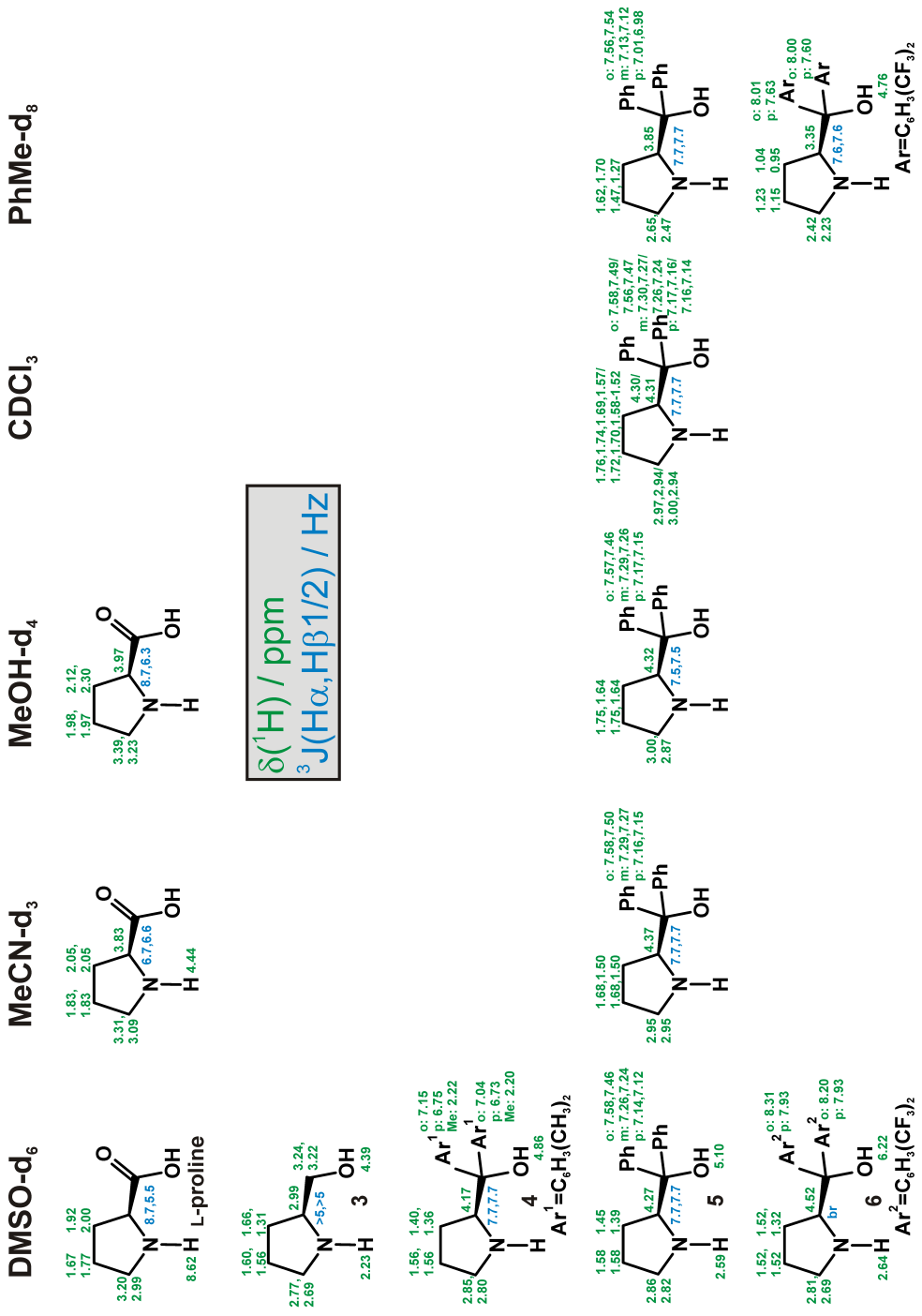

Figure 7.11: ^{1}H chemical shift assignment and relevant coupling constants of the prolinol organocatalysts. (Note: Chemical shifts of Hβ1, Hγ1 and Hδ1 are listed below those of Hβ2, Hγ2, Hδ2.)

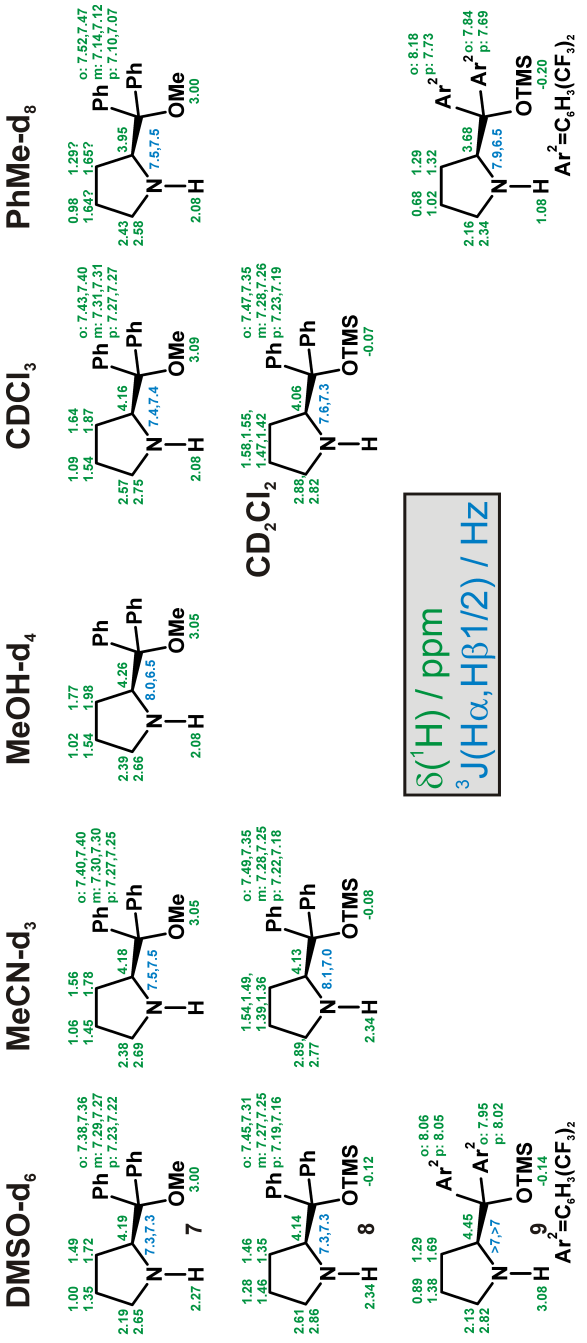

Figure 7.12: ^{1}H chemical shift assignment and relevant coupling constants of the prolinol ether organocatalysts. (Note: Chemical shifts of Hβ1, Hγ1 and Hδ1 are listed below those of Hβ2, Hγ2, Hδ2.)

7.4 Additional Experimental Findings

7.4.1 Aggregation Trends of Amine Organocatalysts in Solution

Introduction

In the field of organocatalysis, the self-aggregation of catalytic systems and the associated implications for their reactivities and selectivities have been a matter of investigations mainly in the context of bifunctional urea- and thiourea-derivatives.[60,79–82] In contrast, studies on the aggregation behaviour of proline-derived amine catalysts and on its potential impact upon the catalyst performance in solution have not become available as yet although the involvement of two proline molecules in the Hajos-Parrish-Eder-Sauer-Wiechert reaction[24,25] was discussed already in the early days of amine catalysis.[83] To fill this gap, we performed NMR diffusion measurements on proline as well as on various prolinol and prolinol ether derivatives in different solvents and with different additives.

Results and Discussion

NMR Diffusion Measurements. Diffusion-ordered spectroscopy (DOSY) experiments[84] deliver information on the translational self-diffusion coefficients of molecules in solution according to the Stejskal-Tanner equation.[85] On this basis and with the help of TMS as a reference compound, the relative diffusivity $D_{rel} = \frac{D_{TMS}}{D_X}$ of an analyte X under investigation is obtained, from which in turn the molecular mass of the analyte can be estimated empirically following equation 7.1 (parametrized for organic solvents).[86]

$$M = 84.5\frac{g}{mol} \cdot D_{rel}^{1.72} \tag{7.1}$$

The comparison of the estimated mass with the actual molecular mass of the analyte then allows for an inkling of the aggregation behaviour of the analyte in solution (Table 7.4).

Prolinol Ethers. The aggregation of neutral molecules in organic solvents is often driven by the formation of H-bonds as major intermolecular interactions. In this respect, prolinol ethers, bearing only one NH moiety as a potentially H-bonding structural motif, are generally less likely to aggregate in organic solvents than proline or prolinol derivatives which can build H-bonds additionally via their COOH or OH groups, respectively. We therefore started our aggregation studies with DOSY investigations on the prolinol ether catalysts **7** (c = 50 mM) and **8** (c = 100 mM) in various solvents and with different basic and acidic additives (Table 7.4). For **8** (M = 325.52 g/mol), the empirical mass estimation approach delivers masses of 320-340 g/mol in DMSO-d_6 and MeCN-d_3 in the temperature range between 293 and 313 K. Lower mass estimations for **8** are obtained only in CD_2Cl_2 at 293 K (269 g/mol) and in DMSO-d_6 at 333 K (291 g/mol). When the basic additives K_2CO_3, NaOAc, or NEt_3 are applied with **8** in DMSO-d_6 at 293 K, slightly increased estimated masses are calculated (332-353 g/mol). These observations suggest that **8** is monomeric

in organic solvents above 290 K. The unexpectedly low estimated masses in DMSO-d_6 at 333 K and in CD_2Cl_2 at 293 K may be attributed to the reduction of the solvent shell owing to the elevated temperature or the lack of H-bond acceptor properties of the solvent. However, it cannot be definitely ruled out as yet that these low values are due to the failure of TMS as a reference compound at elevated temperatures and to the lacking proof of the applicability of the mass estimation approach in CD_2Cl_2.[86] In contrast, the slight elevation of the estimated masses in the presence of basic additives may be interpreted as an indication of a weak aggregation tendency between **8** and the additives, potentially via H-bonding interactions. The monomeric state of prolinol ether organocatalysts in organic solvents was to be verified on the example of **7** (M = 267.37 g/mol) in DMSO-d_6. In addition, since **7**, in contrast to **8**, does not undergo ether cleavage in DMSO upon addition of acidic additives (see section below), the influence of benzoic acid as an additive on the aggregation behaviour of **7** could be studied. At 300 K the DOSY-based mass estimation delivers 264 g/mol for pure **7** and 303 g/mol when one equivalent of PhCOOH is added. This suggests that pure **7** is monomeric in DMSO and that there is a slight tendency to form aggregates with benzoic acid, possibly through H-bonding or π-π interactions.

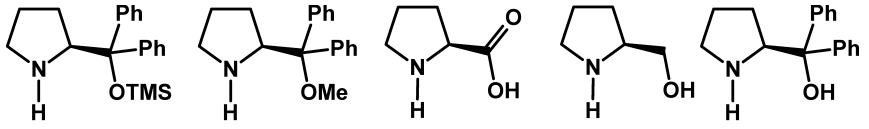

8 **7** **proline** **3** **5**

catalyst	M / g/mol	c / mM	additive (1eq)	DOSY-based mass estimation / g/mol solvent and temperature					
				DMSO-d_6				MeCN-d_3	CD_2Cl_2
				293 K	300 K	313 K	333 K	293 K	293 K
8	325.52	100	—	320-340[a]		339	291	323	269
			K_2CO_3	332					
			NaOAc	353					
			NEt_3	352					
7	267.37	50	—		264				
			PhCOOH		303				
proline	115.13	100	—	243-249[a]		224	224		
		40	—		242				
		30	—		243				
		20	—		233				
		10	—		228				
3	101.15	50	—		123				
5	253.35	17	—	297-311[a]		313	251	277	229
			K_2CO_3	299					
			NaOAc	319					
			NEt_3	316					
		100	—	348 (monomer)		350	279		
			—	567 (dimer)					
			PhCOOH	404					
			PhCOOH (5eq)	509					
			HI (*in situ*)	511[b]					

[a] values obtained with different pulse sequences and with or without sample spinning at 20 Hz
[b] based on DMSO as the reference compound

Table 7.4: DOSY-based molecular mass estimation of various organocatalysts in solution.

Proline. Proline can be regarded as the antipode of prolinol ethers with respect to their expected aggregation behaviour in organic solvents. It possesses an NH group and a COOH group which both bear the potential to act as dual H-bond donors and acceptors at the same time, which privileges proline for its aggregation in solution. Accordingly, for

proline (M = 115.13 g/mol) in DMSO-d_6, mass estimations of 224-249 g/mol are obtained in the temperature range between 293 and 333 K and when concentrations of 10-100 mM were applied (although proline was not soluble in such high concentrations). These values exceed the mass of monomeric proline by far and are rather indicative of a proline dimer (M = 230.26 g/mol) in DMSO. For the rationalization of such a dimeric structure, a preliminary conformer distribution calculation (based on MMFF-based molecular mechanics)[78] was performed which yielded the dimer structure depicted in Figure 7.13 as the lowest energy dimer. It is stabilized by a cooperative network of two moderate[77,87] intramolecular and one moderate[77,87] intermolecular H-bond (see Figure 7.13B for the H-bond parameters).

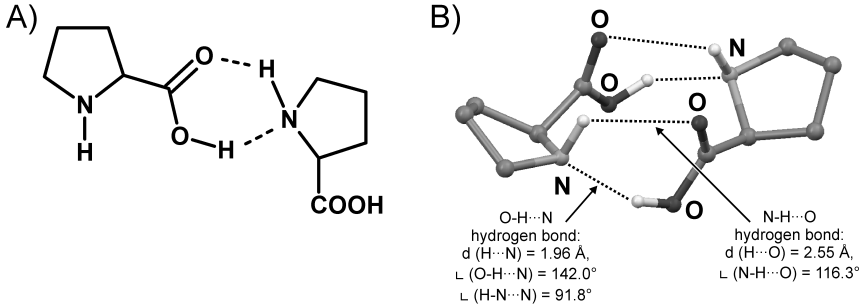

Figure 7.13: A) Hypothetical H-bond pattern between two proline molecules. For the sake of clarity, only one of the two six-membered H-bonded ring arrangements between NH and COOH is depicted; B) MM-minimized[78] structure of a proline dimer.

Prolinols. Similarly to proline, prolinol **3** possesses two potentially H-bonding moieties, the NH and the OH group. However, the OH group in prolinol is a poorer H-bond acceptor than the COOH group of proline and, in addition, the H-bond donor ability of OH is, in line with its lower acidity, lower than the one of COOH. Accordingly, the tendency of prolinol **3** to aggregate in solution can be expected to be less pronounced than for proline. The DOSY-based mass estimation for a 50 mM solution of prolinol **3** (M = 101.15 g/mol) in DMSO-d_6 at 300 K yields a value of 123 g/mol. This clearly evidences that prolinol **3**, in contrast to proline, does not form dimers in DMSO, but is rather monomeric. As outlined above, this may be explained by the reduced H-bond abilities of prolinol compared to proline.

Finally, we investigated the aggregation behaviour of diphenylprolinol **5**. In principle, its aggregation tendency should parallel the one of prolinol **3** because of the identical potential H-bonding pattern. However, the geminal-diaryl effect present in **5** is expected to hamper the rotation around the neighboring C-C bond in comparison to **3**. Therefore, upon dimerization, the entropically unfavorable conformational restriction of the rotation around this bond should be less critical for the aggregation in the case of **5** as compared to **3**. Thus, diphenylprolinol **5** may exhibit a higher level of aggregation in solution than prolinol **3**. First, diphenylprolinol **5** was investigated at an estimated concentration of 15-

20 mM as an impurity in the samples of diphenylprolinol silyl ether **8**. In the temperature range of 293-313 K in DMSO-d_6, optionally with the basic additives K_2CO_3, NaOAc, or NEt_3, and at 293 K in MeCN-d_3, the DOSY-estimated molecular masses for diphenylprolinol **5** (M = 253.35 g/mol) were between 277 and 319 g/mol (again, only in the cases of DMSO at 333 K and in CD_2Cl_2, were lower values obtained, 251 and 229 g/mol, respectively, which may be rationalized as outlined above for **8**). These values basically indicate the monomeric nature of diphenylprolinol **5** at low concentrations in solution.

However, when its concentration is increased to 100 mM in DMSO-d_6, two different species of diphenylprolinol **5** are indicated by two different sets of NMR signals, for which the EXSY spectrum reveals vivid interconversion. According to its chemical shift pattern, the major species, accounting for 97.5 % of the total amount of **5** at 293 K (98.9 % at 313 K and 99.5 % at 333 K), is identical to the one observed at lower concentrations. For this species, the molecular mass estimation yields again values (348 g/mol and 350 g/mol at 293 K and at 313 K, respectively) that agree best with a monomeric structure, but they are increased in comparison to the case of lower concentrations of **5** (277-319 g/mol). This can be interpreted as a hint at a slight tendency of **5** to aggregate at higher concentrations in DMSO.

The minor species of **5** is characterized ^{1}H NMR-spectroscopically by an upfield shift of the proton Hγ2 to 0.39 ppm (*cf.* 1.58 ppm for the monomer) and scalar coupling constants of Hα to Hβ1/2 of 9.0 and 3.0 Hz (*cf.* a triplet of 7.0 Hz for the monomer). Most remarkably, according to our conformation criteria for prolinol (ether) enamines established above (chapter 7.2), this indicates that this minor diphenylprolinol species adopts, in contrast to monomeric diphenylprolinol **5**, the *down* conformation of the pyrrolidine ring and the *sc-exo* conformation around the exocyclic Cα-Cϵ bond. At a total concentration of **5** of 100 mM in DMSO, the minor species accounts for only 2.5 % of **5** at 293 K, for 1.1 % at 313 K, and for 0.5 % at 333 K. This *decrease* of its ratio with increasing temperature indicates that the minor species is not simply a different, less populated conformer of monomeric diphenylprolinol as, in this case, its amount should *increase* with increasing temperatures according to the Boltzmann distribution. Instead, by the temperature-dependence of its amount, the minor species is suggested to represent an aggregate of **5**. Indeed, the DOSY-based mass estimation at 293 K evidences a mass of 567 g/mol which is in reasonable agreement with the mass of a diphenylprolinol dimer (M = 506.70 g/mol). Thus, our NMR spectroscopic investigations of **5** at a concentration of 100 mM in DMSO-d_6 show that monomeric and dimeric diphenylprolinol **5** coexist in an equilibrium in DMSO at higher concentrations and that they exhibit different conformational features.

For the rationalization of these different structures of **5** in solution, one may consider intramolecular and intermolecular H-bonds as the driving forces for the stabilization of the monomer or the dimer, respectively. For monomeric diphenylprolinol **5**, a single crystal could be obtained from a solution of **5** in THF by slow evaporation of the solvent.

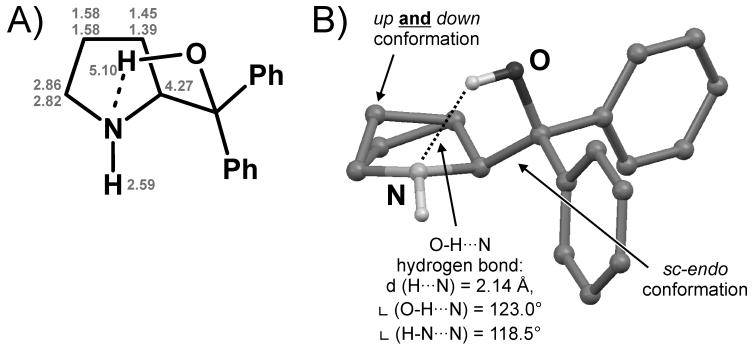

Figure 7.14: A) Intramolecular H-bond in monomeric diphenylprolinol **5** and ^{1}H NMR assignment in DMSO-d$_6$ at 300 K (in ppm); B) crystal structure of **5** obtained upon slow evaporation of the solvent THF.

The crystal structure (Figure 7.14) reveals the stabilization of the monomer by a moderate[77,87] intramolecular O-H···N H-bond (d (H···N) = 2.14 Å, ∠ (O—H···N) = 123.0°, ∠ (H—N···H) = 118.5°; the position of the OH proton was in fact evidenced experimentally by X-ray analysis.). The diphenylmethanol substituent adopts the *sc-endo* orientation since the H-bonding interaction is the most effective in this conformation. For the pyrrolidine ring, however, no preference for the *up* or *down* conformation was found in the single crystal analysis. As these findings are in agreement with the NMR spectroscopic data for monomeric **5**, *i.e.* no upfield shift of Hγ2 and a triplet for Hα (see discussion above), one may well assume that this conformation of the monomer in the crystal is also predominant in solution. Interestingly, this conformation is in contrast to a recently proposed pre-transition state assembly of **5** and a β-ketoester in the H-bond acceptor-catalyzed sulfenylation of β-ketoesters, for which an *sc-exo* conformation of **5** has been postulated.[88]

Beyond the NMR-evidenced *down* conformation of the pyrrolidine ring and the *sc-exo* conformation of the diphenylmethanol substituent for the dimer of **5** in DMSO, we can only speculate about the origin of the observed dimerization of **5**. We can nevertheless state that in the *sc-exo* conformation of the dimer, in contrast to the *sc-endo* conformation of the monomer, the OH and the NH group as potentially H-bonding moieties are pointing towards the same face of the molecule, thereby creating a possible dimerization site via cooperative intermolecular H-bonds. The MMFF-based conformer distribution calculation[78] of a dimer of **5** suggests one possibility for such a network of intra- and intermolecular hydrogen bonds that realizes the experimentally observed conformational properties (Figure 7.15). In this model of the dimer, the *sc-exo* conformation of the diphenylmethanol substituents allow for two intramolecular O-H···N, for two intermolecular N—H···O H-bonds, and, together with the *down* conformation of the pyrrolidine rings, for two intramolecular CH/π interactions between the pyrrolidine protons Hγ2 and the phenyl rings. The intramolecular O-H···N hydrogen bonds (d (H···N) = 1.95 Å, ∠ (O—H···N) = 127.9°) are expected to be weaker than in the monomer because the OH protons do not point towards the nitrogen lone pair appropriately in the *sc-exo* conformation

(∠ (H—N···H) = 82.0°, *cf.* 118.5° for the *sc-endo* conformation in the monomer). However, the two additional intermolecular N—H···O hydrogen bonds ((d (H···O) = 1.99 Å, ∠ (N—H···O) = 154.1°) and the potential CH/π interactions may partially compensate this loss of conformational stabilization so that the dimer can be observed in solution. Altogether, this structure model of the diphenylprolinol dimer (Figure 7.15B) agrees well with the NMR spectroscopic findings on the conformation of **5** in the dimer and the cooperative H-bond network may help to rationalize the dimerization of diphenylprolinol in DMSO.

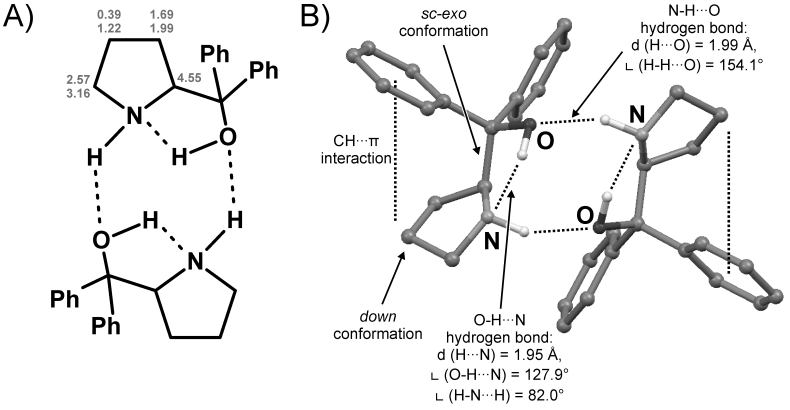

Figure 7.15: A) Intra- and intermolecular H-bonds in dimeric diphenylprolinol **5** and ^{1}H NMR assignment in DMSO-d_6 at 300 K (in ppm). B) MMFF-based[78] structure model of dimeric **5**.

Finally, the influence of acidic additives on the aggregation behaviour of diphenylprolinol **5** was investigated. Upon addition of one equivalent of benzoic acid to a 50 mM solution of **5** in DMSO, the salt of **5** and PhCOOH precipitates rapidly. The molecular mass of the remaining species of **5** in solution is estimated to be 404 g/mol. This value rises to 509 g/mol when 5 equivalents of PhCOOH are applied. This can be taken as a hint that equimolar amounts of **5** and PhCOOH basically form ion pairs in DMSO (sum of molecular masses: 375.47 g/mol) and that additional benzoic acid molecules may further attach to these ion pairs or lead to the aggregation of ion pairs by an H-bond network. This is in line with the well-known dimerization tendency of benzoic acid (M = 122.12 g/mol) in organic solvents (DOSY-estimated mass at a concentration of 0.45 M in DMSO-d_6 at 293 K: 203.7 g/mol) and the crystal structure of **5**/PhCOOH presented in the following section.

In addition, it was studied in how far the release of hydrogen iodide HI in the course of an organocatalytic alkylation reaction influences the aggregation behaviour of diphenylprolinol **5**. Indeed a **5**-derived species was detected in such experimental setups (see chapters 9 and 10.2 also for further related amine catalyst-derived species), for which the mass estimation (here, based on the solvent DMSO, not on TMS) resulted in a value of 511 g/mol. This suggests an aggregate of **5**, possibly a hydrogen-bonded iodide salt. However, the observation that the amount of catalyst-aggregates is typically about twice the amount

of those detected products, from which HI had been released (similarly for other amine catalysts than **5**, chapter 10.2), can be interpreted as an indication that not single ion pairs between protonated **5** and iodide are formed, but larger aggregates involving twice as many molecules of **5** as iodide anions. However, more detailed investigations will be necessary to further clarify this issue.

Conclusion

In summary, a preliminary study on the aggregation of amine catalysts in solution is presented. Diarylprolinol ethers are found to be monomeric in solvents from DMSO to dichloromethane. In contrast, proline forms dimers even in the highly polar DMSO. For prolinols, a certain tendency towards aggregation is evidenced; in the case of diphenylprolinol, the coexistence of the monomer and the dimer in DMSO is revealed. Based on a crystal structur of the monomer and NMR spectroscopic findings on the dimer, the dimerization is suggested to be accompanied by a conformational switch of the diphenylmethanol substituent from *sc-endo* to *sc-exo* which allows for different H-bonding interactions in the monomer or in the dimer. Finally, diphenylprolinol is shown to form aggregates upon the addition of benzoic acid and upon the release of HI in the course of organocatalytic alkylation reactions. Since the aggregation behaviour of amine catalysts in solution has not been a matter of in-depth discussions so far, its relevance for synthetic applications cannot be judged with ease at this stage of our investigations. Still, various findings on organocatalyst performances presented in this work may be connected to the observed aggregation behaviour of the catalysts: Two proline-derived species are shown to participate in the Mannich-type aldol condensation of aldehydes (chapter 5.2), the combination of diphenylprolinol and benzoic has proven superior performances in the coupling of nitroalkenes to enynes (chapter 9), and the release of HI in the course of organocatalytic reactions appears to deactivate amine catalysts in solution (chapters 9 and 10.2). Hence, together with these experimental observations, this aggregation study should inspire to more detailed considerations on the impact of catalyst aggregation tendencies in solution upon the organocatalytic properties of secondary amines.

7.4.2 Mind the Gap—Deprotection of Prolinol Silyl Ethers

Introduction

The loss of the silyl group in diarylprolinol silyl ether organocatalysts has been well-known as a potential source of eventual catalyst deactivation, for instance by the hardly reversible formation of oxazolidines with carbonyl species (chapter 6.2).[39,89–91] However, a systematic investigation of this unwanted catalyst deprotection in solution has been due, although such knowledge would be of high value for the optimization of organocatalytic reaction conditions. We therefore investigated the influence of solvents of different polarity and of basic and acidic additives upon the cleavage of the silyl protecting group of diarylprolinol silyl ether organocatalysts **8** and **9** (c = 100, 50, or 25 mM).

Results and Discussion

The NMR spectroscopic analysis of mixtures of **8** and its desilylated analog **5** or of **9** and its desilylated analog **6** in solution reveals different chemical shifts of the pyrrolidine protons of **8** and **5** or **9** and **6**, respectively (see chapter 7.3). On this basis, the identification of the silylated and desilylated species can be accomplished either via their different diffusion coefficients in DOSY spectra or via NOE contacts from the pyrrolidine protons to the TMS protons or the OH proton, respectively (the latter detectable in DMSO). The first striking observation during our TMS-cleavage study was the fact that the commercially purchased catalysts **8** and **9** from Sigma-Aldrich contained at least 10 - 15 % of their deprotected analogs **5** and **6**. However, since in principle different modes of stereocontrol with opposite stereoinductions, namely H-bonding or steric shielding, can be executed by prolinols **5**, **6** or prolinol ethers **8**, **9**, respectively (see chapter 7.2), the observed purity grade of the purchased catalysts is far from being acceptable. Instead it is therefore highly advisable to purify prolinol silyl ethers before their use as organocatalysts.

Solvent Effects. First, the impact of the polarity of the solvent on the TMS cleavage in **8** was investigated. In the low-polarity solvent chloroform (with a dielectric constant ϵ of 4.8)[92] the ratio of **8**:**5** remained constant at 84:16 over three weeks. In the more polar acetonitrile ($\epsilon = 35.9$),[92] however, the ratio of **5** in solution grew from 18 % after one day to 62 % after one month. Similarly in methanol ($\epsilon = 32.7$),[92] a linear increase from 16 % to 40 % in only 4 days was monitored (Figure 7.16). In the highly polar DMSO ($\epsilon = 46.5$), the amount of the desilylated catalyst **5** went up from 25 % after 2 days to 77 % after one month. Altogether this indicates that the cleavage of the TMS group of **8** is promoted in polar solvents rather than in nonpolar ones. Presumably it is the fastest in methanol which may be linked to its excellent H-bond donor properties.

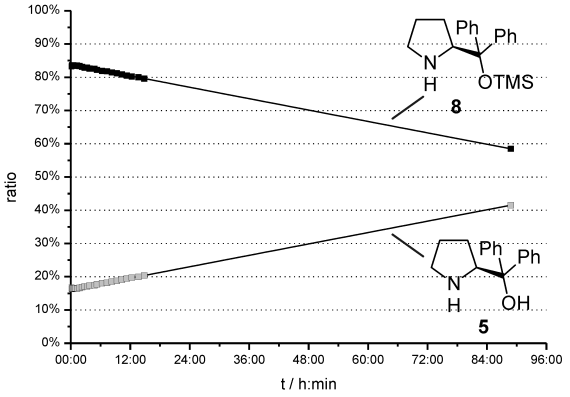

Figure 7.16: Progress of the desilylation of **8** in MeOH-d_4 at 300 K.

Additive Effects. In a further step, the influence of the basic additive potassium carbonate (K_2CO_3) and of the acidic additives succinic acid and benzoic acid (PhCOOH) upon the desilylation of **8** in DMSO (c = 50 mM, each) was studied. K_2CO_3 was found to

retard the cleavage of the TMS group: The ratio of **5** was 21 % after 2 days, but reached only 48 % after 5 weeks (*cf.* 77 % after 1 month in pure DMSO). In contrast, benzoic acid that is often used as an acidic additive in organocatalytic reactions[93] leads to the nearly complete cleavage of the TMS group of **8** within only 6 hours (Figure 7.17A) and the desilylation rate was comparably high in the case of succinic acid (here, the ratio of **8** dropped below 10 % after about 10 hours). This loss of the TMS group under the influence of PhCOOH was furthermore observed to be similarly fast for the enamine **8.2** in DMSO. Even more severe is the finding for catalyst **9**: Desilylation was quantitative within only one hour in DMSO upon addition of PhCOOH. For organocatalysts **8** and **9**, the desilylation in DMSO with the additive PhCOOH occurs on a time scale that is certainly highly relevant for organocatalytic processes that often require relatively long reaction times. In summary, the desilylation of diarylprolinol silyl ether organocatalysts in DMSO is promoted by acidic and retarded by basic additives.

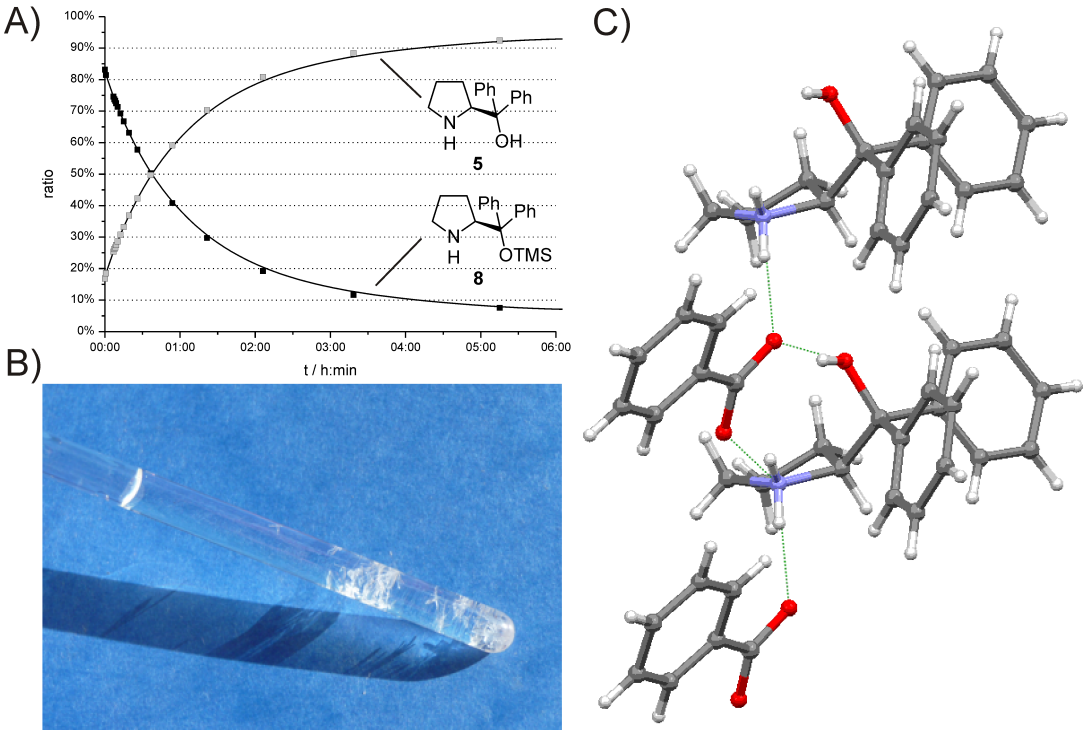

Figure 7.17: A) Progress of the desilylation of **8** with 1 equivalent of PhCOOH (0.1 M, each) in DMSO-d_6 at 300 K; B) crystals obtained from this reaction mixture after 2 days; C) corresponding crystal structure as determined by X-ray structure analysis.

For the combination of **8** with PhCOOH, the progress of the TMS cleavage in DMSO is easily observable by precipitation or crystallization (Figure 7.17B) of the benzoate salt of **5** within few hours. The corresponding crystal structure of this salt is depicted in Figure 7.17C. The structure is maintained by a network of hydrogen bonds between the anion of benzoic acid and the ammonium cation of **5**. Here, the carboxylate moiety acts as a three-fold H-bond acceptor: In a salt-bridge-like manner, it interacts with the OH

proton (d (H···O) = 1.82 Å, ∠ (O—H···O) = 167.9°) and with one of the NH protons of the cation (d (H···N) = 1.89 Å, ∠ (O—H···O) = 153.8°). This H-bond motif is made possible by the adoption of the *sc-endo* conformation around the exocyclic Cα-Cϵ bond of **5**.[94] In addition, one of the benzoate oxygen atoms acts as a bifurcated H-bond acceptor to saturate the H-bond donor ability of the second NH proton (d (H···O) = 1.83 Å, ∠ (O—H···N) = 162.2°, ∠ (H···O···H) = 100.4°) and thereby to bridge the cation-anion pairs through the crystal. That a similar interaction pattern between benzoic acid and **5** may also be present in solution, is indicated by the aggregation of PhCOOH and **5**, which was evidenced by DOSY (see section above). Most interestingly, this overall arrangement of the cation-anion interaction in our crystal structure agrees very well with the recently postulated transition state of the asymmetric epoxidation of 2-arylidene-1,3-diketones by *tert*-butyl-hydroperoxide, non-covalently catalyzed by **5**: In this proposed transition state, protonated **5** adopts the *sc-endo* conformation to develop a two-fold H-bond to the 1,3-diketone. The second NH proton, however, forms an H-bond to tert-butyl-peroxide thereby directing this epoxidating agent selectively towards one face of the diketone double-bond.[95]

Towards the Origin of Desilylation. To move towards an understanding of the processes, that underlie the desilylation of **8** and **9** under the influence of carboxylic acids, we studied the solvent dependence of the desilylation phenomenon as well as the fate of the silyl protecting group. First, we tried to reproduce the *O*-silyl deprotection by PhCOOH in other solvents than DMSO, namely in toluene, chloroform, methanol, and acetonitrile. However, neither for **9** in toluene, nor for **8** in methanol or in chloroform could we observe an acceleration of the TMS-cleavage upon addition of PhCOOH. In contrast, for the addition of PhCOOH to **8** in MeCN-d_3, the desilylation was almost equally fast as in DMSO.[c] These surprising findings indicate that the hydrogen-bond *acceptor* properties of DMSO and MeCN might play a particular role in the desilylation process under the influence of carboxylic acids. Together with the observation that the acid-free desilylation is most rapid in the H-bond *donor* solvent methanol, one may conclude that carboxylic acids and H-bond *acceptor* solvents form a cooperative H-bond network (with H-bond *donating* properties) that facilitates the cleavage of the TMS protecting group.

To further pursue this hypothesis, we applied ^{1}H, ^{13}C, and ^{29}Si NMR spectroscopy to obtain insights into the fate of the silyl protecting group. In all solvents used, the methyl silyl regions of the 1D ^{1}H spectra revealed the formation of the well expected degradation products TMS-OH and TMS-O-TMS (at 0.01 ppm and 0.06 ppm, respectively, in DMSO-d_6; Figure 7.18A). However, one additional proton resonance at 0.36-0.37 ppm was observed exclusively in DMSO-d_6 and MeCN-d_3 upon the addition of PhCOOH, but independently of **8** or **9** as the starting material. Therefore, this unknown species **10**

[c] In fact, the desilylation appears to be a little slower in acetonitrile and did not reach completion. However, since in acetonitrile, the benzoate of **5** precipitated immediately (in contrast to the slow precipitation/crystallization process in DMSO), the experimental conditions are not fully comparable.

was considered a degradation product that might shed some light on the desilylation process of **8** and **9** by PhCOOH in DMSO. However, interestingly, the monitoring of the desilylation process revealed that the formation of **10** does not start immediately in the reaction mixture, but only after an induction period of more than one hour, when the condensation of TMS-OH to TMS-O-TMS has basically reached its equilibrium state (Figure 7.18A). This suggests that the formation of **10** is *not* directly connected to the desilylation process of **8** and **9** itself. Nevertheless, knowledge on the structure and origin of **10** might also help to understand the properties of the reaction mixture that promote the silyl ether cleavage. Accordingly, further spectroscopic and chemical efforts were made to elucidate the molecular structure of **10** in DMSO.

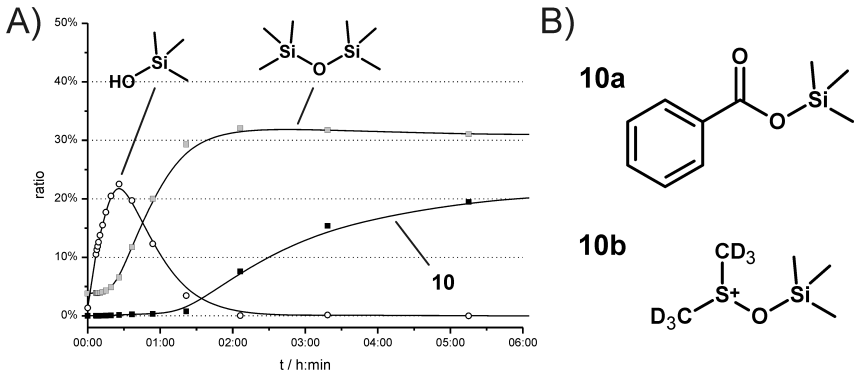

Figure 7.18: A) Concentration-time-curves of the silyl degradation products of **8** in DMSO-d_6 after the addition of one equivalent of PhCOOH at 300 K; B) potential molecular structures of **10**: the TMS benzoate **10a** and the DMSO-stabilized TMS cation **10b**.

The ^{1}H,^{13}C-HSQC revealed that the carbon atoms of the TMS group resonate at -0.5 ppm (referenced to the solvent residual peak). In the one-dimensional ^{29}Si NMR spectrum, the silicon resonance of the TMS group in **10** was found to be 24.5 ppm (referenced to external TMS). The ^{1}H DOSY spectrum in DMSO at 293 K revealed that **10** diffuses faster than benzoic acid and than the catalysts **8** and **5**, but slower than TMS-O-TMS and TMS-OH. However, besides the signal at 0.36 ppm, no other proton resonance with the same diffusion coefficient was observed. Likewise, the ^{1}H,^{1}H-NOESY spectrum did not provide clear-cut evidence for additional proton resonances in **10**: Only one very weak NOE from 0.36 ppm to an aromatic resonance at 7.92 ppm can be observed, but it is so low above the noise level that a reasonable structure interpretation is not possible on this basis. Besides these spectroscopic findings, chemically relevant information on **10** was collected in addition to its delayed formation in the reaction mixtures (Figure 7.18A): Most notably, the amount of **10** decreases with increasing amounts of water in the sample; in fact, the presence of **10** can be totally quenched by the addition of 1/6 vol% of water to DMSO and in turn the amount of TMS-OH increases by doing so, hence indicating the hydrolysis of **10**. This observation of the facile hydrolysis of **10** can be taken as a hint that **10** contains a Si-O or a Si-N bond. However, the missing NOE network of the TMS protons in **10** rules out the *N*-silylation of one of the catalyst species. This is also supported

by the constant ^{1}H chemical shift of **10** independent of **8** or **9** as the starting material as well as by the faster diffusion of **10** than of **8** and **9**. **10** can hence be assumed to be a silyl ether or silyl ester species. Based on our experimental data, considering possible reaction pathways, and by comparison with literature data, two potential structures can be suggested for **10**: the trimethylsilyl benzoate **10a** and the DMSO-stabilized trimethylsilyl cation **10b** (Figure 7.18B).

The experimental data agree reasonably with the molecular structure **10a**. In the literature, ^{1}H chemical shifts of 0.21 ppm (in CCl_4),[96] 0.31 ppm (in CCl_4),[97] 0.43 ppm (in CCl_4),[98] and 0.57 ppm (in C_6D_6)[99] have been reported for **10a**. More characteristic is the congruence with the silicon chemical shift $\delta(^{29}\mathrm{Si})$ of 23.6 ppm (in CCl_4).[98] The structure **10a** also matches the observed relative diffusion coefficient as well as the experimental finding of the release of TMS-OH upon the addition of water. Yet, neither were proton resonances in the aromatic region detected that would indicate a further PhCOOH-derived species, nor could NOESY spectra in DMSO or MeCN provide clear evidence for the structure **10a**. In addition, an analogous TMS ester of succinic acid, which also induces desilylation in DMSO and which has an almost identical first pK_a (4.19) in water as benzoic acid (4.20), was not observed by NMR. Furthermore, all attempts to create **10a** under similar conditions as in the TMS-cleavage study *in situ* and hence to prove **10a** as the unknown compound **10** have failed so far: The proton resonance at 0.36 ppm was not observed at all when equimolar amounts of benzoic acid and the silylating agent TMS-Cl were mixed in DMSO in the presence of piperidine as a secondary amine base. Likewise, this NMR signal was only very tiny in the reaction mixture of benzoyl chloride (PhCOCl) with sodium trimethylsilanolat (NaOTMS). Hence an alternative structure model for **10** may be considered. As such, though certainly a lot more exotic, the DMSO-stabilized TMS cation **10b** can be regarded that has already been described in the literature. **10b** has been characterized by NMR in solution:[100] The ^{13}C chemical shift of 0.7 ppm, reported for the triflate of **10b** in DMSO-d_6,[100] is in line with our experimental data. On the other hand, the literature values for $\delta(^{29}\mathrm{Si})$ (42.8 ppm and 42.7 ppm for the poorly coordinating triflate and iodide counterions, respectively, in DMSO-d_6)[100] do not match our observed values and hence do not support the structure **10b** for the unknown compound. However, the deviation of our experimental $\delta(^{29}\mathrm{Si})$ might also be accounted for by the influence of the more strongly coordinating benzoate counterion within the solvent shell of **10b**.

In a nutshell, the true nature of compound **10** has not been clarified irrevocably. The majority of experimental findings supports the TMS benzoate **10a**, but final proof for this structure is still missing and may be provided by the purposeful synthesis and spectroscopic characterization of **10a**. The silylium ion **10b** represents a less likely alternative. It may nevertheless point out that benzoate is not the only donating species to possibly stabilize the cleaved TMS group. Hence, **10a** and **10b** might also constitute the two sides of the same coin in that both can contribute in a cooperative fashion to the stabilization of the TMS group in solution, that is to the desilylation of organocatalysts **8** and **9**.

Conclusion

Altogether, the desilylation process of diarylprolinol silyl ethers in solution has been monitored NMR spectroscopically in different solvents and with various additives. In the additive-free case, the TMS cleavage is the fastest in the polar protic solvent methanol. On the other hand, in the polar aprotic acetonitrile and DMSO, the addition of carboxylic acids accelerates the desilylation drastically. It is completed within hours and, in the case of the addition of benzoic acid, the precipitation or crystallization of the corresponding salt can be followed visually. A crystal structure of the benzoate salt of diphenylprolinol was obtained which displays an intermolecular H-bond network that is in line with previously postulated H-bonding interactions of diphenylprolinol-substrate adducts in non-covalent organocatalysis. However, the mechanism of the desilylation process has not been disclosed as yet. Further variations of solvent and additive properties should help to clarify this issue in more detail. Likewise, the structure elucidation of a still unknown silyl species observed in solution may aid in understanding the underlying reactivities that lead to the loss of the TMS protecting group.

7.4.3 Supramolecular Mimicking of Proline´s Bifunctionality

The excellent properties of proline to catalyze aldol and Mannich reactions can be ascribed to its bifunctionality: While the Lewis-basicity of the pyrrolidine nitrogen can promote the formation of enamine species, the Brønsted acidity of the carboxylic moiety can direct and activate an electrophile via H-bonding (in the List-Houk model).[46,101] However, as is also reflected by the elusiveness of proline enamines for many years, the tendency of proline to form enamines is rather low so that typically long reaction times have to be accepted in proline-catalysis. On the other hand, prolinol and prolinol ether derivatives have proven outstanding performances in enamine catalysis, but they are poor catalysts for the homo-aldol reaction of aldehydes,[16] which may be rationalized by their missing bifunctionality: either the formation of enamines is low (**3**-**6**) or the activating functionality of the carboxylic proton is missing (**7**-**9**). Based on the already known aggregation of **5** and benzoic acid in DMSO from DOSY investigations (see above), we therefore tried to externally replace the missing bifunctionality by adding benzoic acid as an additive. Thus, reaction mixtures of propionaldehyde **2** (50 mM) with the catalysts **3**-**9** were prepared in DMSO-d_6 at 300 K either with or without PhCOOH as an additive. The formation of aldol or condensation products of **2** was investigated via reaction monitoring by 1D ^{1}H spectra.

For proline as the reference catalyst, the condensation of **2** in DMSO reached a conversion of more than 90 % after 12 hours.[45] In contrast, despite their high tendencies to form enamines with aldehydes (chapter 6.2), the *O*-protected catalysts **7**, **8**, and **9** did not yield aldol addition or condensation products at all or the conversion was below 1 %. Similarly, for L-prolinol **3**, though it simultaneously provides low enamine amounts and the additional option of H-bonding interactions to an electrophile, no products were

detected. This may be rationalized by the absence of sufficient amounts of electrophiles since all the aldehyde molecules were involved in the formation of adducts with **3**. More importantly, the missing conformational restriction of the rotation around the exocyclic Cα-Cϵ bond in **3**, owing to the missing gem-aryl effect, may prevent the hydroxylic group of **3** from working efficiently as an activating and directing group for an incoming electrophile. This line of argument is indicated by the observation that diphenyl prolinol **5** does catalyze the homo-aldol reaction of **2**. However, in this case, because of the rapid and irreversible cyclization of the enamine to the oxazolidine (chapter 6.2), the C-C bond formation is limited to the short time slot (about 30 minutes) during which the enamine is present in solution in considerable amounts. Nevertheless, the aldol addition product is formed in this time window with a yield (determined *in situ* by integration of the NMR resonances) of about 20 % in terms of the non-hydrolyzed product oxazolidine (similarly with the catalysts **4** and **6** in yields of 30 % and 15 %, respectively.).

To check for beneficial effects of acidic additives, the reactions were then run in the presence of 100 mol% of benzoic acid, but under otherwise identical conditions. In the case of **5**, which yielded the product oxazolidines in the absence of PhCOOH, the influence of PhCOOH was detrimental: The hardly reversible formation of the **2**-derived oxazolidine was even accelerated by PhCOOH (*cf.* chapter 10.1) so that no enamine was detected at all and the dimerization products of **2** were formed below 1 %. For **8** as the catalyst, the addition of PhCOOH indeed led to an increase in the catalytic activity: The condensation product of **2** was formed in a yield of about 5 %.[d] However, this experimental setup suffers from the above-mentioned desilylation of **8** followed by irreversible deactivation in terms of the oxazolidine. To overcome this problem on the basis of the known desilylation tendencies, toluene was chosen as an alternative solvent for the silyl ether catalyst **9** and, in a different experimental setup, **7** as a catalyst that does not lose the *O*-protecting group under our experimental conditions. In fact, when **9** was applied as a catalyst in toluene, the addition of PhCOOH triggered the condensation of **2** with a yield of about 15 %. Even more successful was the use of the methyl ether **7** with PhCOOH in DMSO: Within 6 hours, the condensation product of **2** was formed in a yield of about 25 %. However, given the performance of proline in the reaction investigated, the success of the supramolecular mimicking of its bifunctionality must be termed mediocre. However, the results may be used as a first starting point for more sophisticated approaches. In particular, the investigation of the different chemoselectivities upon addition of PhCOOH or K_2CO_3 may be rewarding and might shed more light on the catalytic performance of prolinolether organocatalysts.

[d] Interestingly under these conditions, the use of K_2CO_3 instead of PhCOOH led to a similar degree of condensation of **2**, but in addition, the formation of the aldol dimers in a yield of about 15 % was observed.

7.5 References

[1] A. Berkessel, H. Gröger, *Asymmetric Organocatalysis - From Biomimetic Concepts to Applications in Asymmetric Synthesis*, Wiley-VCH, Weinheim, **2005**.

[2] *Enantioselective Organocatalysis: Reactions and Experimental Procedures* (Ed.: P. I. Dalko), Wiley-VCH, Weinheim, **2007**.

[3] *Chem. Rev.* **2007**, *107*, 12 (special issue on organocatalysis).

[4] *Ernst Schering Foundation Symposium Proceedings "Organocatalysis"* (Eds.: M. T. Reetz, B. List, S. Jaroch, H. Weinmann), Springer, Berlin, **2008**.

[5] P. M. Pihko, I. Majander, A. Erkkilä, *Top. Curr. Chem.* **2010**, *291*, 29–75.

[6] J. Seayad, B. List, *Org. Biomol. Chem.* **2005**, *3*, 719–724.

[7] D. W. C. MacMillan, *Nature* **2008**, *455*, 304–308.

[8] T. Hashimoto, K. Maruoka, *Chem. Rev.* **2007**, *107*, 5656–5682.

[9] A. G. Doyle, E. N. Jacobsen, *Chem. Rev.* **2007**, *107*, 5713–5743.

[10] *Hydrogen Bonding in Organic Synthesis* (Ed.: P. M. Pihko), Wiley-VCH, Weinheim, **2009**.

[11] K. Etzenbach-Effers, A. Berkessel, *Top. Curr. Chem.* **2010**, *291*, 1–27.

[12] T. Akiyama, *Chem. Rev.* **2007**, *107*, 5744–5758.

[13] D. Kampen, C. M. Reisinger, B. List, *Top. Curr. Chem.* **2010**, *291*, 395–456.

[14] S. E. Denmark, G. L. Beutner, *Angew. Chem. Int. Ed.* **2008**, *47*, 1560–1638.

[15] B. List, *Chem. Commun.* **2006**, 819–824.

[16] P. Melchiorre, M. Marigo, A. Carlone, G. Bartoli, *Angew. Chem. Int. Ed.* **2008**, *47*, 6138–6171.

[17] S. Bertelsen, K. A. Jørgensen, *Chem. Soc. Rev.* **2009**, *38*, 2178–2189.

[18] S. Mukherjee, J. W. Yang, S. Hoffmann, B. List, *Chem. Rev.* **2007**, *107*, 5471–5569.

[19] A. Erkkilä, I. Majander, P. M. Pihko, *Chem. Rev.* **2007**, *107*, 5416–5470.

[20] J. B. Brazier, N. C. O. Tomkinson, *Top. Curr. Chem.* **2010**, *291*, 281–347.

[21] T. D. Beeson, A. Mastracchio, J.-B. Hong, K. Ashton, D. W. C. MacMillan, *Science* **2007**, *316*, 582–585.

[22] J. J. Devery III, J. C. Conrad, D. W. C. MacMillan, R. A. Flowers II, *Angew. Chem. Int. Ed.* **2010**, *49*, 6106–6110.

[23] J. M. Um, O. Gutierrez, F. Schoenebeck, K. N. Houk, D. W. C. MacMillan, *J. Am. Chem. Soc.* **2010**, *132*, 6001–6005.

[24] U. Eder, G. Sauer, R. Wiechert, *Angew. Chem. Int. Ed.* **1971**, *10*, 496–497.

[25] Z. G. Hajos, D. R. Parrish, *J. Org. Chem.* **1974**, *39*, 1615–1621.

[26] B. List, R. A. Lerner, C. F. Barbas III, *J. Am. Chem. Soc.* **2000**, *122*, 2395–2396.

[27] Y. Chi, S. H. Gellman, *Org. Lett.* **2005**, *7*, 4253–4256.

[28] M. Marigo, T. C. Wabnitz, D. Fielenbach, K. A. Jørgensen, *Angew. Chem. Int. Ed.* **2005**, *44*, 794–797.

[29] Y. Hayashi, H. Gotoh, T. Hayashi, M. Shoji, *Angew. Chem. Int. Ed.* **2005**, *44*, 4212–4215.

[30] C. Palomo, A. Mielgo, *Angew. Chem. Int. Ed.* **2006**, *45*, 7876–7880.

[31] A. Mielgo, C. Palomo, *Chem. As. J.* **2008**, *3*, 922–948.

[32] L. W. Xu, L. Li, Z. H. Shi, *Adv. Synth. Catal.* **2010**, *352*, 243–279.

[33] A. Lattanzi, *Chem. Commun.* **2009**, 1452–1463.

[34] G. Zhong, J. Fan, C. F. Barbas III, *Tetrahedron Lett.* **2004**, *45*, 5681–5684.

[35] D. Enders, S. Chow, *Eur. J. Org. Chem.* **2006**, *2006*, 4578–4584.

[36] Y. Hayashi, T. Itoh, S. Aratake, H. Ishikawa, *Angew. Chem. Int. Ed.* **2008**, *47*, 2082–2084.

[37] Y. Hayashi, S. Samanta, T. Itoh, H. Ishikawa, *Org. Lett.* **2008**, *10*, 5581–5583.

[38] D. Seebach, U. Grošelj, D. M. Badine, W. B. Schweizer, A. K. Beck, *Helv. Chim. Acta* **2008**, *91*, 1999–2034.

[39] U. Grošelj, D. Seebach, D. M. Badine, W. B. Schweizer, A. K. Beck, I. Krossing, P. Klose, Y. Hayashi, T. Uchimaru, *Helv. Chim. Acta* **2009**, *92*, 1225–1259.

[40] S. Bertelsen, M. Marigo, S. Brandes, P. Diner, K. A. Jørgensen, *J. Am. Chem. Soc.* **2006**, *128*, 12973–12980.

[41] S. Lakhdar, T. Tokuyasu, H. Mayr, *Angew. Chem. Int. Ed.* **2008**, *47*, 8723–8726.

[42] J. Franzén, M. Marigo, D. Fielenbach, T. C. Wabnitz, K. A. Jørgensen, *J. Am. Chem. Soc.* **2005**, *127*, 18296–18304.

[43] P. Dinér, A. Kjærsgaard, M. A. Lie, K. A. Jørgensen, *Chem. Eur. J.* **2008**, *14*, 122–127.

[44] J.-Q. Zhao, L.-H. Gan, *Eur. J. Org. Chem.* **2009**, *2009*, 2661–2665.

[45] M. B. Schmid, K. Zeitler, R. M. Gschwind, *Angew. Chem. Int. Ed.* **2010**, *49*, 4997–5003.

[46] S. Bahmanyar, K. N. Houk, H. J. Martin, B. List, *J. Am. Chem. Soc.* **2003**, *125*, 2475–2479.

[47] D. A. Bock, C. W. Lehmann, B. List, *Proc. Natl. Acad. Sci. U. S. A.* **2010**, *107*, 20636–20641.

[48] M. Karplus, *J. Chem. Phys.* **1959**, *30*, 11–15.

[49] C. Allemann, J. M. Um, K. N. Houk, *J. Mol. Catal. A: Chem.* **2010**, *324*, 31–38.

[50] T. Kanzian, T. A. Nigst, A. Maier, S. Pichl, H. Mayr, *Eur. J. Org. Chem.* **2009**, 6379–6385.

[51] J. Ammer, M. Baidya, S. Kobayashi, H. Mayr, *J. Phys. Org. Chem.* **2010**, *23*, 1029–1035.

[52] M. Nishio, M. Hirota, Y. Umezawa **1998**.

[53] S. Tsuzuki, A. Fujii, *Phys. Chem. Chem. Phys.* **2008**, *10*, 2584–2594.

[54] M. Nishio, Y. Umezawa, K. Honda, S. Tsuboyama, H. Suezawa, *CrystEngComm* **2009**, *11*, 1757–1788.

[55] M. Brandl, M. S. Weiss, A. Jabs, J. Sühnel, R. Hilgenfeld, *J. Mol. Biol.* **2001**, *307*, 357–377.

[56] G. Toth, S. G. Bowers, A. P. Truong, G. Probst, *Curr. Pharm. Des.* **2007**, *13*, 3476–3493.

[57] M. Nishio, M. Hirota, *Tetrahedron* **1989**, *45*, 7201–7245.

[58] M. Nishio, Y. Umezawa, M. Hirota, Y. Takeuchi, *Tetrahedron* **1995**, *51*, 8665–8701.

[59] M. Nishio, *Tetrahedron* **2005**, *61*, 6923–6950.

[60] G. Tárkányi, P. Király, S. Varga, B. Vakulya, T. Soós, *Chem. Eur. J.* **2008**, *14*, 6078–6086.

[61] L.-S. Sonntag, S. Schweizer, C. Ochsenfeld, H. Wennemers, *J. Am. Chem. Soc.* **2006**, *128*, 14697–14703.

[62] D. A. DiRocco, K. M. Oberg, D. M. Dalton, T. Rovis, *J. Am. Chem. Soc.* **2009**, *131*, 10872–10874.

[63] M. Cai, Y. Huang, J. Liu, R. Krishnamoorthi, *J. Biomol. NMR* **1995**, *6*, 123–128.

[64] Z. L. Mádi, C. Griesinger, R. R. Ernst, *J. Am. Chem. Soc.* **1990**, *112*, 2908–2914.

[65] E. L. Eliel, S. H. Wilen, L. N. Mander, *Stereochemistry of Organic Compounds*, Wiley, New York, **1994**.

[66] C. Sparr, W. B. Schweizer, H. Senn, R. Gilmour, *Angew. Chem. Int. Ed.* **2009**, *48*, 3065–3068.

[67] L. W. Reeves, W. Schneider, *Can. J. Chem.* **1957**, *35*, 251–261.

[68] C. E. Johnson Jr., F. A. Bovey, *J. Chem. Phys.* **1965**, *29*, 1012–1014.

[69] M. P. Patil, A. K. Sharma, R. B. Sunoj, *J. Org. Chem.* **2010**, *75*, 7310–7321.

[70] M. Tiecco, A. Carlone, S. Sternativo, F. Marini, G. Bartoli, P. Melchiorre, *Angew. Chem. Int. Ed.* **2007**, *46*, 6882–6885.

[71] Q. Zhu, Y. Lu, *Org. Lett.* **2008**, *10*, 4803–4806.

[72] E. Marqués-López, R. P. Herrera, T. Marks, W. C. Jacobs, D. Könning, R. M. de Figueiredo, M. Christmann, *Org. Lett.* **2009**, *11*, 4116–4119.

[73] Y. Chi, S. H. Gellman, *J. Am. Chem. Soc.* **2006**, *128*, 6804–6805.

[74] H. Gotoh, Y. Hayashi, *Chem. Commun.* **2009**, 3083–3085.

[75] I. Mager, K. Zeitler, *Org. Lett.* **2010**, *12*, 1480–1483.

[76] R. M. de Figueiredo, R. Fröhlich, M. Christmann, *Angew. Chem. Int. Ed.* **2008**, *47*, 1450–1453.

[77] G. A. Jeffrey, *An Introduction to Hydrogen Bonding*, Oxford University Press, Oxford, **1997**.

[78] `http://www.wavefun.com`.

[79] S. H. Oh, H. S. Rho, J. W. Lee, J. E. Lee, S. H. Youk, J. Chin, C. E. Song, *Angew. Chem. Int. Ed.* **2008**, *47*, 7872–7875.

[80] H. S. Rho, S. H. Oh, J. W. Lee, J. Y. Lee, J. Chin, C. E. Song, *Chem. Commun.* **2008**, 1208–1210.

[81] J. W. Lee, T. H. Ryu, J. S. Oh, H. Y. Bae, H. B. Jang, C. E. Song, *Chem. Commun.* **2009**, 7224–7226.

[82] P. Király, T. Soós, S. Varga, B. Vakulya, G. Tárkányi, *Magn. Reson. Chem.* **2010**, *48*, 13–19.

[83] C. Agami, J. Levisalles, C. Puchot, *J. Chem. Soc. Chem. Commun.* **1985**, 441–442.

[84] C. S. Johnson Jr., *Prog. Nucl. Magn. Reson. Spectrosc.* **1999**, *34*, 203–256.

[85] E. O. Stejskal, J. E. Tanner, *J. Chem. Phys.* **1965**, *42*, 288–292.

[86] C. A. Crutchfield, D. J. Harris, *J. Magn. Reson.* **2007**, *185*, 179–182.

[87] T. Steiner, *Angew. Chem. Int. Ed.* **2002**, *41*, 48–76.

[88] L. Fang, A. Lin, H. Hu, C. Zhu, *Chem. Eur. J.* **2009**, *15*, 7039–7043.

[89] E. Alza, M. A. Pericàs, *Adv. Synth. Catal.* **2009**, *351*, 3051–3056.

[90] M. C. Varela, S. M. Dixon, K. S. Lam, N. E. Schore, *Tetrahedron* **2008**, *64*, 10087–10090.

[91] M. Schmid, K. Zeitler, R. M. Gschwind, *J. Am. Chem. Soc.*, *submitted*.

[92] C. Reichardt, *Solvents and Solvent Effects in Organic Chemistry*, Wiley-VCH, Weinheim, **1988**.

[93] D. Enders, C. Wang, J. Bats, *Angew. Chem. Int. Ed.* **2008**, *47*, 7539–7542.

[94] M. Schmid, K. Zeitler, R. M. Gschwind, *J. Am. Chem. Soc.*, *submitted*.

[95] A. Russo, A. Lattanzi, *Org. Biomol. Chem.* **2010**, *8*, 2633–2638.

[96] Y. H. Chang, F.-T. Chiu, G. Zon, *J. Org. Chem.* **1981**, *46*, 342–354.

[97] R. Tacke, H. Lange, *Chem. Ber.* **1983**, *116*, 3685–3691.

[98] W. McFarlane, J. M. Seaby, *J. Chem. Soc. Perkin Trans. 2* **1972**, 1561–1564.

[99] C. M. Yam, A. K. Kakkar, *J. Chem. Soc. Chem. Commun.* **1995**, 907–909.

[100] M. Arshadi, D. Johnels, U. Edlund, C.-H. Ottosson, D. Cremer, *J. Am. Chem. Soc.* **1996**, *118*, 5120–5131.

[101] B. List, L. Hoang, H. J. Martin, *Proc. Natl. Acad. Sci. U. S. A.* **2004**, *101*, 5839–5842.

8 Product Inhibition in Iminium Catalysis by Immobilized Diarylprolinol Ethers

Letter

"Efficient, Enantioselective Iminium Catalysis with an Immobilized, Recyclable Diarylprolinol Silyl Ether Catalyst"

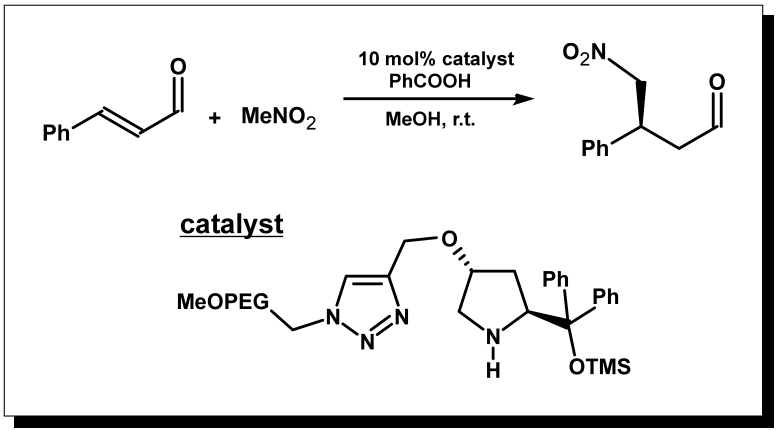

Ina Mager and Kirsten Zeitler

Org. Lett. **2010**, *12*, 1480–1483.

8.1 Summary of the Manuscript

α,α-Diarylprolinol derivatives have proven excellent performances as enantioselective organocatalysts via both enamine and iminium activation of substrates. Nevertheless, for their application as homogeneous catalysts in solution, high catalyst loadings and cumbersome purification procedures had to be put up with. To bypass these drawbacks, immobilization strategies have emerged as a tool to simplify the product separation and to increase the synthesis efficiency by catalyst recovery and reuse. In particular soluble-polymer supported catalysts offer the option to combine the advantages of hetero- and homogeneous catalysis: Synthesis protocols that have been established for non-supported catalysts can be taken over, but the workup of the reactions is largely simplified.

Against this background, Mager and Zeitler designed and successfully synthesized MeOPEG-immobilized diphenyl prolinol ethers for asymmetric iminium catalysis (Figure 8.1A). These catalysts were applied in the Henry-type Michael addition of nitromethane to iminium-activated cinnamaldehydes in methanol to yield γ-nitro aldehydes (Figure 8.1B). Under these conditions, the MeOPEG-supported catalysts shows unchanged excellent reactivities and selectivities in comparison to the non-supported analogs.

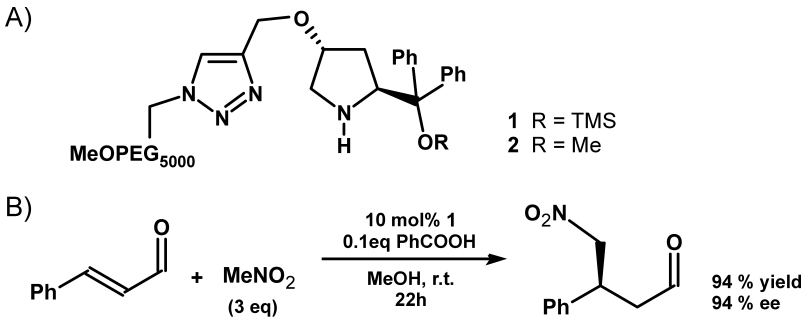

Figure 8.1: A) MeOPEG-immobilized diphenyl prolinol ether catalysts investigated, B) the Michael addition of nitromethane to cinnamaldehyde via iminium activation, used as a model reaction.

Moreover, the product could be accessed straightforwardly without column chromatographic purification by the diethyl ether-triggered precipitation of the catalyst, followed by filtration and washing with a saturated $NaHCO_3$ solution. The catalyst was recovered in more than 95 % and could be reused without any loss of selectivity. However, a prolongation of the reaction times until full conversion was observed with the recycled catalyst. Since this loss of activity was observed for both **1** and **2**, it cannot be explained by the often postulated desilylation of prolinol silyl ether catalysts like **1**. Therefore, NMR spectroscopic techniques were employed to elucidate potential deactivation modes of **2**. Indeed, an unreleased iminium species was observed to be still bound to the recycled catalyst and was hence suggested to deactivate the recycled catalyst through product inhibition. On this basis, simple stirring of the recycled catalyst with a solution of the starting aldehyde could be developed as a straightforward, yet highly efficient approach to fully restore the catalyst´s initial activity.

8.2 NMR Spectroscopy of MeOPEG-Supported Organocatalysts

To check for possible deactivation modes of MeOPEG-immobilized diphenyl prolinol ethers, NMR spectroscopic investigations were undertaken on catalyst **2** which had been recovered from the iminium-catalyzed Michael addition of nitromethane to cinnamaldehyde in methanol with benzoic acid as additive (Figure 8.1). The choice of the methyl ether catalyst **2** for our investigations allowed us to preclude the potential loss of the *O*-protecting group (as might occur in the case of TMS instead of Me, chapter 6.2 and **??**) as an additional source of spectral complexity. Still, in the one-dimensional proton spectrum of the recycled catalyst **2**, at least four different considerable methylated species (**3**, **4**, **5**, and **6**) could be distinguished with the help of the readily observed singlets of the methyl group (Figure 8.2A). The structures of these compounds were to be determined by more detailed 2D NMR investigations.

The NMR spectroscopic challenge of these studies was to efficiently suppress the MeOPEG-5000 resonances, which were by far the most intensive signals and hence largely sensitivity-limiting (Figure 8.2A). For homonuclear two-dimensional experiments, the well-established signal suppression strategies like presaturation or WATERGATE could be adapted straightforwardly for the removal of the MeOPEG resonances (Figure 8.2B,C). In our experimental system, the best results for the ^{1}H,^{1}H-COSY and ^{1}H,^{1}H-NOESY spectra were obtained with the help of a presaturation sequence. Different approaches had to be chosen for heteronuclear 2D experiments. In ^{1}H,^{13}C-HMBC spectra, the suppression of the unwanted MeOPEG-signals was achieved by a combination of presaturation and low-pass *J*-filtering (for the suppression of the $^{1}J_{H,C}$ coupling). A common presaturation sequence was not applicable to the ^{1}H,^{13}C-HSQC spectrum, since in this case both ^{13}C-satellites had to be suppressed at the same time. This was hence accomplished by applying the WET sequence which uses selective saturation pulses under continuous ^{13}C decoupling together with defocusing by pulsed-field gradients for the simultaneous suppression of multiple NMR signals (Figure 8.2D). Exemplary results of these suppression strategies are displayed on the example of the proton spectrum of recycled **2** (Figure 8.2).

Based on these concepts, homo- and heteronuclear two-dimensional NMR spectra of **2** in $CDCl_3$ at 300 K were recorded which, despite the challenges of heavy resonance overlap and low signal intensities, enabled us to gain insight into the nature of the different methylated species. Compound **3** was identified as methyl benzoate; this assignment is in good agreement with the available literature data.[1] However, more detailed investigations would be necessary to clarify the origin of the esterification of benzoic acid, i.e. whether the methyl group stems from the reactant nitromethane, from the solvent methanol, or from the catalyst **2**. The last-mentioned case might also be seen in mechanistic analogy to the putative formation of TMS benzoate from prolinol silyl ether catalysts and benzoic acid in DMSO or MeCN (see chapter **??**). In contrast to **3**, the complete elucidation of the molecular structure of **4** was not allowed by the spectral quality obtainable, but only fragmentary information could be gathered. For the methyl group of **4**, neither a cross-

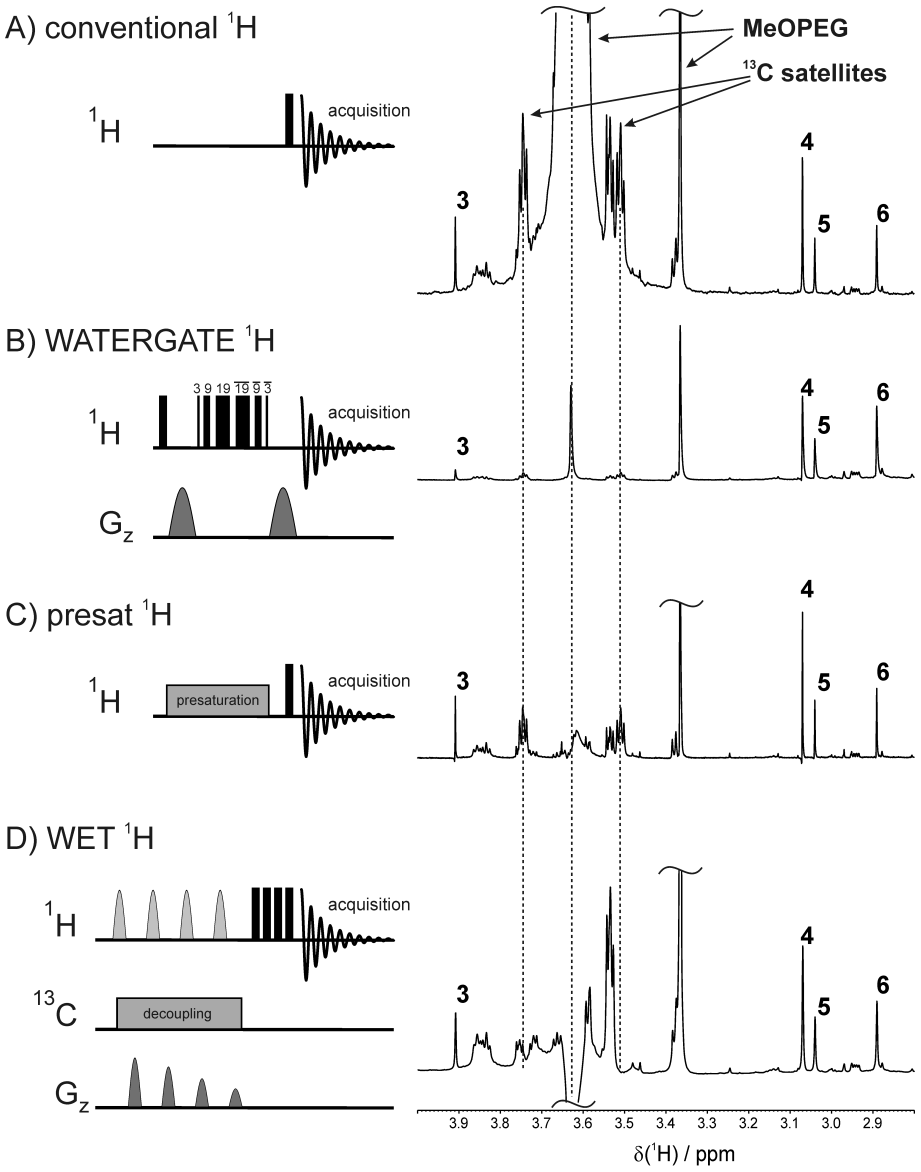

Figure 8.2: Sections of different 1D ^{1}H spectra of recycled **2** in $CDCl_3$ at 300 K with the associated pulse sequences (left) and resulting spectra (right): A) conventional, B) WATERGATE, C) presat, and D) WET ^{1}H experiment. The most effective suppression of the MeOPEG signal is achieved in the case of presaturation (C). The application of the WET sequence (D) allows for the removal of the ^{13}C satellites.

peak from the methyl protons to the quaternary carbon (at about 85 ppm, *cf.* Figure 8.3) in the ^{1}H,^{13}C-HMBC spectrum could be detected nor NOEs between the methyl protons and any aromatic protons. Therefore, we can definitely rule out that this methyl group belongs to a $CPh_2(OMe)$ motif of a catalyst-derived species. Instead, the ^{13}C chemical shift of 38.0 ppm for the methyl group of **4** indicates an *N*-methyl group rather than an *O*-methyl group (for which chemical shifts of about 52 ppm would be expected, *cf.* Figure 8.3). However, the inability to detect NOEs from the methyl to aryl protons clearly shows that the *N*-methyl group is not located at the pyrrolidine nitrogen; instead, possibly

N-methylation occured at nitrogen atoms of the unloaded polymer. Next, investigations on the structure of **5** led to the almost complete assignment of its diphenylprolinol methyl ether moiety (Figure 8.3). No NMR spectroscopic indication was found that suggests any kind of encumbrance of the catalytic unit of **2** in this case. Still, unusually large chemical shifts of the protons in proximity to the pyrrolidine nitrogen atom may be taken as a hint at protonation of the secondary amine. Hence, we suppose that compound **5** is a protonated form of catalyst **2**, possibly the salt of the benzoic acid that had been applied as an additive in the catalyzed reaction.

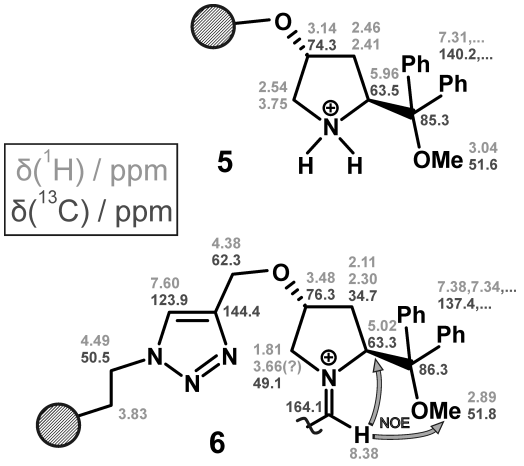

Figure 8.3: NMR assignments of compounds **5** (top) and **6** (bottom) in $CDCl_3$ at 300 K. Proton data is given in light gray, carbon data in dark gray. In the case of diastereotopic protons, the upper value refers to the proton above the plane of projection.

Finally, compound **6** was considered as a potential origin of the drop of activity of catalyst **2** after recycling. **6** could be identified as a species derived from **2** by an almost full NMR assignment of its diphenylprolinol methyl ether unit. Most interestingly an unexpected NOE between the methyl protons of **6** and a proton resonating as a singlet at 8.38 ppm was observed. This proton was revealed by the ^{1}H,^{13}C-HSQC spectrum to be bound to a carbon with a resonance at 164.1 ppm and it furthermore showed an NOE to the α-proton of the prolinol unit. Both the ^{1}H and the ^{13}C chemical shift are in a range that is typical for diarylprolinol ether-derived iminium ions, as has been reported earlier in the literature.[2,3] Hence, together with the observed NOEs, this indicates **6** to be an *E*-configured iminium species. This can be interpreted in terms of residual product that is still bound to the catalyst and thereby leads to its reduced activity. In fact, this hypothesis could be confirmed by the successful displacement approach for the recovery of the full catalytic activity of **2**.[4] The thereby observed product release furthermore shows that this iminium species is not derived from the starting aldehyde, but in fact from the non-released product. However, first attempts to monitor this product release from recycled **1** have not been successful so far because of solubility problems and should be repeated under improved experimental conditions.

In summary, suitable NMR spectroscopic signal suppression approaches for the investigation of MeOPEG-supported diarylprolinol ether organocatalysts were found and they were applied to characterize different molecular species present in the recovered catalytic system. As the major source of catalyst deactivation during the recycling process, a product inhibition of the catalyst by the non-hydrolyzed catalyst-product iminium adduct was identified. Based on this finding, a facile and rapid displacement approach could be developed to fully restore the catalyst´s activity.

8.3 References

[1] SDBSWeb, `http://riodb01.ibase.aist.go.jp/sdbs/`.

[2] S. Lakhdar, T. Tokuyasu, H. Mayr, *Angew. Chem. Int. Ed.* **2008**, *47*, 8723–8726.

[3] U. Grošelj, D. Seebach, D. M. Badine, W. B. Schweizer, A. K. Beck, I. Krossing, P. Klose, Y. Hayashi, T. Uchimaru, *Helv. Chim. Acta* **2009**, *92*, 1225–1259.

[4] I. Mager, K. Zeitler, *Org. Lett.* **2010**, *12*, 1480–1483.

9 The Dimerization of Nitralkenes to Enynes

"Towards Novel Organocatalytic Transformations—
Nitro-Michael-Initiated Nitroalkene-Coupling to Enynes"

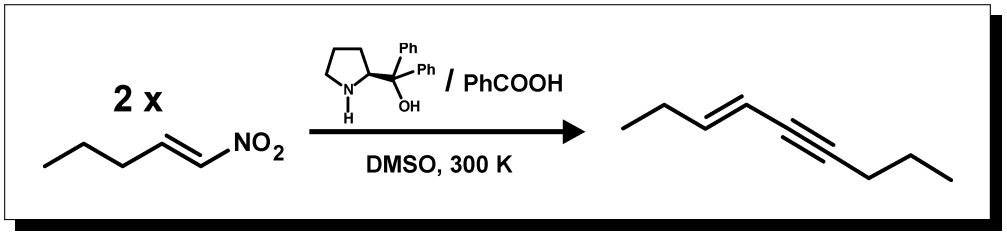

The syntheses of compounds **14** and **19** were conducted by Veronika Kropf under supervision of Felicitas von Rekowski. NMR spectroscopic investigations on reactions involving these compounds were performed in close collaboration with Felicitas von Rekowski, Veronika Kropf and Carina Koch. Compound **16** was synthesized by Dr. Kirsten Zeitler.

Markus B. Schmid, Kirsten Zeitler, and Ruth M. Gschwind

9.1 Nitroalkene Dimerization to Enynes

Introduction

Conjugated enynes constitute a class of organic compounds with an intriguing variety of potential applications. The enyne structure motif is found in natural products, antitumor drugs, and transition metal ligands as well as in synthons and intermediates in organic chemistry (*e.g.* Pauson reactions, Bergman cyclizations, or metathesis reactions).[1] Enynes are typically accessed by Pd/Cu-catalyzed cross-couplings, *i.e.* the formation of a C-C single bond between an alkene and an alkyne moiety (*e.g.* Sonogashira coupling).[2] The formation of enynes by connecting two carbon atoms via a C-C triple bond in one pot, however, has not been reported so far. Neither is an organocatalytic enyne formation protocol known to date. Nitro*alkenes* belong to the most widely used acceptor species in organocatalytic Michael reactions because of their high electrophilicities ("super-electrophiles")[3] and hence their ready reaction with ketone- or aldehyde-derived enamines. In contrast, nitro*alkanes* are well-known to act as α-nucleophilic species under the influence of bases, for instance, in additions to carbonyl species (Henry reaction) or to electron-poor alkenes.[4,5] In particular, the addition of nitro*alkanes* to nitro*alkenes*, promoted by bases,[6] *Cinchona* alkaloids,[7] ammonium bifluorides,[8] or bifunctional amine-thioureas[9,10] has been used to build synthetically valuable 1,3-dinitro-compounds. On the other hand, according to the Baylis-Hillman reaction scheme, α-nucleophilic reactivity is known also for nitro*alkenes* under the influence of tertiary amine bases. This chamaeleon-like reaction option of nitro*alkenes*, as an α-nucleophile and as a β-electrophile at the same time, is presumably also responsible for the observation of a nitroalkene dimer as a by-product during the synthesis of a β-nitronitriles in the presence of cyanide[11] and for the known tendency of nitroalkenes to polymerize,[3,4] especially under basic conditions. Against this background, it is striking to note that there are to the best of our knowledge no systematic studies on the dimerization or oligomerization of nitroalkenes under the influence of amines — neither in terms of an unwanted side-reaction, nor as a potentially productive reaction pathway. To fill this gap, we present here our study on the amine-catalyzed dimerization of nitroalkenes, followed by an unexpected fragmentation to enynes.

Results and Discussion

Nitroalkene Homo-Dimerization to Enynes. The starting point for our investigations on nitroalkene dimerizations was the observation that, upon addition of 20 mol% of diphenylprolinol **3** to an equimolar mixture of nitropentene **5** (synthesized according to the published protocol[12] in a yield of 44 %) and propionaldehyde (50 mM each) in DMSO, the envisaged Michael addition did not take place in noticeable amounts, but the nitropentene was consumed nevertheless to a remarkable degree (see chapter 10.1). To check whether this nitropentene conversion was due to a productive, potentially valuable reaction, nitropentene **5** was mixed with 100 mol% of one of the amine catalysts **1**-**4** (Figure 9.1A) or

of a combination of an equimolar mixture of **4** and the additive benzoic acid in DMSO-d_6 (the final concentration of the reactants was 50 mM each). The events in the reaction mixtures, for which the color change to yellow or orange and the development of gas bubbles macroscopically indicated vivid reactivity, were monitored by 1D ^{1}H spectra at 300 K. Indeed the formation of products in reasonable amounts was revealed and, most surprisingly 3-nonen-5-yne **9** could be identified by 2D NMR techniques as the main product in the reaction mixtures with **3**, **4** and **3**/PhCOOH as catalysts (Figure 9.1A). Best results for this conversion were obtained with **3**/PhCOOH (similarly for the crystalline **3** benzoate salt), for which the NMR-determined *in situ* yield reached 35 % after 7 hours, but was still rising at that stage of the reaction (see Figure 9.1B; assuming full conversion of the dimers **7** to the enyne **9**, the yield of **9** may reach up to 60 %.). In addition to the formation of **9**, various reaction intermediates with different kinetic profiles were detected. In particular with the help of reaction mixtures with L-proline **1**, for which the nitropentene conversion proceeded a lot slower, these intermediates could be characterized by 2D NMR spectroscopy as the catalyst-nitroalkene-adduct **6** as well as the *E*- and *Z*-configured, diastereomeric nitroalkene dimers **7a**,**b** (see Figure 9.1C for the NMR assignments). Interestingly, throughout this study, the *Z*-configured **7a**,**b** were found in higher amounts than the *E*-isomers; the ratio *Z*-**7**:*E*-**7** was about 3:1 (with diastereomeric ratios *Z*-**7a**:*Z*-**7b** of 1.4:1 and *E*-**7a**:*E*-**7b** of 1.5:1) in the case of catalysis by **1** (for which the reaction stopped at the stage of the nitroalkene dimers). Additionally to the enyne **9**, compound **8** was observed as a minor byproduct when **3** or **4** were applied as catalysts, and it was even the only product in case of catalysis by **2**. Based on its NMR characterization, **8** might be the nitronic acid tautomer of **7a**,**b**. Finally, nitromethane was detected as a byproduct in all the reaction mixtures investigated (though not in the stoichiometric amounts expected, see below). Altogether, these findings characterize an unprecedented organocatalytic enyne formation pathway through the dimerization of nitroalkenes, in which two carbon atom get linked by a C-C triple bond in one pot.

Mechanistic Proposal. Based on the reaction intermediates detected, we suggest the following mechanism for this unprecedented organocatalytic nitroalkene coupling to enynes (Figure 9.2): Our mechanistic proposal comprises a Baylis-Hillman-type nitroalkene dimerization and a fragmentation of the dimer intermediate to the enyne: First, the nucleophilic secondary amine catalyst attacks the highly electrophilic β-carbon of the nitroalkene, resulting in the addition of **3** to the C-C double bond of **5** to form **6**. Upon deprotonation of **6** in α-position to the nitro-group, the α-carbon can nucleophilically attack another molecule of **5**. From the resulting catalyst-nitroalkene-nitroalkene-adduct, the catalyst is eliminated and the C-C double bond is reconstituted. Notably, compared to the original nitropentene **5**, the double-bond is now shifted and the deconjugated β,γ-unsaturated nitroalkene **7** is formed. However, this finding is in line with early reports that the ratio of deconjugated nitroalkenes is increased by α-substitution.[13] In addition, the same regiochemical outcome was reported for the amine base-mediated addition of α,β-unsaturated nitroalkenes

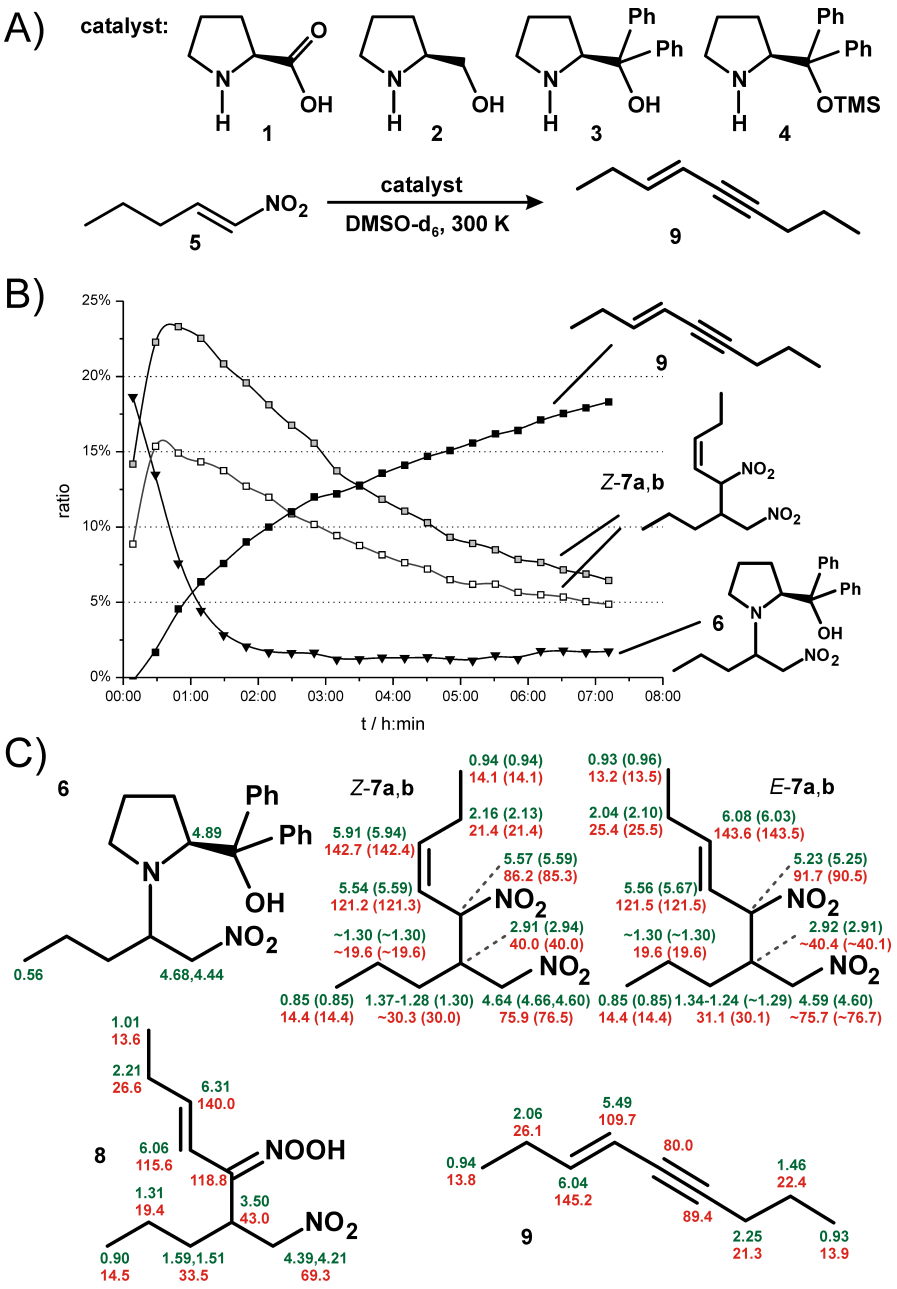

Figure 9.1: A) The reaction investigated and the catalysts employed; B) reaction profile of a mixture of nitropentene, **3** and benzoic acid in DMSO-d_6 (not shown: **5** was consumed within one hour; *E*-**7a**,**b** was detected only in tiny amounts; note: The sum of all **5**-derived moieties detected in the first spectrum was set to 100 %.); C) NMR assignments of reaction intermediates and products (**6** was assigned in analogy to the adduct of **1** and **5** for which the covalent N-C bond could be proven by ^{1}H,^{13}C-HMBC spectra.)

to aldehydes,[5] for the DBU-induced Baylis-Hillman reaction using nitroalkenes,[14] and for the tetramethylguanidine-catalyzed Michael addition of $\alpha\beta$-unsaturated nitroalkenes to electron-deficient olefins, such as α,β-unsaturated ketones, esters, nitriles, or sulfones.[5] Moreover, the unexpected preference of the *Z*-configuration of the nitroalkene dimer corresponds with a previous report on the observation of the dimer of 1-nitro-hept-1-ene (**13**

in Figure 9.3).[11] The resulting nitroalkene-dimer **7** then undergoes fragmentation to the enyne **9**. Since no further reaction intermediates could be detected, the proposed mechanism for this process has to remain on the level of speculation: The exclusive observation of the *E*-configured enyne **9** suggests that the formation of **9** proceeds from *E*-**7** only and that *E*-**7** is recovered in solution by isomerization of *Z*-**7** (potentially through an allylic stage). This hypothesis is supported by the fact that the *E*-isomer of **7** is easily observed in the case of proline catalysis (for which virtually no enyne formation was detected), but on the other hand *E*-**7** was hardly observable for **3**/PhCOOH as catalyst system (for which enyne formation proceeded easily). The fragmentation of **7** may be initiated by deprotonation in the allylic position, that is moreover α to the nitro group, which should hence be a readily occurring process in the presence of amine bases. Since the nitromethylene anion can act as a reasonable leaving group, the formation of the 5-nitro-nona-3,5-diene **10** is a plausible suggestion. It is also supported by the observation of nitromethane in all the reaction mixtures studied. The final step of the enyne formation would then consist of the elimination of nitrous acid HNO_2 from **10**. This is certainly unexpected, but the loss of HNO_2 from a 2-nitro-diene moiety was already reported in a different context.[15] Nevertheless, the observation of gas bubbles as well as the coloring of the reaction mixtures would be in line with the release of nitrous gases.

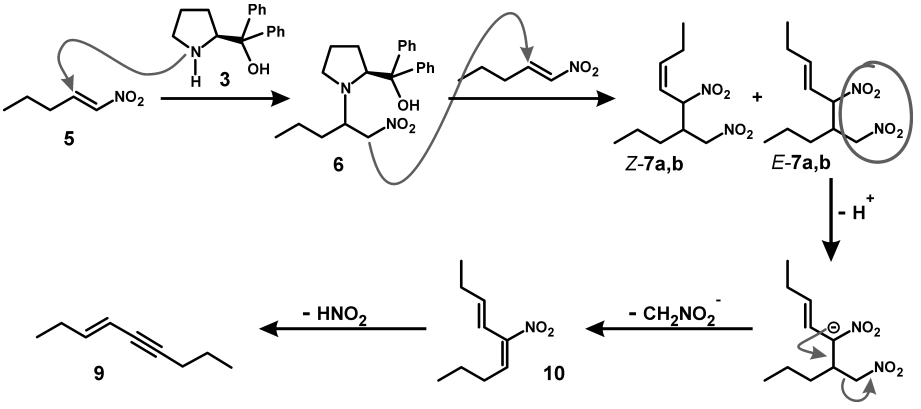

Figure 9.2: Mechanistic proposal for the enyne formation by homo-coupling of nitroalkenes, followed by fragmentation.

On any account, this mechanistic proposal, especially the fragmentation of the nitroalkene-dimer **7**, certainly necessitates further experimental confirmation. For that purpose, more detailed investigations are to be performed, in particular, the application of the α- or β-disubstituted nitroalkenes **11**[16–19] and **12**[20] (Figure 9.3) under the experimental conditions outlined above for the nitroalkene **5**. Because of the changed substitution patterns of **11** and **12** compared to **5**, the fragmentation of the nitroalkene dimer is expected to be incomplete and the detection of intermediates of the fragmentation process might hence provide insights into the underlying mechanism. In addition, the directed synthesis and isolation of nitroalkene-dimers like **7** should be conducted either by proline catalysis (for which fragmentation to the enyne was not observed) or following the synthetic protocol

for **13** that has become available recently.[11] Such dimers could then be exposed to experimental conditions that potentially trigger the fragmentation to enynes. For instance, the use of different catalysts with varying nucleophilicities and H-bond donor properties may help to elucidate whether covalent Lewis-base catalysis or non-covalent H-bond catalysis via supramolecular aggregates is operative in the enyne formation. In addition, the application of excesses or shortages of either acidic or basic additives might clarify the importance of proton transfers in the fragmentation mechanism of the nitroalkene dimers. In addition, radical scavengers such as TEMPO (2,2,6,6-tetramethylpiperidine-1-oxyl) or BHT (butylated hydroxytoluene) could be added to rule out potential radical pathways.

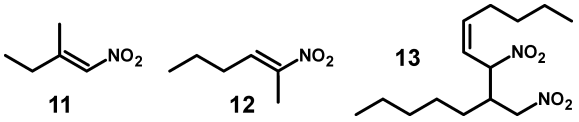

Figure 9.3: Nitroalkenes to be synthesized in order to elucidate the mechanism of the dinitroalkene fragmentation.

Thus, based on a better mechanistic understanding of the enyne formation, an optimization of the reaction conditions should be feasible. Because, despite the promising first results, this novel nitroalkene coupling to an enyne needs to be improved to become a competitive tool in organic chemistry. In particular, higher yields, estimated to be on the order of 35 % so far, and lower catalyst loadings are highly desirable. So far, it has only been shown that the enyne coupling is operative with 20 mol% of **3** in principle, too. In contrast, no efforts have been made towards using other solvents than DMSO or other reaction temperatures than room temperature. In particular, raising the temperature should facilitate the elimination steps of the fragmentation process for entropic reasons and might therefore improve the enyne yields significantly. Additionally, the catalytic system needs to be optimized: Based on the experience available so far and reaction conditions presented in the literature, further amine bases like pyrrolidine, DABCO (1,4-diazabicyclo[2.2.2]octane),[5] or DBU (1,8-diazabicyclo[5.4.0]undec-7-ene)[14] should be tested as well as different tertiary alkyl and aryl phosphines, possibly with different acidic or basic additives. In addition, the catalytic potential of thioureas[9,10] and guanidines[5] in the enyne formation should be explored. Finally, since there are also reports on organocatalytic Henry reactions to form nitroalkenes, catalytic systems to go directly from aldehydes via nitroalkenes and nitroalkene dimers to enynes in a one-pot process might be within reach.

Substrate Scope. We were furthermore interested in the substrate scope of the nitroalkene homo-coupling to enynes. For that purpose, the synthesis of the nitroalkenes **14**[12,21] and **15**[22,23] (Figure 9.4) was envisaged since their predicted enynes should be stabilized even better than the enyne of **5** because of inductive or mesomeric effects, respectively. In addition, the competition of the nitroalkene dimerization with S_N-type alkylations, owing to the presence of leaving groups, was to be investigated on the example of **16**[24,25] which bears an iodide in ϵ-position to the nitro group.

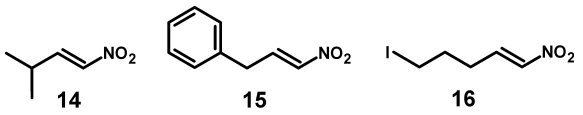

Figure 9.4: Nitroalkenes to be synthesized in order to explore the substrate scope of the enyne formation.

First, **14** (final concentration 100 mM) was mixed with 50 mol% of **3**/PhCOOH in DMSO-d_6 at 300 K, which had turned out to be the optimum catalyst system for the enyne formation in the case of **5**. The reaction progress was monitored by 1D ^{1}H spectra. Overall, the obtained reaction profile showed great similarity to the case of **5**. Analogously to the homo-coupling of **5**, the addition product of the catalyst and **14** as well as the dimer of **14** were detected as intermediates, also with a similar kinetic profile as in the case of **5**. Likewise, the **14**-derived enyne was formed with a comparable rate and the *in situ* yield after 6 hours reached about 35 %. This finding indicates that aliphatic α- and β-unbranched nitroalkenes are widely accepted as substrates in the enyne formation. The transferability of this result onto aromatic nitroalkenes is to be confirmed on the example of **15**. This should then provide a good basis for a further extension of the substrate scope study, in particular with respect to the exploration of other electron-deficient alkenes as substrates, such as sulfonates, phosphonates, or carboxylates.

In contrast to these encouraging findings, for **16**, the iodide leaving group in ϵ-position to the nitro-group was not tolerated by the enyne formation process. When **16** (final concentration 50 mM) was mixed with 100 mol% of **3**/PhCOOH in DMSO-d_6 at 300 K, no enyne product was observed. Instead, as the main product, the (*E*-2-nitroethenyl)-cyclopropane **17** was detected in an estimated *in situ* yield of about 30 % (Figure 9.5). The formation of this unexpected product of an intramolecular S_N-type cyclopropanation can be rationalized by the base-induced deprotonation of **16** in γ-position, resulting in a nitro-stabilized allylic anion that nucleophilically attacks the ϵ-carbon atom and releases the iodide leaving group. Further experiments would be necessary to explore the potential of this γ-alkylation of nitroalkene towards synthetically valuable processes. In addition to this cyclopropanation, leading to **17** under the formal release of HI, the formation of another species **18** was observed. In a different experimental setup (see chapter 10.2), this species could be identified as the protonated catalyst **3**, most probably existing as the iodide salt (as the same species was observed in the absence of PhCOOH). The NMR characterization revealed three distinct resonances for the three exchangeable protons of **18** (even in the presence of PhCOOH; see Figure 9.5). Additionally, COSY crosspeaks of the ammonium protons with each other as well as with the vicinal protons of the pyrrolidine ring were detected. Together with the EXSY observation of only tiny exchange of the ammonium protons with water, this strongly indicates, that the ammonium protons in **18** are involved in a rather stable hydrogen bonding network. This was verified by DOSY investigations (chapter 7.4) which evidenced that **18** is not monomeric in DMSO, but forms larger aggregates. Whether this phenomenon is associated with the deactivation of the catalytic properties of **3** (see chapter 10.2) needs to be investigated in more detail.

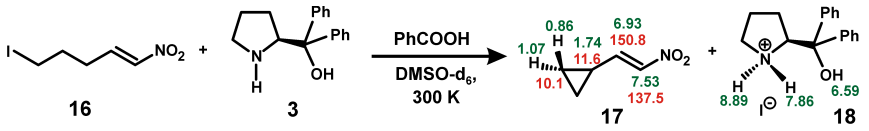

Figure 9.5: Intramolecular S_N-type cyclopropanation of **16** under the influence of **3**/PhCOOH in DMSO-d_6 at 300 K.

Nitroalkene Hetero-Dimerization to Enynes. Since the organocatalytic homo-dimerization of nitroalkenes to enynes had brought about first promising results, the extension of this approach towards the cross-coupling of different nitroalkenes was considered as a further important task. The option to reach this aim is provided by the fact that the nucleophilic reaction partner experiences a shift of the nitroalkene C-C double bond from the α,β- to the β,γ-position. Nitroalkenes, for which this shift is highly unfavorable, are therefore expected to react only as the electrophilic reaction partner and should hence allow for nitroalkene cross-couplings. Therefore, nitrostyrenes **19**,[12,26] **20**,[27] and **21**[12] were selected as designated electrophilic reaction partners of nitroisopentene **14** (Figure 9.6A). The different electron-withdrawing or -releasing properties of the substituents of **19**-**21** should furthermore allow to obtain insights into the influence of electronic effects on the enyne formation. In a first attempt, the most electrophilic nitrostyrene of the series, **19**, was mixed with an equimolar amount of **14** (final concentrations 50 mM) and 100 mol% of **3** and PhCOOH in DMSO-d_6. The reaction progress at 300 K was again monitored by 1D ^{1}H spectra (Figure 9.6B).

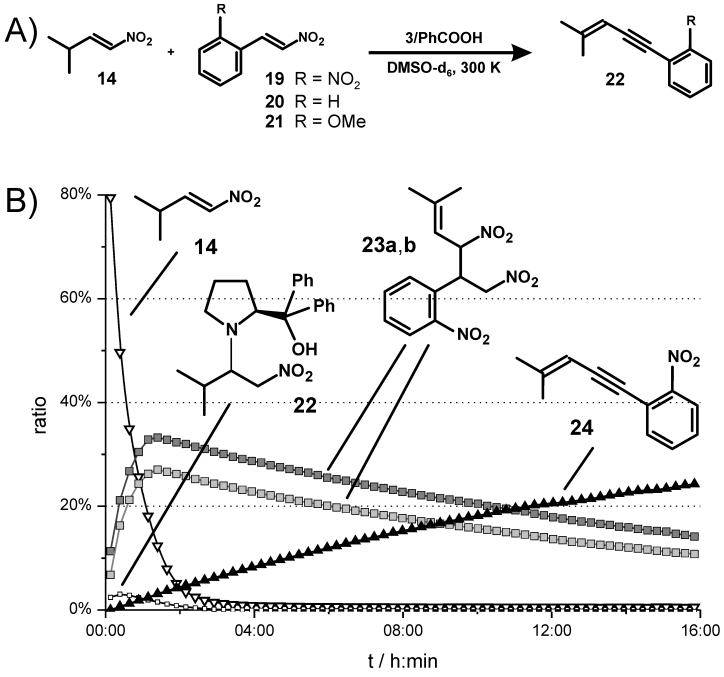

Figure 9.6: A) Envisaged organocatalytic cross-coupling of nitroalkenes using nitrostyrenes **19**-**21** as electrophilic reaction partners; B) reaction profile of the **3**/PhCOOH-catalyzed coupling between **14** and **19**. (not shown: **19** is consumed within one hour; note: The sum of all **14**-derived moieties detected in the first spectrum was set to 100 %.)

To our delight, we could in fact observe the envisaged reaction between **14** and **19**. As anticipated by the reaction progress of the homo-dimerizations of **5** and **14**, the catalyst-nitroalkene adduct **22** was detected as a first intermediate. Next, **23a**,**b**, the diastereomeric hetero-dimers of **14** and **19**, were observed and finally the cross-coupled enyne species **24** in a yield of about 25 %. The yield was still rising after 15 hours and, in view of the residual amounts of the dimers **23**, a final yield of up to 50 % may be reached. Hence, these observations evidence that the organocatalytic cross-coupling of different nitroalkenes to form asymmetric enyne species can be achieved in principle. Given the fact that the reaction conditions have not been optimized yet, this first experimental attempt of a nitroalkene cross-coupling is very promising and encouraging enough to further pursue this reaction pathway. In particular, the effective suppression of the homo-dimerizations of the reaction partners needs to be achieved. Interestingly, in the reaction between **14** and **19**, no homo-dimers of **14** were detected. On the other hand, the less expected homo-dimerization of **19** was observed as a substantial side-reaction and consumed more than 10% of the initial amount of **19**. However, the nature of this dimer of **19** could not be elucidated so far despite a separate experiment in which **19** was mixed with 50 mol% **3**/PhCOOH in DMSO-d_6 at 300 K. In this experimental setup, the dimer of **19** accounted for 30% of the initial amount of **19** used. It might therefore represent a further intriguing target for more detailed investigations in particular with respect to a better understanding of the mechanisms underlying the fragmentation of nitroalkene dimers.

Conclusion

Altogether, our study provides evidence for the first organocatalytic homo- and hetero-dimerizations of nitroalkenes, followed by fragmentation to the corresponding enynes. This represents the first metal-free formation of enynes known to date. Moreover, to the best of our knowledge, this is the only process reported so far, in which two carbon atoms get linked by the direct generation of a triple bond in one pot. As a mechanistic proposal for this unprecedented organocatalytic enyne formation pathway, we suggest the amine base-induced dimerization of nitroalkenes via C-C bond formation between the α-nucleophilic and the β-electrophilic positions. These dimers undergo fragmentation to the enyne under release of nitromethane and nitrous acid. The NMR-detected *in situ* yields of the homo- and hetero-dimerizations under our still non-optimized organocatalytic reaction conditions were estimated to reach up to 50-60 %. These first results are encouraging enough to put more efforts into studying the underlying reaction mechanism and into optimizing reaction conditions. In view of the relevance of enynes the exploitation of this novel synthesis strategy for enyne moieties can be expected to be highly rewarding.

9.2 References

[1] G. Gervasio, P. J. King, D. Marabello, E. Sappa, *Inorg. Chim. Acta* **2003**, *350*, 215–244.

[2] K. Sonogashira, Y. Tohda, N. Hagihara, *Tetrahedron Lett.* **1975**, *16*, 4467–4470.

[3] D. Seebach, A. K. Beck, D. M. Badine, M. Limbach, A. Eschenmoser, A. M. Treasurywala, R. Hobi, W. Prikoszovich, B. Linder, *Helv. Chim. Acta* **2007**, *90*, 425–471.

[4] R. Ballini, G. Bosica, D. Fiorini, A. Palmieri, M. Petrini, *Chem. Rev.* **2005**, *105*, 933–972.

[5] N. Ono, I. Hamamoto, A. Kamimura, A. Kaji, R. Tamura, *Synthesis* **1987**, 258–260.

[6] M.-P. D. Alcántara, F. C. Escribano, A. Gómez-Sánchez, M. J. Diánez, M. D. Estrada, A. López-Castro, S. Pérez-Garrido, *Synthesis* **1996**, *1996*, 64, 64–70.

[7] J. Wang, H. Li, L. Zu, W. Jiang, W. Wang, *Adv. Synth. Catal.* **2006**, *348*, 2047–2050.

[8] T. Ooi, S. Takada, K. Doda, K. Maruoka, *Angew. Chem. Int. Ed.* **2006**, *45*, 7606–7608.

[9] X.-Q. Dong, H.-L. Teng, C.-J. Wang, *Org. Lett.* **2009**, *11*, 1265–1268.

[10] C. Rabalakos, W. D. Wulff, *J. Am. Chem. Soc.* **2008**, *130*, 13524–13525.

[11] J. C. Anderson, A. J. Blake, M. Mills, P. D. Ratcliffe, *Org. Lett.* **2008**, *10*, 4141–4143.

[12] B. M. Trost, C. Müller, *J. Am. Chem. Soc.* **2008**, *130*, 2438–2439.

[13] G. Hesse, R. Hatz, H. König, *Liebigs Ann. Chem.* **1967**, *709*, 79–84.

[14] R. Ballini, L. Barboni, G. Bosica, D. Fiorini, E. Mignini, A. Palmieri, *Tetrahedron* **2004**, *60*, 4995–4999.

[15] C. Dell'Erba, A. Giglio, A. Mugnoli, M. Novi, G. Petrillo, P. Stagnaro, *Tetrahedron* **1995**, *51*, 5181–5192.

[16] A. Lambert, A. Lowe, *J. Chem. Soc.* **1947**, 1517–1519.

[17] F. Lehr, J. Gonnermann, D. Seebach, *Helv. Chim. Acta* **1979**, *62*, 2258–2275.

[18] W. Y. Lee, S. Y. Jang, W. K. Chae, O. S. Park, *Synth. Commun.* **1993**, *23*, 3037–3046.

[19] J. C. Ferrand, R. Schneider, P. Gérardin, B. Loubinoux, *Synth. Commun.* **1996**, *26*, 4329–4336.

[20] P. Mikesell, M. Schwaebe, M. DiMare, R. D. Little, *Acta Chem. Scand.* **1999**, *53*, 792–799.

[21] G. Kumaran, G. H. Kulkarni, *Synthesis* **1995**, *1995*, 1545–1548.

[22] J. M. Concellón, P. L. Bernad, H. Rodríguez-Solla, C. Concellón, *J. Org. Chem.* **2007**, *72*, 5421–5423.

[23] B. R. Fishwick, D. K. Rowles, C. J. M. Stirling, *J. Chem. Soc. Perkin Trans. 1* **1986**, 1171–1179.

[24] M. Lautens, J.-F. Paquin, S. Piguel, M. Dahlmann, *J. Org. Chem.* **2001**, *66*, 8127–8134.

[25] D. Enders, C. Wang, J. Bats, *Angew. Chem. Int. Ed.* **2008**, *47*, 7539–7542.

[26] G. Kumaran, G. H. Kulkarni, *Tetrahedron Lett.* **1994**, *35*, 9099–9100.

[27] P. J. Black, G. Cami-Kobeci, M. G. Edwards, P. A. Slatford, M. K. Whittlesey, J. M. J. Williams, *Org. Biomol. Chem.* **2006**, *4*, 116–125.

10 The Organocatalytic Michael Addition and α-Alkylation

"Beyond Dimerizations—Amine-Catalyzed Michael Additions of Aldehydes to Nitroalkenes and Subsequent α-Alkylations"

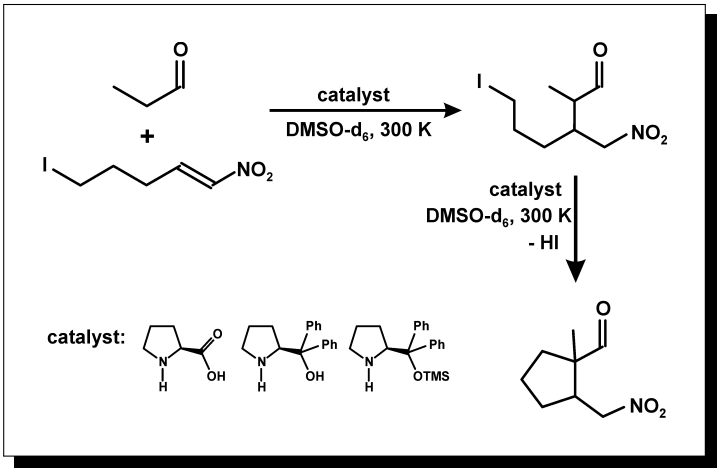

The synthesis of compound **11** was conducted by Dr. Kirsten Zeitler.

Markus B. Schmid, Kirsten Zeitler, and Ruth M. Gschwind

10.1 Michael Addition of Propionaldehyde to Nitropentene

Introduction

The organocatalytic Michael addition constitutes one of the benchmark reactions of amine catalysis. Thereby, aldehydes as nucleophiles in the form of enamines and nitroalkenes as "super-electrophiles"[1] are among the most frequently applied substrates for studying the performance of catalysts in Michael additions. On the basis of our detailed knowledge on homo-dimerizations of both aldehydes (chapters 3 and 5) and nitroalkenes (chapter 9) under amine catalysis, we also studied the organocatalytic Michael reaction between these two compound classes in terms of the detection of intermediates and of differences in catalyst performances. As our model reaction, we chose the Michael addition of propionaldehyde **1** to nitropentene **2** (c = 50 mM, each) under catalysis of the secondary amines L-proline **4**, diphenylprolinol **5**, or diphenylprolinol trimethylsilyl ether **6**, respectively, in DMSO-d_6 at 300 K (Figure 10.1A).

Results and Discussion

Catalysis by Proline. First we applied 20 mol% of L-proline **4**. The Michael addition products **3a**,**b** were formed within 4 hours in a total yield of about 90 % and a diastereomeric ratio of about 3.5:1 (Figure 10.1B). Interestingly and in contrast to the proline-catalyzed self-aldolization of **1** (chapter 3.2), however, intermediates formed from **1** and proline **4** could not be detected in this Michael addition approach. This is attributed to the "super-electrophilicity" of nitropentene **2**; it reacts vividly with the enamine of **1** and **4** so that the concentration of the intermediates of **1** and **4** is below the detection limit. This superiority of **2** as an electrophile is also evidenced by the observation that products of the aldehyde self-aldolization hardly exceeded 5 % yield after 20 hours of reaction time. Nevertheless, instead of proline substrate intermediates, proline product adducts were readily observed: In addition to the product-oxazolidinones, that could be well expected in view of our finding on the aldehyde self-aldolization (*cf.* chapter 3.2), the diastereomeric product-enamines **7a**,**b** were detected, too (Figure 10.1B and C). Again, these proline-derived enamines **7a**,**b** could be characterized by NOESY analysis as *E*-configured s-*trans* enamines. But in contrast to the enamine-oxazolidinone equilibrium of **1**, in which the enamine accounted for only 9 % of the total intermediate amount in DMSO (chapter 3.2), here the share of the enamines **7a**,**b** in the equilibrium with the oxazolidinones was on the order of 40 %. This striking observation may be rationalized by a relative destabilization of the oxazolidinones with respect to the enamines in the case of the product-catalyst adducts: The larger size of the product residue of **3a**,**b** (in comparison to the propyl residue of **1**) may cause heavier steric conflicts with the bicyclic structure of the oxazolidinones than with the monocyclic enamines **7a**,**b**, leading to a reduction of the oxazolidinone equilibrium ratio. Moreover, since comparable product enamines have not been observed for the self-aldolization of propionaldehyde, one may also speculate about the potential involve-

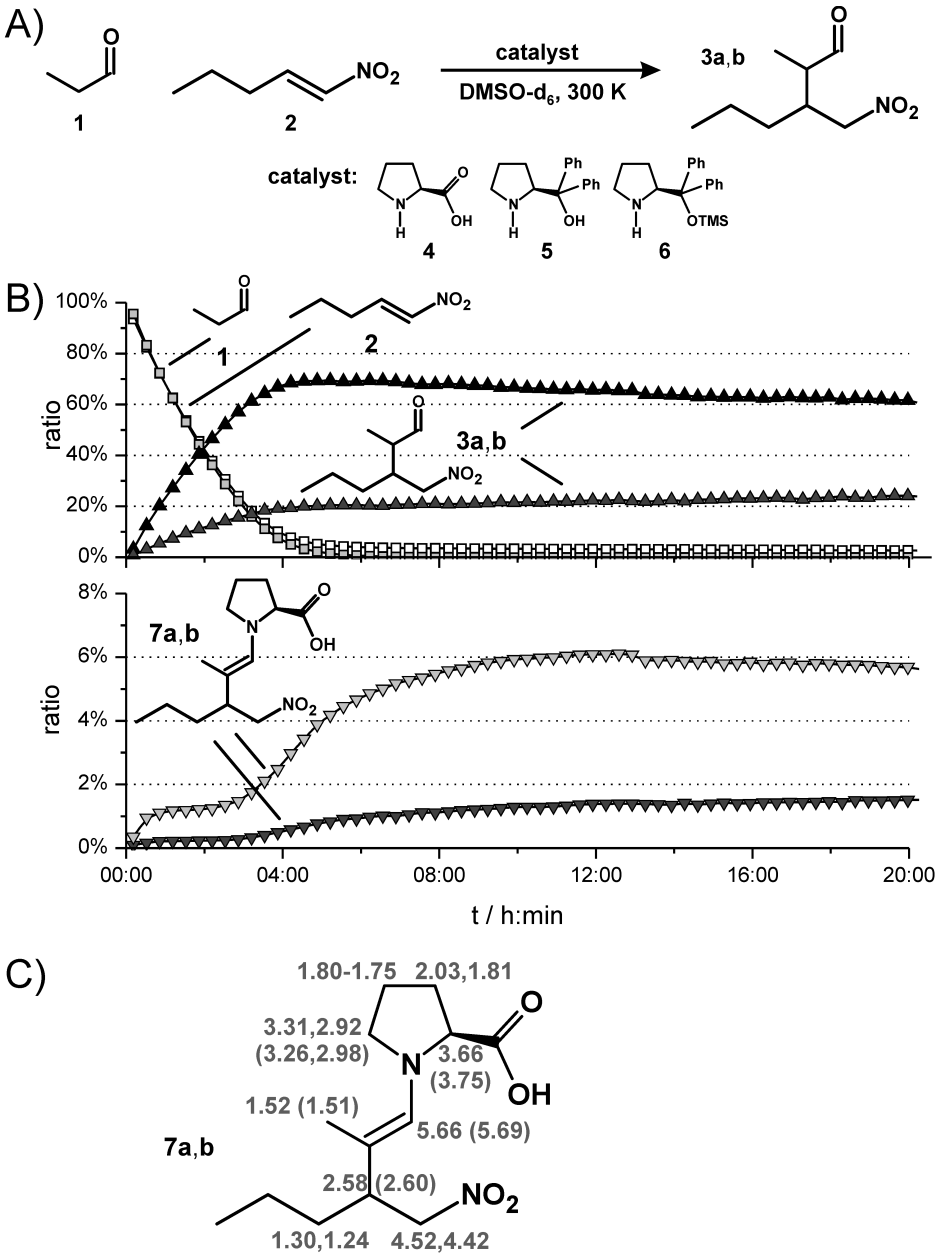

Figure 10.1: A) Amine-catalyzed Michael addition of **1** to **2** and catalysts employed; B) reaction profile of the Michael addition of **1** to **2** under catalysis of L-proline **4** in DMSO-d_6 at 300 K (The various product oxazolidinones are not displayed for the sake of clarity; note: The sum of all **2**-derived moieties detected in the first spectrum was set to 100 %.); C) ^{1}H NMR assignments of the product enamines (in ppm; values for the minor diastereomers are given in brackets.)

ment of the nitro group of **7a**,**b** as an H-bond acceptor in the enamine stabilization. In addition, the slow thermodynamic equilibration of the two diastereomeric pairs of enantiomers **3a** and **3b** was observed in the course of the Michael reaction (see Figure 10.1B): The diastereomeric ratio **3a**:**3b** drops from 3.5:1 after 4 hours to 2.5:1 after 20 hours. This may be accounted for by the interconversion of the diastereomers **3a**,**b** via the inversion of the α-configuration through the enamine stage. Hence, the diastereomeric outcome of

proline-catalyzed Michael additions of aldehydes to nitroalkenes is shown to be dependent on the time scale of the reaction. Interestingly, this parallels the time-dependent selectivity of the proline-catalyzed aldol addition although, most notably, the origin of the drop of selectivity was essentially due to different rates of the retro-aldolizations in this case (chapter 5.2).

Catalysis by Diphenylprolinol. In a next step, the same experimental setup was used, but proline **4** was replaced by 20 mol% of diphenylprolinol **5**. As mentioned earlier (chapter 9), no notable amounts of Michael product were observed under these experimental conditions even after more than 20 hours of reaction time. Still, a product enamine **9** was detected as an intermediate species, but vanished in favor of the product oxazolidines **10a**,**b**; the yield of the latter reached almost 15 % after 22 hours. From these oxazolidines, in turn, the slow release of product could be triggered by adding benzoic acid as an additive (data not shown). To study these processes in more detail, we increased the amount of catalyst **5** to 100 mol% (Figure 10.2). Under these experimental conditions, about 35 % of the propionaldehyde **1** were consumed by the formation of the oxazolidine **8**; its amount remained stable over the reaction time observed (*cf.* chapter 5.2). The corresponding enamine, however, could not be detected at all; just like in the case of proline-catalysis (see above), this unability to detect the enamine derived from **1** (though it had well been detected in the case of the homo-aldol reaction, see chapter 3.2 and 5.2) can be ascribed to the rapid reaction of the enamine with the "super-electrophile" **2**. Indeed, in the reaction mixture of **1**, **2**, and **5**, large quantities of product-derived species could be observed. Only small amounts of the products **3a**,**b**, however, were released from its adducts with the catalyst **5**. Instead, most of the product species was still present as the product-enamine **9** or as a product-oxazolidines **10a**,**b**. The kinetic profiles of these species suggest (Figure 10.2), that first the enamine **9** is generated after the C-C bond formation and it is then slowly converted to the thermodynamically more stable oxazolidine **10a**,**b** over a time span of presumably more than one day. This long lifetime of a diphenylprolinol-derived enamine is highly surprising given the fact that the enamine of **1** and **5** was not detected at all under Michael addition conditions and that it was completely converted into the oxazolidines under aldol addition conditions within only one hour (see chapter 6.2). Again, just like for the unexpectedly high amounts of proline-derived product enamines (see above), the increased steric bulk of **3a**,**b** compared to **1** should again guide the line of argument to explain this striking observation: Firstly, the increased steric demand of the α-disubstituted enamine **9** should prevent further reactions with additional "super-electrophilic" nitroalkenes. Therefore, the fast reaction between enamines and nitropentene **2**, that was made responsible for the unability to detect enamines of **1** and **5** under Michael conditions, is now eliminated as a source of enamine **9** consumption. Secondly, ring closure of the s-*trans* enamine **9** (supposedly via the *E*-iminium ion) leads to the *endo*-oxazolidine which is generally prone to steric repulsions between the *endo*-substituent and the pyrrolidine moiety. Increasing the size of the *endo*-substituent such as in **10a**,**b** is therefore expected to thermodynam-

ically destabilize the *endo*-oxazolidine. Likewise, one may assume, that the transition state leading to this *endo*-oxazolidine is sterically disfavored which drastically reduces the rate of the formal ring closure of enamine **9**. Altogether, this should hence explain the unexpectedly large amounts and the long lifetime of enamine **9** under the experimental conditions applied.

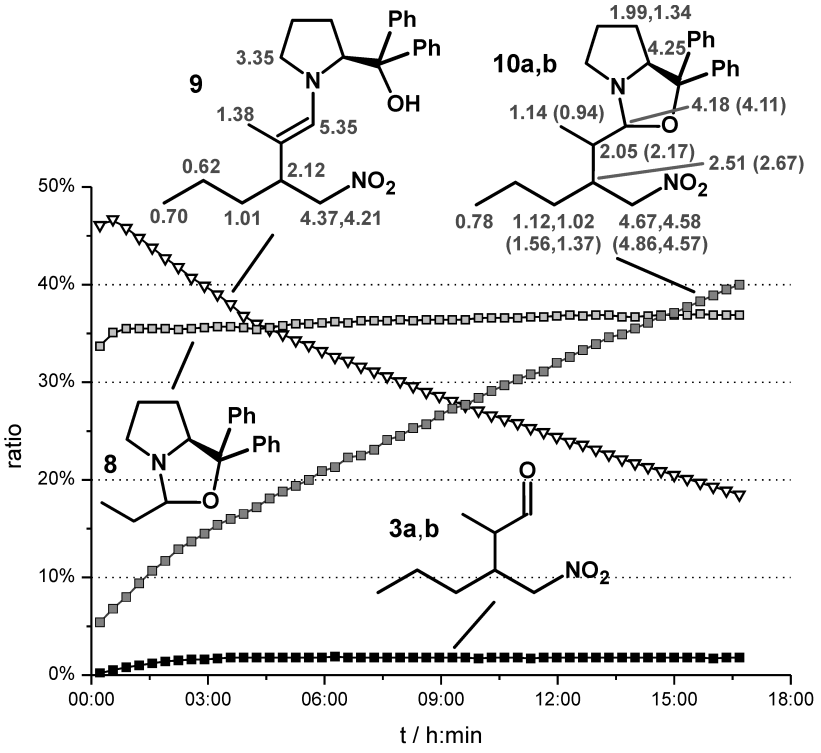

Figure 10.2: Reaction profile of a mixture of propionaldehyde **1** and nitropentene **2** (c = 50 mM, each) with 100 mol% of diphenylprolinol **5** in DMSO-d_6 at 300 K (note: The total amount of all **2**-derived moieties detected in the first spectrum was set to 100 %.)

Catalysis by Diphenylprolinol/Benzoic Acid. Based on these findings and together with the knowledge, that the products **3a**,**b** are released under the influence of benzoic acid, we reasoned that the addition of PhCOOH to the discussed experimental setup might significantly increase the yield of the **5**-catalyzed Michael addition of **1** to **2**. However, as presented earlier (chapter 9), the combination of **5** and benzoic acid constituted the ideal conditions for the nitroalkene homo-dimerization to enynes in DMSO. To suppress this and other unwanted reaction pathways, we applied the following procedure. First, propionaldehyde **1** (final concentration 100 mM) was mixed with 50 mol% of **5** and PhCOOH in DMSO-d_6. This was expected to lead to the fast formation of the oxazolidine, thereby largely suppressing the unwanted homo-aldol reaction of **1** (see chapter 7.4). At the same time, by the addition of benzoic acid, the oxazolidine ring opening (see above) should nevertheless provide small amounts of enamine. In addition, by using an excess of **1**, no free catalyst molecules should be available to catalyze the nitroalkene-dimerization. Indeed, the ^{1}H NMR spectrum of this reaction mixture after half an hour revealed no amounts

of free catalyst or **1**-derived enamine, but only oxazolidine **8** as well as tiny amounts of the homo-aldoldimer oxazolidine and additional starting material **1**. Then 0.5 equivalents of **2** were added to the mixture and the reaction progress was again monitored by 1D ^{1}H spectra (Figure 10.3).

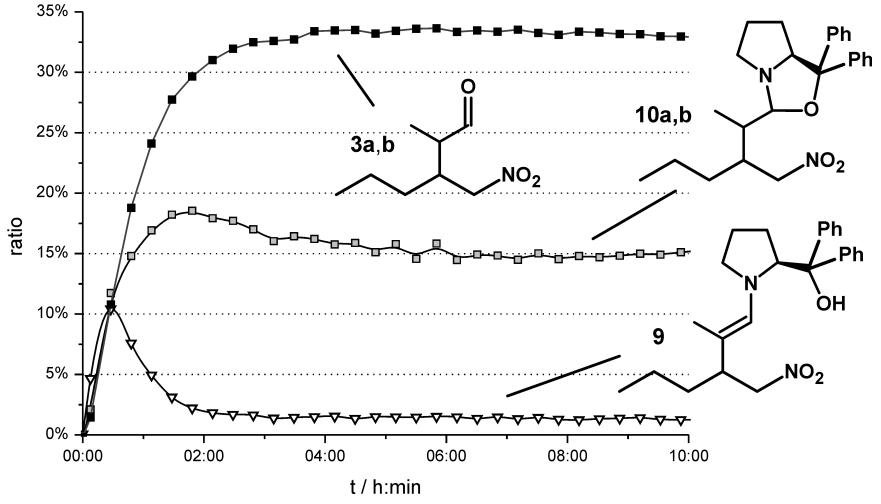

Figure 10.3: Formation of the Michael addition products **3a**,**b**, of the product-oxazolidines **10a**,**b** and of the product enamine **9** in a reaction mixture of propionaldehyde **1**, nitropentene **2**, and 100 mol% of **5**/PhCOOH in DMSO-d_6 at 300 K (See the text for the experimental procedure.).

Again, the product enamine **9** was formed first. However, as envisaged and in contrast to the acid-free case discussed above, the enamine species **9** is not accumulated in large amounts and is not converted into the oxazolidinones **10a**,**b** at a very slow rate only. Instead, the concentrations of **10a**,**b** exceed the one of **9** already after half an hour (compared to more than 9 hours without PhCOOH, *cf.* Figure 10.3 and Figure 10.2); this indicates that the formal ring closure of the enamine **9** is accelerated by the additive benzoic acid, as was also evidenced for the oxazolidine **8** (chapter 7.4). Moreover, as expected, PhCOOH leads to the release of the products **3a**,**b** in a yield of more than 30 % within only two hours (compared to less than 2 % yield after 16 hours without benzoic acid, Figure 10.2). Hence, the idea of adding an acidic additive to release the Michael products from their adducts with catalyst **5** proved to work in principle (similarly to the homo-aldol reaction, chapter 7.4), however, the performance of proline **4** as a catalyst for the Michael addition was not achieved in terms of the yield. The main factor for this inferiority of **5**/PhCOOH against proline **4** was recognized to be the nitroalkene dimerization. Despite the fact that no free catalyst could be observed NMR-spectroscopically before the addition of nitropentene **2**, approximately 25 % of **2** was consumed by the unwanted nitroalkene-dimerization. This must be attributed to the fact that the additive PhCOOH provides, by hydrolysis of catalyst-adducts, small amounts of the free catalyst **5**, undetectable by NMR, but sufficient for the catalysis of the nitroalkene homo-coupling.

Catalysis by Diphenylprolinol Silyl Ether. Finally, the performance of diphenylprolinol trimethylsilyl ether **6** as a catalyst for the Michael addition of **1** to **2** was tested. For that purpose, equimolar amounts of **1** and **2** were mixed with 20 mol% of **6** in DMSO-d_6 at 300 K. Since in contrast to **5**, the silyl ether **6** cannot form stable product-oxazolidines, the release of the products **3a**,**b** was expected to be improved in the case of **6**. Indeed, **3a**,**b** were formed slowly, but continuously and the *in situ* yield reached approximately 25 % after 16 hours. In addition, the existence of at least three enamine species (with a total ratio of about 15 %) was suggested by 1D ^{1}H spectra. This is surprising, since only two diastereomeric *E*-configured product enamines (the silyl ethers of **9**) are expected to be formed. However, the nature of these putative enamine species could not be clarified so far and needs to be investigated in more detail (*e.g.* with 100 mol% of **6**), in particular with regard to potential *E*/*Z* isomers or even stable rotamers around the exocyclic C-C bond.

Conclusion

Altogether, the organocatalytic Michael addition of propionaldehyde to nitropentene in DMSO was investigated by NMR reaction monitoring. Among other product intermediates, α-branched product enamines derived from proline and diphenylprolinol were found for the first time in substantial amounts. In the case of proline, the presence of these product enamines was made responsible for the eventual decay of the diastereomeric ratio of the products. However, further investigations will be necessary to elucidate in detail the origins of the observed thermodynamic and kinetic stabilizations of such product enamines, especially the involvement of steric shielding or intramolecular H-bonding therein. In particular, the revelation of stabilization trends by varying catalyst and aldehyde scaffolds, for instance by the employment of differently substituted diphenylprolinols or α,β-branched aldehydes, is expected to promote the understanding of the observed high enamine amounts. This will also help to relate these results to our previous finding of only tiny amounts of isobutyraldehyde-derived enamines (chapter 3.2),[2] to our inability to detect product enamines in the propionaldehyde self-aldolization (chapter 3.2 and 5.2), and to the rapid oxazolidine formation of α-unbranched aldehydes with prolinol catalysts (chapter 6.2). Moreover, the first observation of large quantities of α-branched enamines makes such species accessible to more detailed conformational analyses. Since the use of α-branched aldehydes as aldol donors in amine-catalysis has not found a general solution yet, such investigations might help to clarify the underlying challenges and thus ultimately lead to the design of tailored organocatalysts for that purpose. In addition, the presented availability of prolinol enamines *in situ*, along with the previously reported oxazolidine-enamine equilibria (chapter 6.2), will also enable studies on the formation pathways of prolinol enamines in solution.

10.2 A Michael Addition - α-Alkylation Cascade

Introduction

An intriguing extension of organocatalytic reactions is the coupling of different consecutive reactions via different organocatalytic activation modes to so-called cascade reactions. This offers the option to generate products with high degrees of chemical and stereochemical complexity from rather easily accessible substrates with one single catalyst in one pot. One example for such a cascade approach was presented by Enders *et al.* in 2008.[3] They designed a cascade reaction consisting of a Michael addition of an aldehyde to a nitroalkene and a subsequent intramolecular α-alkylation of the resulting aldehyde by an alkyl iodide moiety. By employing (*E*)-5-iodo-1-nitropent-1-ene **11** as an electrophile they could hence build up optically pure γ-nitro aldehydes (Figure 10.4A) that could potentially be converted into valuable γ-amino acids. To investigate whether *in situ* NMR spectroscopy could contribute to the understanding of this reaction cascade and the catalyst performances reported,[3] mixtures of propionaldehyde **1**, iodonitropentene **11**[3,4] (c = 50 mM, each), and one of the catalysts **4**-**6** were prepared and the ongoing events were monitored by 1D ^{1}H spectra.

Results and Discussion

Catalysis by Proline. First 20 mol% of L-proline **4** were applied. In agreement with our previous findings, the proline-catalyzed Michael addition of **1** to **11** proceeded smoothly to **12a**,**b** within 5 hours, with a yield of more than 50 % *in situ* and a diastereomeric ratio of about 10:1. In contrast, the subsequent α-alkylation of **12a**,**b** did not proceed well under our experimental conditions applied: The cyclized products **13a**,**b** were formed in a diastereomeric ratio of 3:1, but the yield was below 5 % after 5 hours which is in striking contrast to the reported overall yield of 59 % (*nota bene* 5 equivalents of aldehyde were used in the original study).[3] In addition to the products of the Michael addition and the complete cascade, various other intermediates and byproducts were detected in the ^{1}H spectra, but could not be identified at catalyst loadings of 20 mol%. In our experimental system the concentrations of both **12a**,**b** and **13a**,**b**, however, remained virtually unchanged for another 17 hours, which indicates that the reaction had come to rest. This observation is all the more striking since substantial amount of the starting materials **1** and **11** (about one third of the initial concentration) were still present in the mixture. Therefore, a certain catalyst deactivation must be assumed as the reason for the standstill of the reaction. Indeed, a catalyst species **14** was detected whose concentration was rising throughout 5 hours and then remained constant, too. It was represented, among others, by broad resonances at 9.55 ppm (half-width > 100 Hz), 9.26 ppm and 8.68 ppm (half-widths of about 30 Hz, each). It was assigned in analogy to **15** (see chapter 9 and discussion below) as an iodide salt of **4** (Figure 10.4B), formed upon α-alkylation of **12a**,**b**. The fact that the detected amount of **14** is about twice the amount of detected **13a**,**b** contradicts

this hypothesis only at first glance. Two rationalizations for this phenomenon come to mind: First, in our reaction mixture with plenty of nucleophiles, also other side-reactions occur that formally release HI from **11**. For instance, the cyclopropylated nitroalkene (**17** in chapter 9) was observed in small amounts in this experimental setup, too. Secondly, not single ion pairs of **14** may be formed, but iodide may trigger the aggregation of protonated **4**, leading to larger complexes whose positive charges are compensated by other anions than iodide; at least for **15**, aggregation could be evidenced experimentally by DOSY (see chapter 7.4 and discussion below).

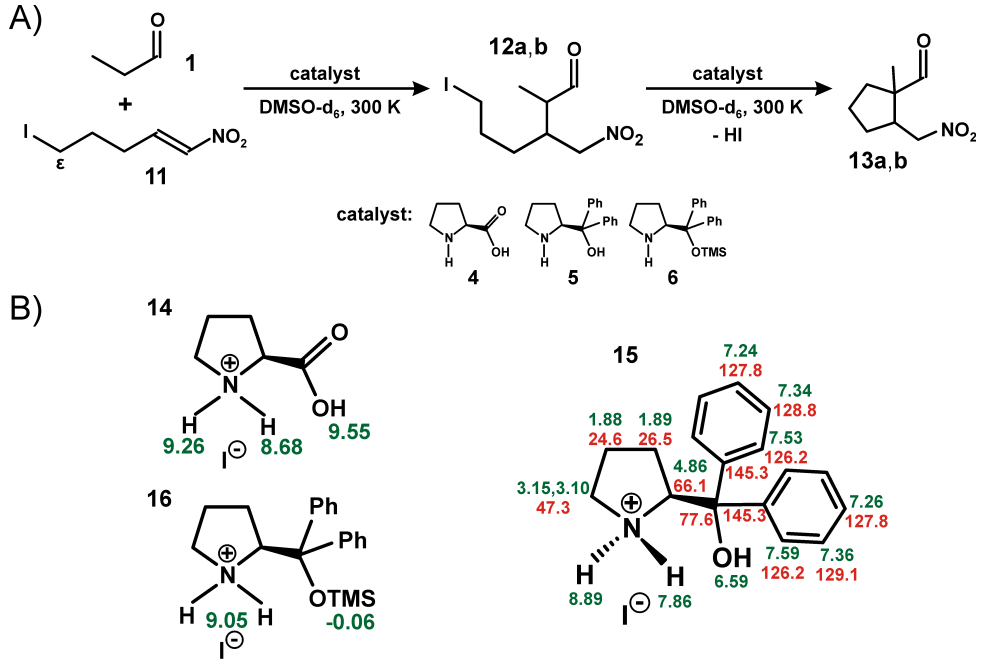

Figure 10.4: A) Amine-catalyzed Michael addition of **1** to **2** and catalysts employed; B) iodide salts **14-16** of catalysts **4-6** and chemical shift assignments. (in ppm relative to the residual solvent signals; values for ^{1}H are given in green, those for ^{13}C in red.)

Catalysis by Diphenylprolinol. When 20 mol% of diphenylprolinol **5** were used as the catalyst instead of proline **4**, the outcome of the reaction between **1** and **11** was very poor. In agreement with the literature,[3] only traces (below 3 %) of the cascade product **13a**,**b** were formed, but in contrast to the original publication,[3] only tiny amounts (about 1 %) of the Michael products **12a**,**b**. In addition, various intermediates and by-products in low yields were detected, among them the cyclopropyl nitroalkene (**17** in chapter 9) and other not yet identified substances. In analogy to the case of proline, a protonated catalyst species **15** was observed and fully characterized by means of 2D NMR spectroscopy (see Figure 10.4B for the assignment). It turned out to be the same species that had occurred in the course of the intramolecular cyclopropanation of **11** (see chapter 9), which supports its identification as an iodide salt of **5**. As outlined earlier (chapter 9), the spectroscopic findings indicate that **15** is involved in a larger aggregate with a rather stable hydrogen-bond network. This might again be considered to be responsible for the lack of catalytic

activity of **5** in this experimental system. Applying 20 mol% of diphenylprolinol **5** and additionally 20 mol% of benzoic acid hardly improved the yield of the reaction: Only 5 % of the Michael products **12a**,**b** and 3 % of the cascade product **13a**,**b** were formed within 15 hours, among a variety of other products and intermediates.

Catalysis by Diphenylprolinol Silyl Ether. Neither by employing 20 mol% of **6** as the catalyst was a significant improvement of the reaction achieved: The yield of the reaction cascade was almost 10 % after 5 hours, but did not rise any further throughout another 15 hours. Again, this standstill of the reaction correlates with the appearance of a protonated catalyst species **16** which may be responsible for the catalyst deactivation. Interestingly, this protonated diphenylprolinol trimethylsilyl ether in DMSO did not experience a significant loss of the TMS protecting group, as was observed upon addition of PhCOOH (see chapter 7.4), but it was stable for at least one day in solution. The combined use of 20 mol% of **6** and of benzoic acid did not enhance the yields of the cascade products **13a**,**b** (close to 10 %) or of the Michael addition products **12a**,**b** (about 3 %) significantly. In contrast, increasing the amount of catalyst **6** to 100 mol% led to a substantial better outcome of the reaction: **13a**,**b** was formed in more than 50 % yield within only 2 hours and the Michael products **12a**,**b** in 7 % yield. This observation may be explained by the assumption that substantial quantities of the catalyst are already engaged in intermediate species before the release of HI and its deactivating influence can become operative.

Conclusion

Altogether, in this study of an organocatalytic reaction cascade, consisting of a Michael addition and an intramolecular α-alkylation, we observed a so far unknown mode of organocatalyst deactivation. This deactivation is triggered by HI that is released in the course of the alkylation reaction. It is associated with the protonation as well as with the aggregation of the catalyst molecules. Because of the discrepancy with the report by Enders *et al.* concerning the performance of organocatalysts in this reaction cascade,[3] one may speculate that this deactivation is only present under our experimental conditions, possibly caused by the lack of sample mixing during the reaction. The catalyst deactivation effects need to be investigated further before a more detailed analysis of the various intermediates and side reactions observed can be undertaken.

10.3 References

[1] D. Seebach, A. K. Beck, D. M. Badine, M. Limbach, A. Eschenmoser, A. M. Treasurywala, R. Hobi, W. Prikoszovich, B. Linder, *Helv. Chim. Acta* **2007**, *90*, 425–471.

[2] M. B. Schmid, K. Zeitler, R. M. Gschwind, *Angew. Chem. Int. Ed.* **2010**, *49*, 4997–5003.

[3] D. Enders, C. Wang, J. Bats, *Angew. Chem. Int. Ed.* **2008**, *47*, 7539–7542.

[4] M. Lautens, J.-F. Paquin, S. Piguel, M. Dahlmann, *J. Org. Chem.* **2001**, *66*, 8127–8134.

11 Summary and Outlook

Catalytic processes are central to the production of the vast majority of chemicals that surround us in everyday life and are therefore indispensable for an economic and sustainable development. With regard to the ever increasing significance of enantiopure substances as agrochemicals or pharmaceuticals, for instance, asymmetric catalysis has been gaining in importance already throughout the second half of the 20th century. While this had majorily been based on transition metals and enzymes as catalytic units, the past decade has seen tremendous scientific progress in the field of asymmetric organocatalysis, *i.e.* catalysis by small organic molecules. However, in this rapidly expanding research area, the mechanistic understanding of the underlying processes often lags behind the development of novel synthetic applications. Yet, intimate knowledge on organocatalytic reaction pathways and on the origin of their stereocontrol should largely promote the catalyst design and facilitate the improvement of the reaction conditions. Therefore, the objective of this thesis was the elucidation of some of the hitherto unsolved mechanistic and conformational issues of aminocatalysis by means of modern NMR spectroscopic techniques.

The major part of this dissertation is devoted to the detection and characterization of enamine key intermediates in aminocatalysis.

In the archetypical proline-catalyzed aldol reaction, the elusive proline enamine intermediates that had evaded their experimental detection despite numerous attempts throughout many years could be snared for the first time *in situ*. On the example of the aldehyde self-aldolization in DMSO, they have been characterized as *E*-configured enamines with a preference for the s-*trans* conformation. Aldehyde-derived proline enamines have been shown to be stabilized by β-alkyl substituents, while α-alkyl substituents reduce the enamine amounts and ketone-derived proline enamines have not been observed at all. The proline enamine detection has furthermore been restricted to dipolar aprotic solvents with pronounced H-bond acceptor properties (DMSO and DMF), which could be attributed to the presence of favorable H-bonding interactions between solvent molecules and the enamine carboxylic acid.

The central role of interactions involving the carboxylic group for the enamine detection has also been highlighted by the transient proline enamine stabilization through deuteration. Even more remarkably, upon deprotonation of the carboxylic group and subsequent ion pair formation with amine bases, permanently and substantially larger enamine quantities have been obtained. In particular with the help of DBU, enaminocarboxylates have hence become accessible in a variety of solvents formerly unsuited for the enamine detec-

tion. Thereby, also the contribution of *Z*-configured enamines to the proline intermediate pool could be evidenced. In addition, the deprotonation of the carboxylic group has been shown to impact on the electron density and hence nucleophilicity of the proline enamine π-electron system.

Beyond enamines derived from proline and simple monomeric aldehydes, a proline dienamine, a proline dienamine carboxylate, an α-oxy-aldehyde-derived proline enamine, and a tripeptide enamine could be detected in DMSO. In addition, significant amounts of α-branched product enamines from a Michael addition of aldehydes to nitroalkenes have been observed.

With regard to the role of proline enamines and related intermediates within the catalytic cycle, the enamines have been found to exist in an equilibrium with the tautomeric oxazolidinones that had previously been termed "parasitic". Yet, in contrast to this common view, it has been revealed that in DMSO proline enamines are formed directly from the oxazolidinones which hence play the part of a bridge between the aldehyde and the enamine. A nucleophile-assisted proton relay mechanism is suggested for the oxazolidinone-enamine interconversion based on its acceleration by nucleophilic rather than by basic additives and on observed substituent and isotope effects.

Concerning the reaction pathways of proline enamines, strong experimental evidence has been provided that the aldol addition and condensation are competing instead of consecutive reaction steps. The aldol condensation presumably proceeds via a Mannich-type mechanism with dual activation of the substrate molecules as a nucleophilic enamine and an electrophilic iminium ion, respectively. Most notably, the competition between the aldol addition and condensation, along with the reversibility of the aldol addition, causes a time- and catalyst amount-dependence of the diastereoselectivity of the aldol addition.

In the field of prolinol (ether) organocatalysts, detailed studies on formation trends, stabilities, and conformational preferences of their aldehyde-derived enamine intermediates have been conducted in view of their high relevance and of unsolved conformational and mechanistic issues. For prolinol catalysts, the first detections of enamine intermediates (and of a carbinolamine intermediate) have been reported in DMSO and their rapid cyclization to the oxazolidines has been evidenced. Means to partially shift this "parasitic equilibrium" through steric and electronic modifications of the prolinol substituents have been demonstrated. On this experimental basis, the performances of different (diaryl) prolinols in enamine catalysis have been rationalized. In addition, a significant kinetic stabilization of an α-branched product enamine from a prolinol-catalyzed Michael addition has been observed.

For diarylprolinol ether catalysts, the aldehyde-derived enamine amounts are substantial in various solvents, but they have been revealed to decrease with increasing sizes of the *O*-protecting group and of the aryl substituents. Moreover, for unfortunate catalyst/solvent/additive combinations, the prolinol ether enamine formation has been found

to be significantly delayed, but a rapid NMR screening method could be introduced to recognize such potentially detrimental conditions. In the case of TMS ethers, the eventual desilylation in DMSO and subsequent cyclization to the oxazolidine could be monitored.

For all prolinol(ether)s, the *E*-configured enamines have been found to be highly preferred over the *Z*-isomers; nevertheless, the latter could be detected in the case of high overall enamine amounts in solution, too. Concerning the controversial orientation of the enamine moiety, it has been proven that only the unsubstituted prolinol allows for a significant population of the s-*cis* enamine conformation, whereas diarylprolinol (ether) enamines exist exclusively in the s-*trans* conformation. Along with the enamine formation, the pyrrolidine ring has been evidenced to preferredly adopt the *down*, which creates a convex enamine half-space opposite to the α-substituent that is easily accessible for an electrophilic attack.

For the disputed arrangement of the diarylmethanol (ether) substituent around the exocyclic C-C bond, distinct conformational differences have been disclosed for prolinol enamines and prolinol ether enamines, respectively, and a rapid 1D ^{1}H NMR screening approach for these differences could be established: Prolinol enamines exist in the *sc-endo* conformation that is mainly favored by the formation of an OH$\cdots$N H-bond. In contrast, prolinol ether enamines adopt the *sc-exo* conformation owing to stabilizing CH/π interactions, which implies the shielding of the "upper" face of the enamine moiety by the *O*-protecting group and by a *meta*-substituent of the aryl moieties. By comparison with literature data, these conformational features have been shown to explain well the catalytic performances of prolinol ethers.

Beyond prolinol ether enamines, investigations on a recycled MeOPEG-supported prolinol ether catalyst have revealed a non-hydrolyzed product iminium species of the catalyzed Michael addition. Since it has been suggested as the origin of the eventual activity loss of such immobilized catalysts, a facile procedure for the restorage of the full catalytic activity could be developed.

In addition to the investigation of intermediate species, proline-derived catalysts themselves have been studied in solution.

Short linear peptides, containing the unnatural amino acid β-ACC, have been analyzed conformationally in chloroform. An intraresidual H-bond has been evidenced as the main source of conformational stabilization of the peptide backbone. On this basis, residual dipolar couplings could be established as valuable novel structural parameters for peptidic foldamers. RDCs have been used to validate the force field parameterization of the rigid amino acid and to gather information on the conformation of the peptide backbone and of the proline side-chains.

Prolinol silyl ethers have been studied with regard to their regularly claimed desilylation in solution. Carboxylic acid additives in dipolar aprotic solvents have been found to

provide the optimum conditions for the TMS-cleavage within few hours, while—among additive-free solvents—methanol has proven to be the best promoter for the deprotection. Altogether this has been interpreted as an indication of complex H-bonding networks being operative in the desilylation process.

Furthermore, the aggregation of proline-derived catalysts in solution has been addressed. The bifunctional proline has turned out to be dimeric in DMSO while prolinol ethers are monomeric. For prolinol derivatives, monomers and dimers as well as their rapid exchange have been detected. Moreover, their aggregation with benzoic acid in solution has been revealed and rationalized with the help of a crystal structure. First observations towards a correlation of aggregation trends and catalytic activities have been presented.

Finally, serendipitous circumstances have led to the discovery of two unprecedented organocatalytic reaction pathways of nitroalkenes. Under aminocatalysis, nitroalkenes have been shown to dimerize and to subsequently undergo fragmentation, under formal loss of nitromethane and nitrous acid, to enynes in promising yields. On the other hand ϵ-iodo-substituted nitroalkenes have been observed to be intramolecularly cyclopropylated in the presence of proline-derived catalysts.

Altogether, this dissertation presents NMR spectroscopic investigations on aminocatalysis, in particular on intermediate species therein, which can be expected to substantially promote the understanding of the underlying principles of reactivity and stereocontrol. The mechanistic and conformational studies should provide valuable information both for synthetically and theoretically working organic chemists in the field of organocatalysis in order to optimize the reaction conditions, to tailor the catalyst design, and to perform focussed calculations. Furthermore, an experimental and methodological foundation is laid for the *in situ* generation and study of further enamine and dienamine species, derived from different aldehydes and different amine catalysts, for the exploration of novel organocatalytic transformations, for investigations on the role of the solvent in organocatalysis, for the disclosure of aggregation trends and their impact on catalyst performances. Future investigations are expected to elucidate these and further issues of aminocatalysis in even more detail.